AD-A048 275 LOCKHEED MISSILES AND SPACE CO INC HUNTSVILLE ALA HU--ETC F/G 1/1
LASER DOPPLER VELOCIMETER MEASUREMENTS OF B-747 WAKE VORTEX CHA--ETC(U)
SEP 77 M R BRASHEARS, A D ZALAY DOT-TSC-1145

UNCLASSIFIED LMSC-HREC-TR-D496975 FAA-RD-77-85 NL

1 OF 3
AD
A048275

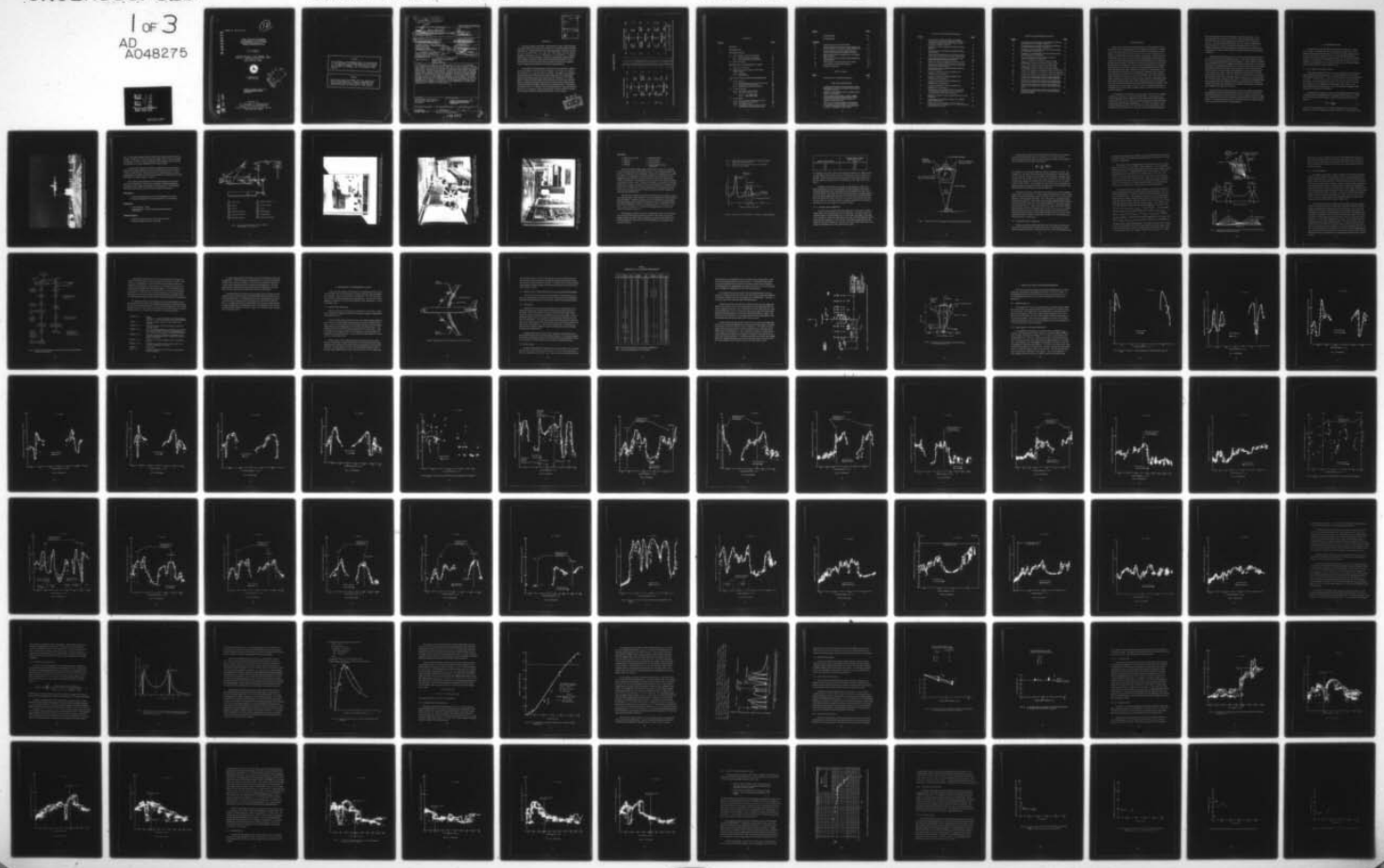

REPORT NO. FAA-RD-77-85

LASER DOPPLER VELOCIMETER MEASUREMENTS OF B-747 WAKE VORTEX CHARACTERISTICS

M. R. Brashears
A. D. Zalay

LOCKHEED MISSLES & SPACE COMPANY, INC.
HUNTSVILLE RESEARCH & ENGINEERING CENTER
4800 Bradford Drive
Huntsville AL 35807

SEPTEMBER 1977
FINAL REPORT

Prepared for

U.S. DEPARTMENT OF TRANSPORTATION
FEDERAL AVIATION ADMINISTRATION
Systems Research and Development Service
Washington DC 20591

NOTICE

This document is disseminated under the sponsorship of the Department of Transportation in the interest of information exchange. The United States Government assumes no liability for its contents or use thereof.

NOTICE

The United States Government does not endorse products or manufacturers. Trade or manufacturers' names appear herein solely because they are considered essential to the object of this report.

(18) FAA-RD, TSC

Technical Report Documentation Page

1. Report No. (19) FAA-77-13	2. Government Accession No.	3. Recipient's Catalog No. (11)
[redacted]-77-85		

4. Title and Subtitle (6)
LASER DOPPLER VELOCIMETER MEASUREMENTS OF B-747 WAKE VORTEX CHARACTERISTICS.

5. Report Date
September 1977

6. Performing Organization Code

7. Author(s) (10)
M. R. Brashears and A. D. Zalay

8. Performing Organization Report No.
DOT-TSC-FAA-77-13
(14) LMSC-HREC-TR-D496975

9. Performing Organization Name and Address
Lockheed Missiles & Space Company, Inc.*
Huntsville Research & Engineering Center
4800 Bradford Drive
Huntsville AL 35807

10. Work Unit No. (TRAIS)
FA705/R7126

11. Contract or Grant No. (15)
DOT-TSC-1145 New

12. Sponsoring Agency Name and Address (12) 220 p.
U. S. Department of Transportation
Federal Aviation Administration
Systems Research and Development Service
Washington DC 20590

13. Type of Report and Period Covered (9)
Final Report,
Nov [redacted]75 — Jan [redacted]77

14. Sponsoring Agency Code

15. Supplementary Notes
*Under Contract to: U. S. Department of Transportation
Transportation Systems Center
Kendall Square
Cambridge MA 02142

16. Abstract

To determine the behavior of the wake vortices of a B-747 at low altitudes and to measure the vortex-decay process behind the B-747 as a function of altitude above ground, flap and spoiler settings, and different flight configurations, a B-747 aircraft flew 54 passes at low level over a ground-based lasser Doppler velocimeter (LDV) system. From the LDV measurements, the location and flow field of the wake vortices and the general vortex roll-up, transport, and decay trends were obtained. Results of the study indicated that the deployment of spoilers and flaps enhanced the decay of the vortex peak tangential velocity in the near wake while aircraft altitude, glide slope, and landing gear deployment had little effect. The report discusses the LDV wake vortex measurements including the instrumentation used, the experimental test sequence, the results of the wake measurements in terms of the vortex roll-up, transport, and decay trends, and a comparison of the wake vortex characteristics for different configurations.

17. Key Words	18. Distribution Statement
Aircraft Wakes, Trailing Vortex, Wake Vortices, Laser Doppler Velocimetry	DOCUMENT IS AVAILABLE TO THE U.S. PUBLIC THROUGH THE NATIONAL TECHNICAL INFORMATION SERVICE, SPRINGFIELD, VIRGINIA 22161

19. Security Classif. (of this report)	20. Security Classif. (of this page)	21. No. of Pages	22. Price
Unclassified	Unclassified	224	

Form DOT F 1700.7 (8-72) Reproduction of completed page authorized

210105

VP

PREFACE

The laser Doppler velocimeter measurements of wake vortex characteristics described in this report were carried out by Lockheed Missiles & Space Company, Inc., Huntsville Research & Engineering Center working in conjunction with AeroVironment, Inc., under the "Wake Decay near the Ground" program sponsored by the U.S. Department of Transportation. Lockheed-Huntsville's role in the program consisted of operating the Lockheed Mobile laser Doppler velocimeter system and collecting measurements of vortex characteristics with the system and processing and analyzing the measurements to determine the dominant vortex decay characteristics.

The following Lockheed-Huntsville personnel made significant contributions to this effort: C.E. Craven, B.B. Edwards, J.L. Jetton, A.J. Jordan, M.C. Krause, T.R. Lawrence, and K.R. Shrider. The authors are grateful to the Optics Branch at NASA-Marshall Space Flight Center for making their filter bank and signal processor available for this study and to J.W. Bilbro and H.B. Jeffreys at NASA-MSFC and to Bill Keenum, Earl Lucas, and Rick Bynum at Computer Sciences Corporation for processing the measurements obtained with the NASA-MSFC filter bank and signal processor. The authors are grateful to Dr. J.N. Hallock, TSC Contracting Officer's Technical Monitor, and to Dr. D.C. Burnham, staff scientist at TSC, for their technical contributions and able assistance during the performance of this contract.

METRIC CONVERSION FACTORS

Approximate Conversions to Metric Measures

Symbol	When You Know	Multiply by	To Find	Symbol
		LENGTH		
in	inches	2.5	centimeters	cm
ft	feet	30	centimeters	cm
yd	yards	0.9	meters	m
mi	miles	1.6	kilometers	km
		AREA		
in^2	square inches	6.5	square centimeters	cm^2
ft^2	square feet	0.09	square meters	m^2
yd^2	square yards	0.8	square meters	m^2
mi^2	square miles	2.6	square kilometers	km^2
	acres	0.4	hectares	ha
		MASS (weight)		
oz	ounces	28	grams	g
lb	pounds	0.45	kilograms	kg
	short tons (2000 lb)	0.9	tonnes	t
		VOLUME		
tsp	teaspoons	5	milliliters	ml
Tbsp	tablespoons	15	milliliters	ml
fl oz	fluid ounces	30	milliliters	ml
c	cups	0.24	liters	l
pt	pints	0.47	liters	l
qt	quarts	0.95	liters	l
gal	gallons	3.8	liters	l
ft^3	cubic feet	0.03	cubic meters	m^3
yd^3	cubic yards	0.76	cubic meters	m^3
		TEMPERATURE (exact)		
°F	Fahrenheit temperature	5/9 (after subtracting 32)	Celsius temperature	°C

Approximate Conversions from Metric Measures

Symbol	When You Know	Multiply by	To Find	Symbol
		LENGTH		
mm	millimeters	0.04	inches	in
cm	centimeters	0.4	inches	in
m	meters	3.3	feet	ft
m	meters	1.1	yards	yd
km	kilometers	0.6	miles	mi
		AREA		
cm^2	square centimeters	0.16	square inches	in^2
m^2	square meters	1.2	square yards	yd^2
km^2	square kilometers	0.4	square miles	mi^2
ha	hectares (10,000 m^2)	2.5	acres	
		MASS (weight)		
g	grams	0.035	ounces	oz
kg	kilograms	2.2	pounds	lb
t	tonnes (1000 kg)	1.1	short tons	
		VOLUME		
ml	milliliters	0.03	fluid ounces	fl oz
l	liters	2.1	pints	pt
l	liters	1.06	quarts	qt
l	liters	0.26	gallons	gal
m^3	cubic meters	35	cubic feet	ft^3
m^3	cubic meters	1.3	cubic yards	yd^3
		TEMPERATURE (exact)		
°C	Celsius temperature	9/5 (then add 32)	Fahrenheit temperature	°F

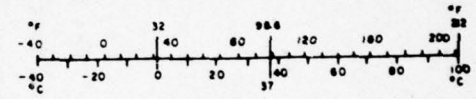

CONTENTS

LIST OF TABLE

LIST OF ILLUSTRATIONS

LIST OF ILLUSTRATIONS (Continued)

LIST OF ILLUSTRATIONS (Concluded)

1. INTRODUCTION

Wake vortex transport and decay parameters near the ground are important factors in determining safe aircraft separation distances for terminal areas. For an operational Wake Vortex Avoidance System (WVAS), a knowledge of the location and intensity of wake vortices near the terminal area is necessary to determine the minimum-delay safe spacings. Under light cross-wind conditions, a wake vortex can remain in the approach corridor, and the minimum aircraft separation distance is dictated primarily by the wake decay process near the ground. Therefore, an important consideration in determining safe aircraft separations is the decay of the wake vortex near the ground. While numerous vortex decay theories have been proposed, there are little full-scale experimental data available for comparison. Experimental vortex decay data near the ground are also lacking for aerodynamic wake minimization concepts where variations in aircraft geometry are used to tailor the wake vortex flow. Flight tests by NASA have shown that certain flap and spoiler settings can reduce the imposed rolling moments on following aircraft (in the near wake); however, wake vortex measurements near the ground for full-scale aircraft with different wake minimization concepts are needed. Thus, for both wake vortex avoidance and wake vortex minimization techniques, a knowledge of the vortex-rollup, transport, and decay characteristics near the ground is important.

To determine the behavior of aircraft wake vortices at low altitudes, a flight test program was conducted by DOT/NASA. The primary goal of the test program was to measure the wake vortex decay process behind a conventional jumbo jet as a function of altitude above ground, flap and spoiler settings, and different flight configurations. To isolate the influence of aircraft and flight parameters on the wake decay process, the flight tests were conducted at the Rosamond Dry Lake test area in California during the

early morning hours when calm atmospheric conditions prevailed. The Rosamond wake decay measurements were sought to quantify the effect of burst, link and viscous decay parameters on the wake vortex dissipation process. The wake decay measurements were also sought to demonstrate the effectiveness of recently developed vortex minimization concepts. In addition to the wake decay measurements, the flight tests were also focused on measuring the wake vortex rollup and transport phenomena in ground plane proximity.

The Rosamond flight tests involved airborne and ground-based meteorological sensors, an acoustic Doppler system, a mobile laser Doppler velocimeter, a flow visualization using smoke and balloons. In this report the measurements obtained with the laser Doppler velocimeter system (LDV) are discussed including: (1) the initial downwash field; (2) the lateral and horizontal transport of the coherent wake vortex; and (3) the decay of the vortex flow in terms of the time history of the circulation, peak tangential velocity, and the diffusion of the viscous core radius. While the application of LDV techniques for the study of wake vortex flows is not novel, this is the first time, to our knowledge, that the details of the vortex formation and decay process have been extracted for a full-scale aircraft using an LDV system. In addition to providing detailed wake measurements for comparison with available theoretical and empirical models, the results show the influence of changes in flap, spoiler, and landing gear settings on the wake characteristics.

The report discusses the LDV wake vortex measurements including the instrumentation used, the experimental test sequence, and the results of the wake measurements in terms of the vortex-rollup, transport, and decay trends, and a comparison of the wake vortex decay characteristics for different configurations. A brief discussion of the LDV wind measurements is given followed by the overall conclusions and recommendations.

2. INSTRUMENTATION

The wake vortex and atmospheric wind measurements were carried out by means of a scanning LDV system contained in a mobile van. Preliminary processing of the data was carried out with a SEL computer aboard the van. Reduction and analysis of the vortex and wind signatures were carried out by off-line processing software using a Univac 1108 and a PDP11 computer. A description of the instrumentation and the data processing methods for the Rosamond tests is given in terms of the LDV system configuration and the data processing techniques used.

2.1 Laser Doppler Velocimeter System

The Lockheed-Huntsville LDV was used to obtain wake vortex measurements during the Rosamond flight tests. A photograph of the van-mounted LDV system is given in Fig. 1. The wake measurements were accomplished as follows: (1) the wake generated by the aircraft was scanned by the CO_2 laser; (2) the radiation backscattered from the aerosol in the wake was collected; (3) the radiation was photomixed with a portion of the transmitted beam on a photodetector; and (4) the intensity and Doppler shift frequency of the signal were displayed.

The difference in frequency between the transmitted and backscattered signal generated at the photodetector, the Doppler shift frequency, is a measure of the aerosol's absolute line-of-sight velocity within the laser focal volume

$$\left|\bar{V}\right| = \frac{\lambda\,\Delta f}{2\cos\gamma}\,, \qquad (1)$$

where $\left|\bar{V}\right|$ is the magnitude of the velocity component in the region being sensed, λ is the laser radiation wavelength (10.6μm), Δf is the Doppler shift,

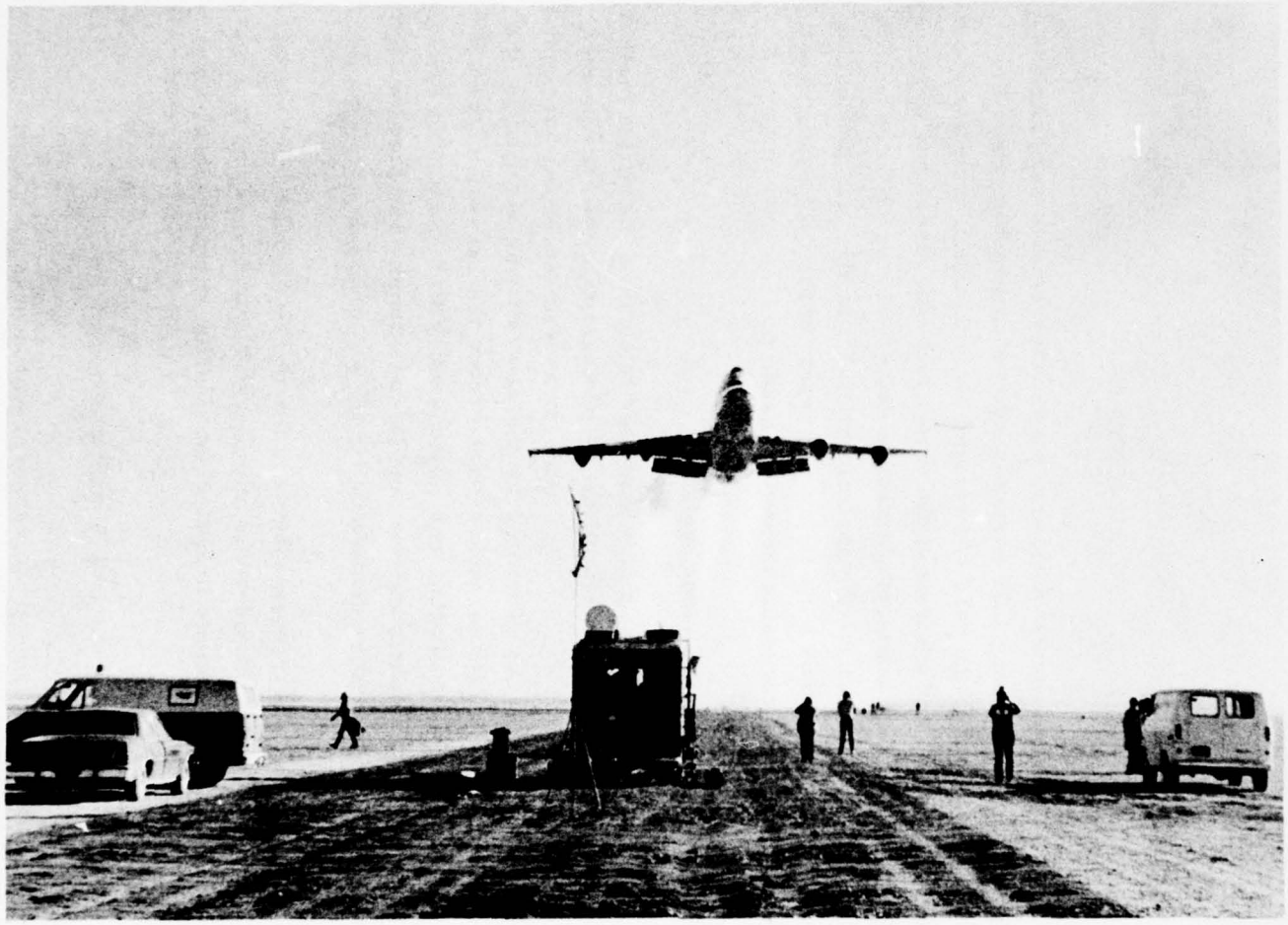

Fig. 1 - Lockheed LDV System Monitoring Wake Vortex Generated by a B-747 Aircraft at the Rosamond, California, Test Site

and γ is the angle subtended by the velocity vector and the optic system line of sight. From Eq. (1), it is noted that the Doppler shift is a direct and absolute measure of aerosol velocity component and a frequency shift of 188 kHz corresponds to a 1 m/sec magnitude line-of-sight velocity.

A sketch of the optical and electronic equipment for measuring the intensity and frequency spectrum of the coherent backscatter from the focal volume is shown in Fig. 2, and described in more detail in Refs. 1, 2, and 3. Photographs of the optical and electronic equipment for measuring the aerosol backscatter are shown in Figs. 3, 4, and 5.

The Lockheed LDV system used in the Rosamond wake vortex tests monitors the magnitude of the velocity component of ambient atmospheric particulate matter within its instantaneous sensing volume. The pertinent *operating* characteristics of the LDV are summarized as follows:

Performance

1. Threshold of Magnitude of Velocity Component: 0.5 m/sec
2. Range of Magnitude of Velocity Component: 0.5 to 28 m/sec

Sample Rate

1. Low Data Rate: 70 Hz
2. High Data Rate: 500 Hz (using the NASA filter bank processor).

Spatial Resolution

1. Range Accuracy: $\pm$0.4 m at 30 m, $\pm$44 m at 300 m
2. Elevation Angle Accuracy: $\pm$0.25 deg.

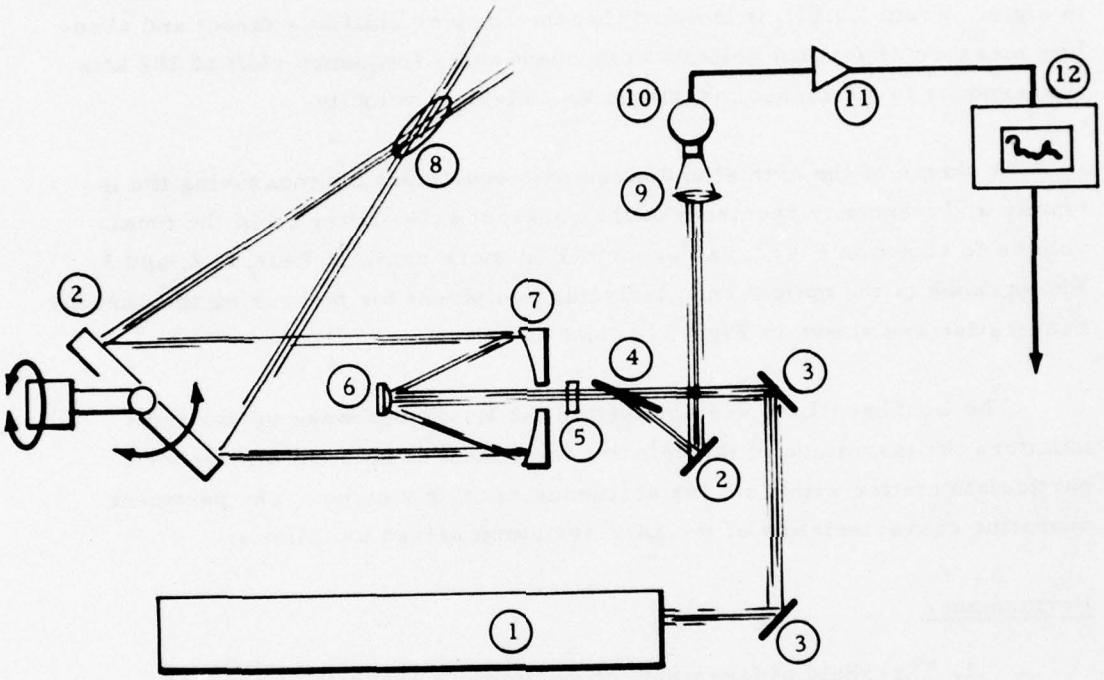

1. CO_2 Laser
2. Mirror
3. Mirror
4. Brewster Window
5. Quarter Wave Plate
6. Secondary Mirror
7. Primary Mirror
8. Focal Volume
9. Lens
10. Photodetector
11. Preamplifier
12. Spectrum Analyzer

Fig. 2 - Component Configuration of the Lockheed Laser Doppler Velocimeter

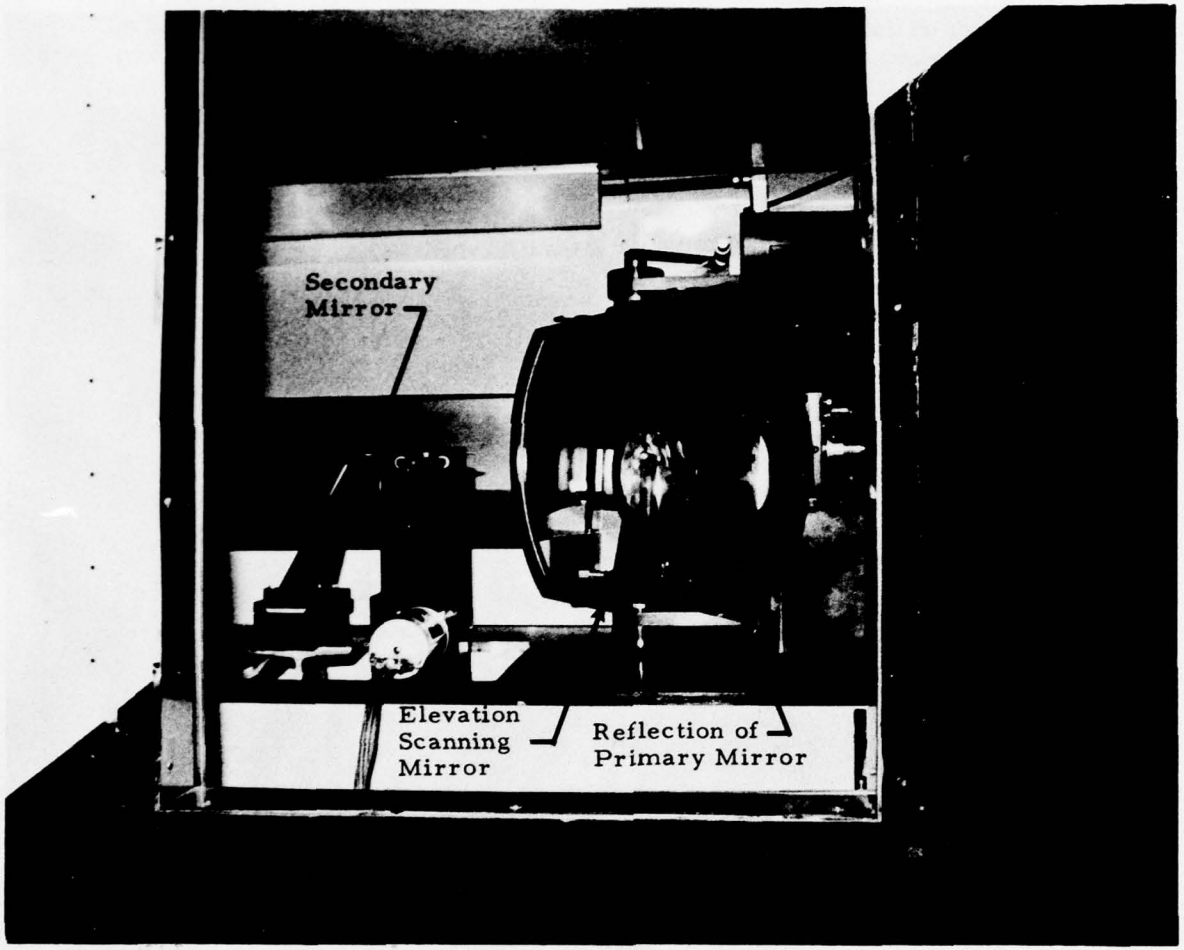

Fig. 3 - View Through Side Window of Laser Doppler Velocimeter Depicting Scanning Optics (Note reflection of telescope primary mirror in elevation scanning mirror)

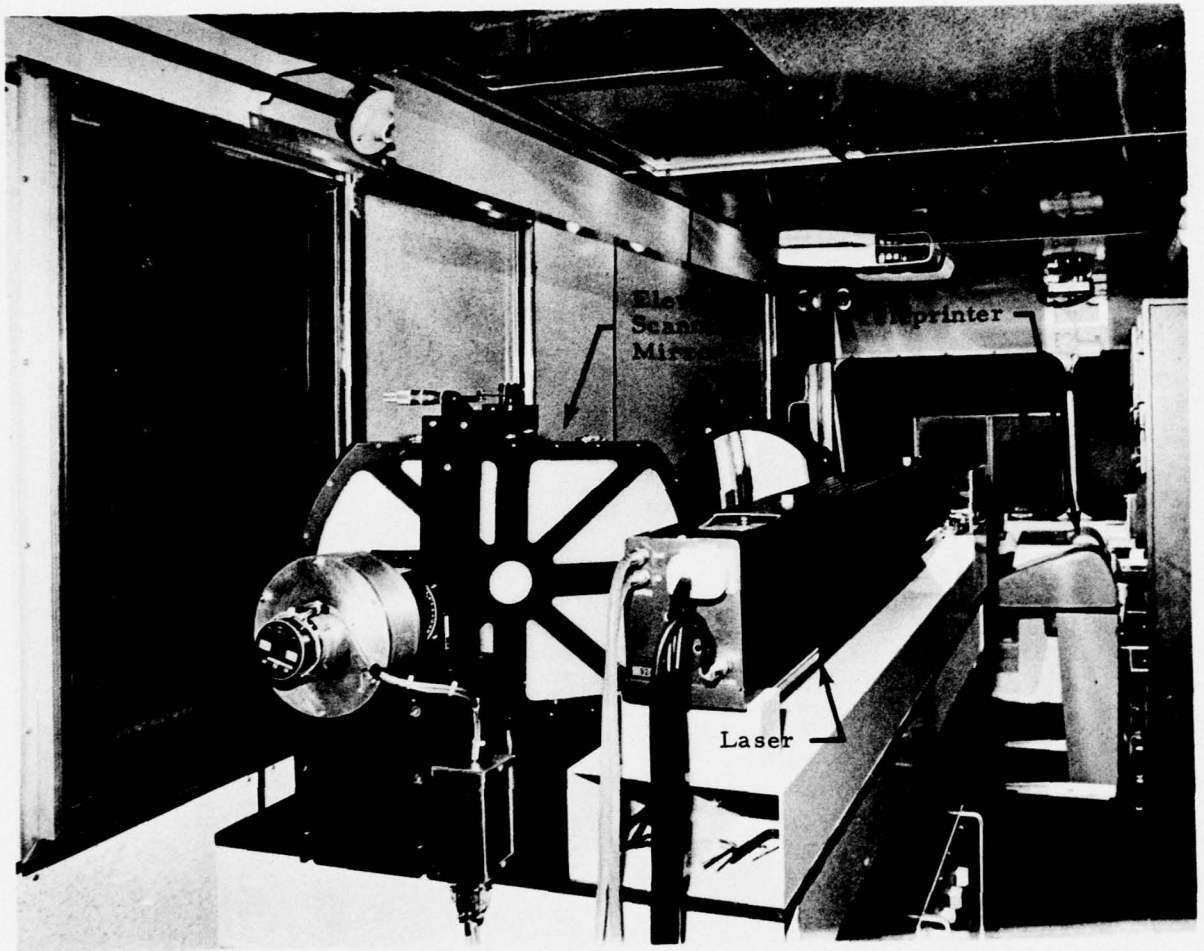

Fig. 4 - Interior View of Laser Doppler Velocimeter Van Looking Forward (Depicted in foreground is elevation scanning mirror on left and laser on right. Teleprinter in right rear.)

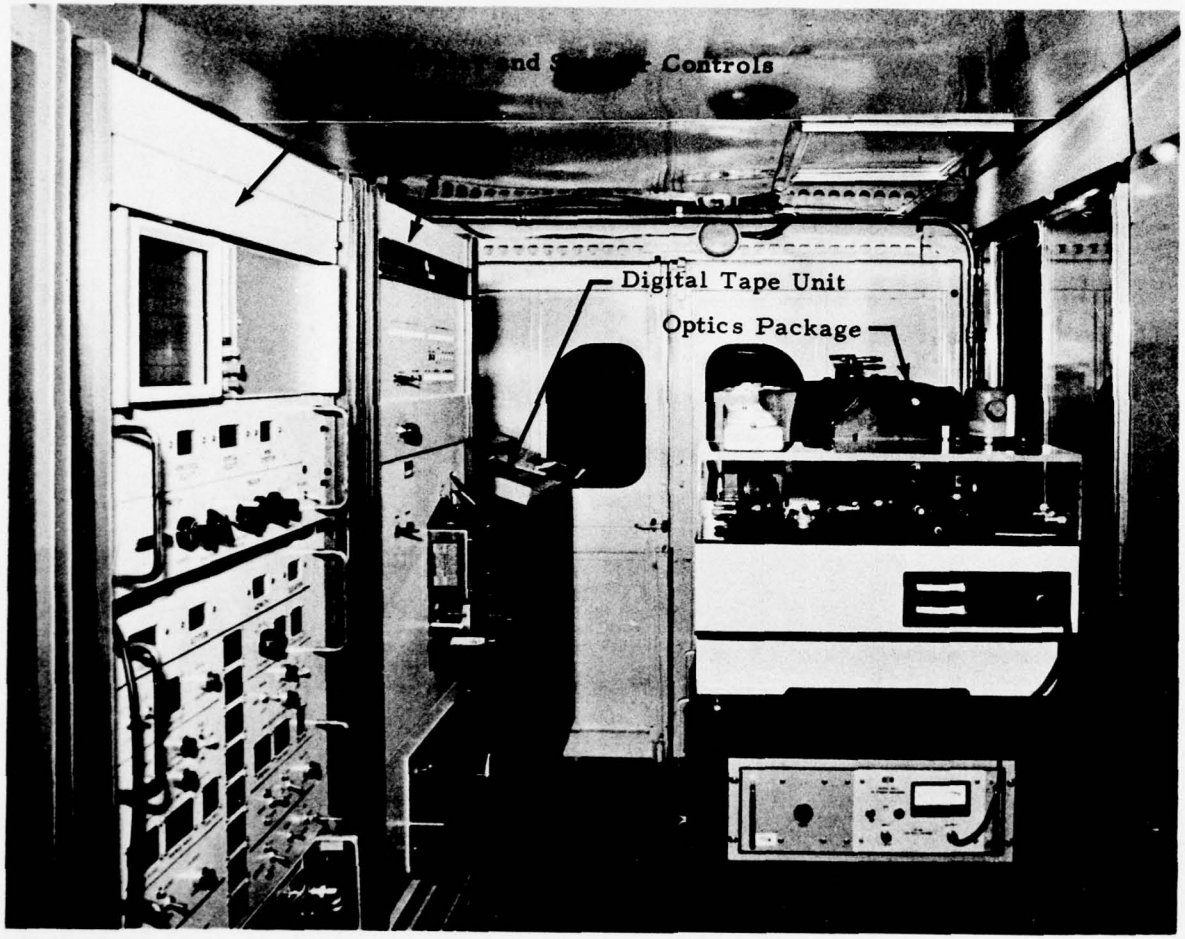

Fig. 5 - Interior View of Laser Doppler Velocimeter Van (Display and scanner controls in first rack, computer in second rack, digital tape unit aft, and optics package on right.)

Scan Modes

1. Range or Line Scan
2. Elevation
3. Altitude
4. Azimuth
5. Horizontal Wind
6. Vertical Wind
7. Wind Direction
8. Line-of-Sight Velocity Component

The characteristic output signal from the LDV system is an intensity versus frequency spectrum illustrated in Fig. 6. The output parameters V_{pk} and V_{ms} are indicative of the magnitude of the velocity component in the LDV focal volume corresponding to the fastest particle (or particles) above the amplitude threshold and the particle (or particles) having the highest backscatter, respectively. The bandwidth, N, is a measure of the range of particle velocities in the focal volume. Intensity and frequency thresholds are applied to the signal, as shown, to eliminate noise and to improve the resolution of the system. For example, in the vortex tracking mode the frequency threshold of the LDV is set relatively high to filter out the low-frequency signal associated with the ambient wind.

The velocity resolution of the LDV is determined by the signal-to-noise-ratio characteristics of the system as well as the atmospheric aerosol particle-size distribution. During the Rosamond tests, no difficulty was encountered detecting the high velocity regions, as high as 28 m/sec, associated with the wake vortex phenomena. The very low ambient winds, on the order of 1 to 2 m/sec, were also detected by the LDV at Rosamond which were above the system's threshold of 0.5 m/sec.

The spatial resolution of the LDV is determined by the size of the laser beam sensing volume where the beam is focused. The extent of the laser Doppler system sensing volume is a function of range which is shown in the following table ($\Delta r = 9.84 \times 10^{-4}\ (m^{-1})\ R^2$) obtained from calibration measurements (Ref. 4).

V_{pk} = Magnitude of velocity component of highest channel above amplitude threshold

V_{ms} = Magnitude of velocity component of the channel having the peak signal

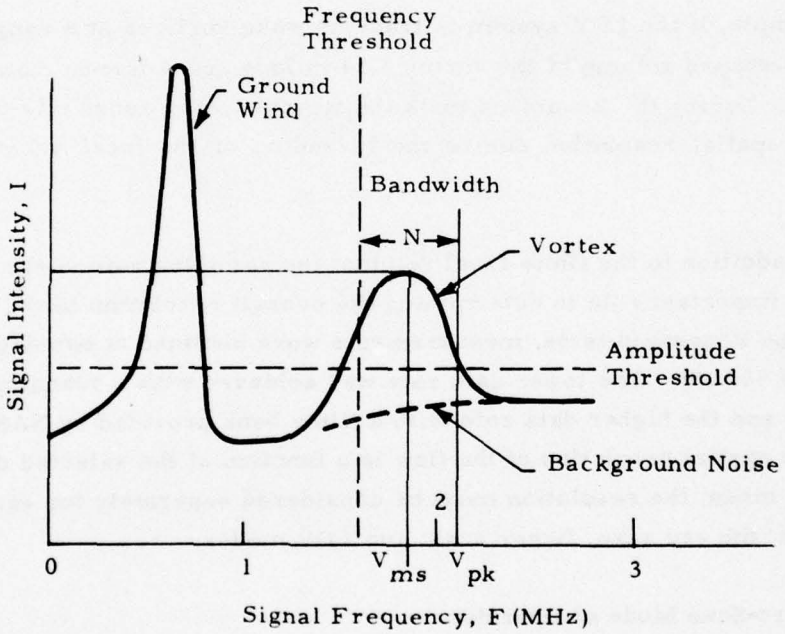

Fig. 6 - Definition of Laser Doppler Velocimeter Output Signature

Range to Focus, R(m)	Sensing Volume Length (Half Power Value) Δr (m)
76	5.68
100	9.84
152	22.73

For example, if the LDV system is tracking wake vortices at a range of 60 m, a needle-shaped volume of the vortex 3.54 m long and 4 mm in diameter is sampled. During the Rosamond tests, the typical vortex range was 60 m so that the spatial resolution due to the spreading of the focal volume was 3.54 m.

In addition to the finite focal volume, the sampling rate of the LDV plays an important role in determining the overall resolution of the system. During the Rosamond tests, measurements were obtained at two data rates, at 70 and 500 Hz. The lower data rate was achieved with a scanning spectrum analyzer and the higher data rate with a filter bank provided by NASA-MSFC. Since the spatial resolution of the flow is a function of the selected data rate and scan mode, the resolution must be considered separately for each type of operation; the arc scan, finger scan, and LDV modes.

2.1.1 Arc-Scan Mode of Operation

In the arc-scan mode, the LDV interrogates the vortex wake at a fixed range along an arc normal to the aircraft flight path. As shown in Fig. 7, the sensing volume is moved between two elevation limits (the typical cone angle is $2\alpha = 30$ deg) at a fixed rate (the typical scan rate is 0.5 Hz) while the vortex drifts past the scanned arc. Thus, the arc scan measurements indicate the spanwise downwash distribution in the wake of the aircraft, provided that vortex range is sufficiently close to the selected scan range.

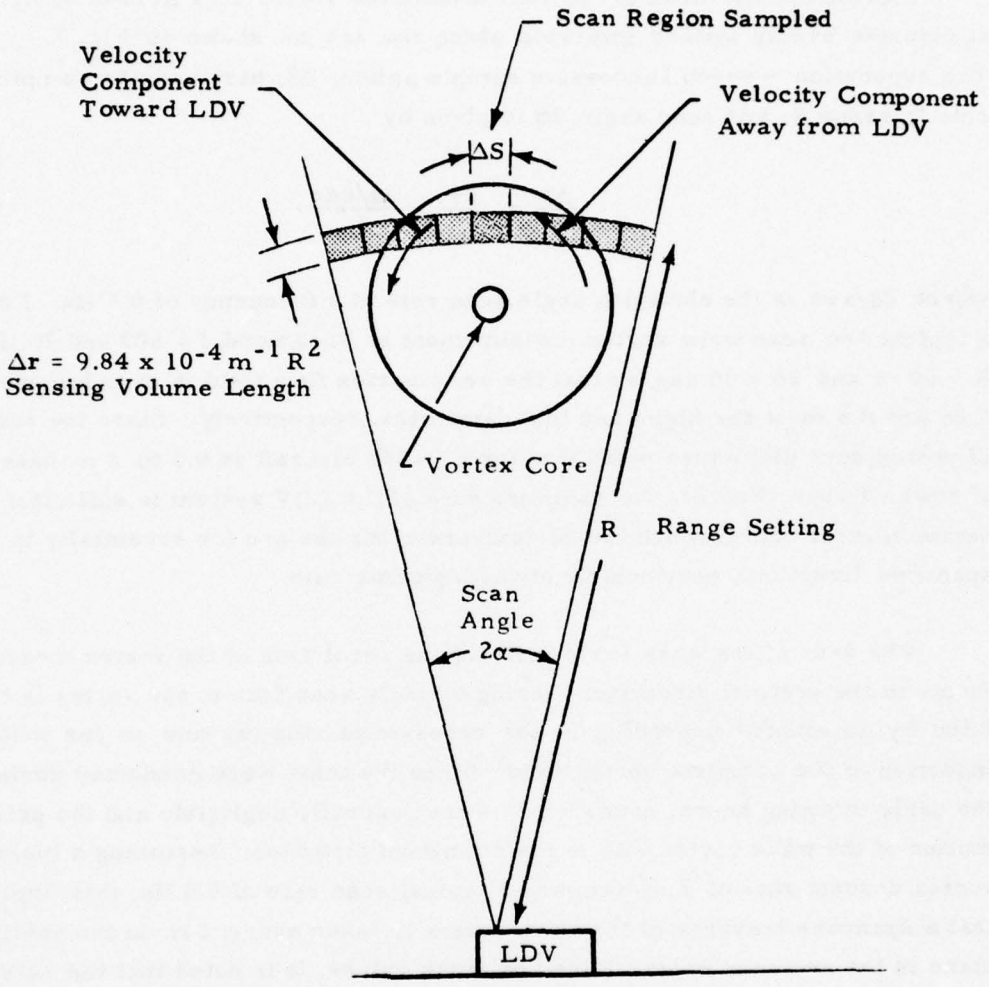

Fig. 7 - Geometry for Arc Scanning for Rosamond Wake Vortex Tests

During one arc scan of the vortex wake, the vortex flow field is sampled at discrete evenly spaced intervals along the arc as shown in Fig. 7. The separation between successive sample points, ΔS, based on the sampling rate f, range R, and cone angle 2α is given by

$$\frac{\Delta S}{R} = \frac{2\pi}{360^{\circ}} \frac{2\alpha/\text{sec}}{f}, \tag{2}$$

where 2α/sec is the elevation angle scan rate at a frequency of 0.5 Hz. For a typical arc scan wake vortex measurement at Rosamond, f = 500 and 70 Hz, R = 60 m and 2α = 30 deg, so that the wake vortex flow field is sampled every 0.06 and 0.4 m at the high- and low-data rates, respectively. Since the range of vortex core diameters measured for a B-747 aircraft is 0.3 to 2 m based of tower flybys (Ref. 5), the sampling rate of the LDV system is sufficient to obtain several cuts through the vortex core along the arc (or essentially in the spanwise direction), particularly at the high data rate.

The drift of the wake vortex affects the resolution of the vortex measurements in the vertical direction. During a single scan frame, the vortex is translated by an amount depending on the cross-wind velocity and on the mutual induction of the complete vortex field. Since the tests were conducted during the early morning hours, cross winds were generally negligible and the primary motion of the wake vortex was in the downward direction. Assuming a typical vortex descent rate of 2 m/sec, and a typical scan rate of 0.5 Hz, this implies that a spanwise traverse of the wake vortex is taken every 2 m in the vertical plane in the arc-scan mode. Based on these values, it is noted that the LDV arc-scan technique can observe the detailed characteristics of the wake vortex phenomena which are larger in extent than 0.06 and 2 m in the horizontal and vertical directions, respectively.

2.1.2 Finger-Scan Mode of Operation

During the Rosamond flight tests, 56% of the LDV wake vortex measurements were conducted using the finger-scan mode. In the finger-scan mode, both the range and elevation of the laser beam were varied simultaneously and

linearly with time, producing a multiple lobe scan pattern with the laser beam as shown in Fig. 8. The settings and sampling rates for the finger-scan mode are given in Appendix A.

The distance between sample points for the finger-scan mode is higher than for the previous arc-scan mode. From Appendix A, it is noted that the typical range scan excursion for the finger scan mode is 105 m, and the normal range rate is 3.5 Hz. It follows that the beam-scan velocity is 735 m/sec. Because the LDV measurements were sampled every 2 and 14.3 msec at the low and high data rates, the wake vortex flow field is measured at every 1.5 and 10.5 m increment in range, respectively. Thus, the finger scan mode can interrogate a large cross-sectional area rapidly, and this is ideal for vortex tracking. In addition, the LDV finger scan measurements contain essential information regarding the wake vortex phenomena.

The characteristic line-of-sight component as a function of range and elevation angle during one finger-scan sweep is shown in Fig. 8. A pair of double-peak patterns is noted in the line-of-sight velocity profile as a function of elevation angle. The maximum values occur at the elevation angles where the line of sight is tangent to the viscous core radius of the vortex. Thus, the mean elevation angle of the local maxima in the V_{pk} vs θ curve yields the elevation angle of the wake vortex, $\theta_{vortex} = (\theta_1 + \theta_2)/2$. Similarly, the difference between the two elevation angles is a measure of the vortex viscous core radius, $r_{vortex\ 1} = R_1 \left| \tan \frac{\theta_1 - \theta_2}{2} \right|$. The peak tangential velocity and core cirdulation of the vortex is given by $V_{pk\ vortex\ 1} = (V_{pk\ \theta_1} + V_{pk\ \theta_2})/2$ and $\Gamma_{vortex\ 1} = 2\pi R_{vortex\ 1} V_{pk\ vortex\ 1}$, assuming circular symmetry. The peak line-of-sight component at the two edges of the vortex, $V_{pk\ \theta_1}$ and $V_{pk\ \theta_2}$ are not necessarily equal due to a contribution by the other vortex and the ambient winds. The range of the vortex, R_1, is given by the local maximum in the line-of-sight component at the two edges of the in the bottom of Fig. 8, and is not affected by the ambient winds. Based on the characteristic LDV signature observed for one scan, it is noted

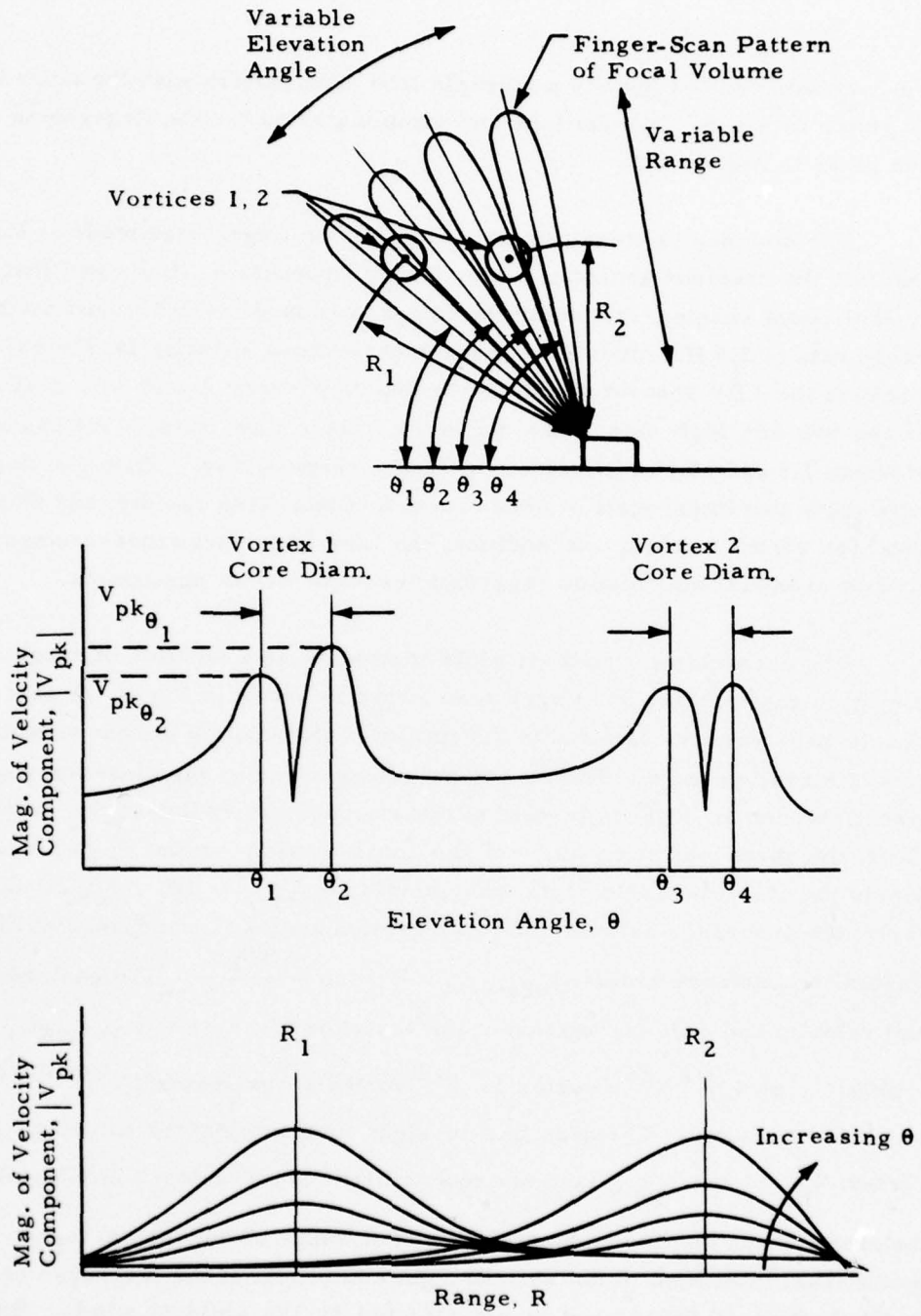

Fig. 8 - Magnitude of Characteristic LDV Velocity Component Observed During One Finger-Scan Sweep

that several successive finger scans contain the essential decay history of the wake vortices, provided that at least two sample points are obtained for each vortex, one upwash and one downwash measurement, where the line of sight is tangent to the viscous core and the mean vortex range is within the LDV focal volume.

2.2 DATA PROCESSING

The output from the LDV system consisting of the coherent backscatter intensity versus frequency from the focal volume as well as the location of the focal volume in space was processed to yield the aircraft downwash field and the wake vortex characteristics. Reduction and analysis of the LDV measurements were carried out as follows: (1) the low-speed signal was digitized and stored on magnetic tape by the onboard SEL computer and subsequently processed off-line on a Univac 1108 computer, and (2) the high-speed data were both digitized and processed off-line on a Univac 1108 computer and the vortex tracks computed on a PDP 11 computer. A flow chart of the data processing sequence used for the Rosamond wake decay study is shown in Fig. 9. The software system for processing the low-speed and high-speed LDV data is described in more detail in Refs. 4 and 6, respectively.

The high-speed processor utilized the raw range and elevation signal, while the low-speed processor used the raw range and commanded elevation signal to determine the location of the LDV focal volume. As a result, the magnitude of the velocity component versus elevation angle measured with the high-speed processor showed scatter due to the $\pm$0.25 deg elevation angle resolution. In addition, noise was present in the elevation angle versus time distribution from the high-speed data characterized by a square wave with a frequency of 14 Hz and an amplitude of 0.7 deg. This was believed to be a sympton of a processing or decode problem. The normal scatter in the elevation angle was not noticeable at the low data rate, but the low-speed data did show a finite lag in the scan pattern. A time lag of approximately 0.3 sec, and a corresponding lag in the position of the LDV focal volume depending on the selected scan rate was observed. The lag in the system resulted from the difference between commanded versus actual angular position of the scanning mirror.

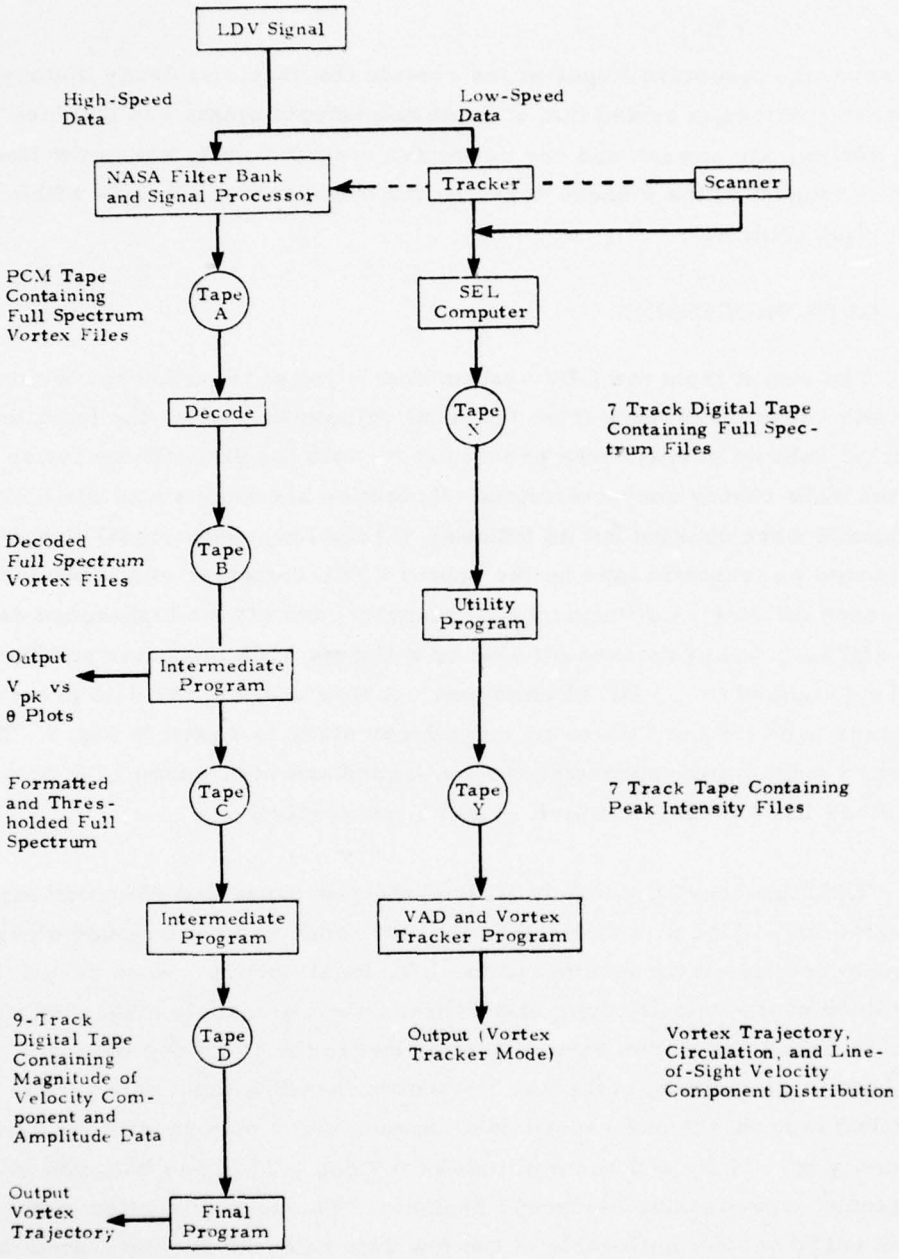

Fig. 9 - Data Processing Sequence Carried Out for the Rosamond Wake Decay Measurements

The manner in which the wake vortex measurements were processed from both the high-speed and low-speed data is summarized as follows. The frequencies and amplitudes associated with the laser Doppler signal were sampled at fixed intervals. The spectrum was recorded if it was above the frequency and amplitude threshold settings (Fig. 6). The amplitude and frequency threshold settings for the Rosamond tests are given in the log sheets in Appendix A. From the array of recorded frequency and intensity points, the magnitude of the line-of-sight velocity component was computed, and the vortex parameters including location and velocity distribution were determined.

To compute the wake vortex transport and decay characteristics from the low-speed line-of-sight velocity component magnitude, the Rosamond measurements were analyzed using the "Velocity Azimuth Display and Vortex Track Program" (Ref. 5). Based on previous experience with the program, the following parameters were selected for the analysis of the Rosamond data:

INTVEL = 2	Flag INTVEL = 1, Velocity oriented vortex determination INTVEL = 2, Intensity oriented vortex determination
NPSUF = 4	Sufficient number of points to determine vortex position
APERCT = 0.1	Fraction of points below the maximum velocity or intensity points
BPERCT = 0.1	Fraction of points within the correlation circle where Q is at least APERCT fraction of the maximum Q (Q is velocity or intensity as determined by INTVEL)
RPERCT = 0.3	Fraction of number of points in correlation circle used for determining vortex 1 (required for determination of vortex 2)
RPERCT = 0.3	Fraction of aircraft wing span used for correlation radius
EPERCT = 2.0	Fraction of correlation radius from vortex 1 for excluding initial point of vortex 2
NOISEF = 0	Noise floor
ADJI = 0.0	Intensity adjustment (fraction of noise floor added to total intensity).

A sample output from the VAD and Vortex Track Program is presented in Appendix B. The intermediate sorting parameters used in determining the location of the vortex core region are also given in the printouts along with "scatter plots" indicating the line-of-sight velocity magnitudes. From the typical line-of-sight velocity magnitude illustrated in Appendix B, the time history of the vortex wake was determined for many of the flybys.

In parallel with the low-speed data acquisition and processing, the LDV signal was also fed into the high-speed NASA-MSFC data processing system as illustrated in Fig. 9. The high-speed data processing technique is similar to the low-speed technique described earlier, and is described in detail in Ref. 6. A sample output from the NASA-MSFC LDV data processing routines is shown in Appendix C, including the listing of the magnitude of the raw line-of-sight velocity component, the plot of $|V_{pk}|$ versus elevation angle, and plots of the vortex trajectory.

3. DESCRIPTION OF EXPERIMENTAL TESTS

A two-day test sequence was carried out to determine the wake vortex characteristics of a B-747 aircraft as a function of spoiler, flap, and landing gear settings, altitude above ground, and glideslope. The test consisted of 54 low level passes during the early morning hours over the LDV system deployed at Rosamond Dry Lake near Edwards AFB, California, on 2 and 3 December 1975.

3.1 FLIGHT TEST PROGRAM

The aircraft used for the tests was a Boeing 747-123 aircraft. A plan view of the aircraft showing the details of the flap and spoiler configurations is presented in Fig. 10.

Aircraft configuration varied from run to run, with dominant emphasis on as close to a normal landing configuration as operating conditions would allow. The clean configuration was also studied, and special flap and spoiler configurations were investigated for vortex alleviation effectiveness. The Boeing 747 flew at 30 to 250 m above the ground level of 700 m MSL. Runs were made in level flight as well as in descending and climbing flight. Descents were at about 250 m/min. A lift coefficient of approximately 1.4 was used for all flaps-down runs.

Of the 54 runs, 35 (or about 65%) were made with the inboard flaps lowered 30 deg and the outboard flaps lowered 30 deg (denoted 30/30); eight (approximately 15%) with 10/10 flaps; and five (approximately 9%) with flaps retracted. The remaining six runs had the inboard flaps lowered 30 deg and the outboard flaps lowered 1 deg, to test the effects of this configuration

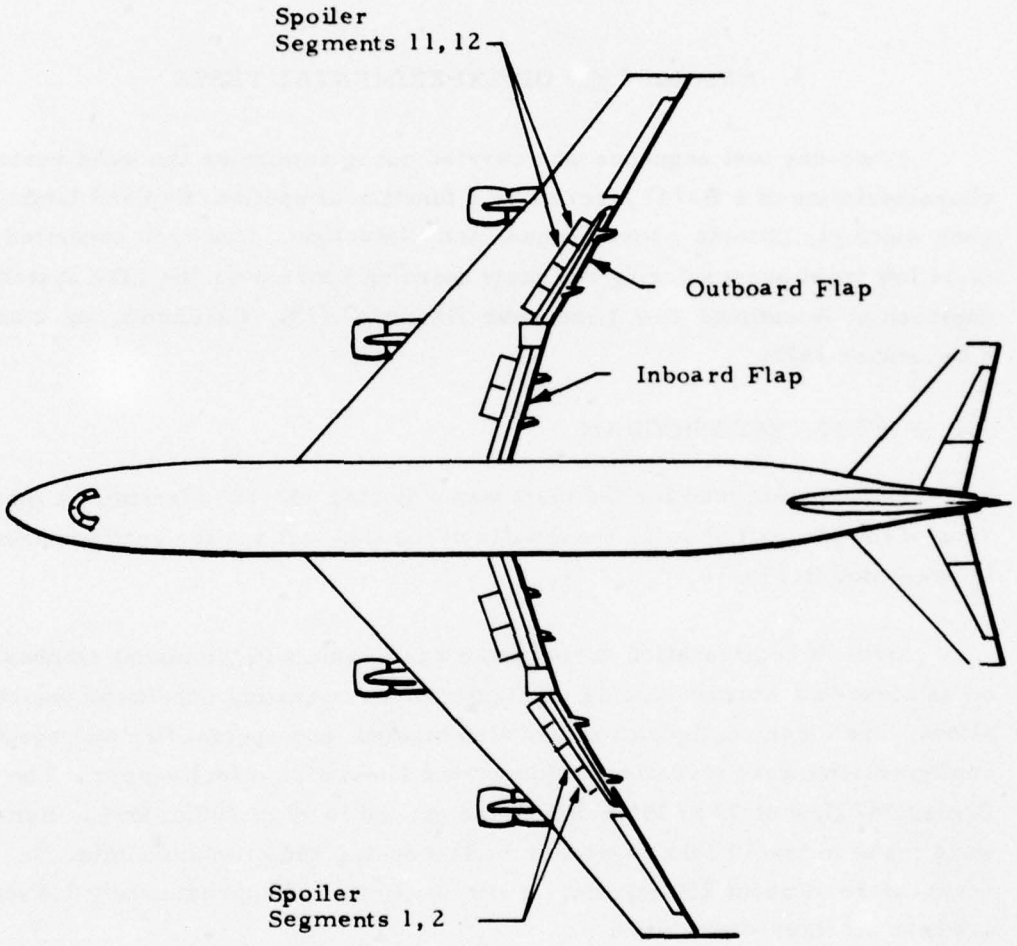

Fig. 10 - Spoiler and Flap Arrangement on B-747 Aircraft

on vortex alleviation. For each flap setting, runs were conducted with the gear down or retracted, and some had spoilers deployed (the extension angle was always 41 deg) in addition to the flap. A summary of the aircraft altitude, speed, weight, and flap, landing gear, and spoiler settings for each of the flybys is given in Table 1.

3.2 OPERATION OF LASER DOPPLER VELOCIMETER REMOTE SENSOR

The LDV system was set up and calibrated at the Rosamond test site prior to conducting the actual wake surveys. A discussion of the calibration procedure and the conduct of the wake vortex surveys is summarized below.

3.2.1 Calibration

During the set-up process, the optical bench was leveled with the external van jacks using a bubble level for reference (estimated accuracy of $\pm$0.5 deg). For the second day of the tests, the scanner was offset 45 deg using a tri-square for reference (estimated accuracy of $\pm$0.5 deg). Prior to the actual wake surveys, the elevation and azimuth angle readouts from the LDV were calibrated. The calibration involved pointing the optical system at the sun and comparing the observed elevation and azimuth angle readouts with those given in the ephemeris. The results indicated that a -3 deg and $\pm$139 deg correction should be applied to the raw elevation and azimuth readouts from the LDV, respectively.

During the Rosamond tests, the range resolution and signal-to-noise ratio characteristics of the LDV were not recalibrated. The range and signal-to-noise ratio calibrations taken a few months earlier and documented in Ref. 4 were assumed to be representative of the systems overall performance.

3.2.2 Wake Surveys

During the Rosamond wake decay tests, 53 aircraft flybys were recorded with the LDV system (flyby 36 was lost due to a loss in electrical power). The test conditions and the LDV scan, range, and elevation settings for the

Table 1

SUMMARY OF B-747 FLIGHT PARAMETERS

Flyby No	Altitude (m AGL)	IAS (knots)	Weight (kg/1000)	Flap (deg)	Spoilers Deployed	Thrust (EPR)	Gear
1	56	146	255	30/30	0	1.25	Down
2	62	146	252	30/30	0	1.21	Down
3	68	145	250	30/30	0	1.25	Down
4	65	145	249	30/30	0	1.22	Down
5	122	144	248	30/30	0	1.22	Down
6	122	144	247	30/30	0	1.23	Down
7	244	143	245	30/30	0	1.23	Down
8	244	143	244	30/30	0	1.20	Down
9	61	143	236	30/30	1, 2, 11, 12	1.26	Down
10	122	143	235	30/30	1, 2, 11, 12	1.26	Down
11	183	142	234	30/30	1, 2, 11, 12	1.25	Down
12	244	142	232	30/30	1, 2, 11, 12	1.25	Down
13	64	142	230	30/30	1, 2, 11, 12	1.24	Down
14	65	138	228	30/30	1, 2, 11, 12	1.20	Down
15	61	138	227	30/30	1, 2, 11, 12	1.20	Down
16	61	138	226	30/30	1, 2, 11, 12	1.18	Down
17	30	141	222	30/1	0	1.19	Down
18	37	141	218	30/1	0	1.18	Down
19	38	141	216	30/1	0	1.18	Up
20	67	139	215	30/1	0	1.18	Down
21	64	139	213	30/1	0	1.16	Up
22	91	139	212	30/1	0	1.23	Down
23	122	148	260	30/30	0	1.24	Down
24	122	220	259	0/0	0	1.03	Up
25	122	147	258	30/30	0	1.24	Down
26	122	215	256	0/0	0	1.06	Up
27	67 (LDG)	146	255	30/30	0	1.20	Down
28	66	146	254	30/30	0	1.20	Down
29	72 (LDG)	146	252	30/30	0	1.14	Down
30	66	145	251	30/30	0	1.24	Down
31	107 (TO)	156	243	10/10	0	1.38	Up
32	65	156	242	10/10	0	1.11	Up
33	57 (TO)	156	241	10/10	0	1.36	Up
34	59	143	240	10/10	0	1.15	Up
35	63	142	239	30/30	0	1.20	Down
36	68	142	238	30/30	0	1.20	Up
37	67	141	237	30/30	0	1.21	Down
38	61	141	236	30/30	0	1.22	Up
39	47 (TO)	151	230	10/10	1, 2, 11, 12	1.36	Up
40	46 (TO)	151	228	10/10	0	1.36	Up
41	48 (TO)	150	227	10/10	1, 2, 11, 12	1.36	Up
42	54 (TO)	150	226	10/10	0	1.40	Up
43	61	138	225	30/30	0	1.24	Down
44	63 (LDG)	138	224	30/30	0	1.12	Down
45	50 (LDG)	138	223	30/30	0	1.16	Down
46	37	137	222	30/30	0	1.24	Down
47	91	135	215	30/30	0	1.15	Down
48	91	135	214	30/30	1, 2, 11, 12	1.20	Down
49	37	134	213	30/30	1, 2, 11, 12	1.20	Down
50	91 (LDG)	134	210	30/30	0	1.11	Down
51	122	200	209	0/0	0	1.11	Down
52	122	200	208	0/0	0	1.03	Up
53	122	133	207	30/30	0	1.22	Down
54	122	200	206	30/30	0	1.05	Up

LDG: Aircraft descending along imaginary glideslope.

TO: Aircraft ascending as in actual takeoff.

Rosamond tests are summarized in the log sheets given in Appendix A, while a list of the flight parameters is given in Table 1. Primarily, those flybys have been processed from the wake measurements where flow visualization and photographic data (photographs were taken of vortices at 1 sec increments) were available for comparison with the LDV measurements.

To maximize the amount of data collected regarding wake vortex trajectories, velocity profiles, and decay rates, the LDV was operated in different scan modes including: arc-scan and, finger-scan configurations. The wake vortex surveys were conducted in the following manner.

On the first test day, the LDV was located directly under the flight path (Fig. 11) and scanned arcs in a plane perpendicular to the flight path (Fig. 12) with a complete scan every 2 sec. Scans were at a fixed range until the vortex passed through the scan arc, at which time the sensor range was lowered and remained fixed again until the vortex descended through the new range. The objective of the overhead arc scan measurements was the measurement of the initial downwash field and the wake vortex roll-up process.

On the second test day, the LDV was moved 60 m north of the flight path (Fig. 11) and scanned simultaneously in elevation and range (finger-scan mode) at a frequency of 0.2 Hz, and 2 to 2.5 Hz, respectively. The objective of the finger scan measurements was to track the location of the vortex pair and to observe the vortex decay rates. The coordinated variations in range and elevation settings for the finger scan mode were selected on the basis of the aircraft wake vortex parameters. In addition, during the last sorties, the azimuth angle was changed during the run to 90- and 180-deg angles to scan both down the vortex (axially) and to follow the vortex drift away from the LDV.

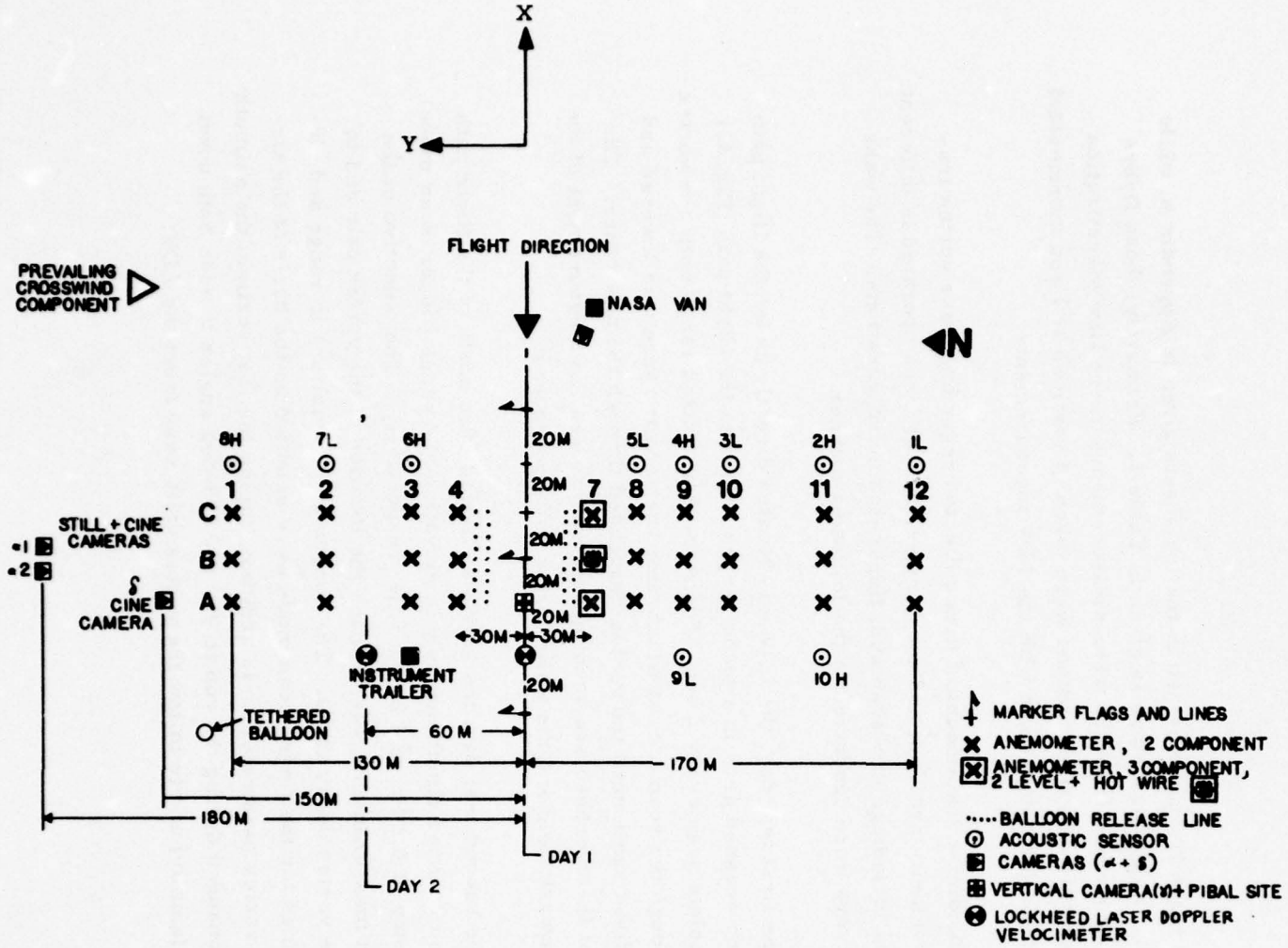

Fig. 11 - Location of Lockheed LDV During the Rosamond Wake Vortex Measurements

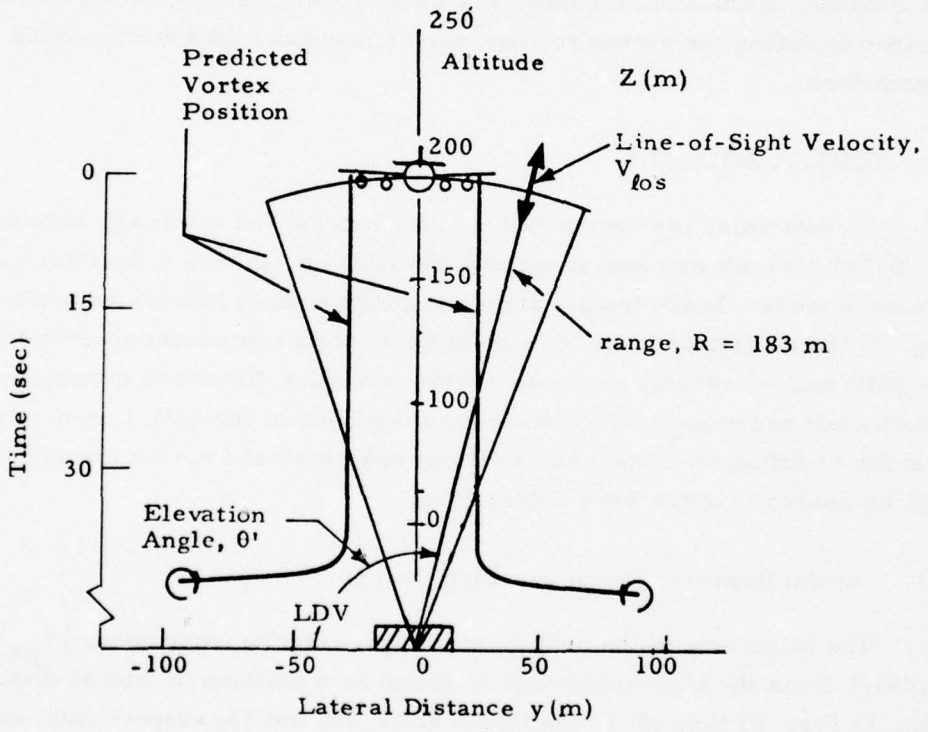

Fig. 12 - Overhead Arc Scan Configuration Illustrated for Rosamond Flyby 11

4. RESULTS OF WAKE VORTEX MEASUREMENTS

The LDV measurements obtained during the Rosamond tests have been analyzed to determine the dominant characteristics of the B-747 wake. In the following discussion, the observed wake vortex characteristics are described including the vortex roll-up, vortex transport, and vortex decay parameters.

4.1 VORTEX ROLL-UP

To determine the vortex roll-up parameters, the downwash field behind the B-747 aircraft was measured with the LDV operated in a constant-range arc-scan mode. In the typical arc-scan configuration, illustrated earlier in Fig. 13, the magnitude of the line-of-sight velocity component observed by the LDV was essentially a measure of the spanwise downwash distribution in the aircraft nearwake. Thus, from the magnitude of the LDV line-of-sight velocity distribution in the near wake the downwash and vortex formation and roll-up characteristics were determined.

4.1.1 Initial Spanwise Downwash Distribution

The magnitude of the peak line-of-sight velocity component, $|V_{pk}|$ (m/sec), from the high-speed data is shown as a function of lateral distance, y(m), in Figs. 13 through 16 for flybys 8, 11, 12, and 13, respectively, over the time interval t = 0 to 8 sec. Each scan is defined as the period between two successive elevation angle reversals and is approximately 1 sec in duration. Occasionally, some overlapping occurs between successive scans due to limitations in the processing software. Therefore, successive scans shown in Figs. 13 tthrough 16 do not always have the same starting and ending limits, and, as a result, the lateral scales can be different. The direction and mid-time of each scan is indicated in the figures. The lateral distance, y, was computed directly from the raw range, R, and raw elevation angle

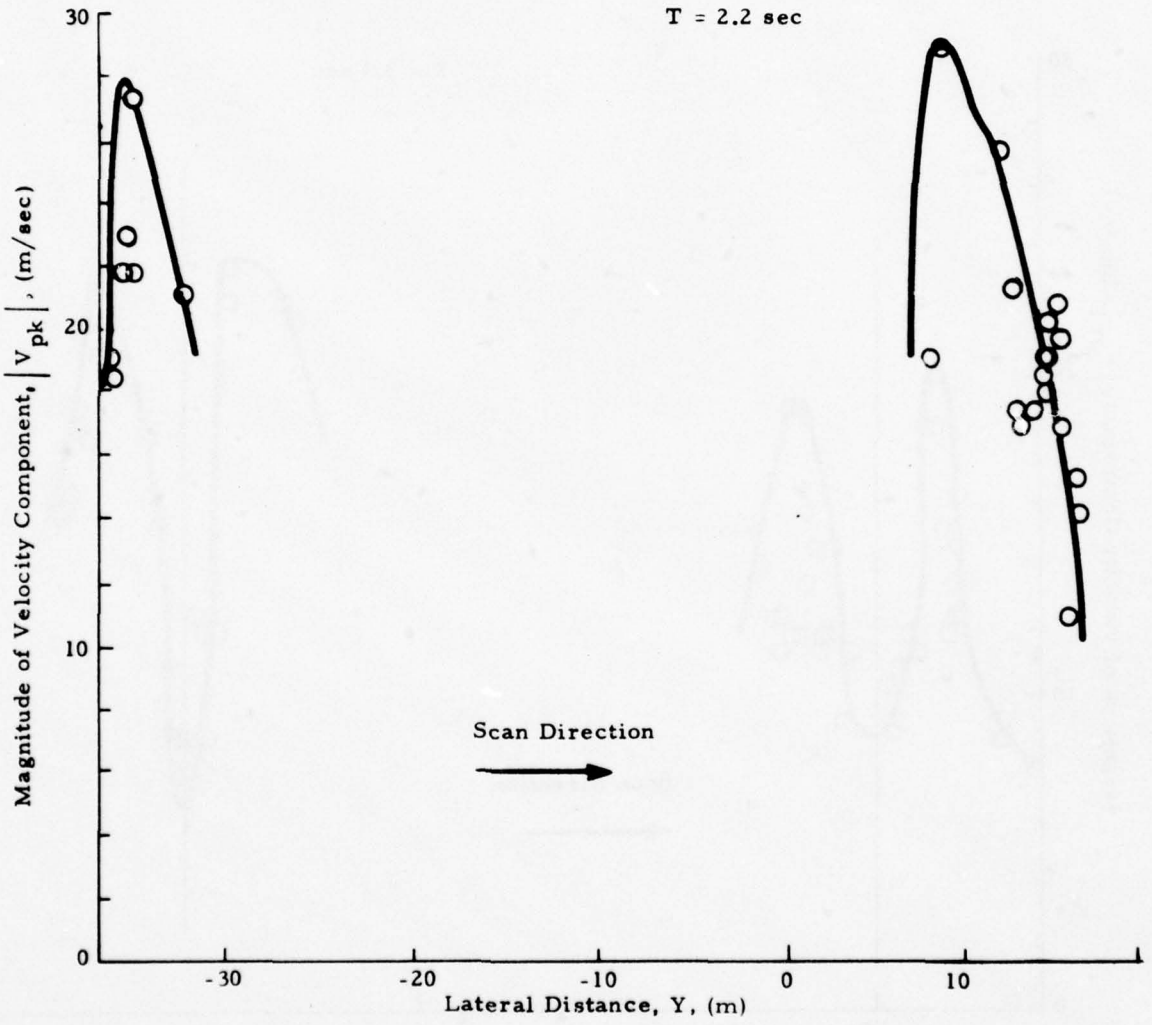

Fig. 13 - $|V_{pk}|$ as a Function of Lateral Distance for Rosamond B-747 Flyby 8

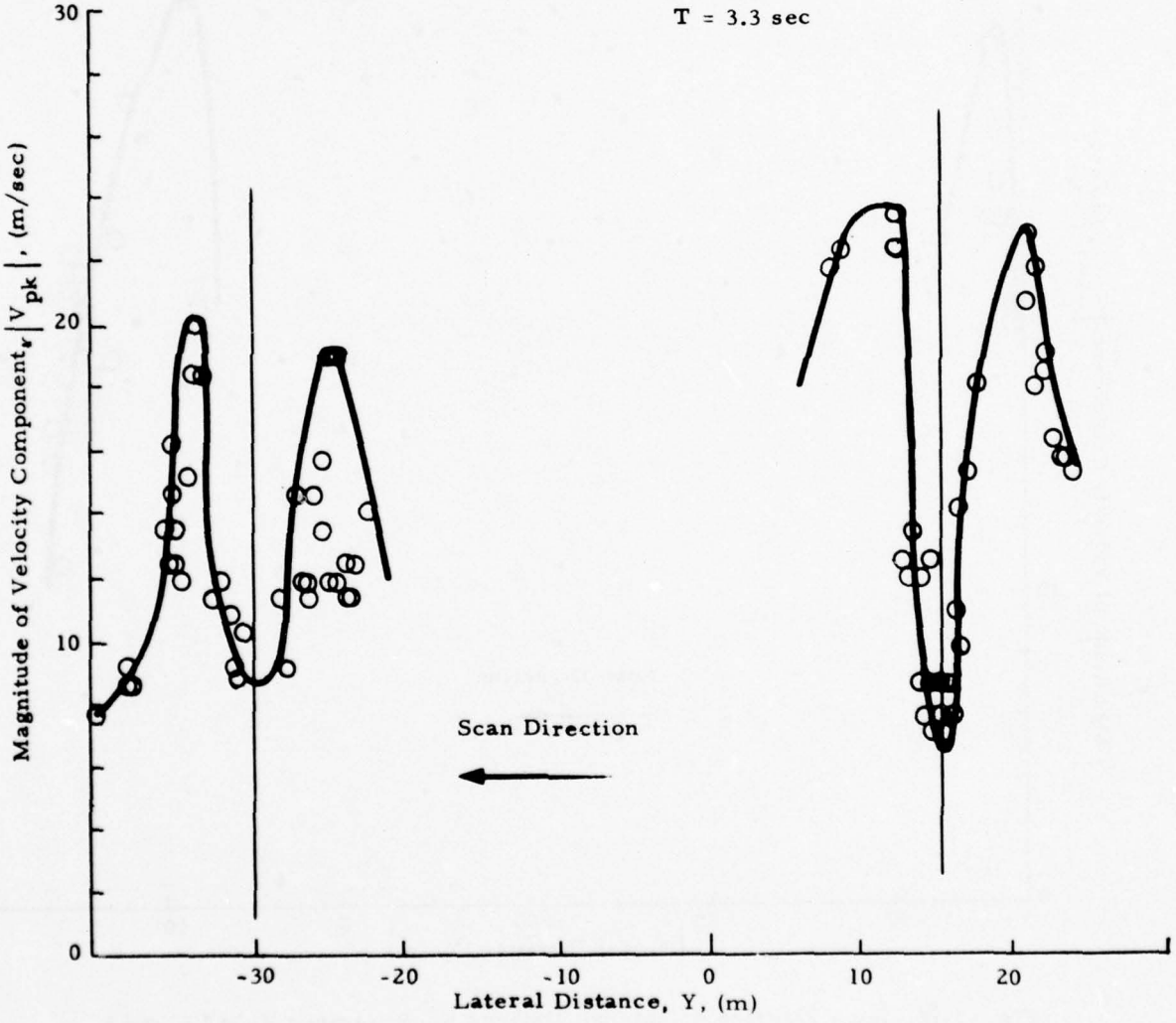

Fig.13 (Continued)

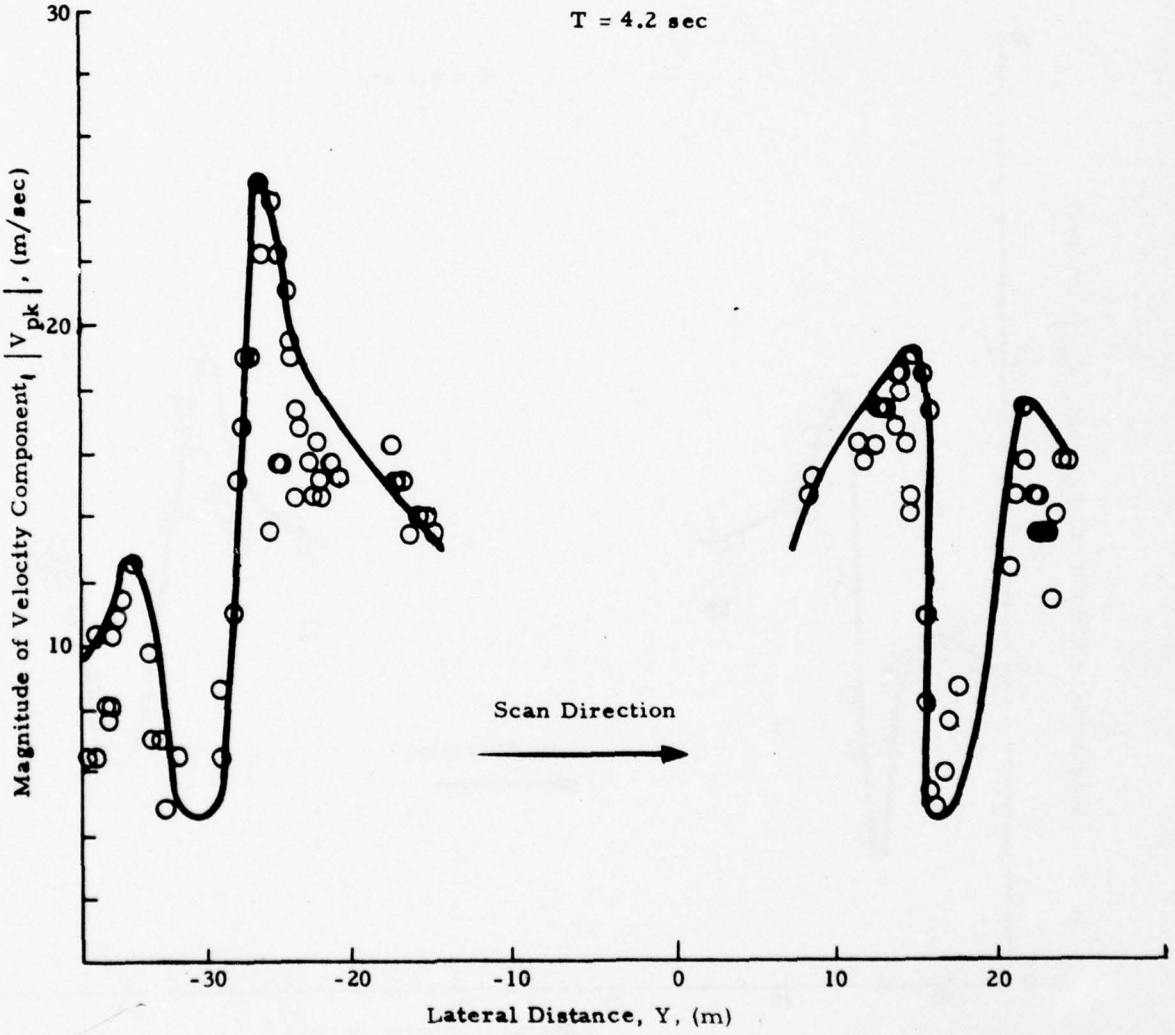

Fig. 13 (Continued)

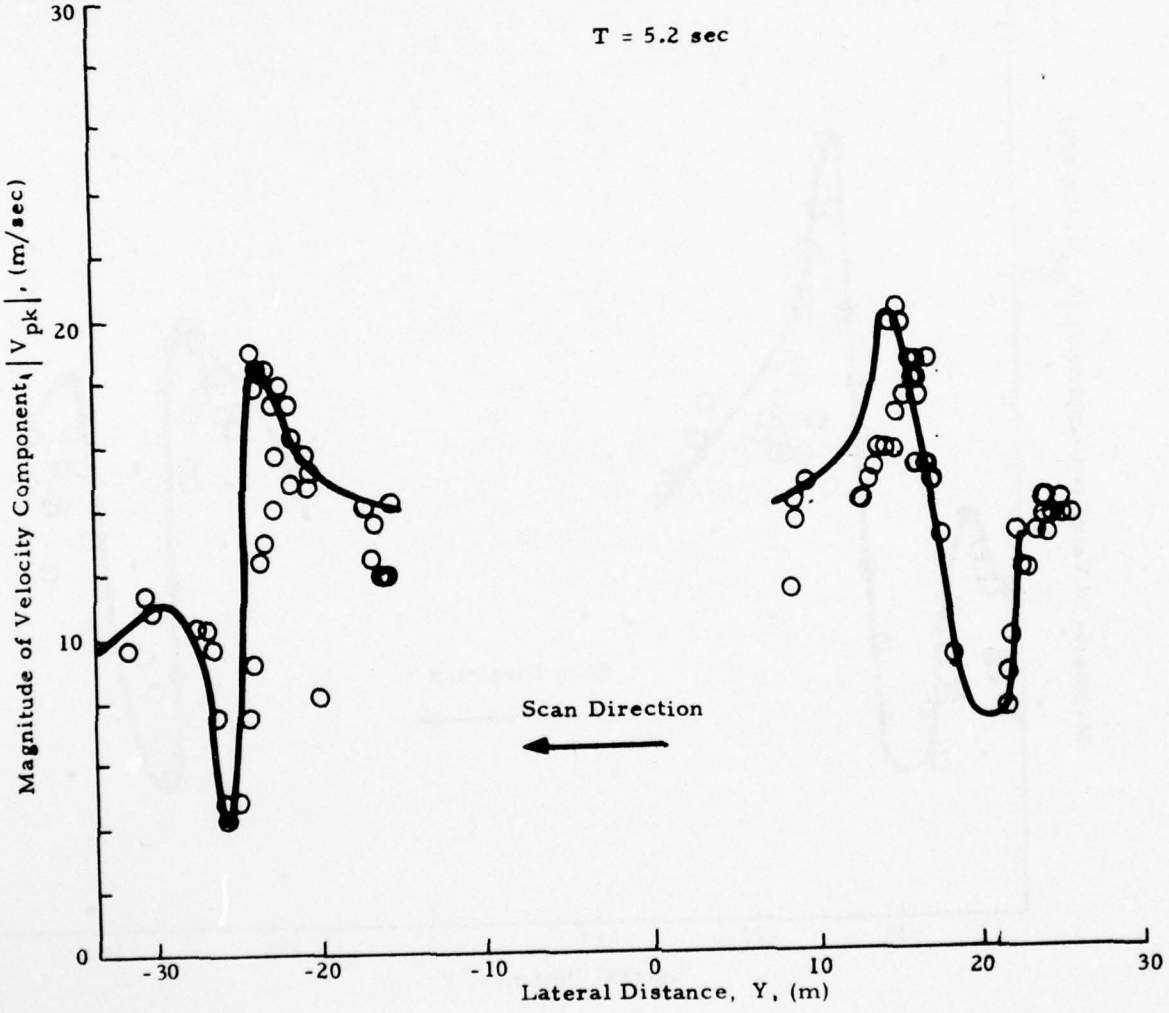

Fig. 13 (Continued)

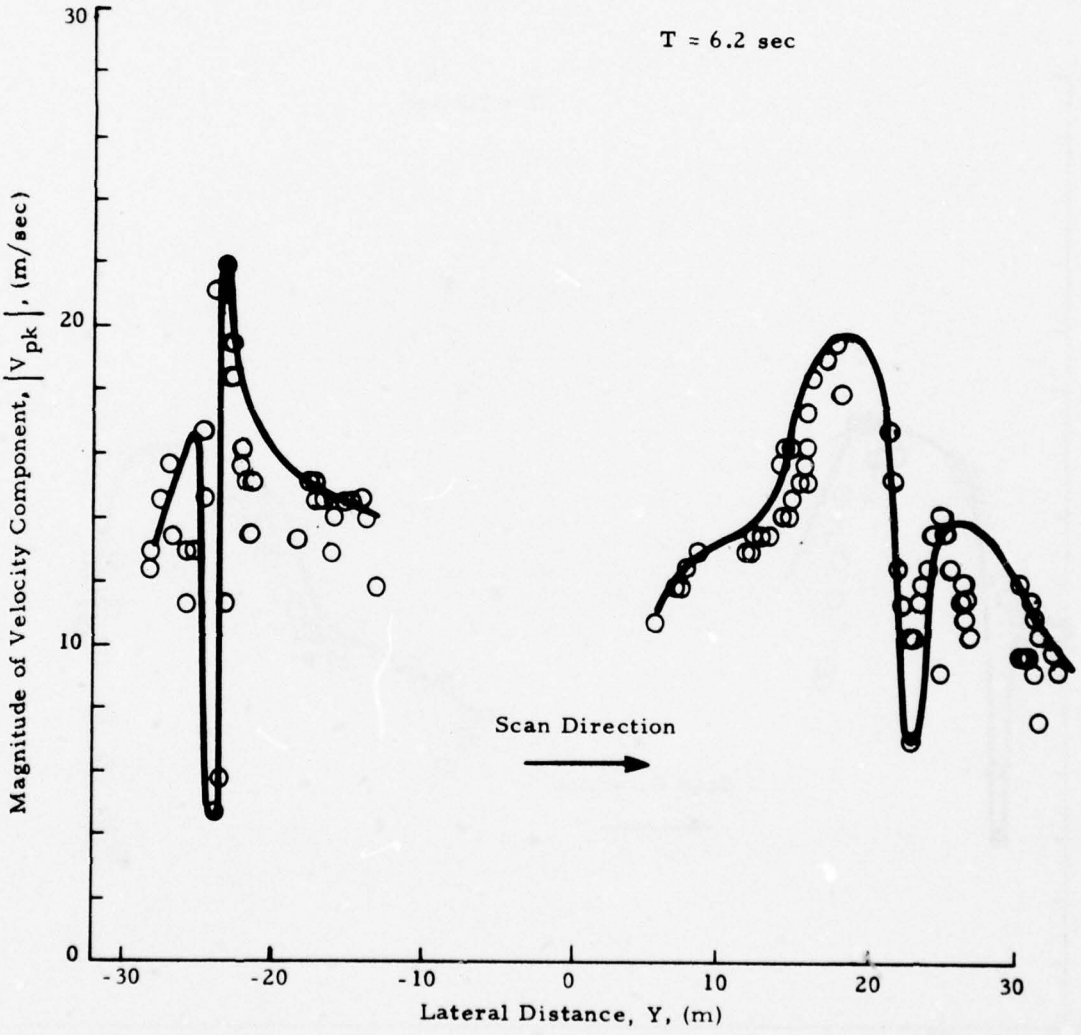

Fig. 13 (Continued)

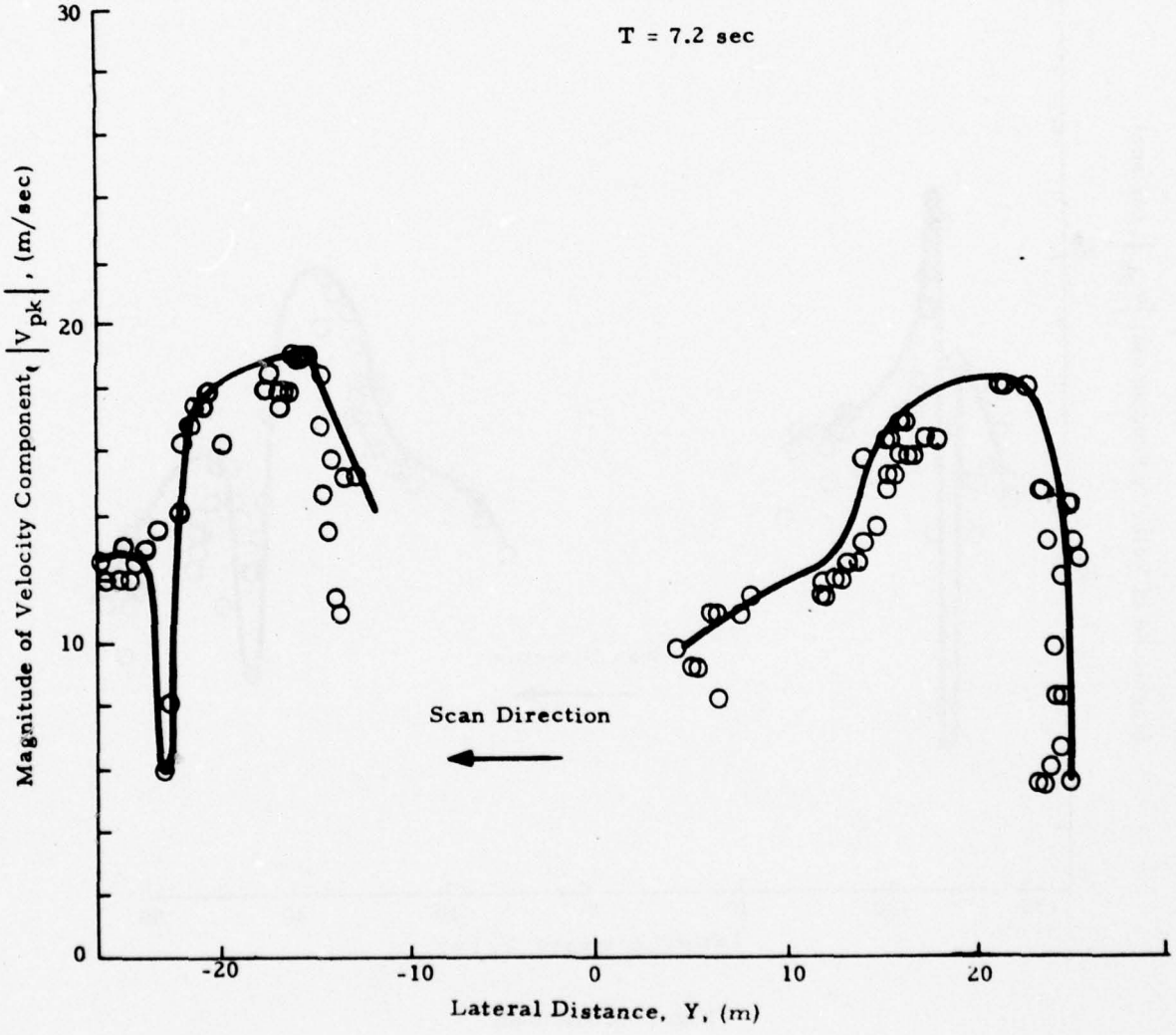

Fig. 13 (Continued)

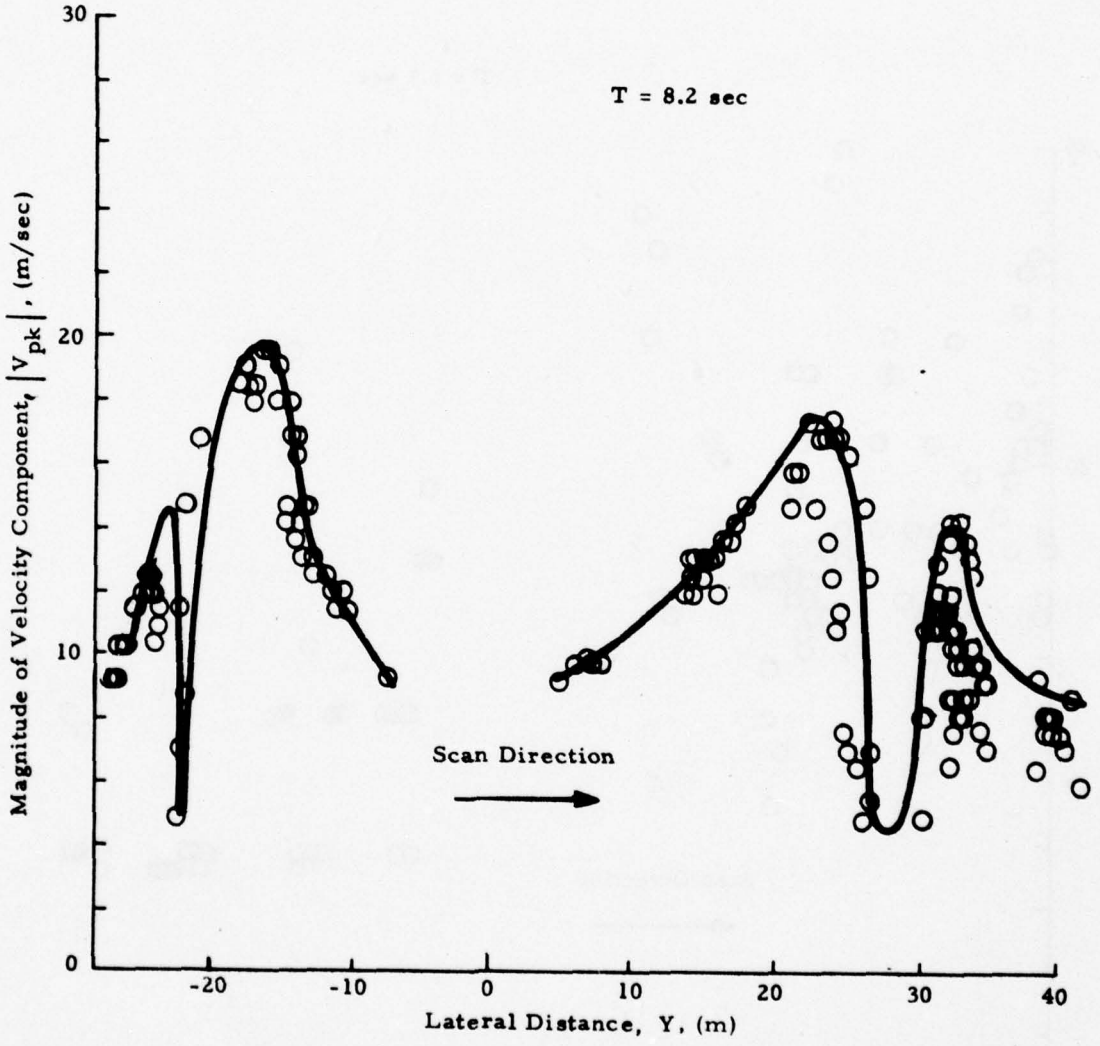

Fig. 13 (Concluded)

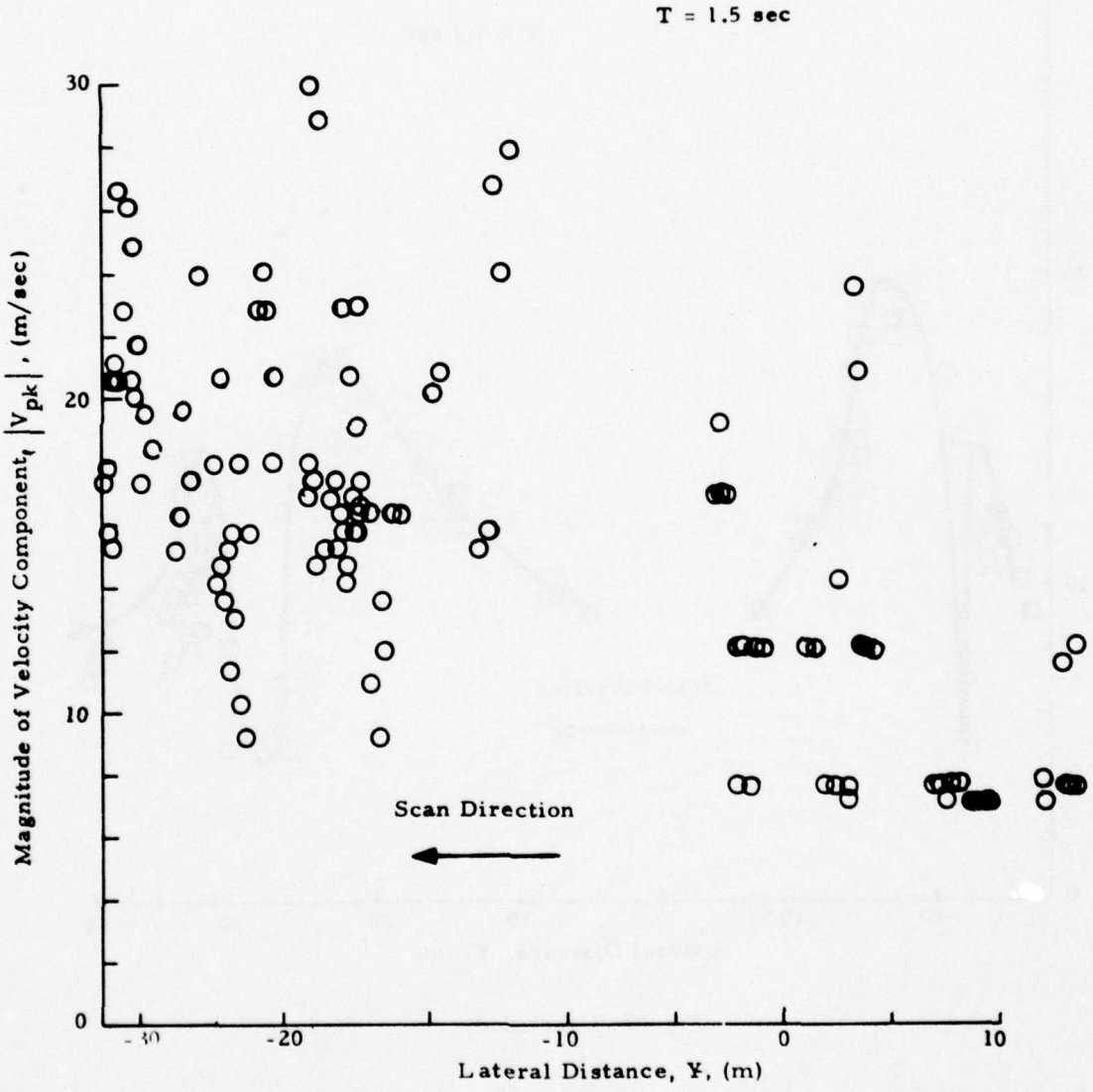

Fig.14 - $|V_{pk}|$ as a Function of Lateral Distance for Rosamond B-747 Flyby 11

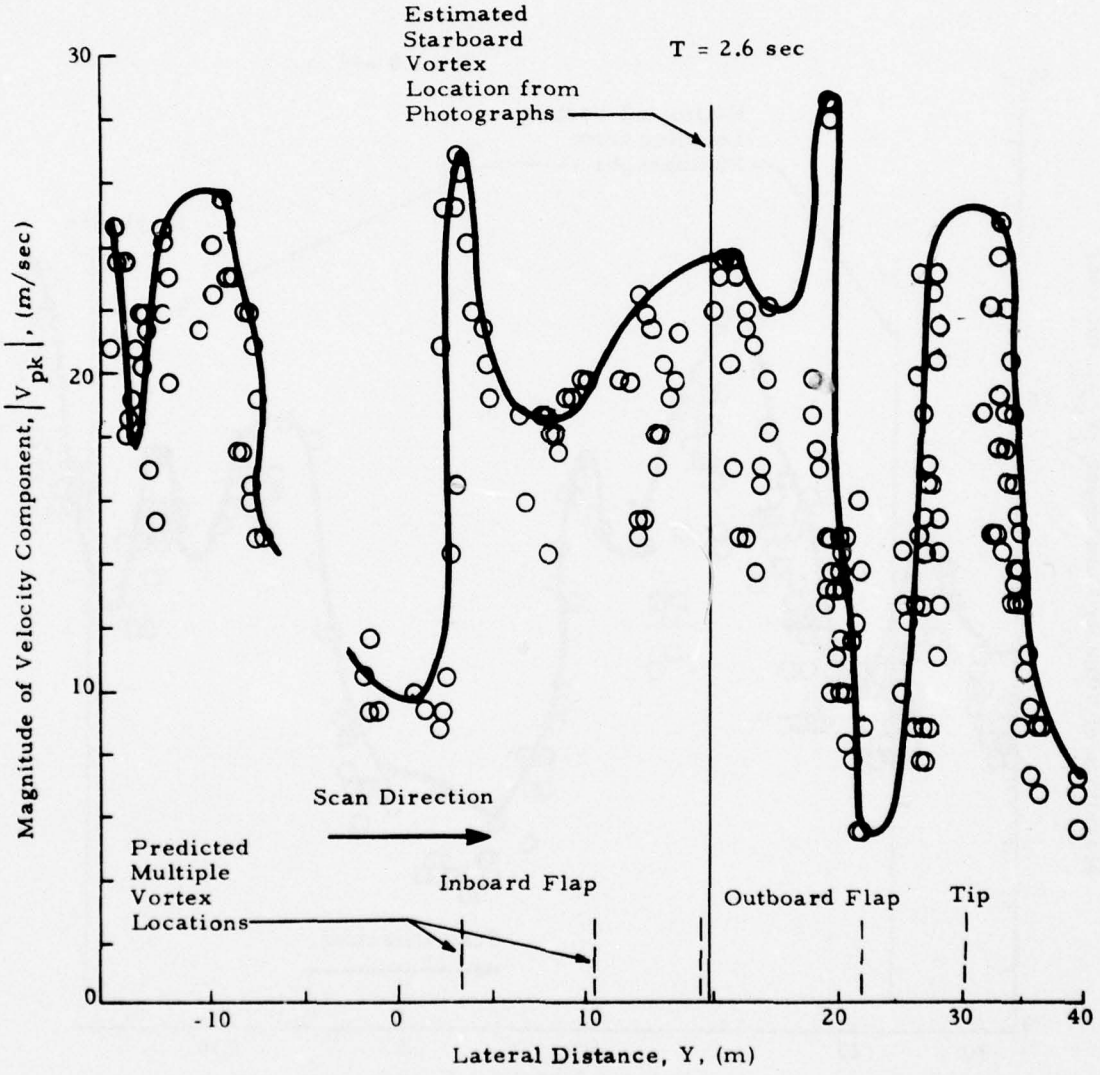

Fig. 14 (Continued)

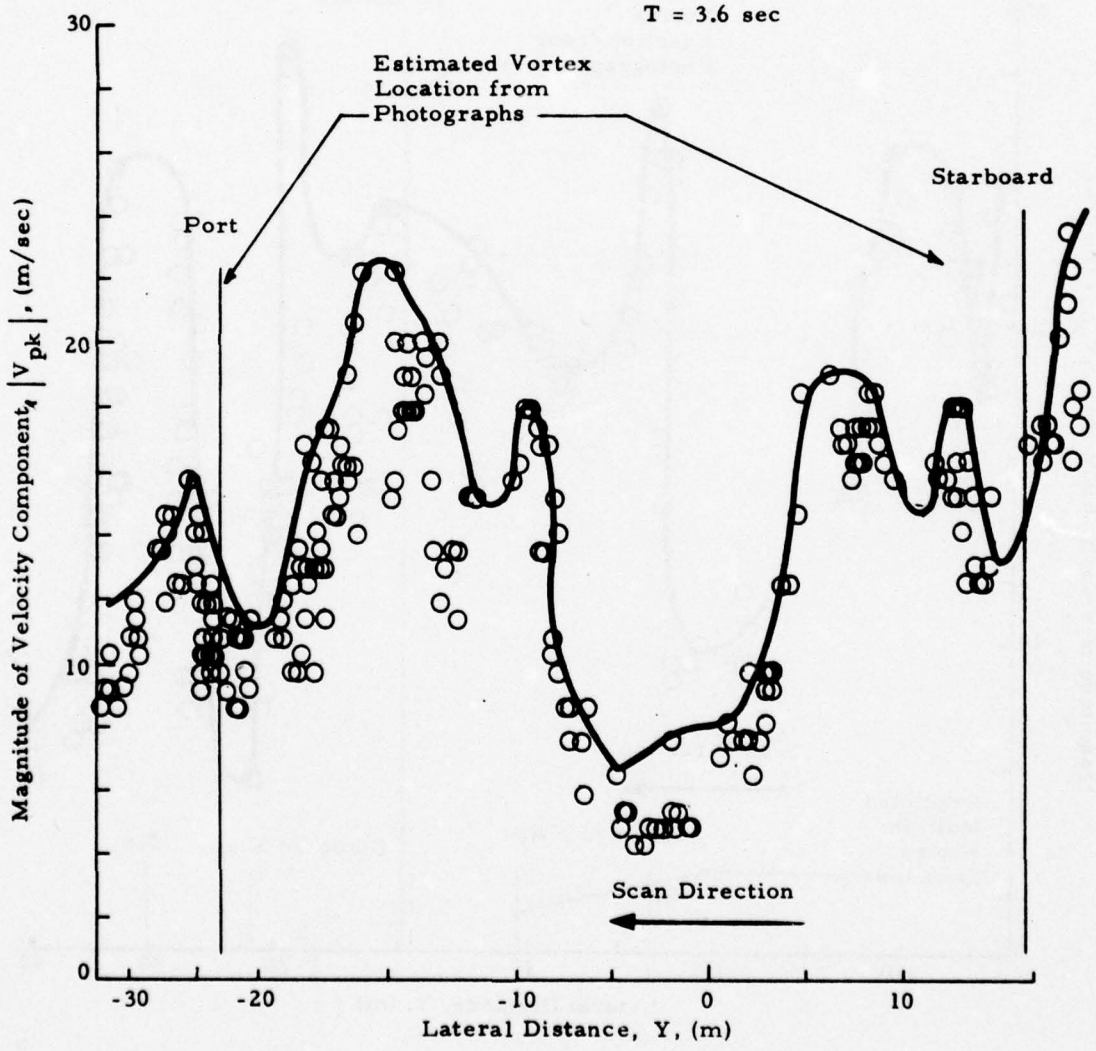

Fig. 14 (Continued)

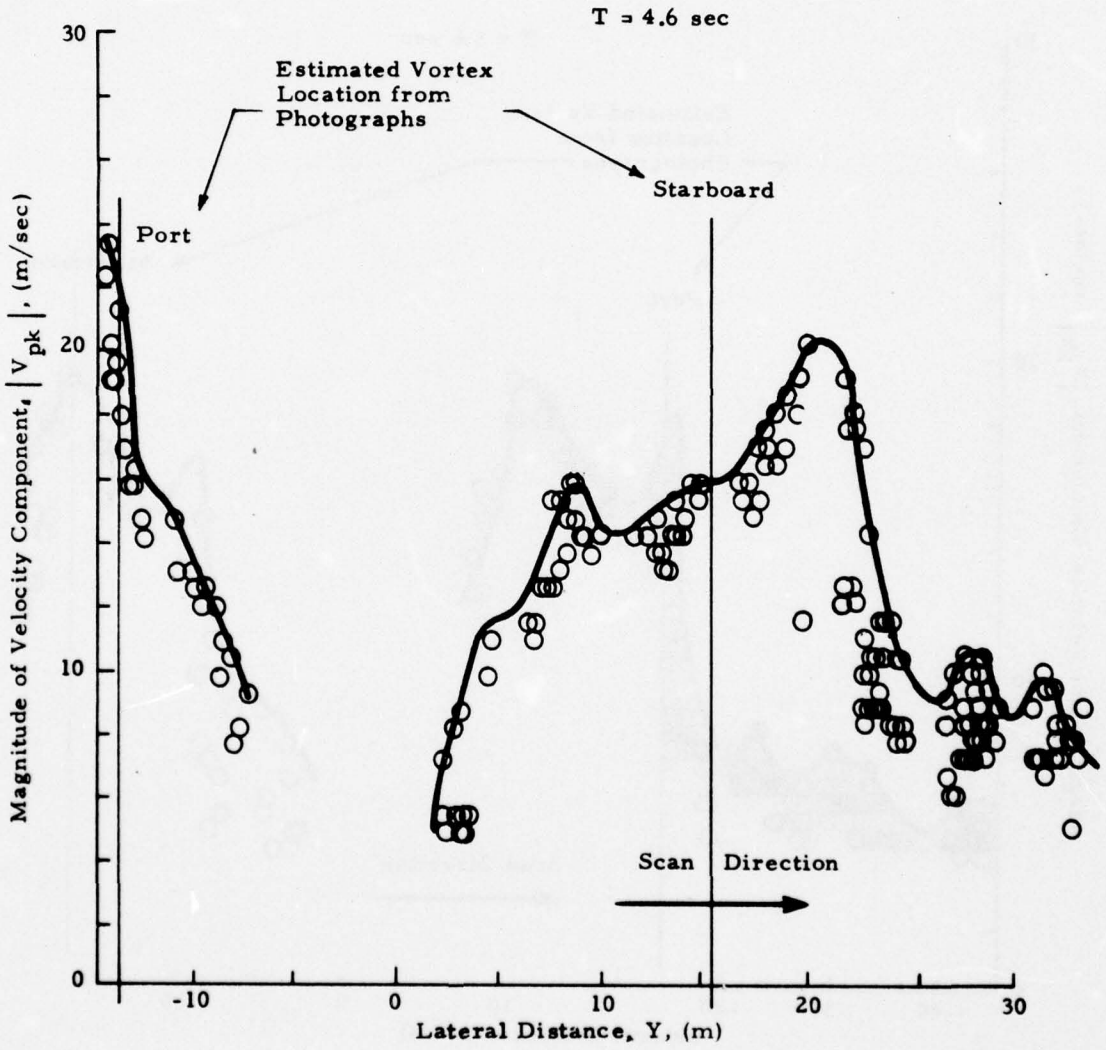

Fig. 14 (Continued)

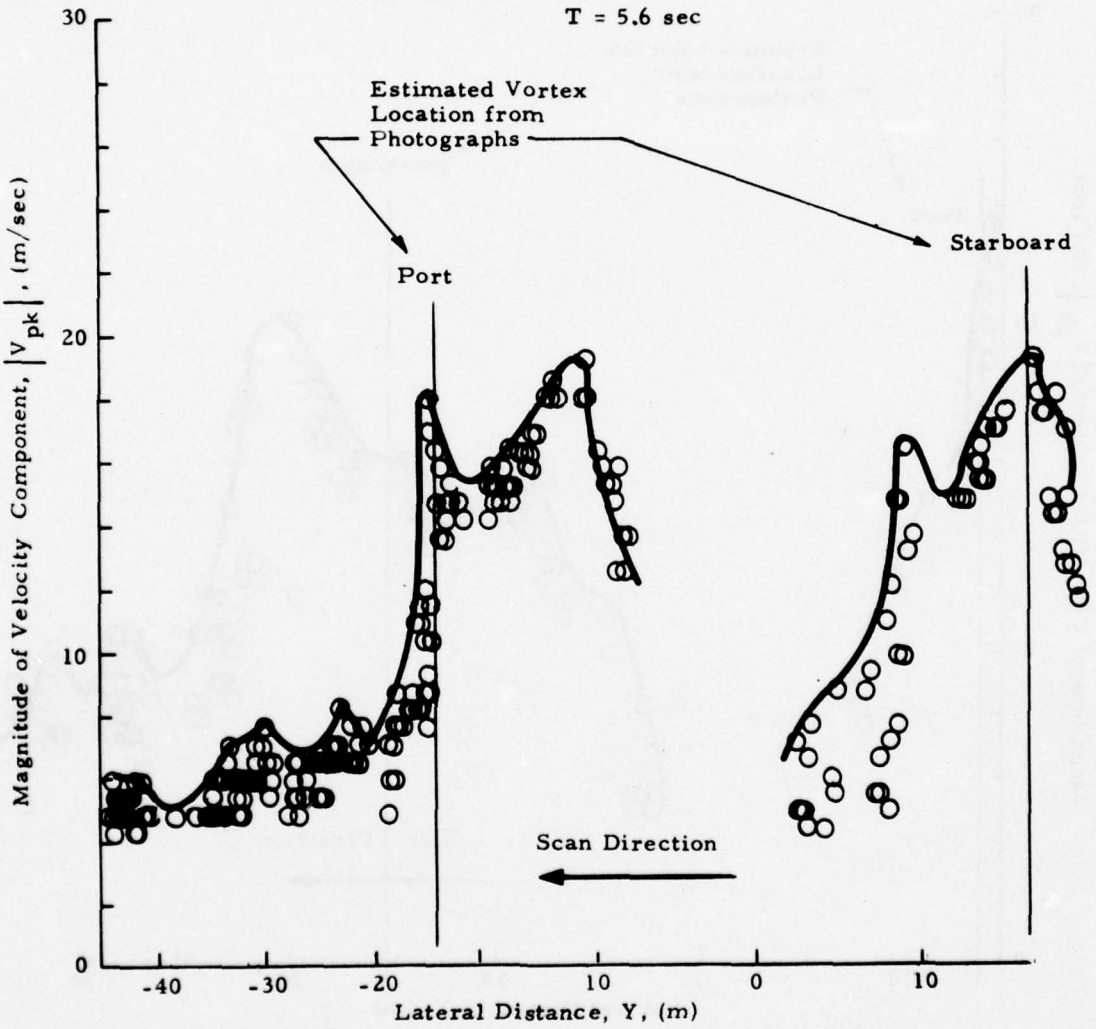

Fig. 14 (Continued)

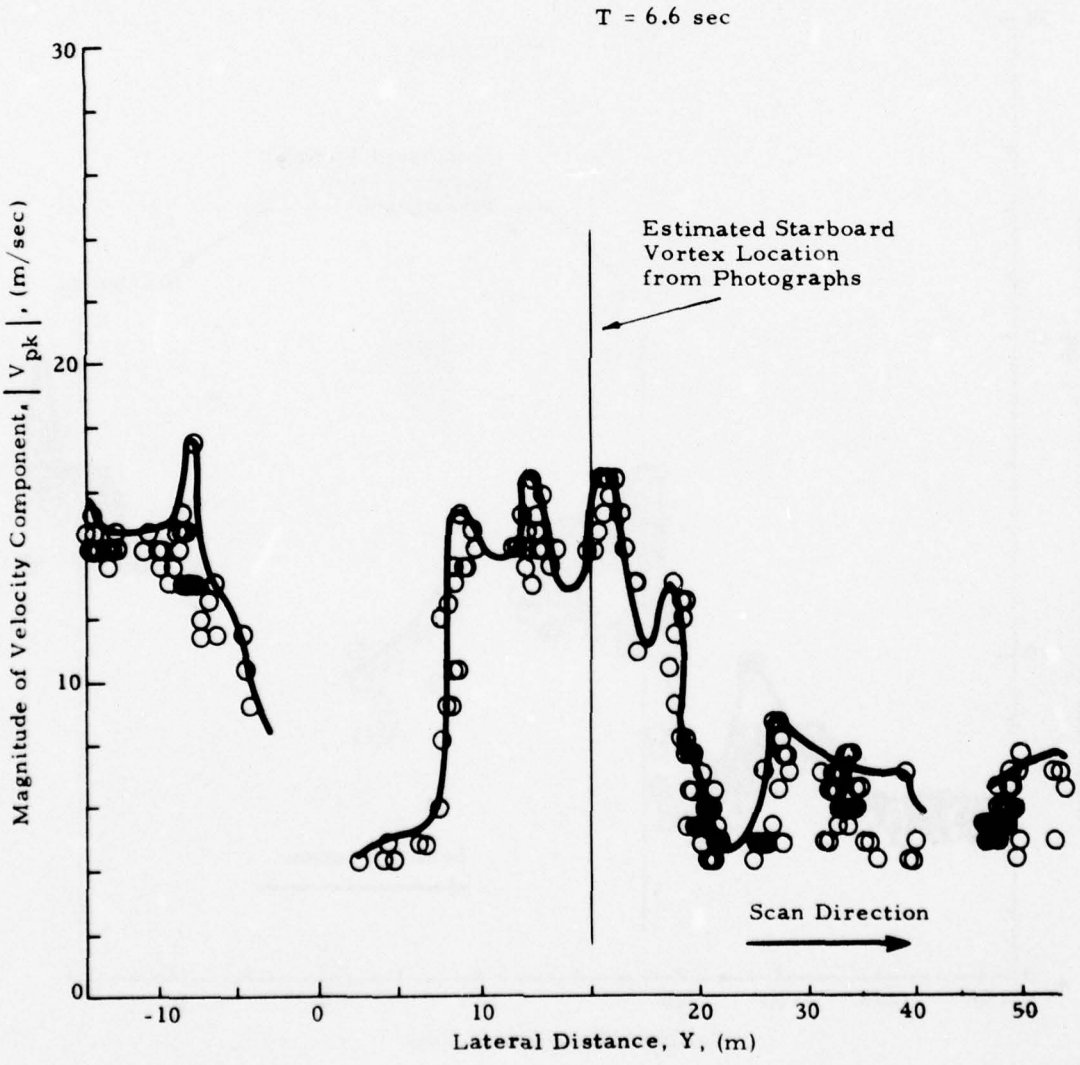

Fig. 14 (Continued)

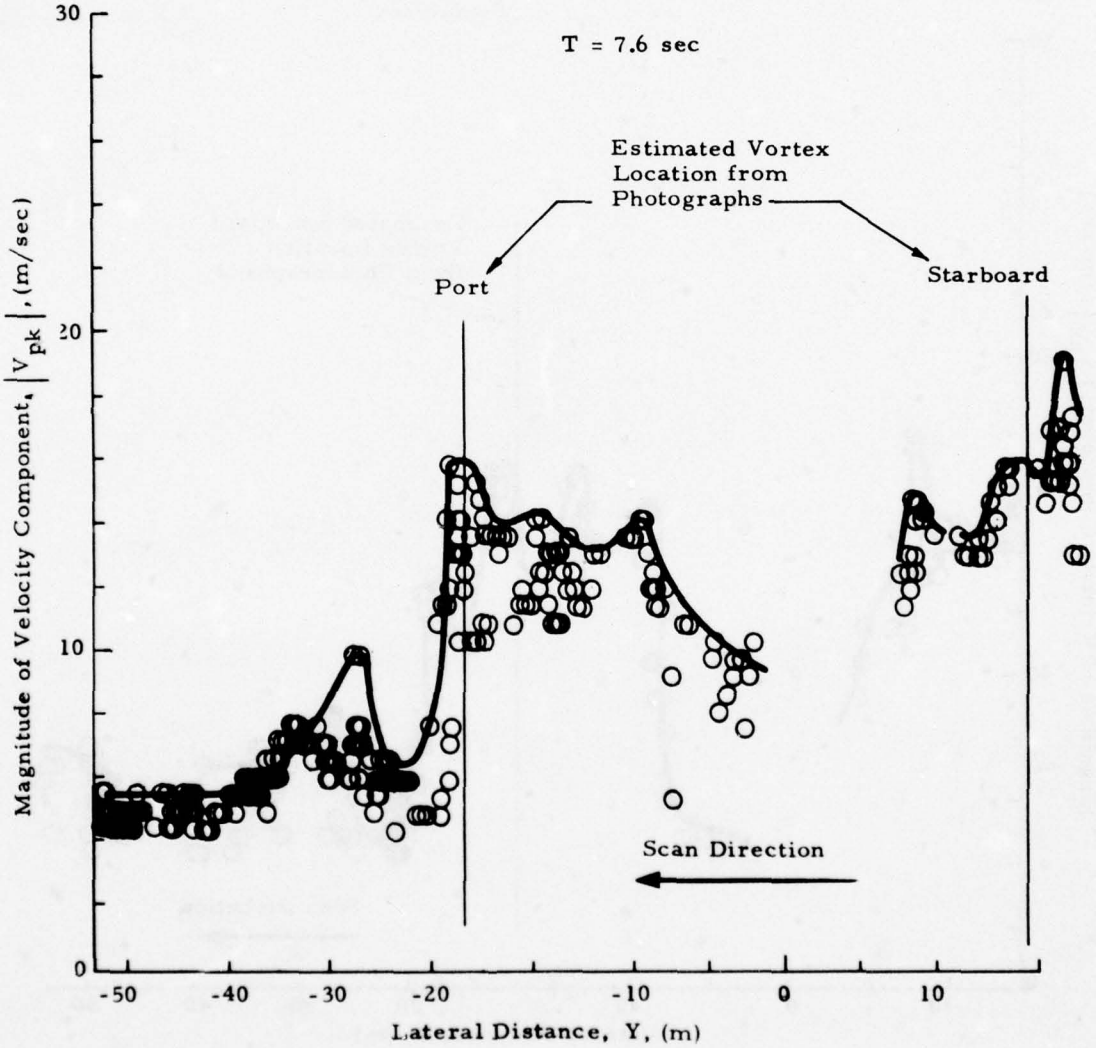

Fig. 14 (Continued)

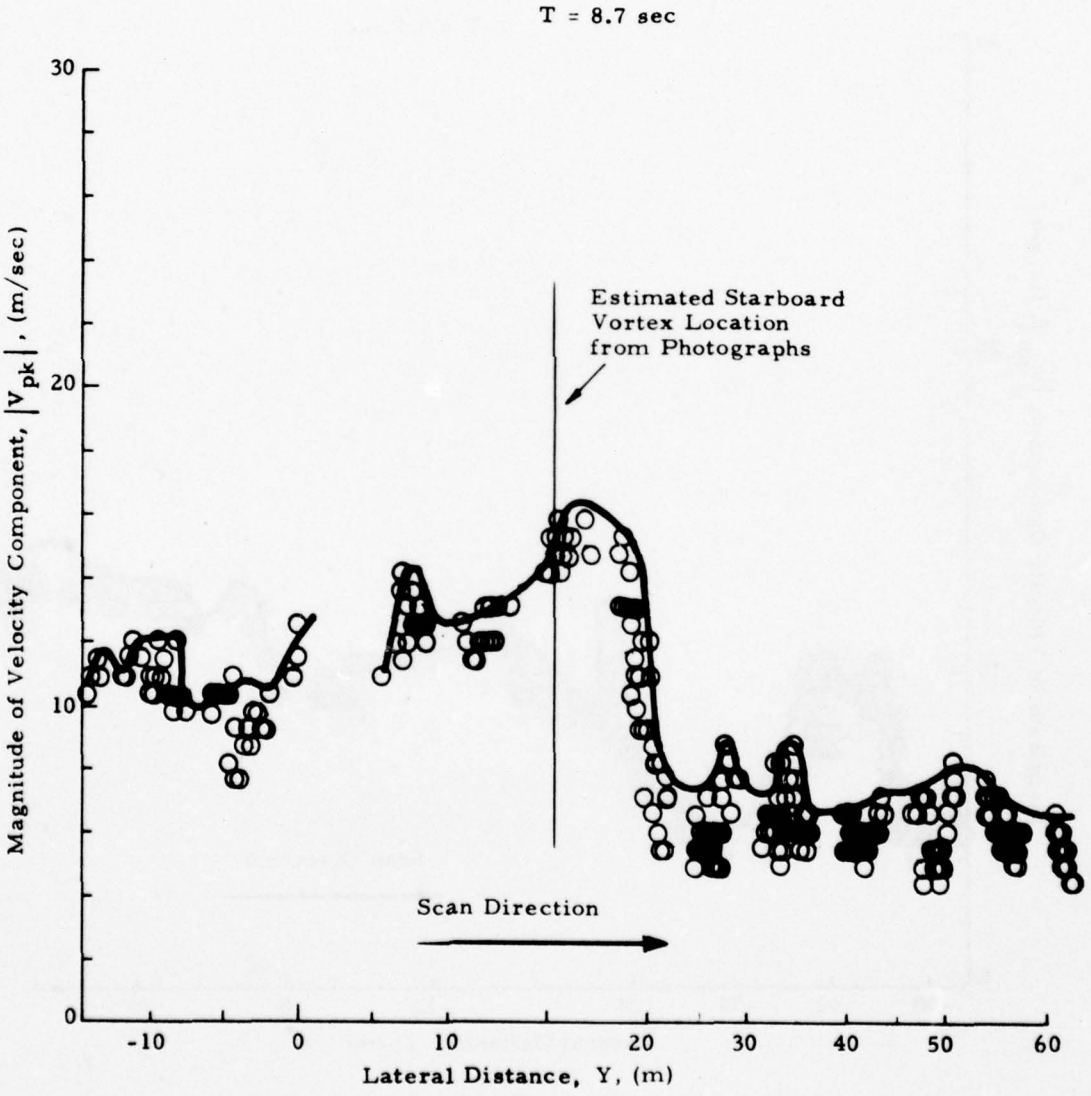

Fig. 14 (Continued)

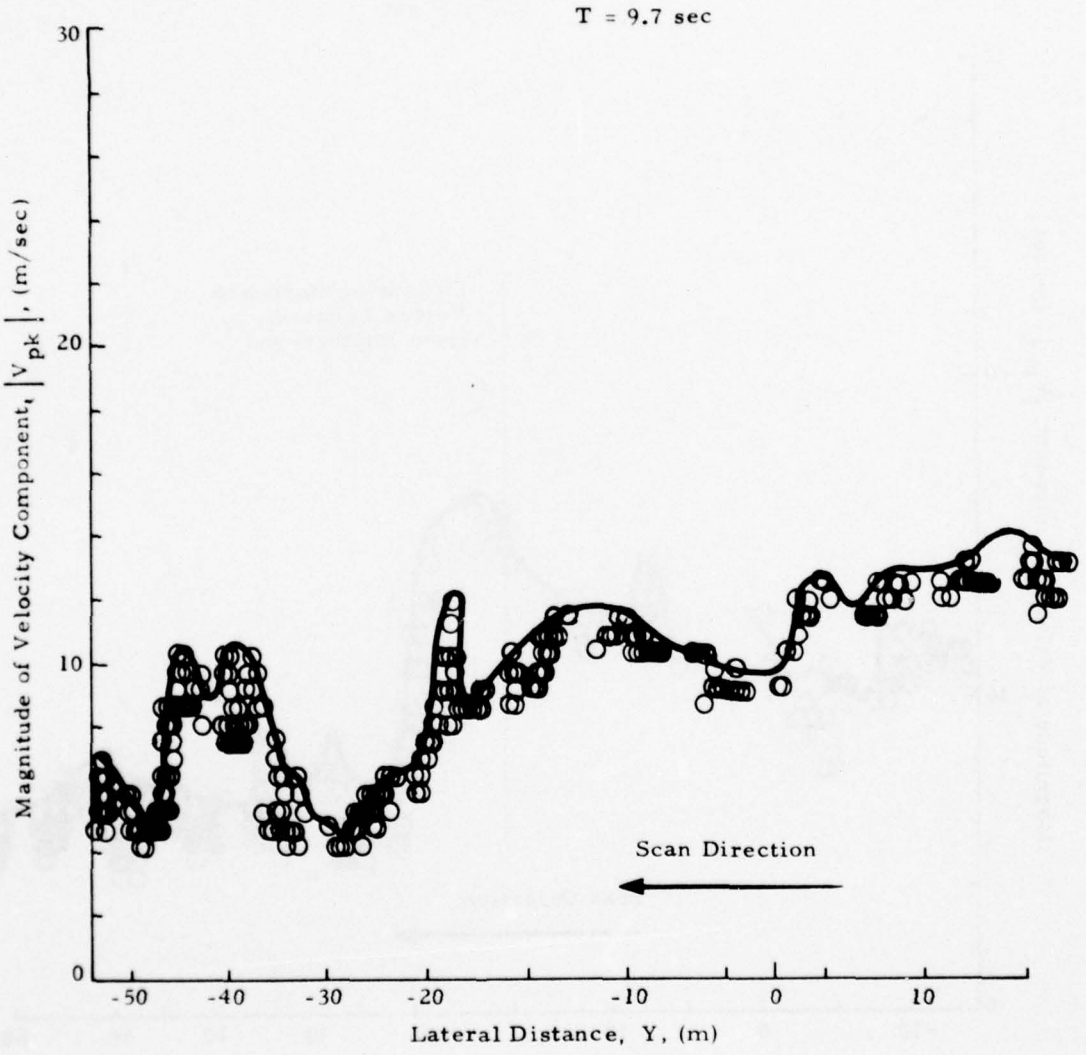

Fig. 14 (Concluded)

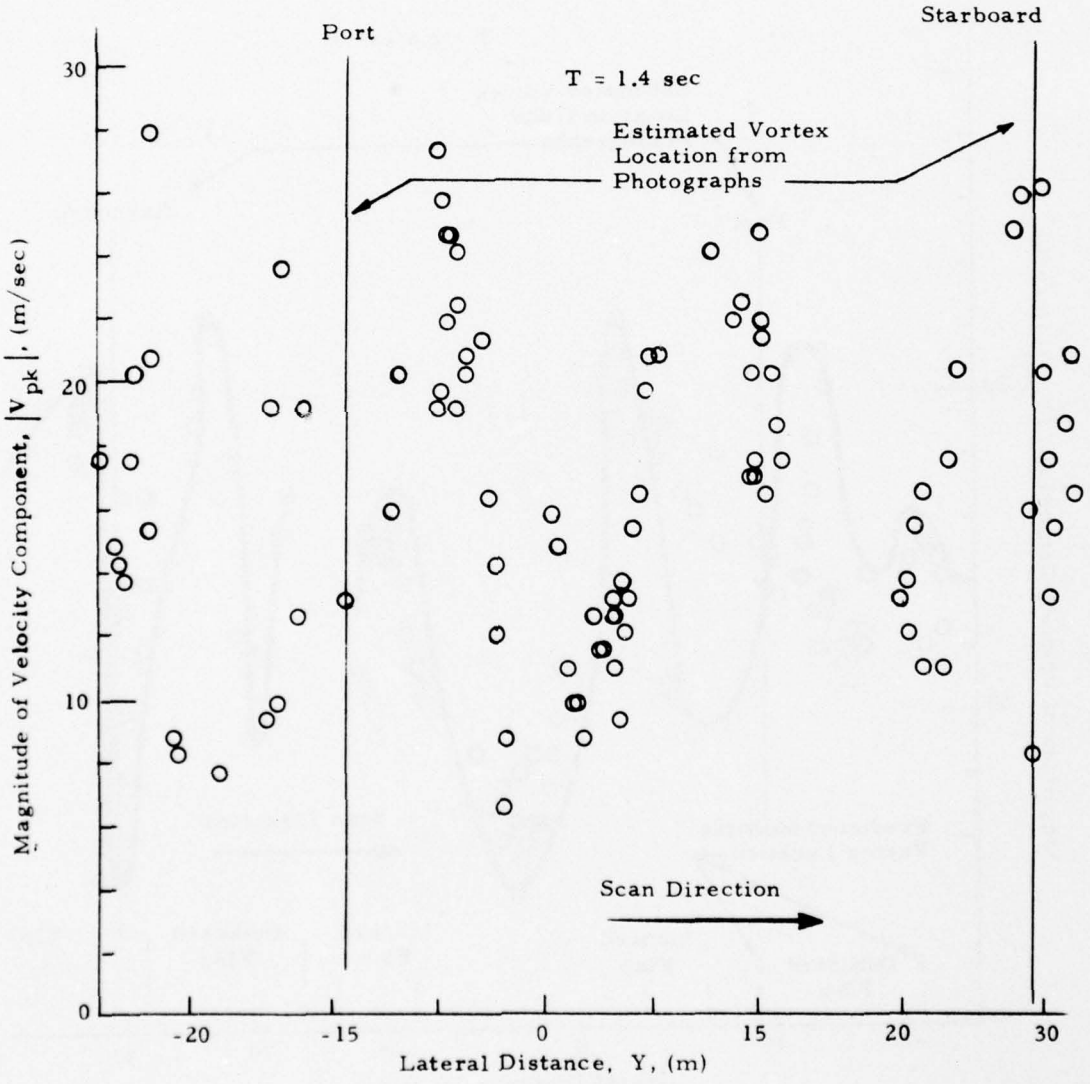

Fig. 15 - $|V_{pk}|$ as a Function of Lateral Distance for Rosamond B-747 Flyby 12

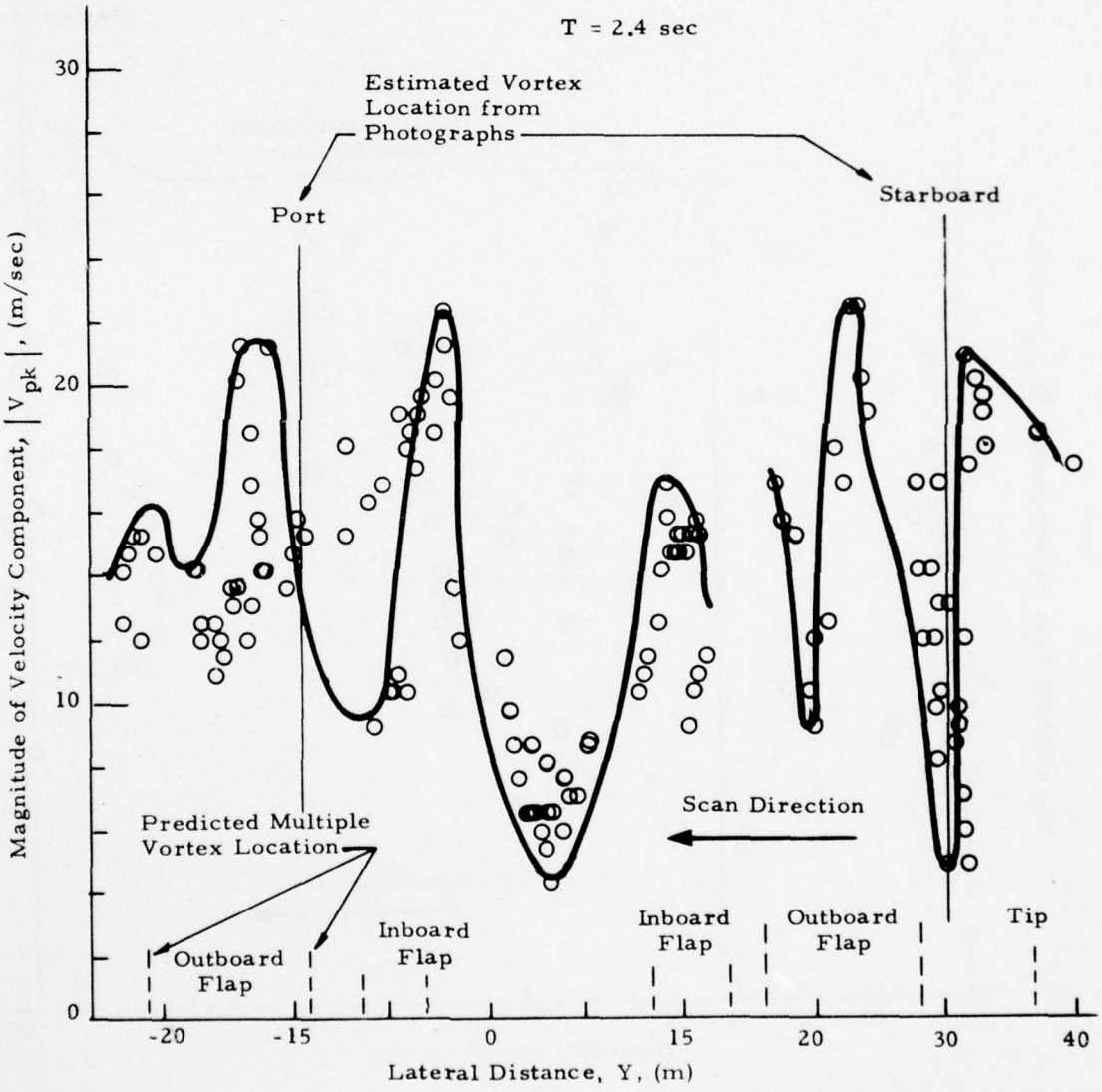

Fig. 15 (Continued)

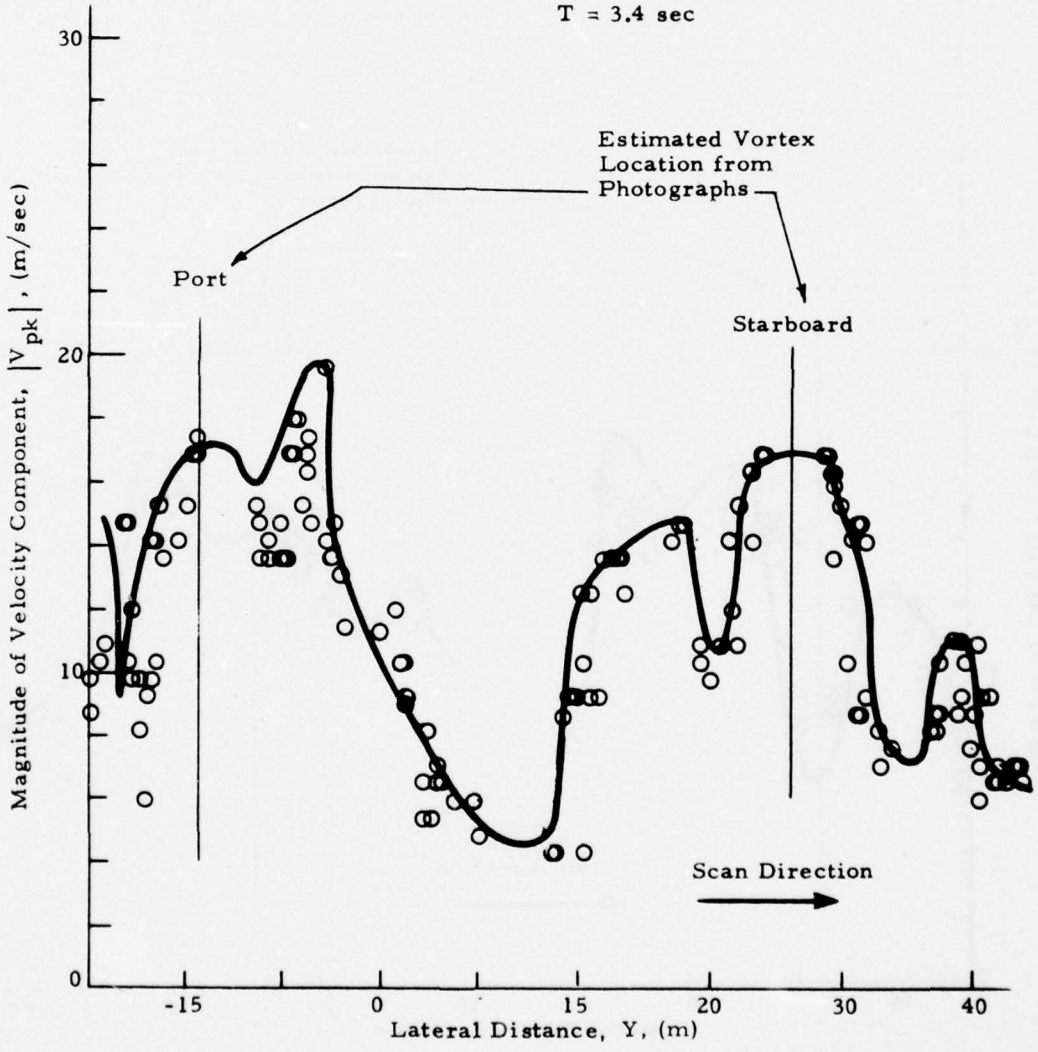

Fig. 15 (Continued)

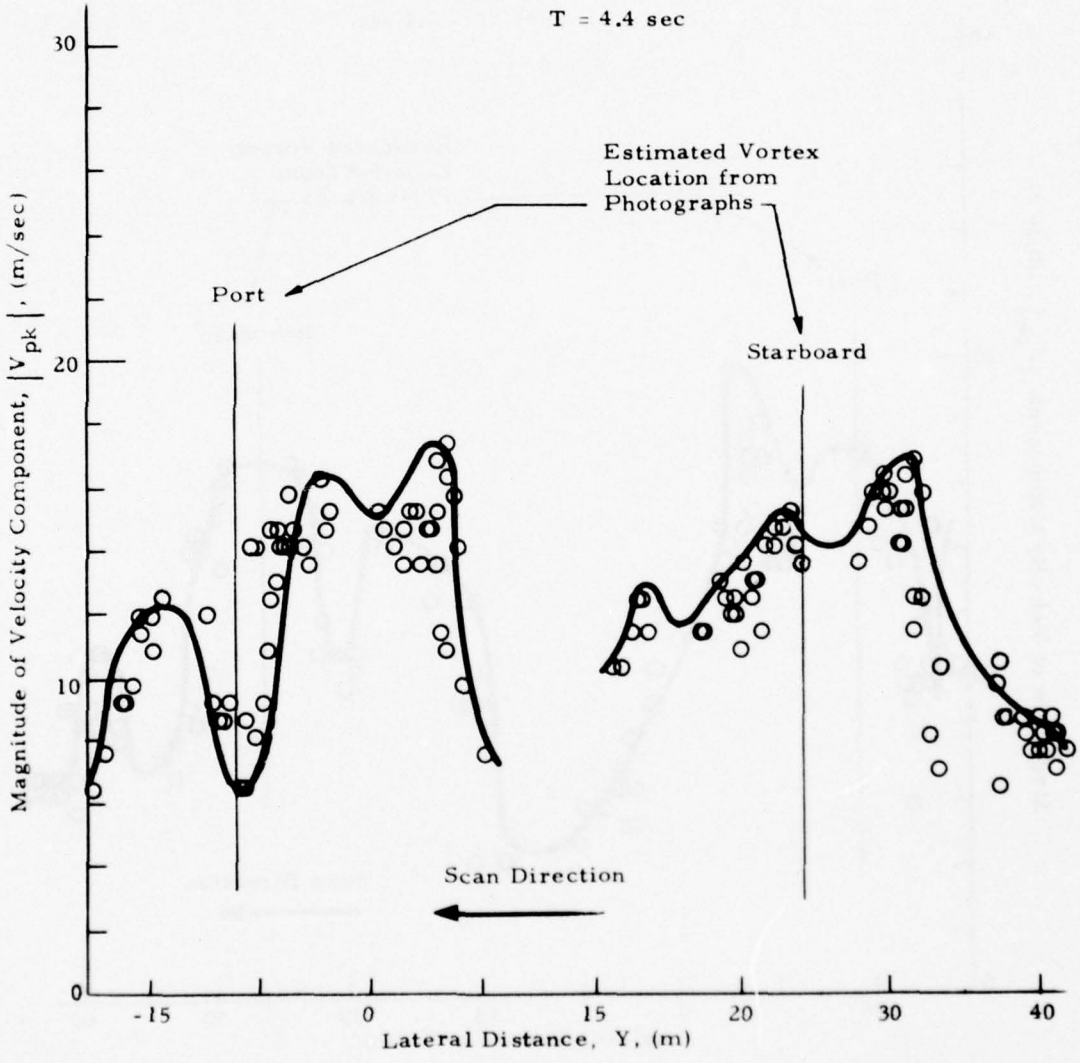

Fig. 15 (Continued)

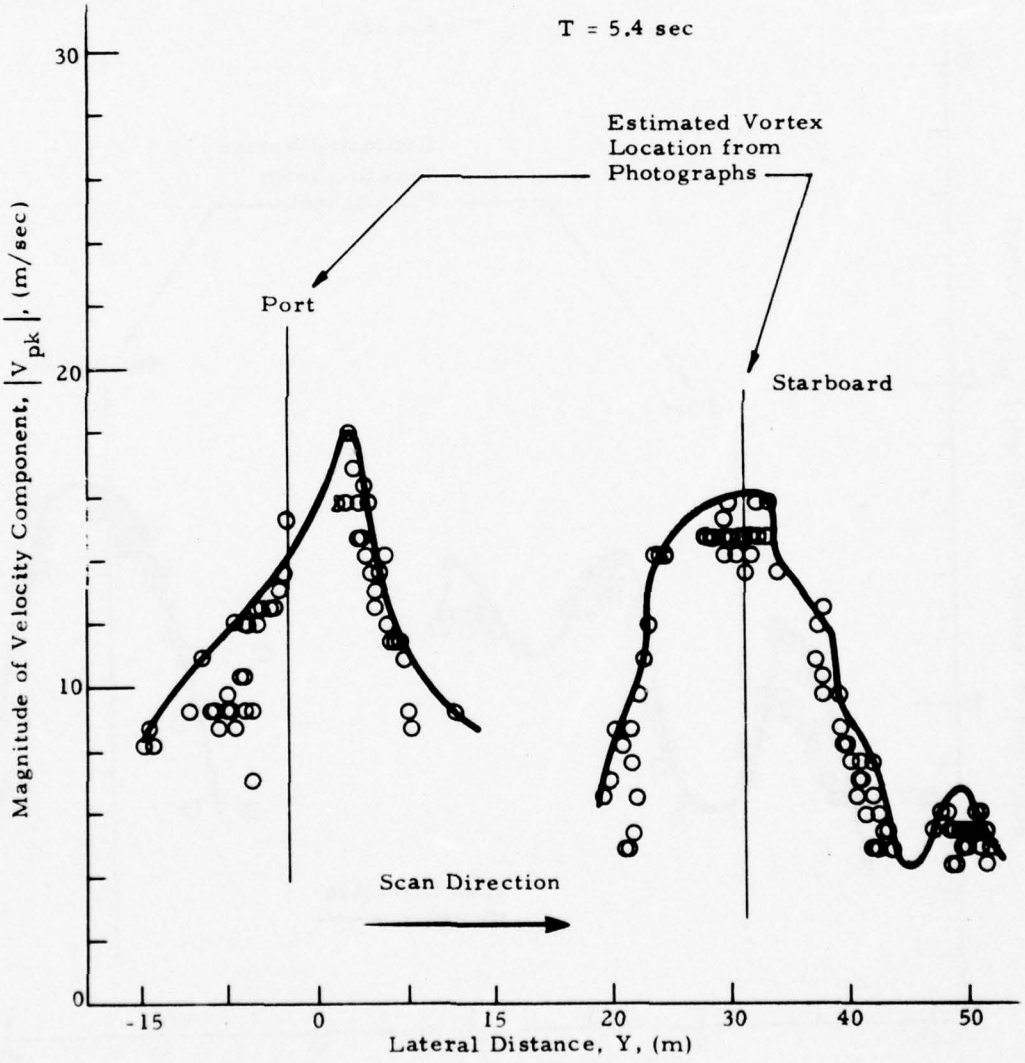

Fig. 15 (Continued)

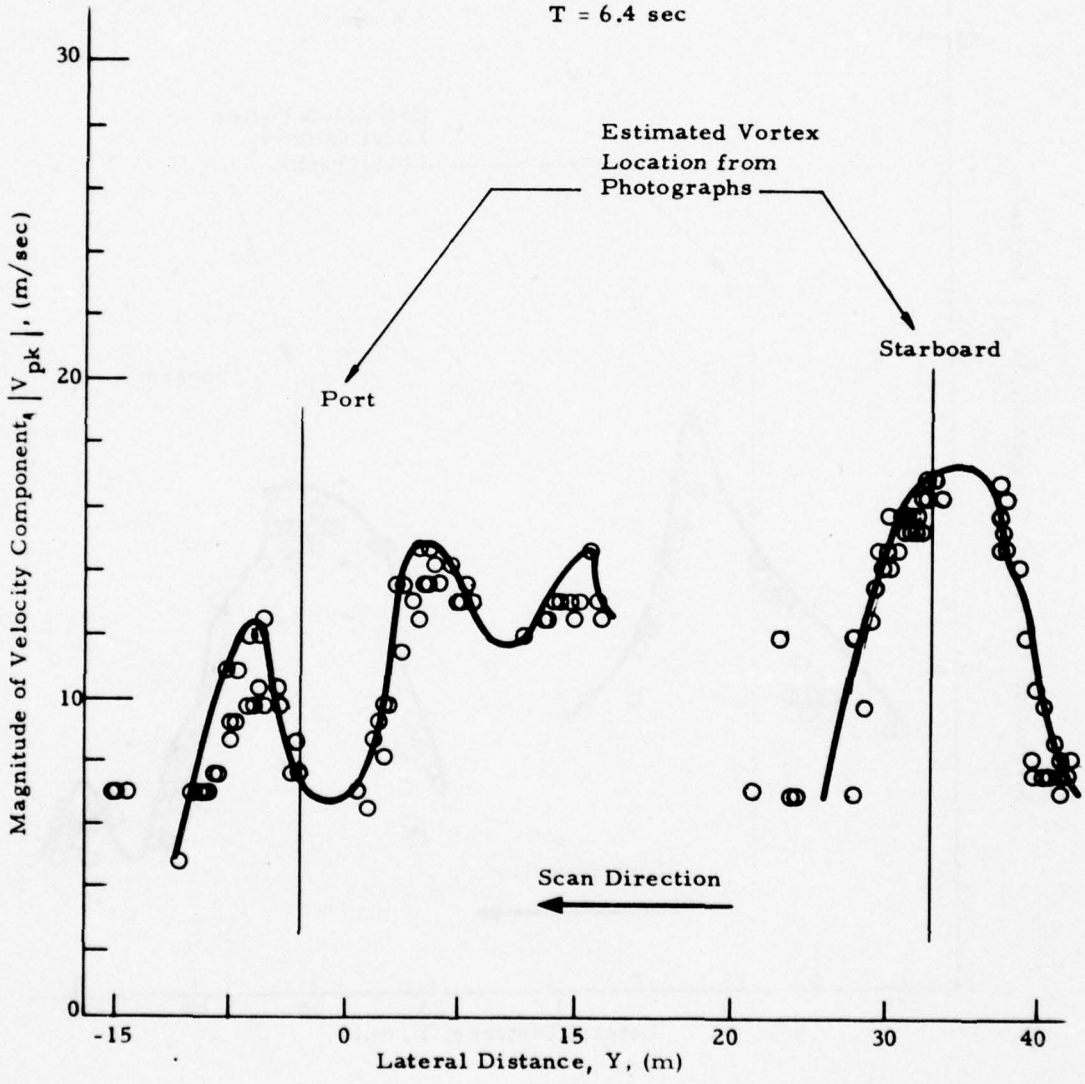

Fig. 15 (Continued)

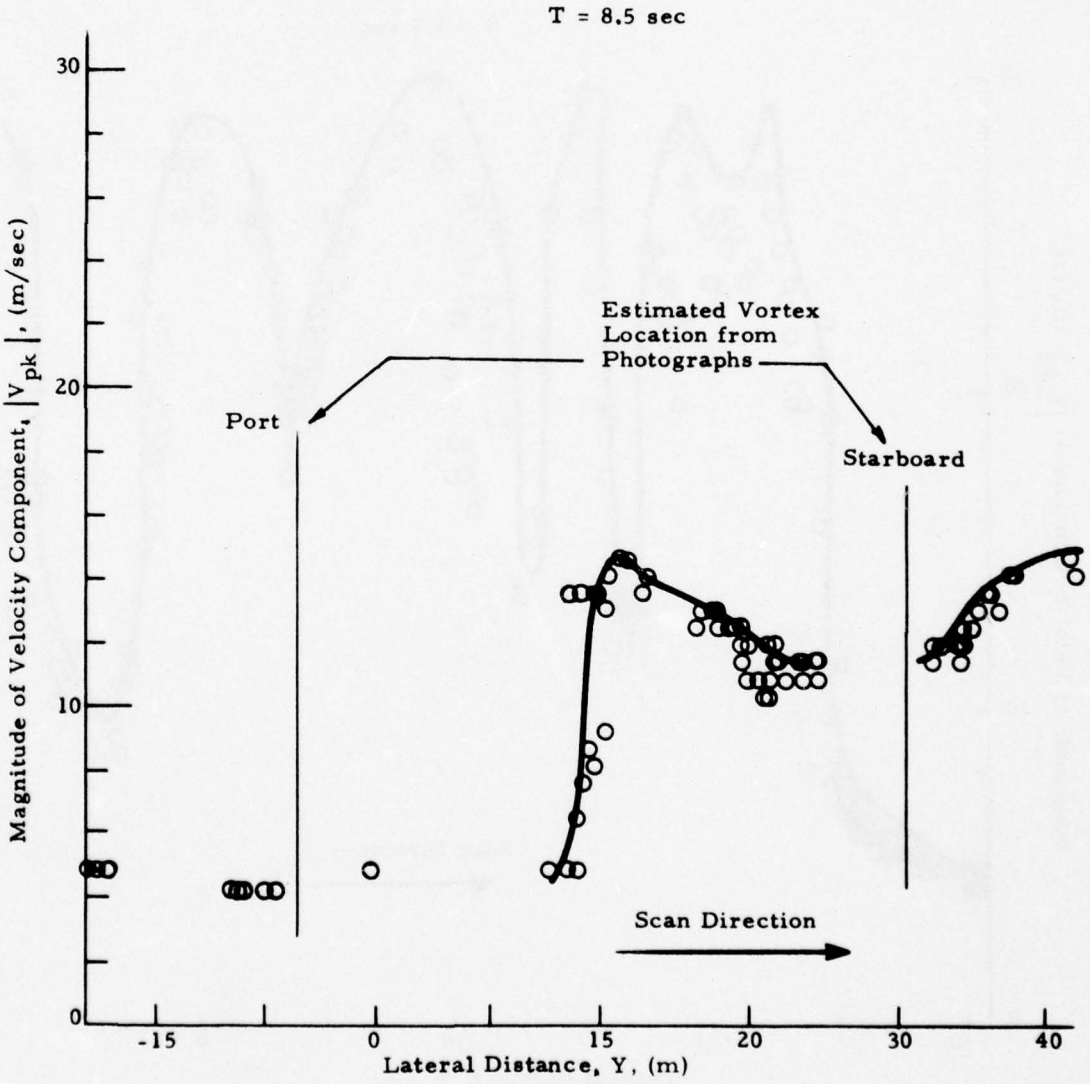

Fig. 15 (Concluded)

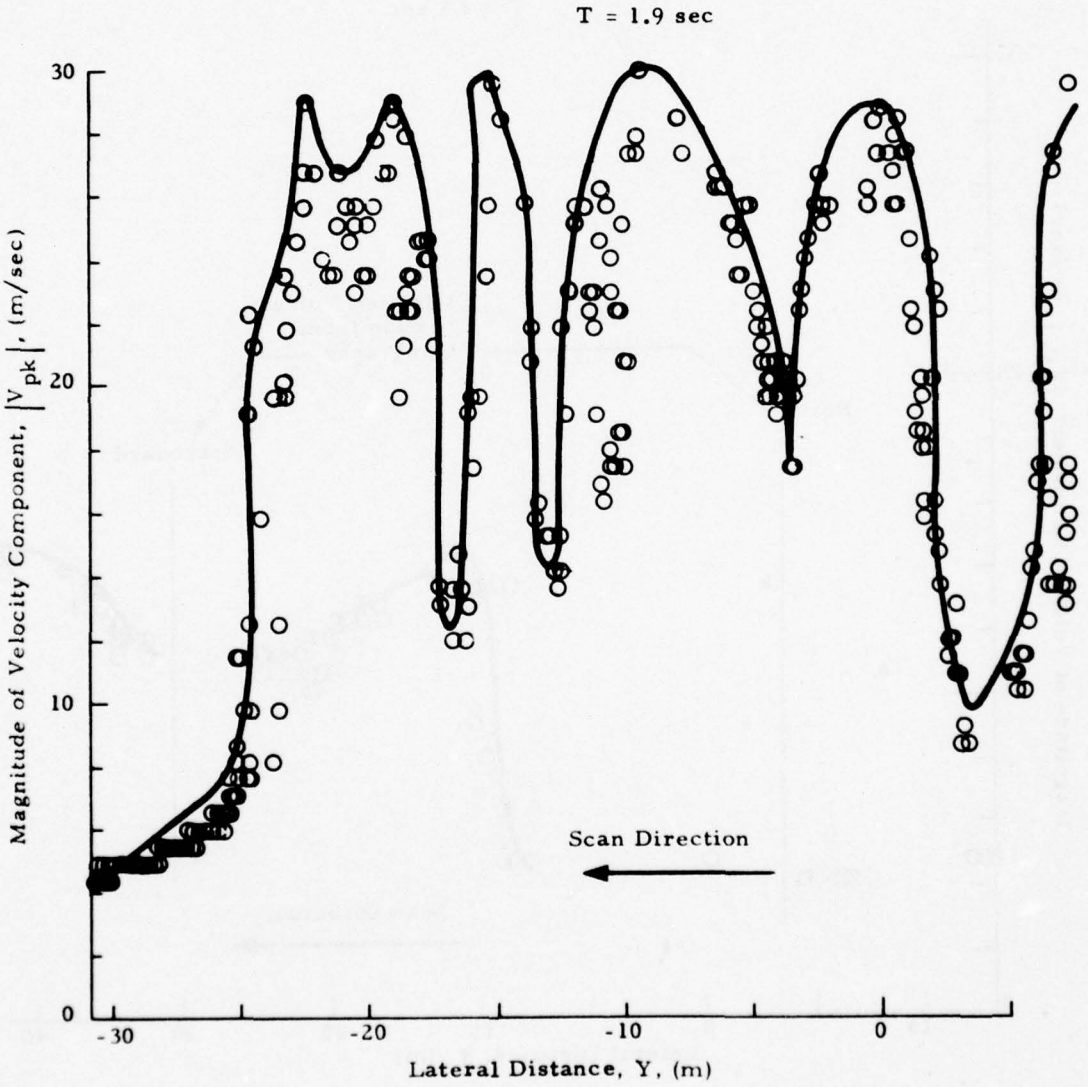

Fig. 16 - $|V_{pk}|$ as a Function of Lateral Distance for Rosamond B-747 Flyby 13

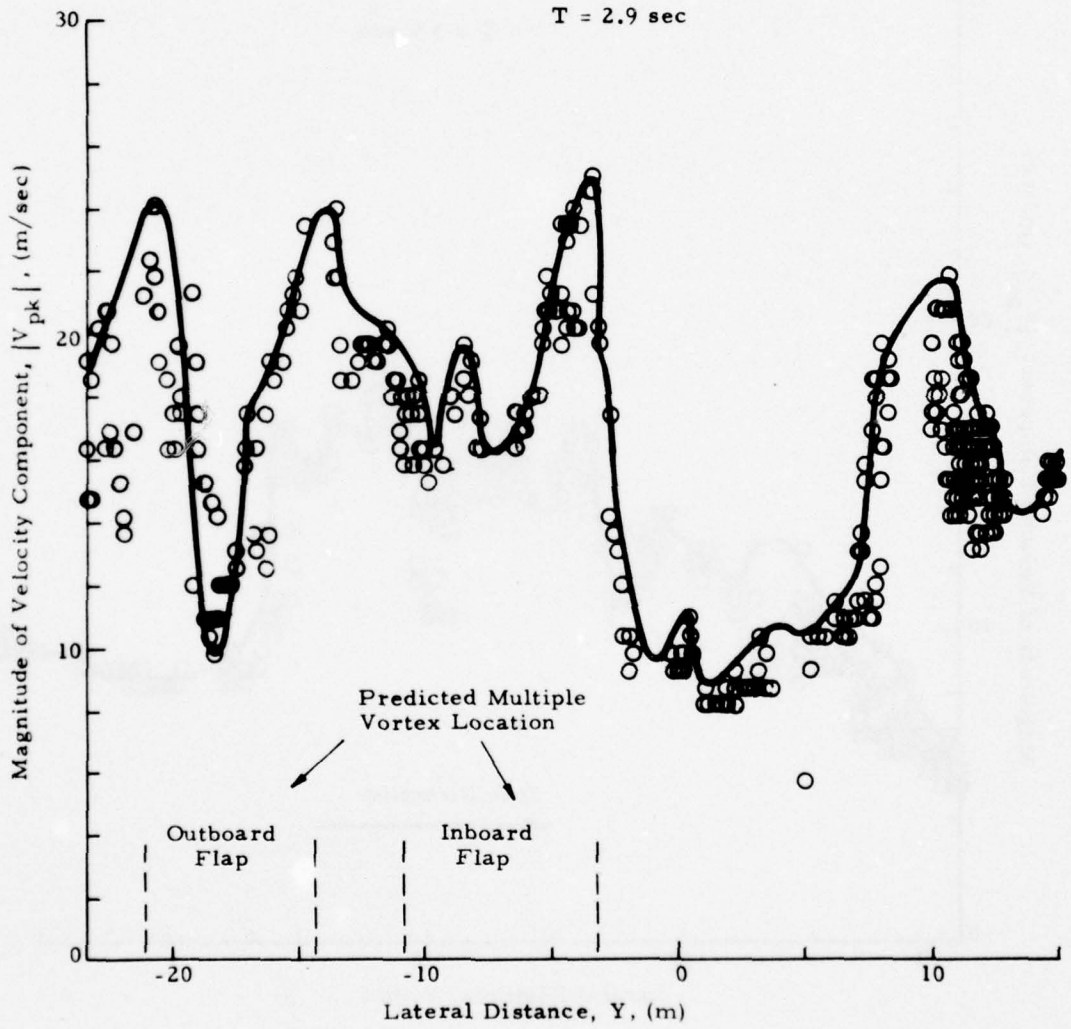

Fig. 16 (Continued)

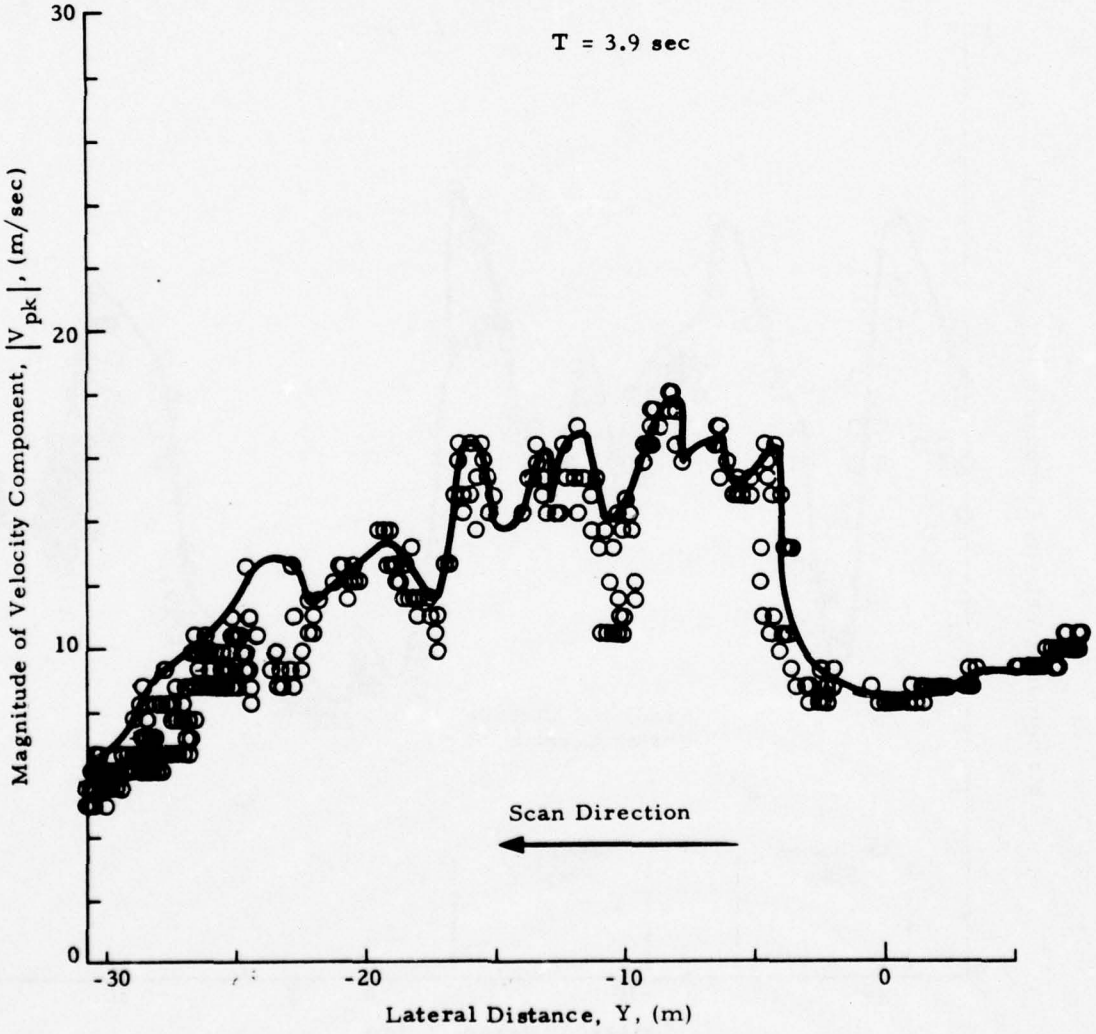

Fig. 16 (Continued)

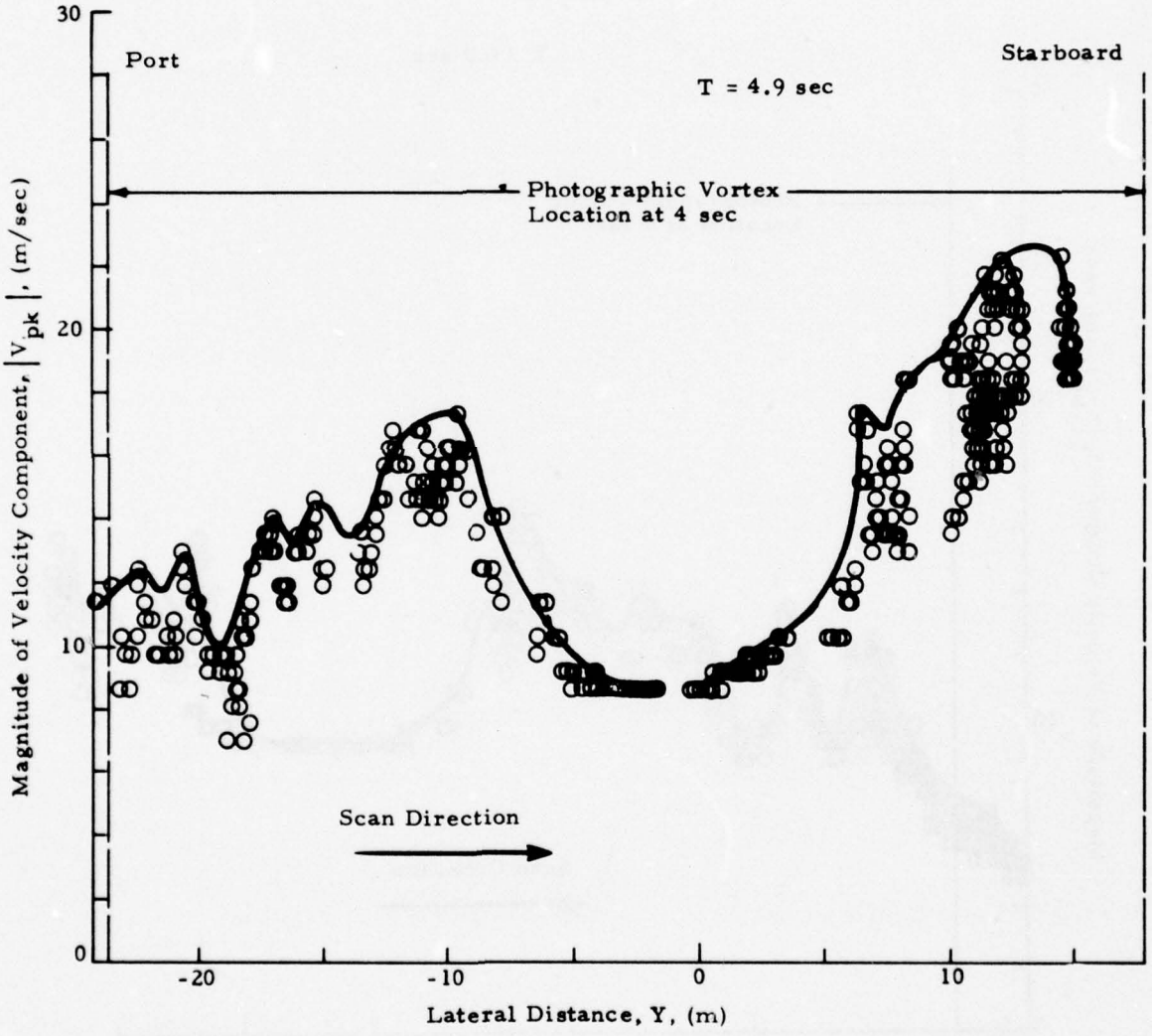

Fig. 16 (Continued)

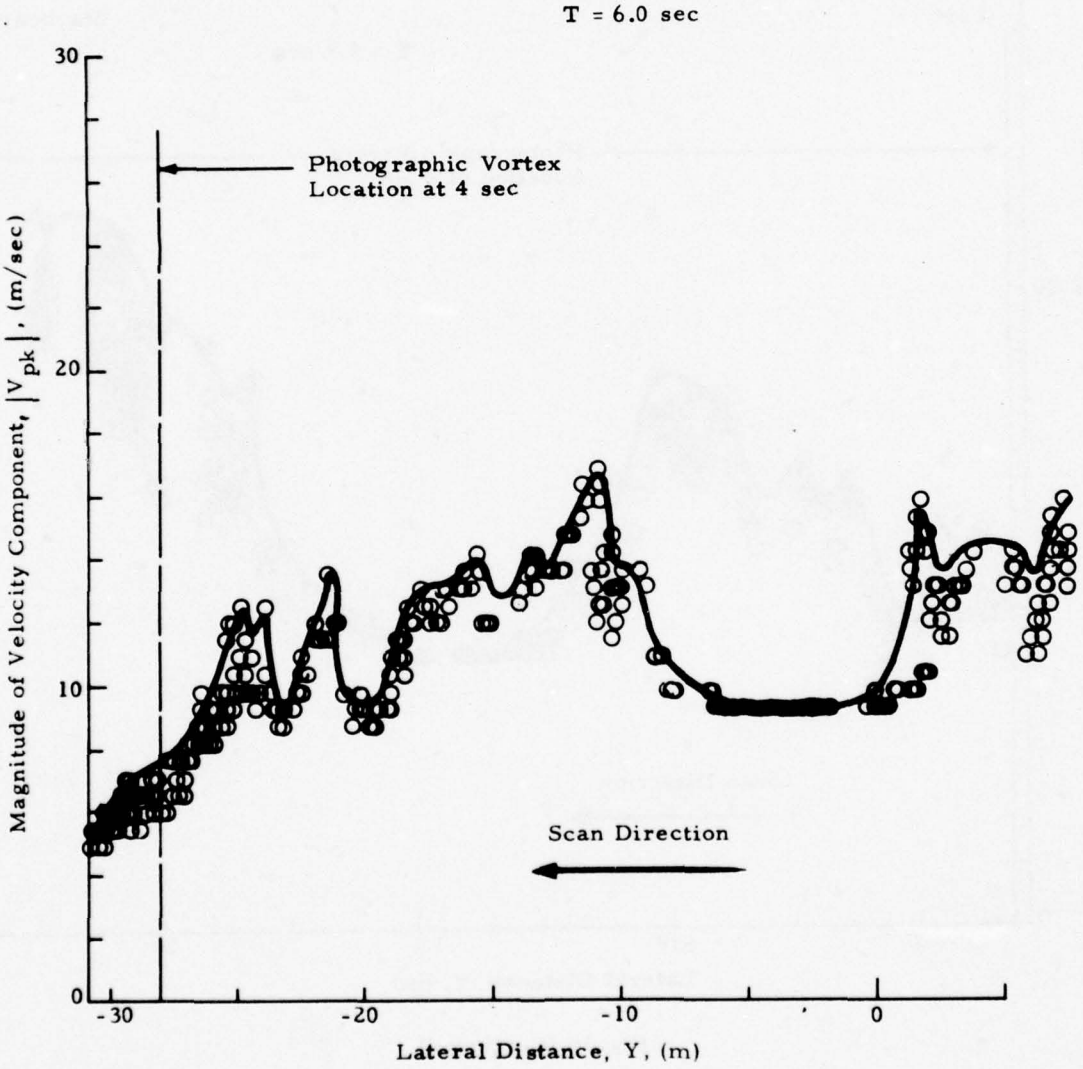

Fig. 16 (Continued)

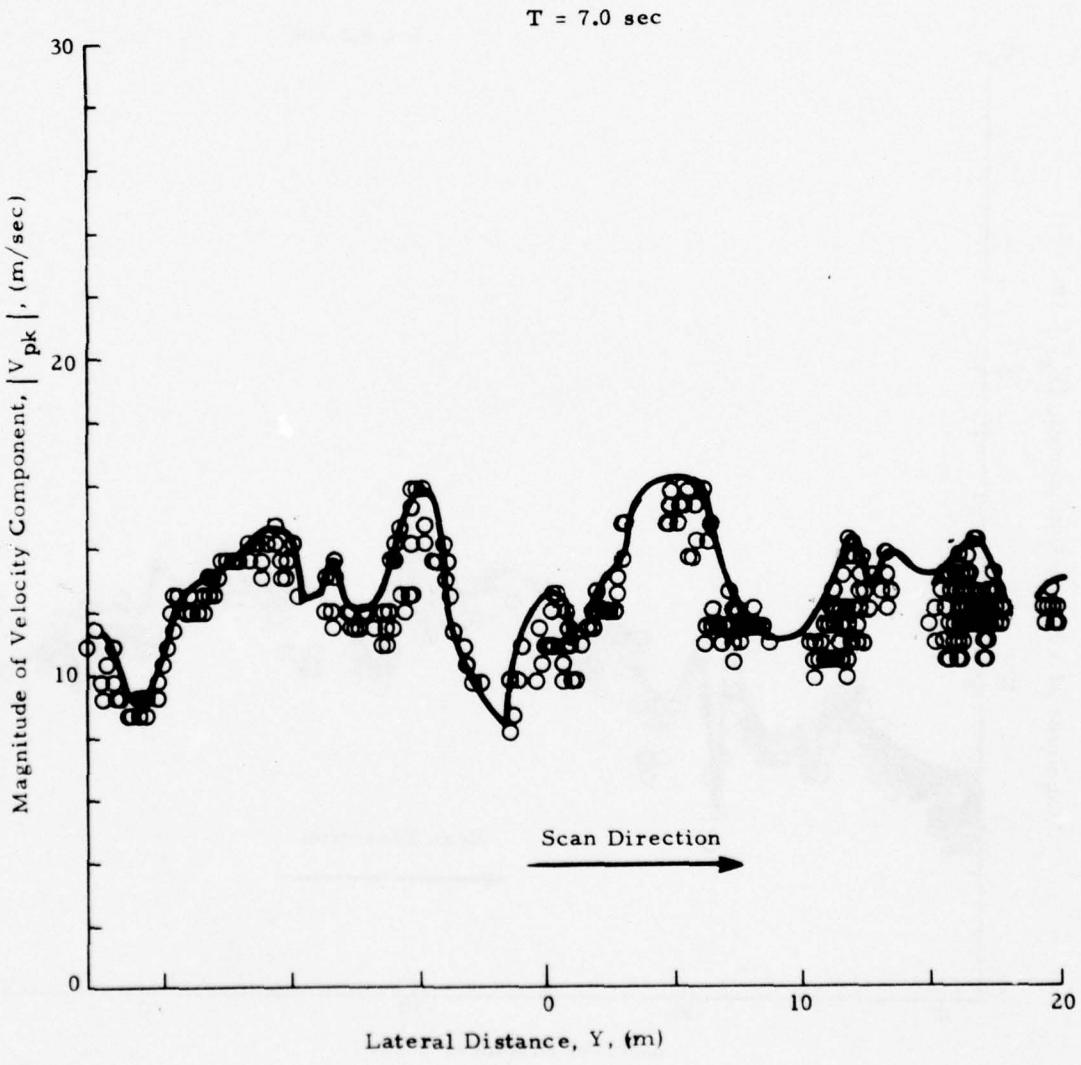

Fig. 16 (Continued)

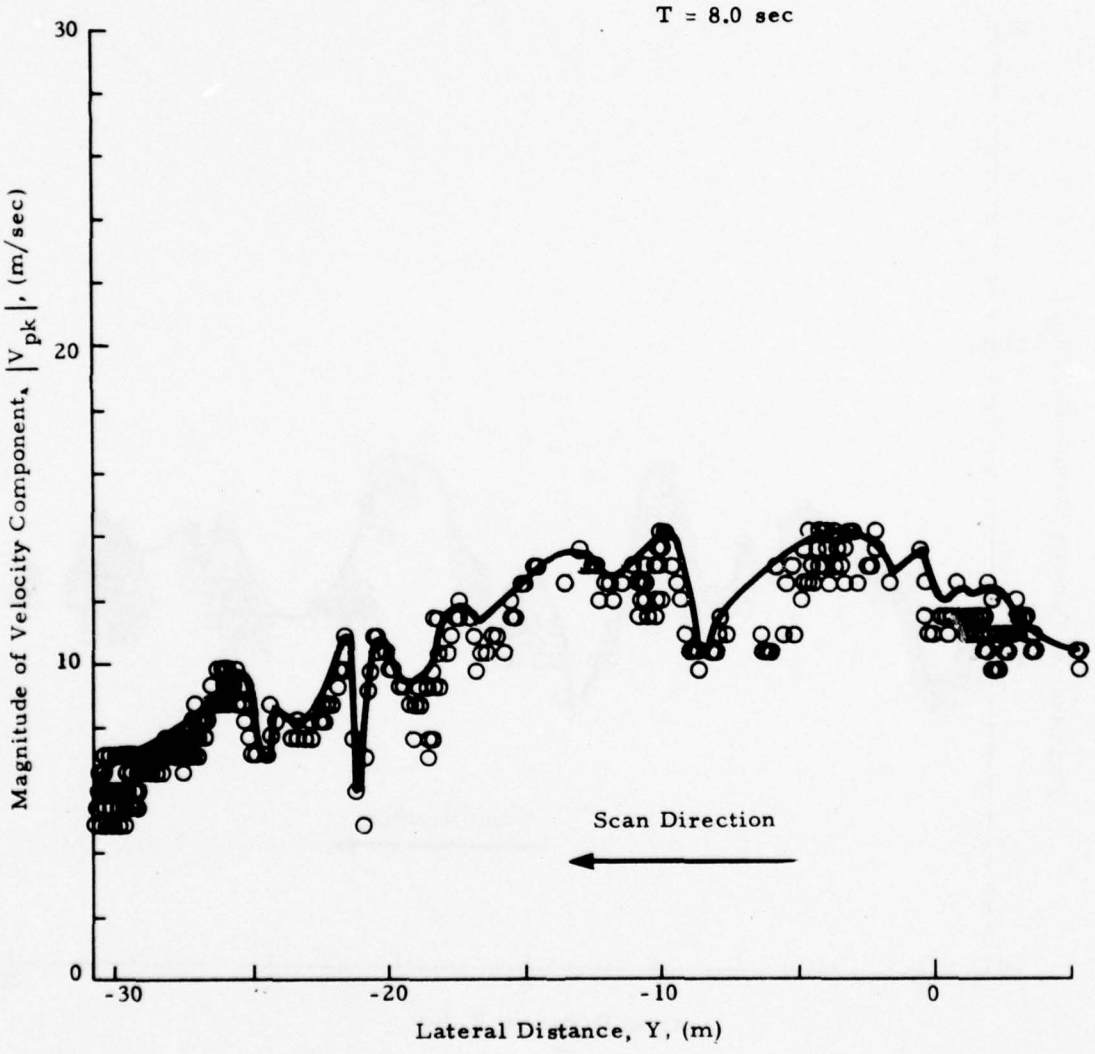

Fig. 16 (Concluded)

measurements, θ, where $y = -R \cos\theta$. This resulted in a nonlinear lateral scale at extended distances from the flight path centerline.

To illustrate the maximum downwash or upwash velocities in the aircraft near wake, the highest values of $|V_{pk}|$ occurring over 1 deg increments were faired by a smooth curve. The solid lines in the plots represent a faired curve through the highest LDV measurements given by the circles. Since the arc-scan measurements were made at an initial range equal or somewhat less than the airplane height, and since the maximum descent rate of the trailing vortices was on the order of 2 m/sec, the wake vortex remained essentially in the focal volume of the LDV system over the time period of 0 to 8 sec. Thus, the solid lines shown in Figs. 13 through 16 are indicative of the peak velocities observed with the LDV system in the aircraft near wake.

Available measurements of vortex lateral position obtained from a triangulation of simultaneous photographs or estimated from overhead photographs are also shown in Figs. 13, 14, and 15.

The spanwise downwash distribution for flyby 8, the 0-spoiler configuration, shows a well defined double-peak signature in most of the plots shown in Fig. 13 which is suggestive of a coherent vortex. For example, in Fig. 13 at t = 2.2 sec, two broad peaks are observed separated by a spacing of 0.76 wingspan. The lack of signature in the inboard regions may be attributed to the lack of high velocities or aerosols near the flight path centerline. The two broad peaks become more well defined at later times (t = 3.3 to 8.2 sec), showing a double-peak signature characteristic of the rotational velocity profile of a viscous vortex. The lateral separation and the maximum speed for the two double-peak signatures do not change significantly over this time range.

In contrast to the coherent wake structure observed earlier for the 0-spoiler configuration (Fig. 13), the downwash field for flybys 11, 12 and 13, where the two outer spoilers were deployed, shows a broad high amplitude region composed of narrower closely spaced peaks. This is suggestive of multiple

vortices and an incomplete vortex roll-up phase. These measurements indicate that the deployment of spoilers has a marked effect on the near-wake strucuture, tending to retard the early formation of a coherent trailing vortex pair. Analysis of the downwash field shown in Figs. 13 through 16 has been carried out to determine the basic characteristics of single and multiple vortices such as location, circulation strength, and the magnitude of the velocity component.

4.1.2 Vortex Pair Characteristics

For the 0-spoiler configuration, the spanwise downwash distribution in the wake shows a well defined double-peak signature (Fig. 13). A double-peak signature is predicted theoretically when a vortex pair is interrogated in the arc-scan mode. For example, the magnitude of the line-of-sight velocity component for Rosamond flyby 11 at $t \sim 2$ sec assuming a fully rolled-up vortex pair is shown in Fig. 17. The magnitude of the line-of-sight velocity generated by a distribution of N line vortices with the LDV located at the origin is given by

$$\left|V_{\ell os}\right| = \frac{1}{2\pi} \sum_{n=1}^{N} \Gamma_n \frac{\left[(Y_n - Y_o) X_o + (X_o - X_n) Y_o\right]}{\left[(X_o - X_n)^2 + (Y_o - Y_n)^2\right] \left[X_n^2 + Y_n^2\right]^{1/2}} \qquad (3)$$

where (X_o, Y_o) is the location of the centroid of the focal volume, and (X_n, Y_n) and Γ_n are the coordinate and circulation strength of the n^{th} vortex, respectively.

In Fig. 17, the magnitude of the computed line-of-sight velocity is shown for a pair of line vortices with spacing $b' = Kb = 41.8$ m and circulation strength $\Gamma = U_\infty \bar{c}\, C_L/2K = 606\ m^2/sec$ where the spanwise loading coefficient, wingspan, flight velocity, mean chord, and lift coefficient are taken to be $K = 0.7$, $b = 59.7$ m, $U = 72.5$ m/sec, $\bar{c} = 8.3$ m, $C_L = 1.41$. The vortex pair was assumed to be located at an altitude of 180 m and the selected arc scan range was 183 m. The magnitude of the computed line-of-sight velocity for the vortex pair shows the characteristic double peak signatures noted earlier in the LDV measurements. The magnitude of the peak velocity is determined by the separation distance between

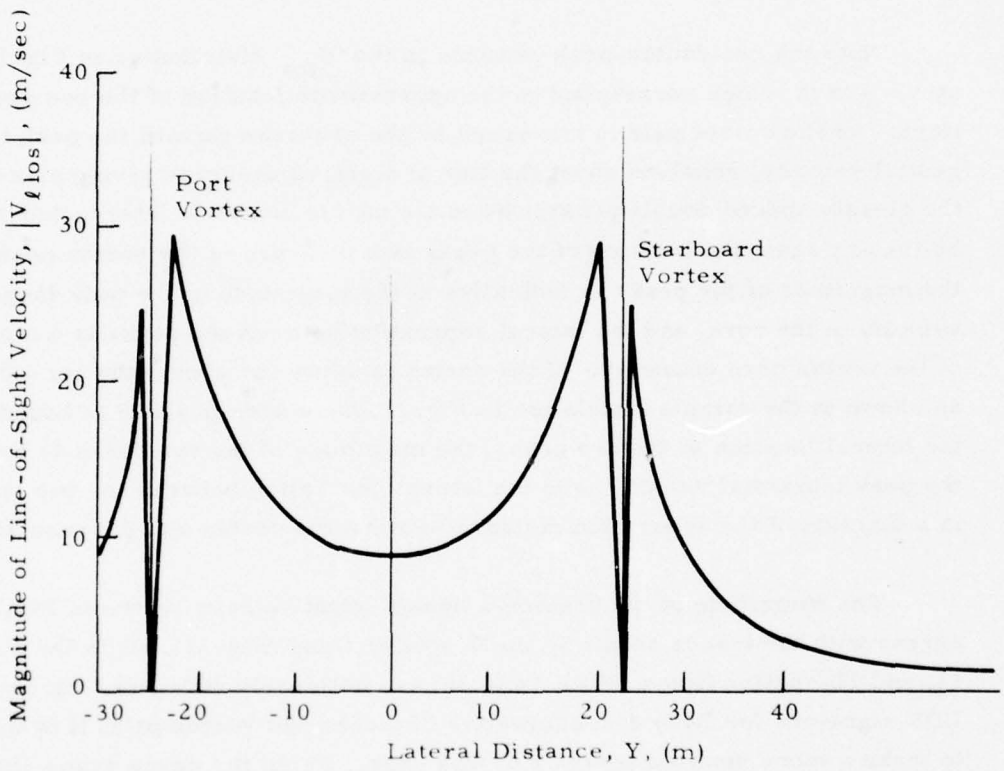

Fig. 17 - Magnitude of Line-of-Sight Velocity Component for Rosamond B-747 Flyby 11 at $t \sim 2$ sec, Computed Assuming a Fully Rolled-Up Vortex Pair

the vortex pair and the scan arc. The slight asymmetry in the double peaks results from the velocity contribution of the adjoining vortex, the scan geometry, and the decrease in the contribution of the vortex rotational velocity along the line of sight at extended lateral distances from the centerline.

Note the two double-peak patterns in the $V_{\ell os}$ distribution in Fig. 17 at $y = \pm 23$ m which correspond to the approximate location of the two vortices. As the vortex pair is traversed by the arc-scan pattern, the peak tangential velocity, resolved about the line of sight, is observed giving rise to the closely spaced double peaks. When the vortex center is intersected exactly by the arc scan, the location of the peaks is a measure of the vortex position, the magnitude of the peaks is indicative of the magnitude of the peak tangential velocity in the core, and the lateral separation between the peaks is a measure of the vortex core diameter. If the vortex is below (or above) the arc-scan, as shown in the sample simulation in Fig. 17, the vortex position is bounded by the lateral location of the two peaks, the magnitude of the two peaks is less than the peak tangential velocity, and the lateral separation between the two peaks is a function of the separation distance between the vortex and the scan arc.

The magnitude of the predicted line-of-sight velocity shown in Fig. 17 agrees with the trends shown by the 0-spoiler flyby (Fig. 13), while the 1, 2, 11, and 12-spoiler flybys (Figs. 14 to 16) are noticeably different. Since the LDV signature for flyby 8 is suggestive of a coherent vortex pair, it is useful to make a more detailed analysis of this case. From the seven scans shown in Fig. 13 the earliest scan showing the two double peak signatures was selected ($t = 3.3$ sec); the minimum points were used to determine the lateral position of the port vortex (vortex altitude was assumed to be the scan range $R = 240$ m), and the peak velocity magnitudes observed by the LDV for the port vortex were plotted as a function of radius about the vortex center in Fig. 18. For comparison, the magnitude of the velocity for a potential line vortex and a turbulent viscous vortex are also shown in Fig. 18 matched to the experimentally measured core circulation and core velocity.

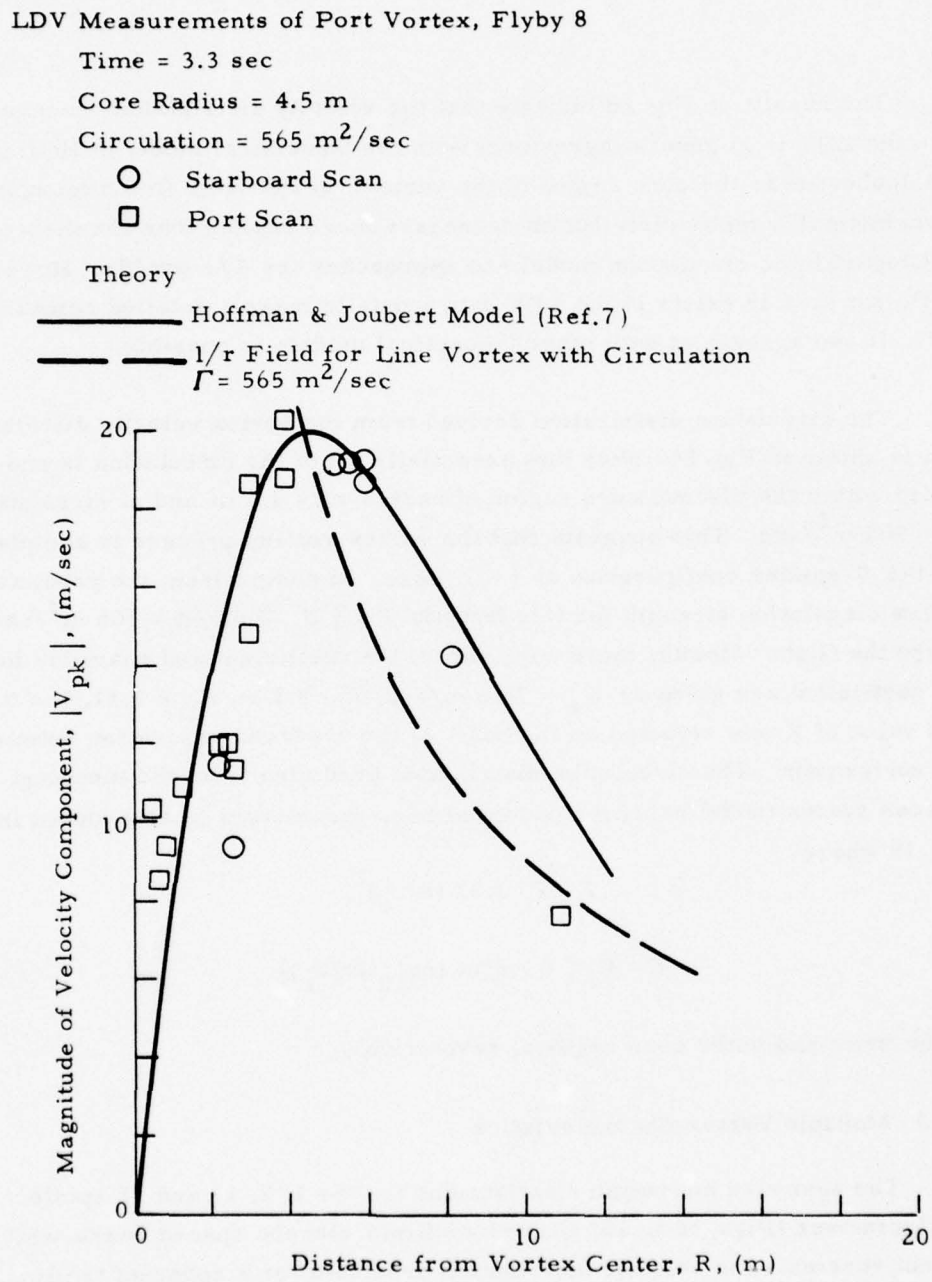

Fig. 18 - Magnitude of Wake Vortex Velocity Distribution with 0 Spoilers

The results in Fig. 18 indicate that the velocity distribution observed with the LDV is in general agreement with the theoretical model of Hoffman and Joubert near the core region of the vortex. In the outer flow region, the experimental velocity distribution decreases more rapidly than the theoretical logarithmic circulation model and approaches the 1/r profile. However, sufficient scatter exists in the LDV data points to make a detailed comparison difficult, and agreement with other theoretical models is possible.

The circulation distribution derived from the vortex velocity distribution is shown in Fig. 19. Note that essentially all of the circulation is contained within the viscous core region of radius $r_c = 4.5$ m and of circulation $\Gamma_c = 565\ m^2/sec$. This suggests that the vortex roll-up process is complete for the 0-spoiler configuration at t = 3.3 sec. In comparison, the predicted vortex circulation strength for this flyby is $\Gamma = \frac{1}{2} U_\infty \bar{c}\, C_L/K = 565\ m^2/sec$, where the flight velocity, mean wing chord, lift coefficient and spanwise loading coefficient, are given by $U_\infty = 73.6$ m/sec, $\bar{c} = 8.3$ m, $C_L = 1.41$, $K = 0.762$. The value of K was selected on the basis of the observed separation between the vortex pair. The circulation distribution predicted from the turbulent viscous vortex model using the observed core parameters is also shown in Fig. 19 where

$$\Gamma = \Gamma_c\ 1.83\ (r/r_c)^2,$$

$$\Gamma = \Gamma_c\ [1 + 2.14 \log_{10} (r/r_c)],$$

in the inner and outer core regions, respectively.

4.1.3 Multiple Vortex Characteristics

The spanwise downwash distributions for the 1, 2, 11, and 12-spoiler configurations (Figs. 14 to 16) showed multiple closely spaced peaks which did not resemble the velocity distribution predicted for a coherent trailing vortex pair (Fig. 17). Since the multiple high-velocity peaks in the near-wake downwash field are found in multiple vortex wakes; and the 1, 2, 11, and 12-spoiler configurations (flybys 11, 12, and 13) have been analyzed to identify possible multiple vortex characteristics.

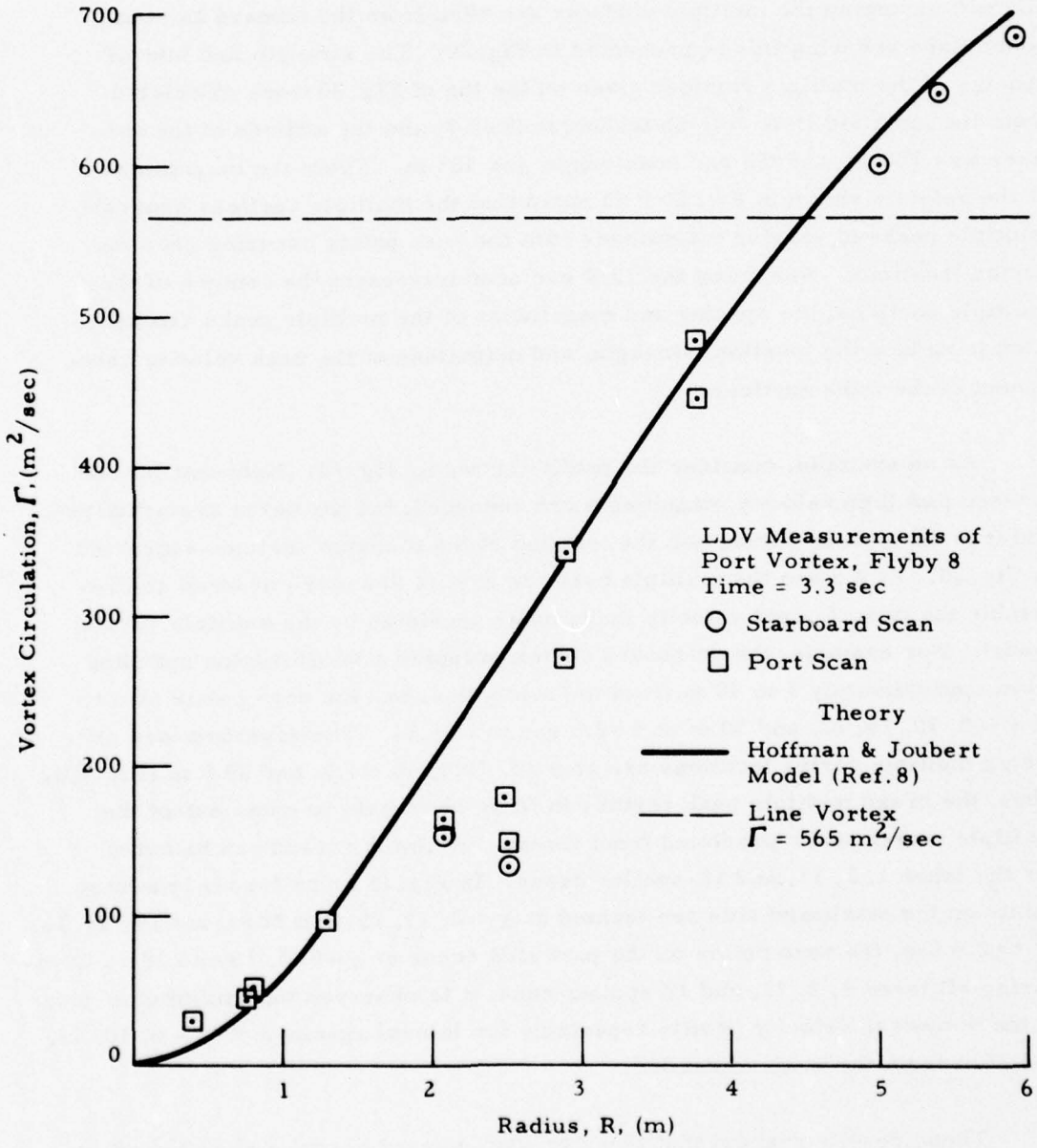

Fig. 19 - Circulation as a Function of Radius for 0 Spoiler Flight Configuration

The magnitude line-of-sight velocity component predicted for a B-747 aircraft assuming the multiple vortices are shed from the inboard and outboard flaps and wing tips is presented in Fig. 20. The strength and lateral spacing of the multiple vortices given on the top of Fig. 20 were calculated from the modified Betz roll-up technique (Ref. 9) and the altitude of the vortices was 180 m, and the arc scan range was 183 m. From the magnitudes of the velocity shown in Fig. 20 it is noted that the multiple vortices generate multiple peaks of varying magnitudes with the zero points occuring near the vortex locations. Assuming the LDV arc scan intersects the centers of the multiple vortices, the spacing and magnitudes of the multiple peaks can be used to deduce the location, strength, and magnitude of the peak velocity component of the wake vortices.

As an example, consider the profile shown in Fig. 14. Note that for the 1.5-sec plot high velocity magnitudes are recorded, but the peaks are scattered and it is difficult to distinguish the location of the multiple vortices suggested in Fig. 20. At 2.6 sec the multiple peaks in Fig. 14 are more ordered and resemble the line-of-sight velocity magnitudes predicted by the multiple vortex model. For example, the starboard vortex occupies a broad region spanning from approximately 3 to 40 m from the centerline, and the zero points occur at $y \sim 0$, 10, 15, 22, and 30 m at $t = 2.6$ sec in Fig. 14, The superimposed predicted multiple vortex locations are at $y = 3$, 10.4, 14, 21.3, and 29.6 m (Fig. 20). Thus, the broad multiple peak regions in flyby 11 contain to some extent the multiple vortex peaks predicted from theory. A similar trend can be noted for the other 1, 2, 11, and 12-spoiler cases. In Fig. 15 at $t = 2.4$ sec, the zero points on the starboard side are located at $y \sim 0$, 17, 25, and 32 m, and in Fig. 18 at $t = 2.9$ sec, the zero points on the port side occur at $y \sim 0$, 5, 10 and 18 m. Comparing all three 1, 2, 11, and 12 spoiler runs, it is observed that minimums occur in the downwash velocity profile repeatedly for lateral spacings of $y \sim 0$, 10, 15, and 25 m from the wake centerline.

These results suggest that three or four merged vortices are present in the near wake for each semispan. A more detailed analysis of the LDV measurements may establish the strength and core radii of these vortices.

Γ_1 = 62.3 m^2/sec, Γ_2 = 433.5 m^2/sec, Γ_3 = -158.4 m^2/sec, Γ_4 = 298 m^2/sec, Γ_5 = -16.2 m^2/sec
Γ_6 = -62.3 m^2/sec, Γ_7 = -433.5 m^2/sec, Γ_8 = 158.4 m^2/sec, Γ_9 = -298 m^2/sec, Γ_{10} = 16.2 m^2/sec
y_1 = 29.6 m, x_i = 180 m, y_2 = 21.3 m, x_2 = 180 m, y_3 = 14 m, x_3 = 180 m, y_4 = 10.4 m, x_4 = 180 m,
y_5 = 3 m, x_5 = 180 m, y_6 = -29.6 m, x_6 = 180 m, y_7 = -21.3 m, x_7 = 180 m, y_8 = -14 m, x_8 = 180 m,
y_9 = -10.4 m, x_9 = 180 m, y_{10} = -3 m, x_{10} = 180 m
(Subscripts 1-5 Starboard Vortices, 6-10 Port Vortices)

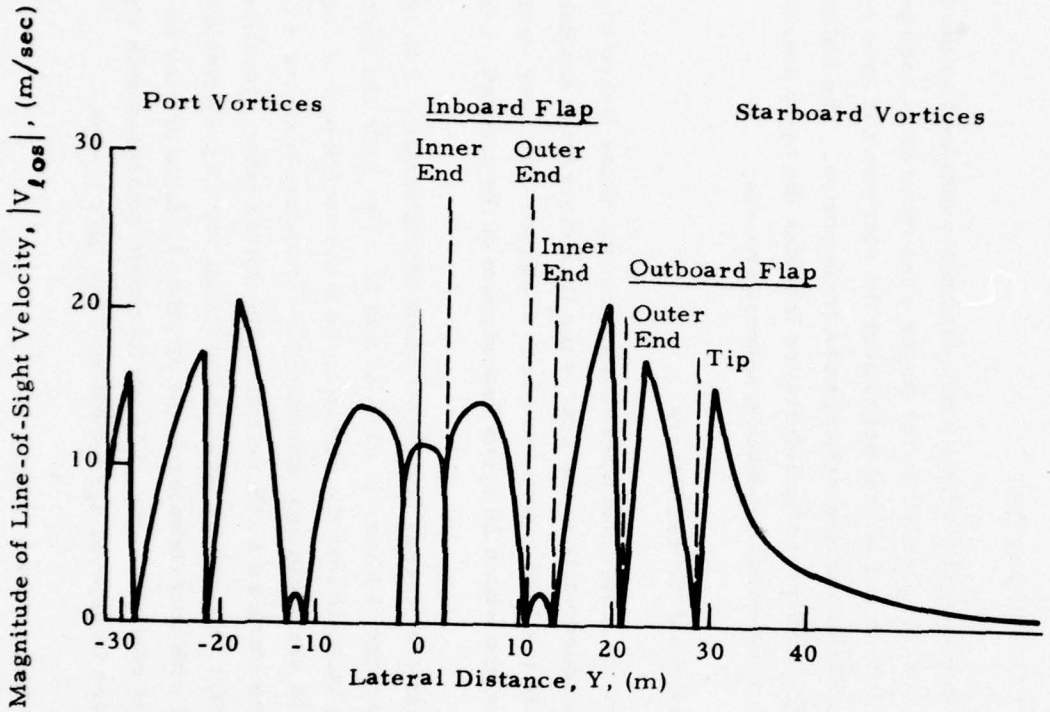

Fig. 20 - Magnitude of Line-of-Sight Velocity Component for Rosamond B-747 Flyby 11 at t~ 2 sec, Computed Assuming Multiple Wake Vortices

However, the LDV measurements have shown that multiple vortices exist in the near wake of the B-747 aircraft when spoilers are deployed, whereas a coherent rolled-up trailing vortex pair exists in the near wake for 0 spoilers.

4.2 VORTEX TRANSPORT

The line-of-sight velocity measurements obtained by the LDV in the wake of the B-747 aircraft in the finger-scan mode have been processed to yield the altitude and lateral position of the vortices, and have been compared with photographic and theoretical wake trajectories. The following analysis of the vortex transport characteristics includes the early near-wake flow as well as the subsequent far-wake transport process.

4.2.1 Near-Wake Vortex Tracks

From the Rosamond wake measurements, those flybys where photographic measurements of the near-wake trajectory were available for comparison with the LDV tracks have been selected. The near wake was assumed to be the region within 20 spans downstream of the aircraft, $x/b \leq 20$.

The lateral versus horizontal wake vortex location 5 to 10 sec after aircraft passage is shown in Figs. 21 and 22. The LDV and photographic measurements indicate that the center of the wake vortex pair is located at approximately 80% semispan and descends at ~ 1.5 m/sec over the 4 to 10 sec interval. However, as much as a 15% scatter in the vortex lateral location and 50% scatter in the descent rate can be noted in the initial vortex trajectories which may be associated with uncertainties in the airplane location or may be due to the different flight configurations. The photographic measurements shown in Figs. 21 and 22 are in general agreement with the LDV trends.

4.2.2 Far Wake Vortex Tracks

The line-of-sight velocity measurements obtained with the LDV system in the finger-scan mode have been processed with the VAD and Vortex Track Program and the I_{pk} program to determine the far-wake vortex trajectories.

Solid Symbols Photo, Open
Symbols LDV Measurements

Flyby	Aircraft Alt. (m)
○ 27	67
◇ 28	66
△ 30	66

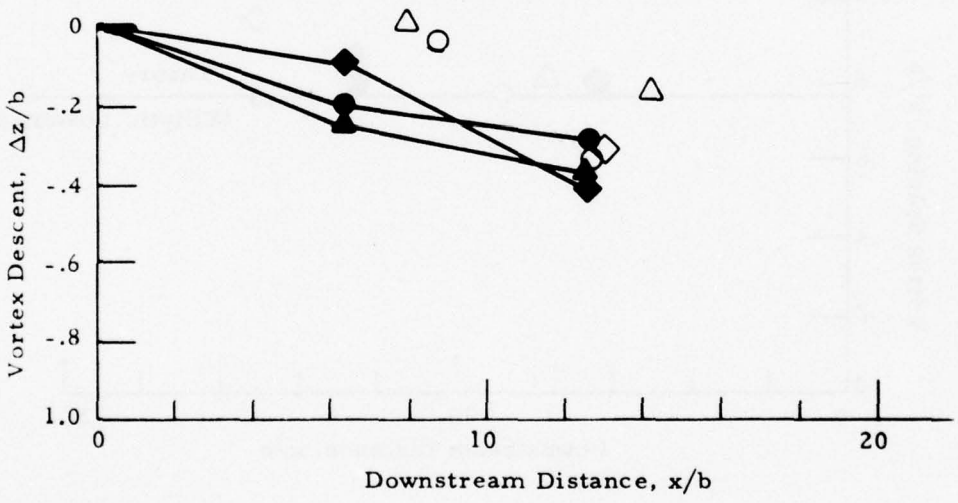

Fig. 21 - Vortex Descent as a Function of Downstream Distance for Flybys with 30/30 Flaps, 0 Spoilers

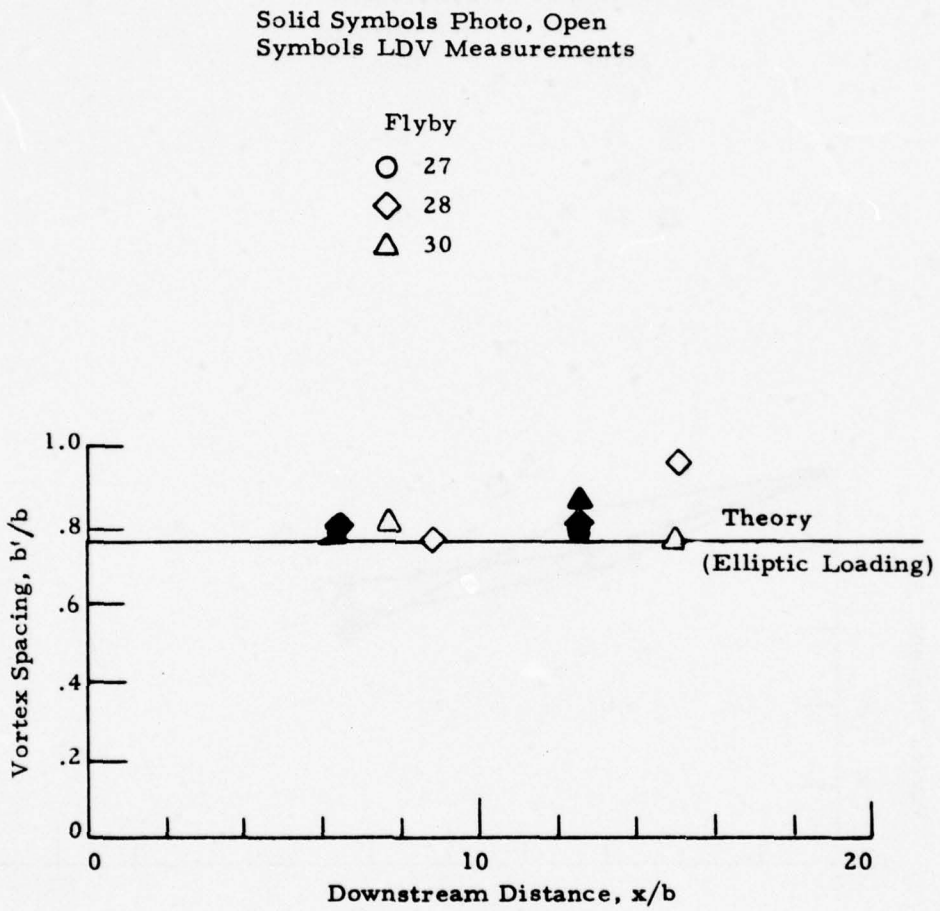

Fig. 22 - Vortex Spacing as a Function of Downstream Distance for Flybys with 30/30 Flaps, 0 Spoilers

The regions of the maximum backscatter intensity were used to locate the vortex core region. The wake vortex tracks from the Rosamond tests include the results from the low-speed data and high-speed data.

4.2.2.1 Low-Speed Data

The wake vortex trajectories from the low-speed LDV measurements are presented in Appendix D. From the wake vortex trajectories presented in Appendix D, the following wake transport characteristics can be noted: (1) the wake vortex descends nearly vertically with very little horizontal motion; (2) the initial descent rate over the period 0 through 20 sec after aircraft passage is in general agreement with the prediction; and (3) the wake descent diminishes after 20 sec and the vortex tends to remain at a constant altitude in ground effect. In addition to the above trends, some scatter is noted in the location of the vortices. Since both the photographic and LDV tracks show the vortex wandering in lateral position and altitude, particularly at late times, this is believed to be the effect of random atmospheric winds and gusts. However, in some cases, a large scatter is noted in the LDV vortex tracks which is not seen in the corresponding photographic measurements. This has been investigated using the high-speed data since accurate determination of the vortex position is a prerequisite in determining other relevant parameters such as the decay of the vortex rotational velocity and circulation strength.

4.2.2.2 High-Speed Data

The wake vortex tracks computed from the high-speed LDV data using the I_{pk} algorithm are given in Appendix E for flybys 27, 28, 44, 47, 48, and 49. The vertical and lateral vortex trajectories computed from the high-speed data show the same trends as the low-speed tracks discussed earlier.

Comparison of the high-speed wake vortex measurements with the observed photographic vortex position is shown in the V_{pk} versus elevation angle curves in Figs. 23 and 24. With the exception of any dominant low

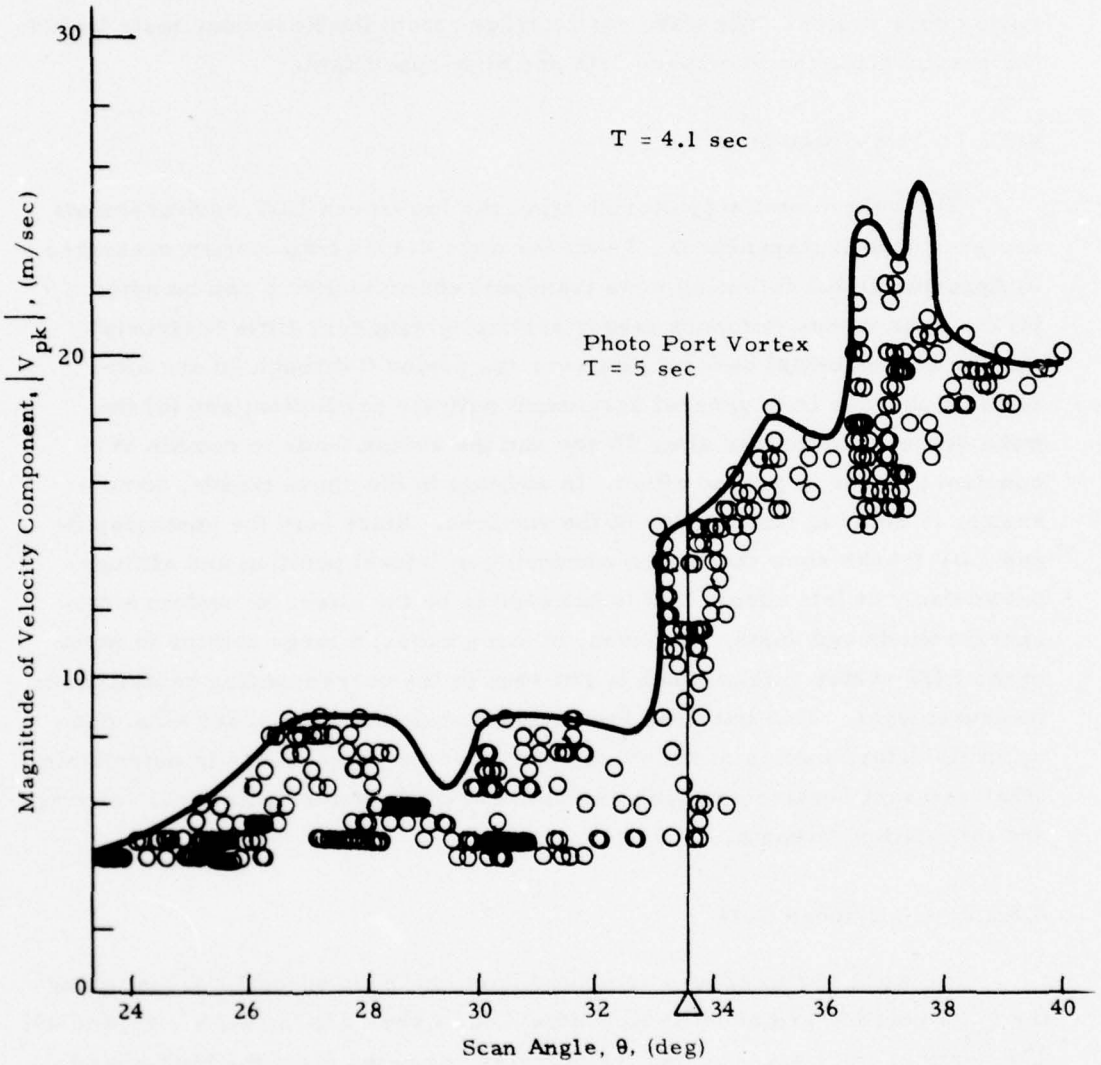

Fig. 23 - Comparison of Photographic and LDV Measurements for Rosamond B-747 Flyby 27

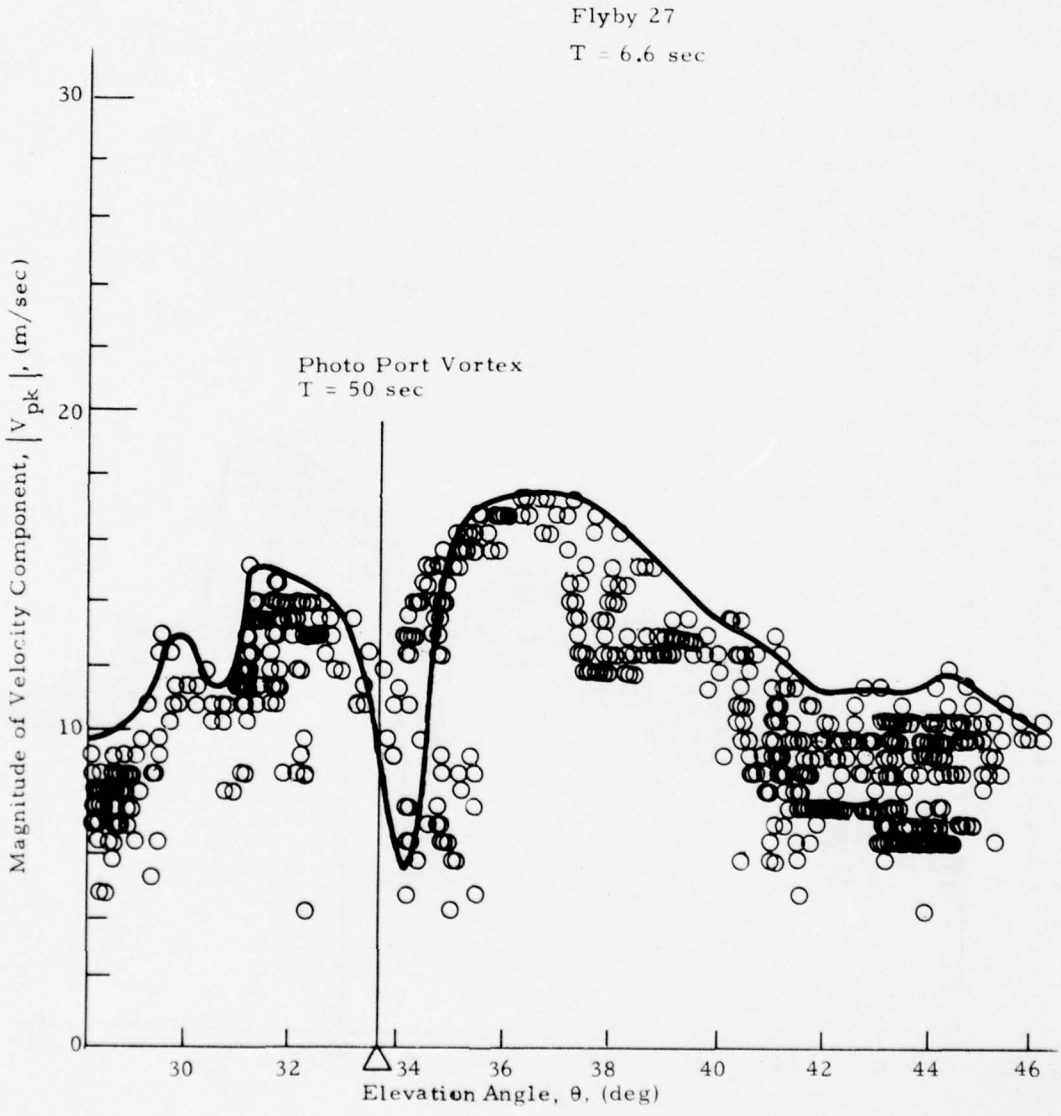

Fig. 23 (Continued)

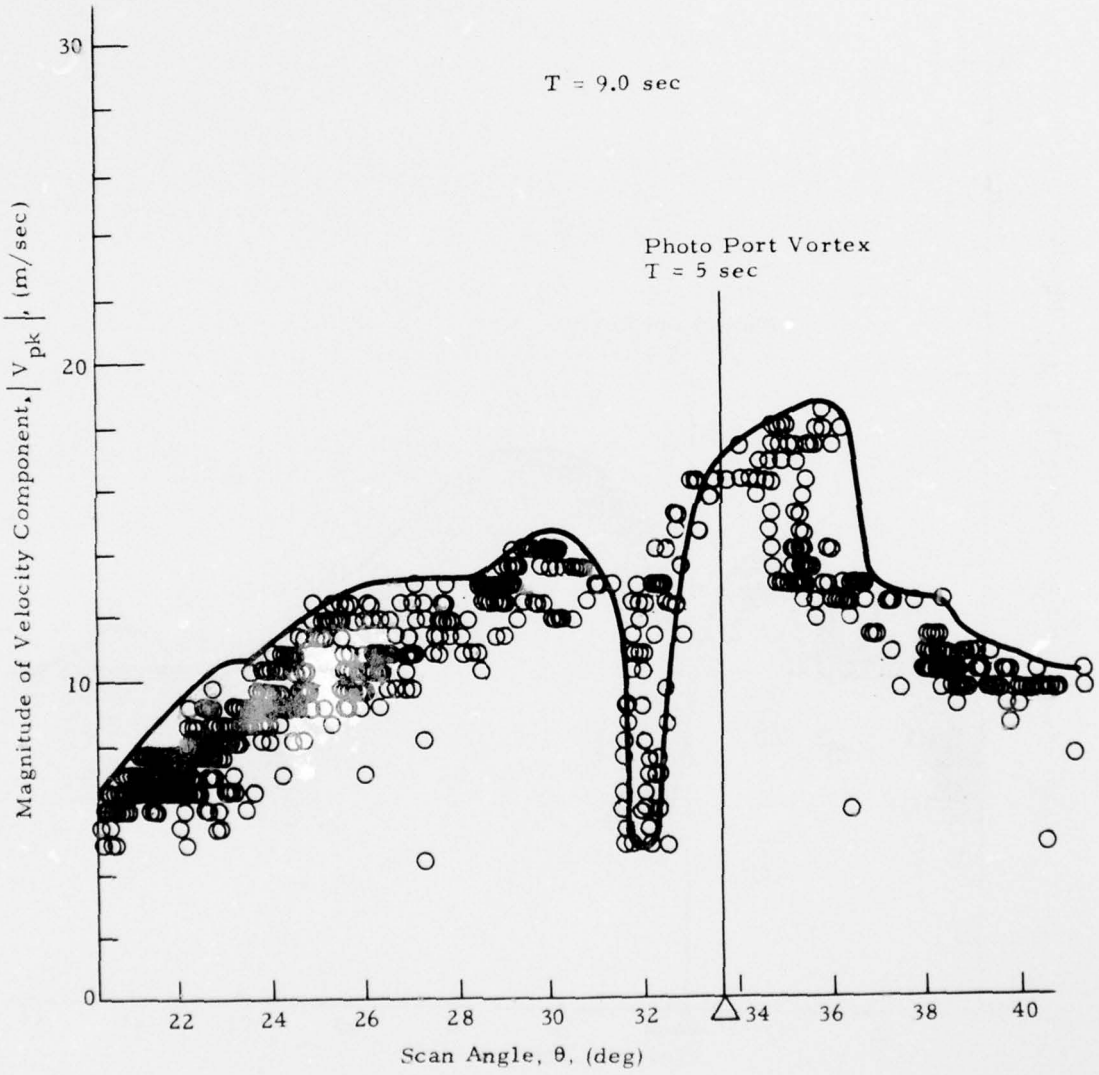

Fig. 23 (Continued)

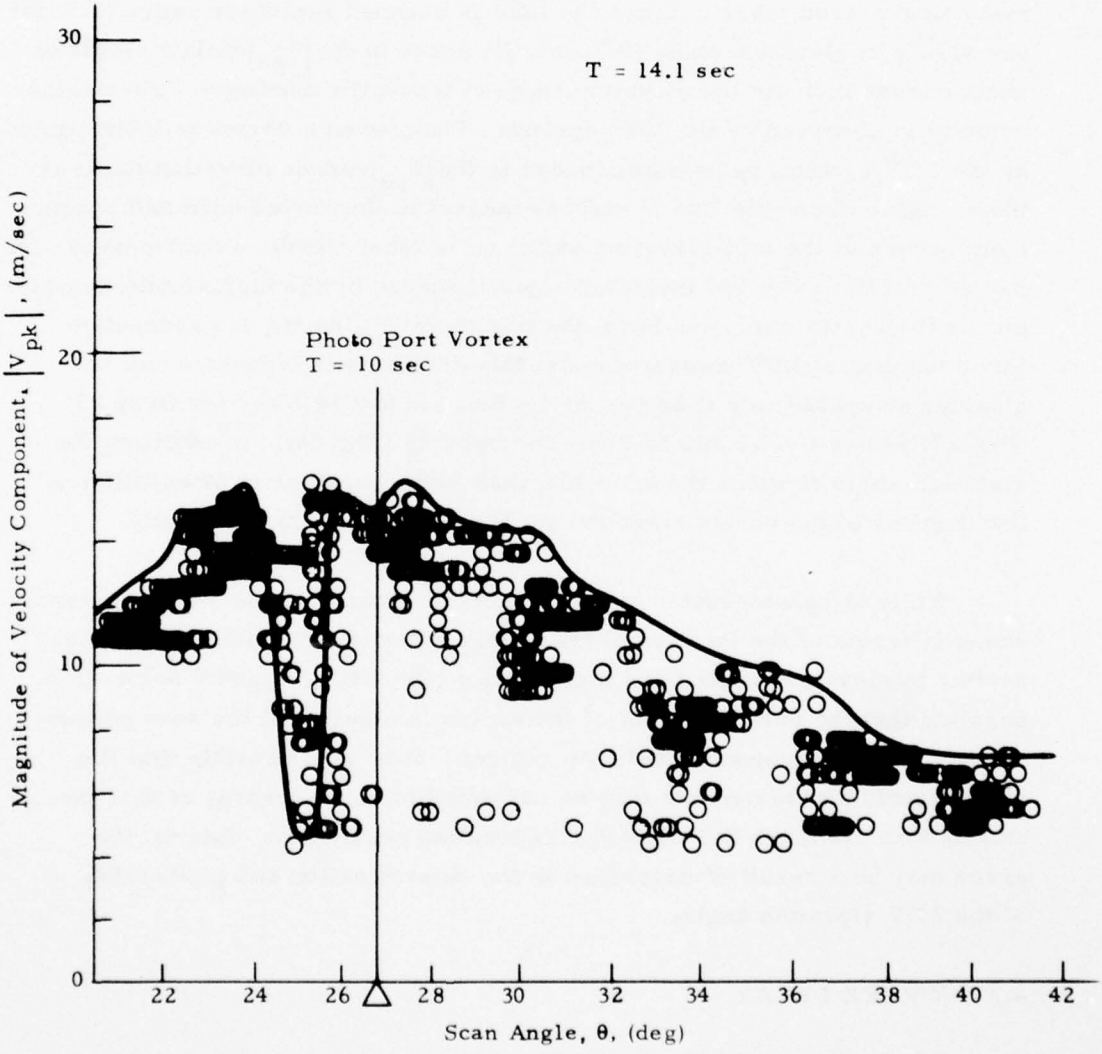

Fig. 23 (Concluded)

magnitude spikes, the solid line in the plots connects the maximum values of $|V_{pk}|$ observed by the LDV in the finger scan mode for one scan between the two elevation angle limits (i.e., it represents the maximum value of $|V_{pk}|$ for many finger-scan lobes). Since the LDV is scanned rapidly in range (3.5 Hz) and slowly in elevation angle (0.2 Hz), the peaks in the $|V_{pk}|$ versus elevation-angle curves indicate the elevation angle at which the maximum line-of-sight velocity is observed by the LDV system. Thus, when a vortex is interrogated by the LDV system, two maxima occur in the $|V_{pk}|$ versus elevation angle at those angles where the line of sight is tangent to the vortex core and a minimum occurs at the mid-elevation angle, or in other words, a double-peak signature results. The low magnitude spike bounded by the high amplitude peaks marks the vortex core, and here, the minimum $|V_{pk}|$ points are connected. For a number of LDV measurements, this double-peak signature can be clearly recognized; for example, at t = 6.6, 9.0 and 14.1 sec for flyby 23 (Fig. 27) and at t = 4.2 and 14.2 sec for flyby 28 (Fig. 24). In addition, the elevation angle at which these double-peak patterns occur is often within a few degrees of the vortex elevation angle measured photographically.

While the photographic and LDV measurements agree well for some scans in terms of the location of the vortex signature, for other scans, the scatter in elevation angle is as high a 6 deg (Fig. 24, t = 5 and 9 sec). It is possible that the core diameter of the vortex is small, and the scan pattern misses the peak-tangential velocity regions. It is also possible that the photographic measurements may be subjected to some errors, or that the smoke does not mark the exact vortex location accurately. Lastly, the error may be a result of anomalies in the determination and processing of the LDV elevation angle.

4.3 VORTEX DECAY

Information regarding the decay of wake vortices such as the time history of the peak tangential velocity, circulation and viscous core radius is contained in the line-of-sight velocity magnitudes measured by the LDV system.

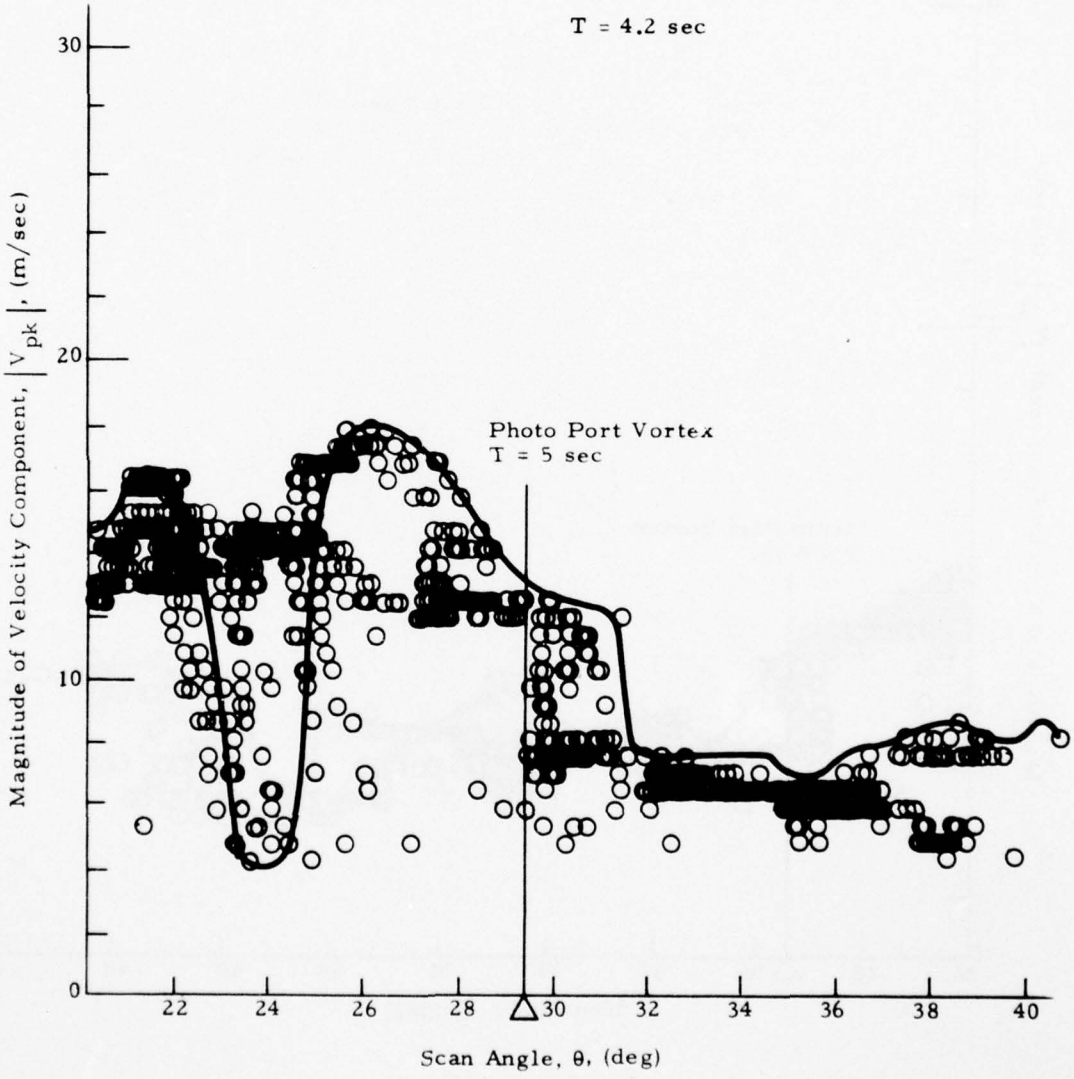

Fig. 24 - Comparison of Photographic and LDV Measurements for Rosamond B-747 Flyby 28

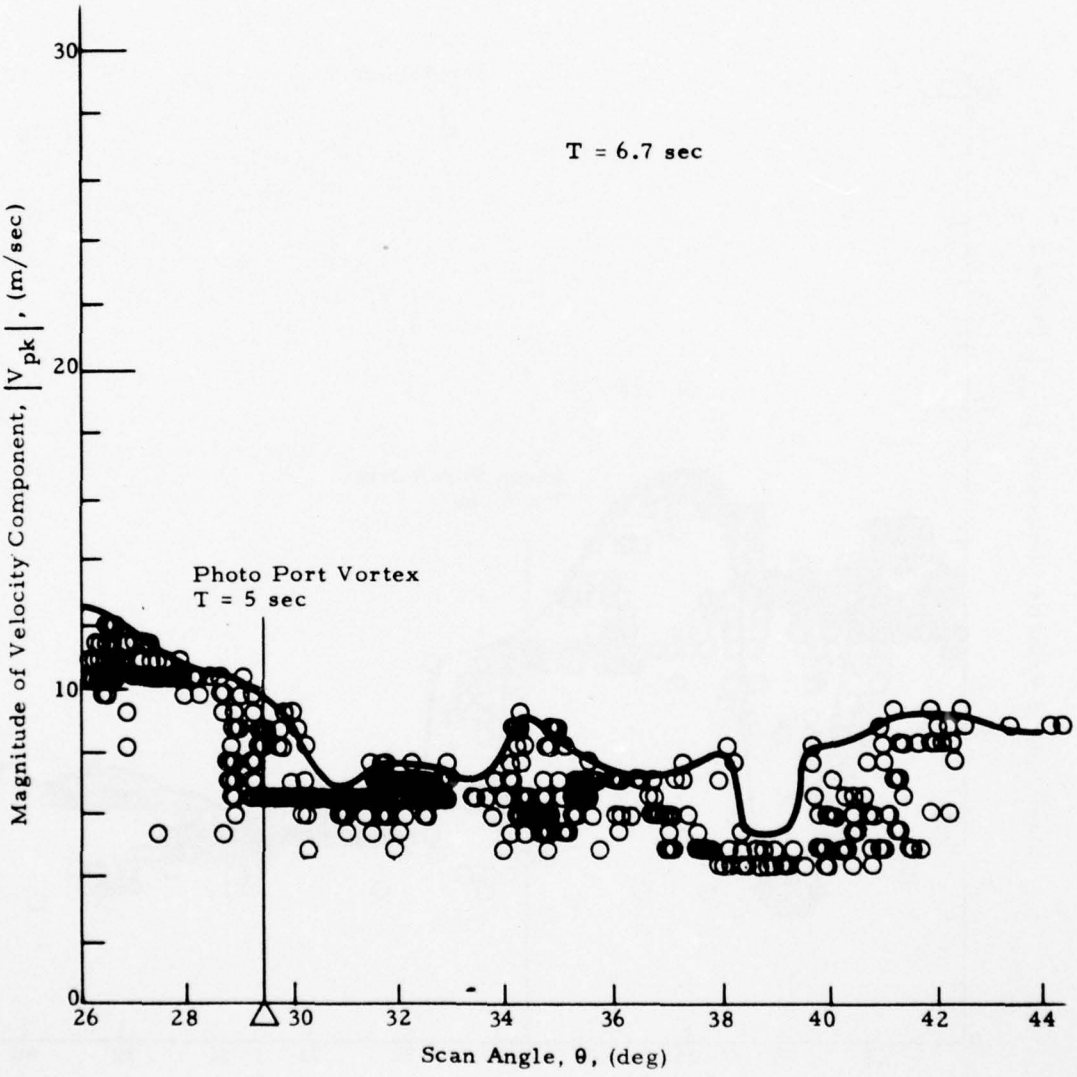

Fig. 24 (Continued)

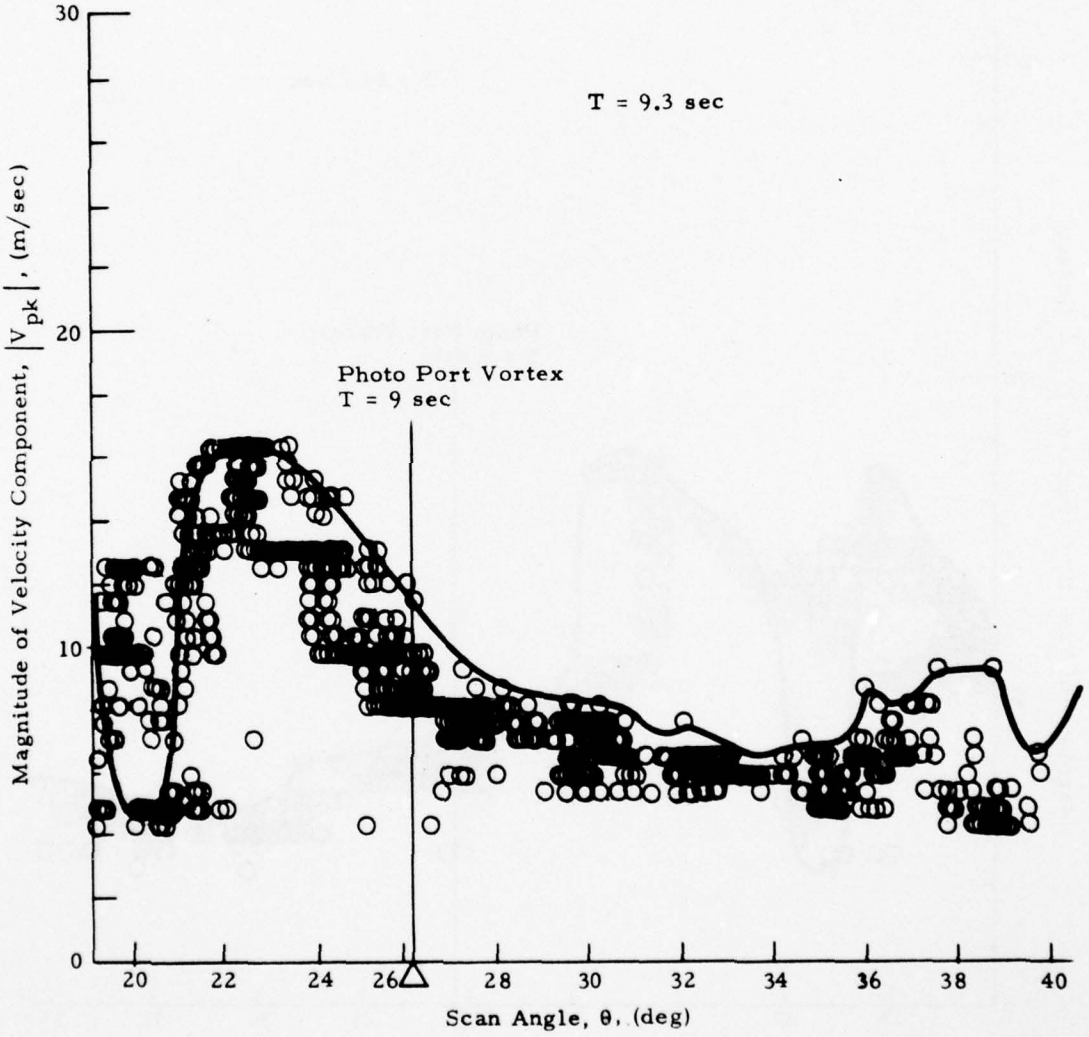

Fig. 24 (Continued)

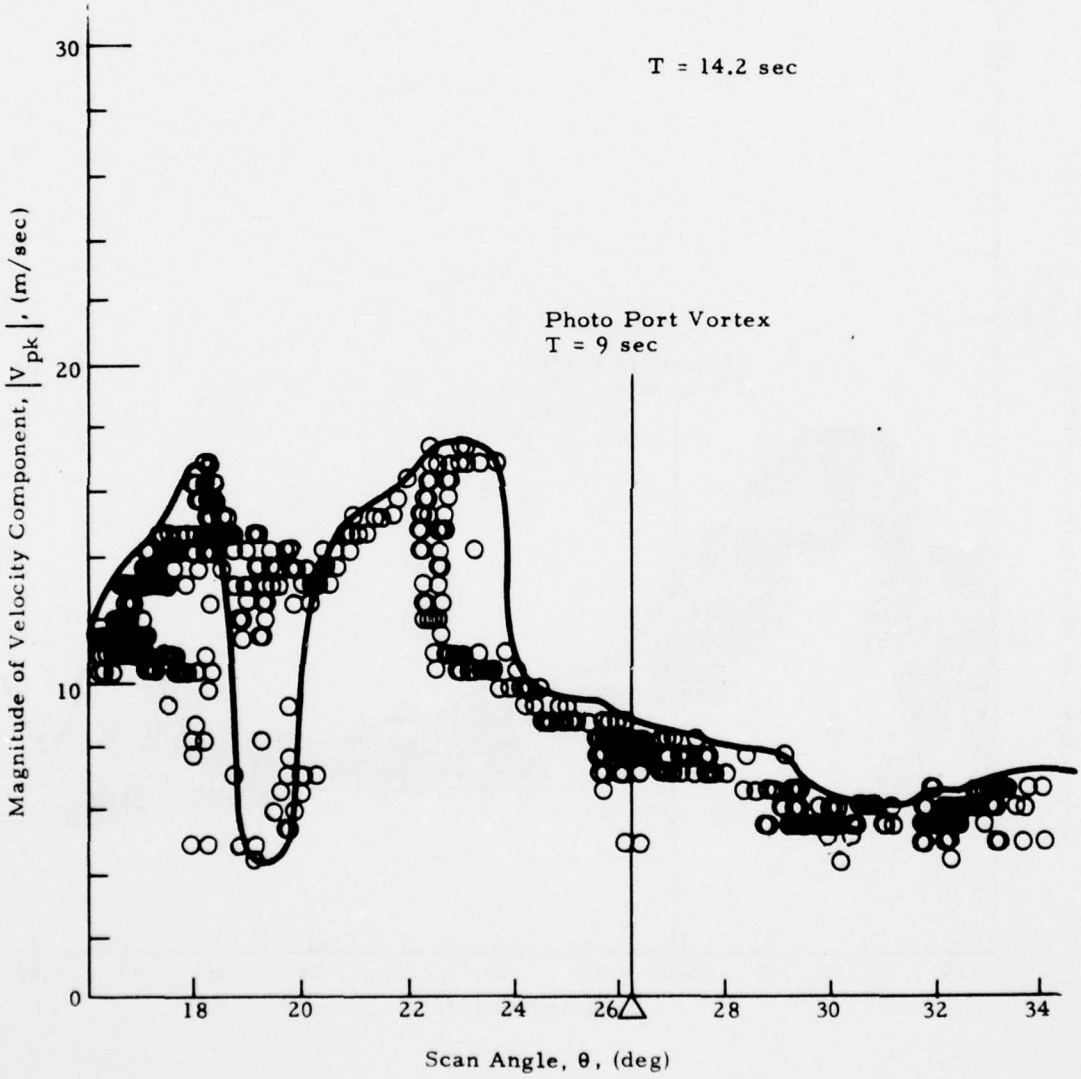

Fig. 24 (Concluded)

4.3.1 Decay of Vortex Rotational Velocity

To determine the decay of the wake vortex rotational velocity from the LDV line-of-sight velocity magnitudes, two basic methods were used to pick out the maximum tangential velocity of the vortex:

a. Selection of the maximum value of $|V_{pk}|$ (or $|V_{ms}|$) occurring during each scan between minimum and maximum elevation settings.

b. Selection of the maximum value of $|V_{pk}|$ occurring within ± 3 deg of the known elevation angle of the vortex.

For both techniques, the maximum value of $|V_{pk}|$ is a good measure of the magnitude of the peak tangential velocity of the vortex if the LDV line of sight is tangent at some point with the circular core region of the vortex, and the vortex range falls within the focal volume. However, in the first approach, the $|V_{pk}|$ time history becomes meaningless if the vortex drifts out of the scan area. To eliminate this uncertainty, in the second approach, other information, i.e., photographic vortex position, is used to establish the approximate location of the vortices. These regions are then searched for the maximum $|V_{pk}|$ values which are associated with the vortex phenomena.

The $|V_{pk}|$ and $|V_{ms}|$ time histories determined using the first technique are shown in Appendix F. A bandwidth criterion of $N \geq 2$ was used in the analysis to filter out random high-frequency noise (i.e., at least two of the 100 frequency bins had to be activated for the data to be used). A sample of the results, presented in Fig. 25, indicates that the wake vortex rotational velocity is nearly constant approximately 50 spans downstream of the aircraft followed by 1/time decay. Some scatter which may be associated with the uncertainty in vortex location may be noted in the velocity decay curve.

Using the photographic vortex tracks to determine the approximate vortex location (the second technique above), the $|V_{pk}|$ time history has been

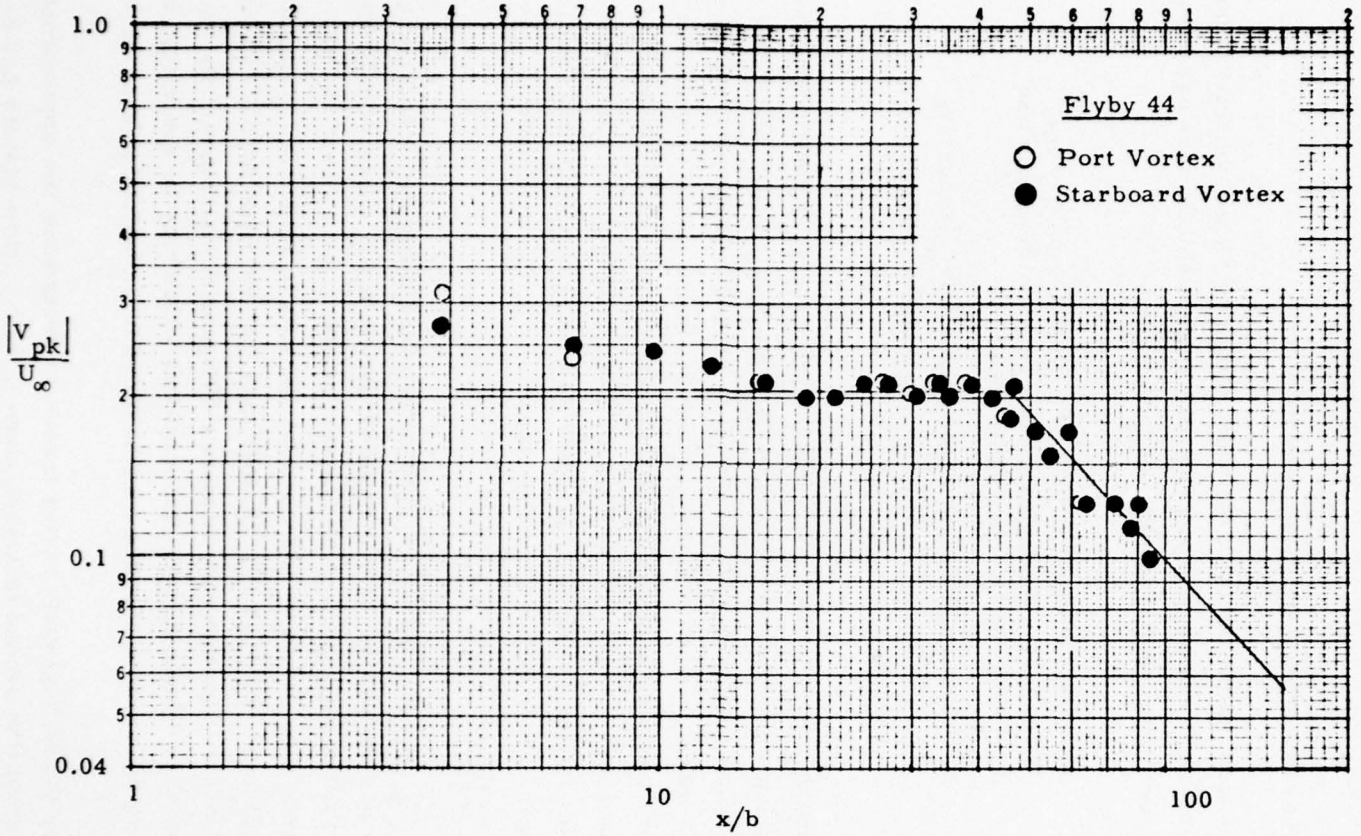

Fig. 25 - Decay of Magnitude of Wake Vortex Rotational Velocity Component for Flyby 44

recomputed for flybys 27 and 28 and is presented in Figs. 26 and 27. The results shown in Figs. 26 and 27 also indicate a nearly constant magnitude of the vortex velocity component within 50 spans downstream of the aircraft. Less scatter occurs in $|V_{pk}|$ versus time plots when the photographic tracks are used to establish the vortex center. Unfortunately, photographic measurements were not available at late times to establish the final vortex decay process.

4.3.2 Core Radius Time History

The vortex core radius was determined from the observed variations in $|V_{pk}|$ with range and elevation angle according to the technique discussed earlier in Section 2.1.2. The computed vortex core radius time history for flybys 27, 28, and 44 is given in Figs. 28, 29, and 30, respectively. Photographic vortex tracks were compared with LDV $|V_{pk}|$ distributions to compute the core radius time history in Figs. 28 and 29, while the predicted vortex tracks were used to compute the core radius time history in Fig. 30. The LDV wake vortex measurements show that the vortex core radius is approximately constant in the aircraft near wake. The observed core radius ranges from 1 to 4 m, and the mean core radius is approximately 2 m.

4.3.3 Circulation Decay

The circulation time history was computed from the observed LDV line-of-sight velocity distribution using: (1) the vortex tracks from the low-speed data, and (2) the photographic tracks to determine the vortex location. In the first technique, the circulation was determined from the average moment of the line-of-sight velocity components within a correlation radius of the computer vortex center. In the second technique, the circulation was computed from the moment of the two maximum $|V_{pk}|$ values adjacent to the center of the vortex as outlined earlier in Section 2.1.2, and the photographic vortex tracks were used to determine the vortex location. It was found that this technique was very sensitive to errors in core radius.

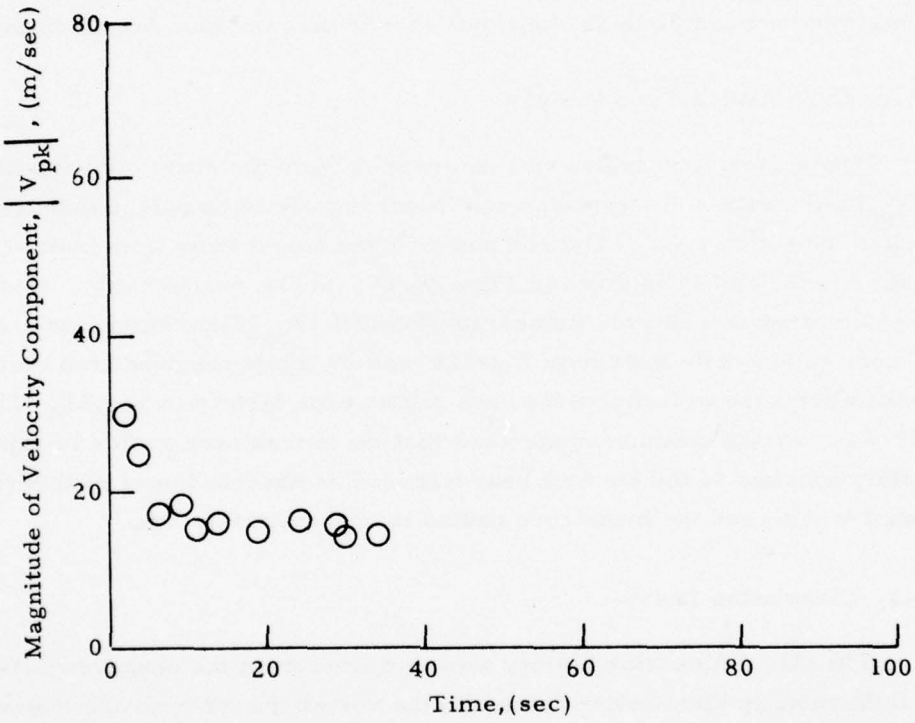

Fig. 26 - $|V_{pk}|$ as a Function of Time for Flyby 27 Using Photographic Tracks to Locate the Vortex Center

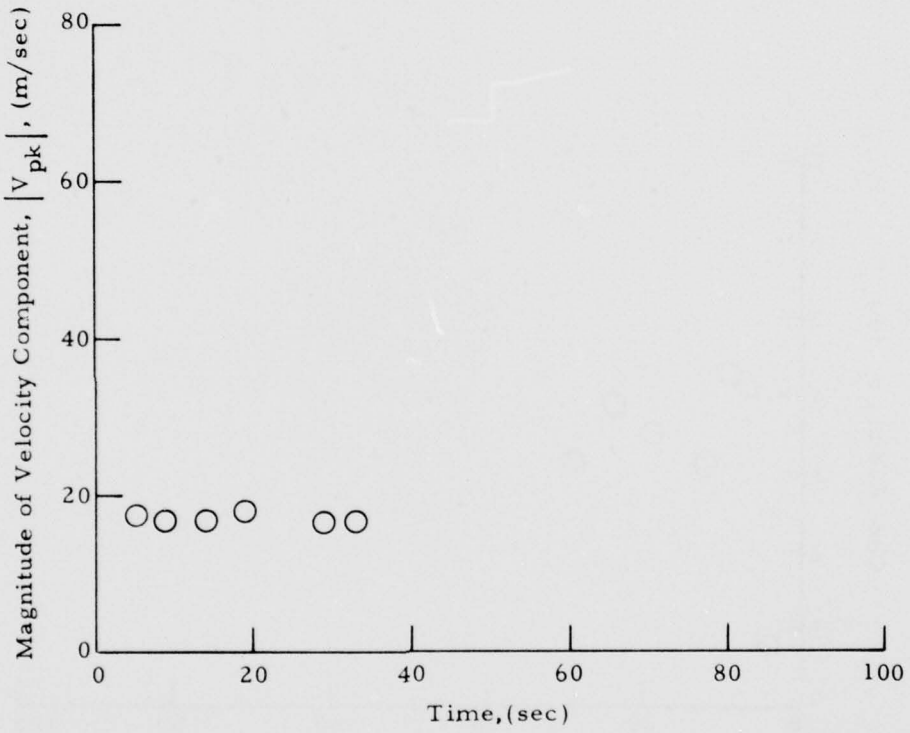

Fig. 27 - $|V_{pk}|$ as a Function of Time for Flyby 28 Using Photographic Tracks to Locate the Vortex Center

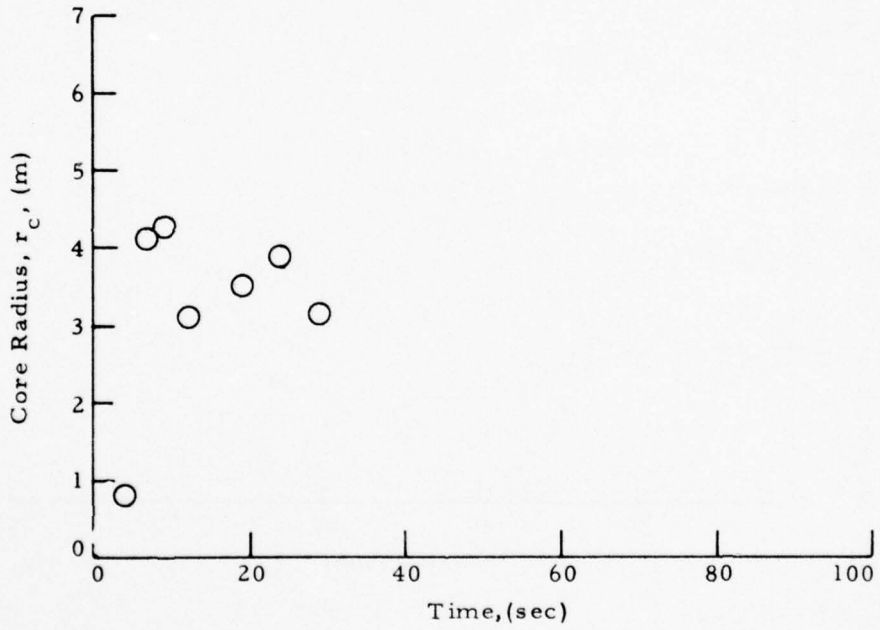

Fig. 28 - Vortex Core Radius as a Function of Time for Flyby 27

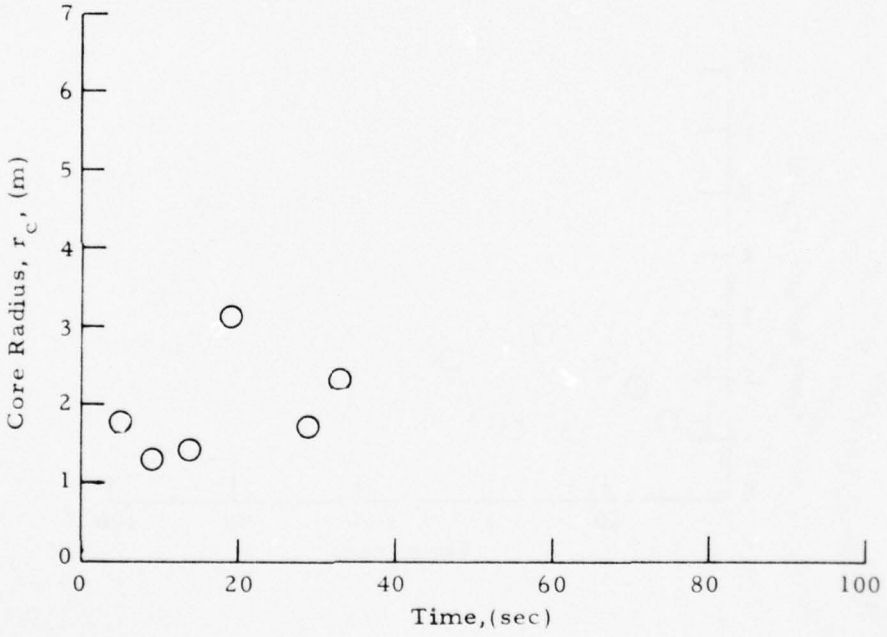

Fig. 29 - Vortex Core Radius as a Function of Time for Flyby 28

AD-A048 275 LOCKHEED MISSILES AND SPACE CO INC HUNTSVILLE ALA HU--ETC F/G 1/1
LASER DOPPLER VELOCIMETER MEASUREMENTS OF B-747 WAKE VORTEX CHA--ETC(U)
SEP 77 M R BRASHEARS, A D ZALAY DOT-TSC-1145
UNCLASSIFIED LMSC-HREC-TR-D496975 FAA-RD-77-85 NL

2 OF 3
AD
A048275

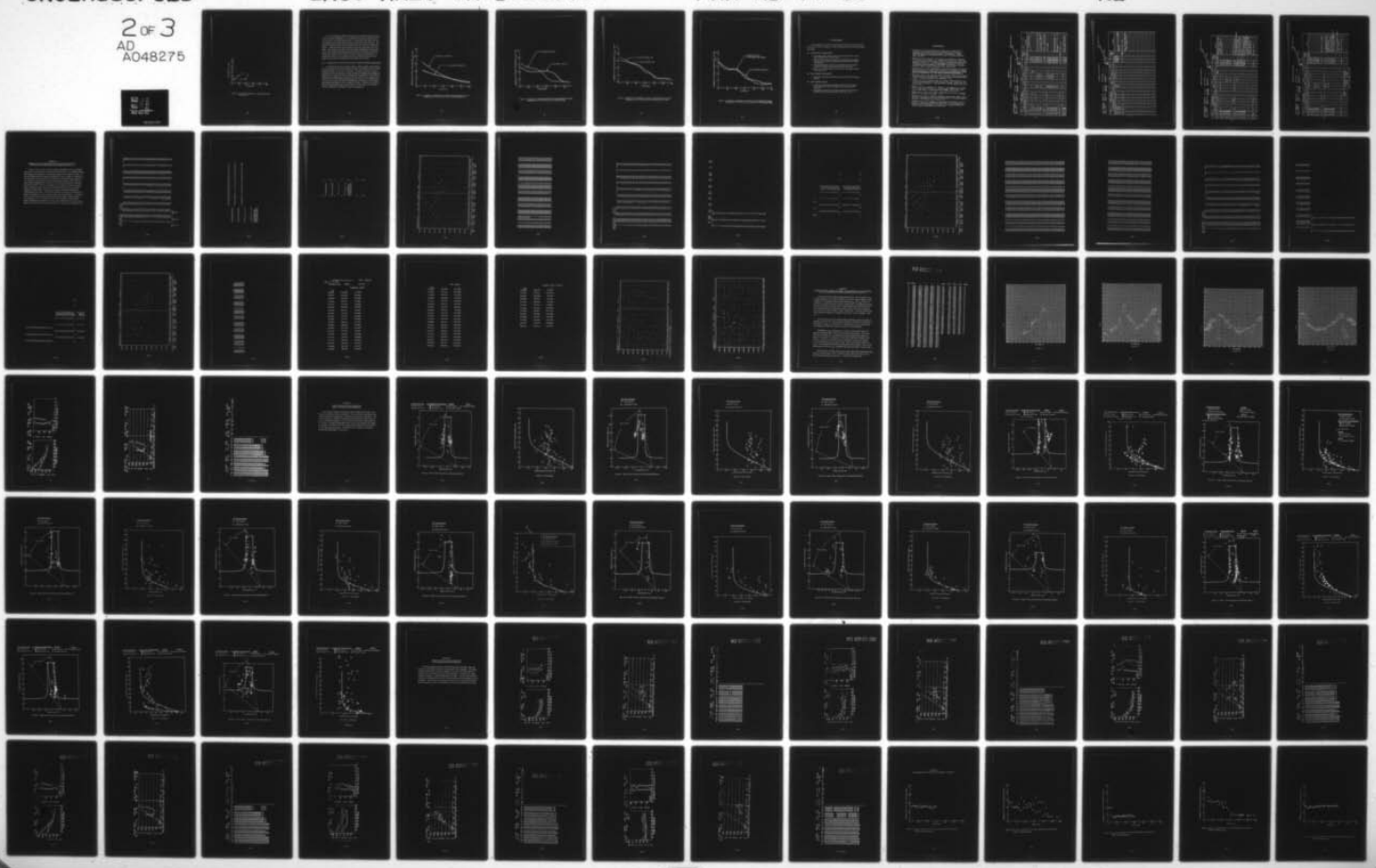

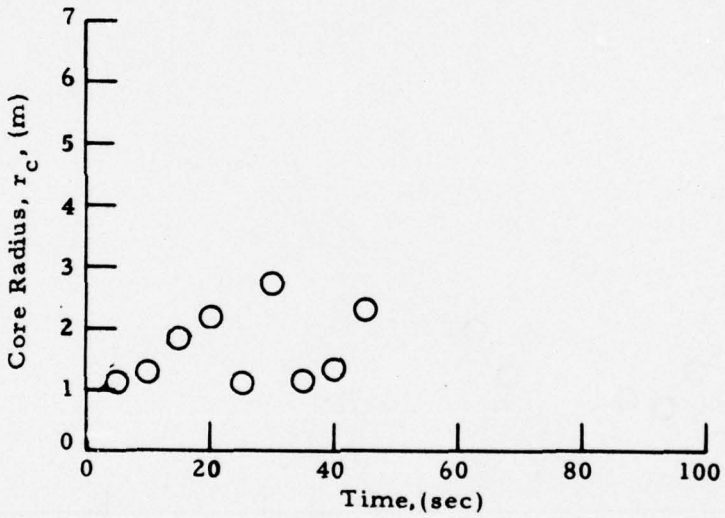

Fig. 30 - Vortex Core Radius as a Function of Time for Flyby 44

The circulation time history computed from the low-speed data vortex tracks is shown in Appendix G. The computed circulation is shown from 20 sec to the time of the last measurement. At periods earlier than a few sec, circulations are not shown since the vortex may not be fully rolled up. The general circulation decay trend is similar to the velocity decay trends noted earlier – relatively small decay initially followed by rapid decay in the far wake. More scatter is evident in the circulation distributions than the velocity or core radius distributions presented earlier because the circulation involves the product of the scatter of the previous two measurements. To reduce this scatter, the circulation has been recomputed using the photographic vortex tracks to define the vortex center more closely.

4.3.4 Comparison of Vortex Decay Trends for Different Flight Configurations

To determine the vortex decay trends for different flight configurations, the time history of the vortex rotational velocity, circulation, and core radius presented earlier can be cross correlated. The decay of the wake vortex rotational velocity for different spoiler and flap and landing gear settings and flight paths is compared in Figs. 31 through 34, respectively. These results indicate that the deployment of spoilers decreases the vortex rotational velocity in the near wake while flap and landing gear settings and aircraft flight path angle do not appear to have a significant effect. However, care must be used in interpreting the above results since for some of the runs the wake vortices drifted out of the field of view (see Appendix D).

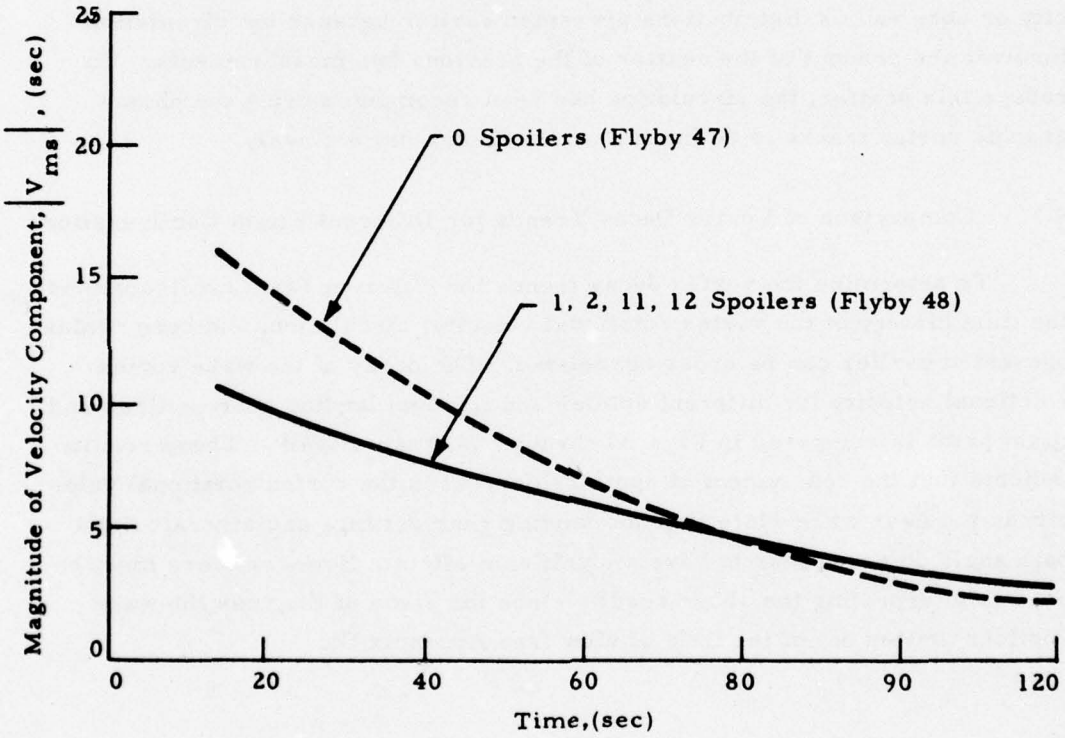

Fig. 31 - Comparison of Magnitude of Wake Vortex Rotational Velocity Component for B-747 Flybys With and Without Spoilers

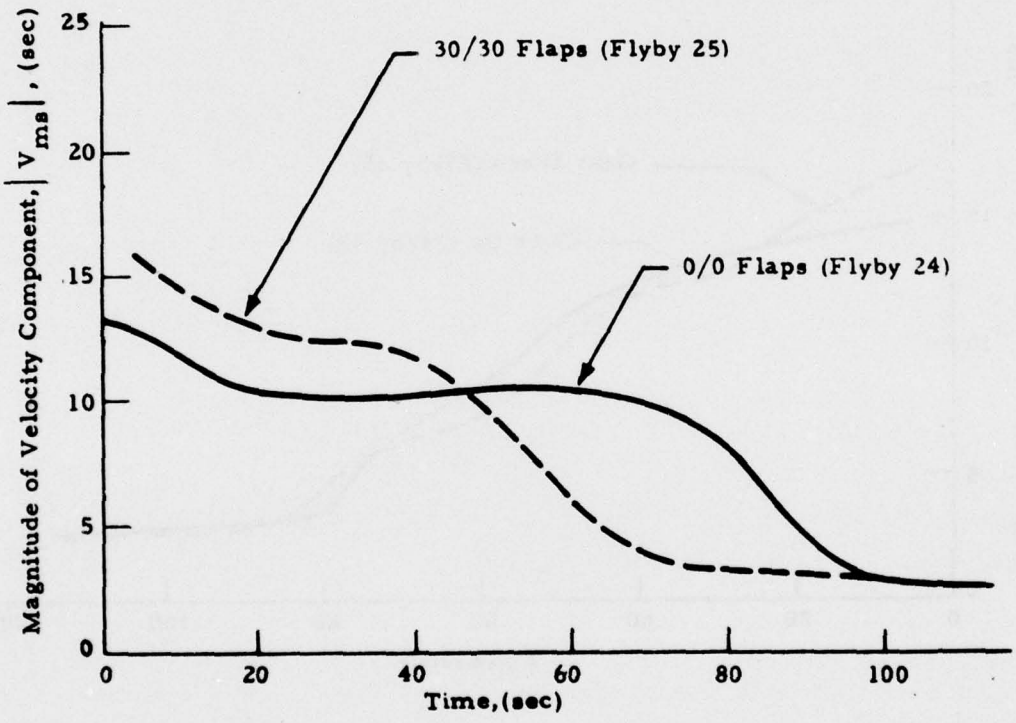

Fig. 32 - Comparison of Magnitude of Wake Vortex Rotational Velocity Component for B-747 Flyby With and Without Flaps

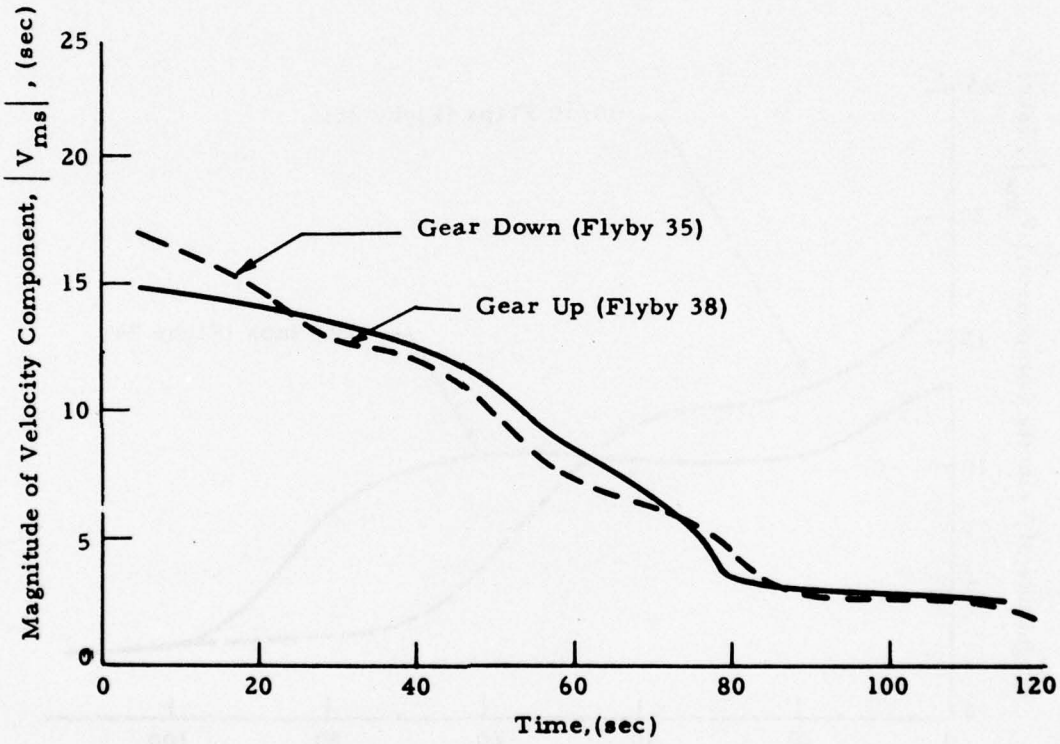

Fig. 33 - Comparison of Magnitude of Wake Vortex Rotational Velocity Component for B-747 Flybys With and Without Gear Down

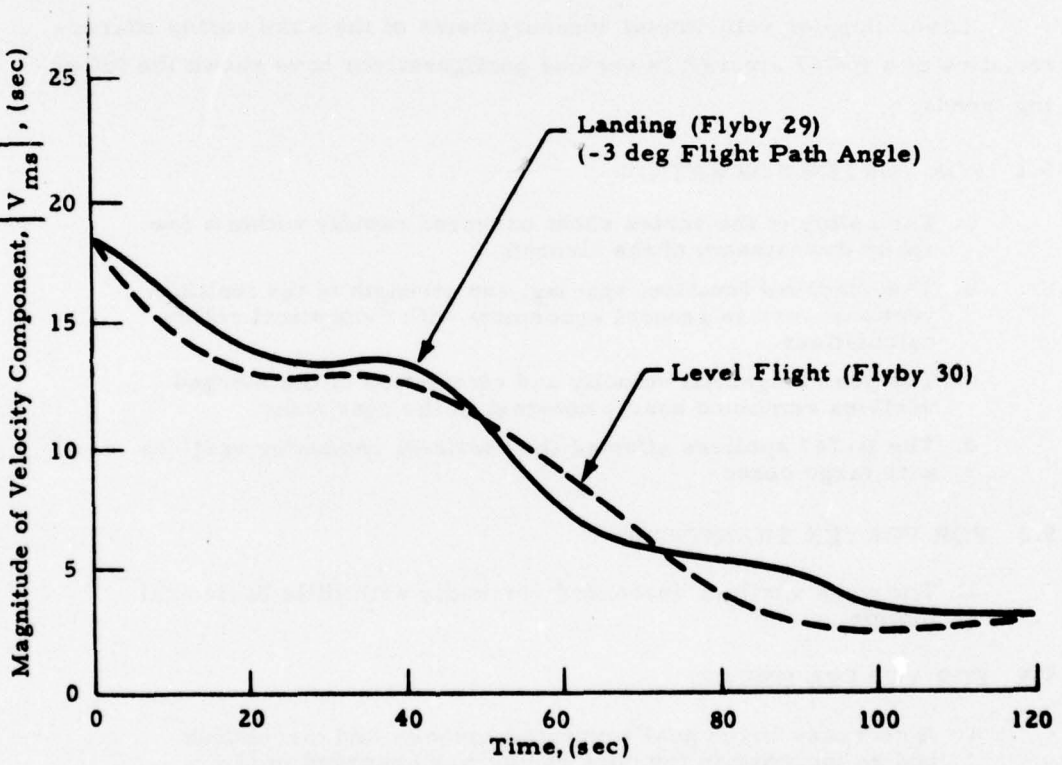

Fig. 34 - Comparison of Magnitude of Wake Vortex Rotational Velocity Component for B-747 in Level Flight and in Descending Flight

5. CONCLUSIONS

Laser Doppler velocimeter measurements of the wake vortex characteristics of a B-747 aircraft in various configurations have shown the following trends.

5.1 FOR VORTEX FORMATION:

a. The rollup of the vortex sheet occurred rapidly within a few spans downstream of the aircraft.

b. The observed location, spacing, and strength of the multiple vortices were in general agreement with theoretical rollup calculations.

c. The peak tangential velocity and circulation of the merged vortices remained nearly constant in the near wake.

d. The B-747 spoilers affected the vortices, producing vortices with large cores.

5.2 FOR VORTEX TRANSPORT:

a. The wake vortices descended vertically with little horizontal motion.

5.3 FOR VORTEX DECAY:

a. A decrease in the peak tangential velocity and circulation and an increase in the core radius was observed in the far wake.

b. Deployment of spoilers and flaps enhanced the vortex peak tangential velocity decay process in the near wake.

REFERENCES

1. Krause, M.C., L.K. Morrison, C.E. Craven, N.A. Logan and T.R. Lawrence, "Development of Theory and Experiments to Improve Understanding of Laser Doppler Systems – Final Report," LMSC-HREC TR D306632, Lockheed Missiles & Space Company, Huntsville, Ala., June 1973.

2. Wilson, D.J., M.C. Krause, E.W. Coffey, C-C. Huang, B.B. Edwards, C.E. Craven, K.R. Shrider, J.L. Jetton and L.K. Morrison, "Development and Testing of Laser Doppler System Components for Wake Vortex Monitoring – Volume I – Scanner Development, Laboratory and Field Testing and System Modeling," LMSC-HREC TR D390159-I, Lockheed Missiles & Space Company, Huntsville, Ala., August 1974.

3. Lawrence, T.R. et al., "Application of a Laser Velocimeter for Remote Wind Velocity and Turbulence Measurements," Proceedings of the International Conference on Aerospace and Aeronautical Meteorology, 22-26 May 1972, Washington, D.C., The American Meteorological Society.

4. Brashears, M.R., T.R. Lawrence and A.D. Zalay, "Mobile Laser Doppler System Check Out and Calibration," FAA-RD-77-48, Lockheed Missiles & Space Company, Huntsville, Ala., September 1976.

5. Garodz, L.J., D.M. Lawrence and N.J. Miller, 'Measurement of the Trailing Vortex Systems of Large Transport Aircraft, Using Tower Fly-by and Flow Visualization," FAA-RD-75-127, NAFEC, Atlanta City, N.J., January 1976.

6. Bilbro, J.W., H.B. Jeffreys, E.A. Weaver, R.M. Huffaker, G.D. Craig, R.W. George, and P.J. Marrero, "Laser Doppler Velocimeter Wake Tests," FAA-RD-76-11 (also NASA TM X 64988), March 1976.

7. Hoffman, E.R., and P.M. Joubert, "Turbulent Line Vortices," J. Fluid Mech., Vol. 16, Part 3, July 1963, p. 395.

8. Snedeker, R.S., and A.J. Bilanin, "Analysis of the Vortex Wakes of the Boeing 727, Lockheed L-1011, McDonnell Douglas DC-10, and Boeing 747 Aircraft," ARAP Report No. 245, July 1975.

9. Brashears, M.R., N.A. Logan, S.J. Robertson, K.R. Shrider, and C.D. Walters, 'Analysis of Predicted Aircraft Wake Vortex Transport and Comparison with Experiment," FAA-RD-74-74, Lockheed Missiles & Space Company, Huntsville, Ala., April 1974.

Appendix A

EXTERNAL LOGS FOR ROSAMOND TESTS

Location: Rosamond Dry Lake
Date: 12/2/15 - Day 1
Sheet 1 of 2

Van X Position Ref. Pt. _____
Van Y Position Ref. Pt. Center of RW

Runway Azimuth: _____
Mirror Azimuth for Switch _____

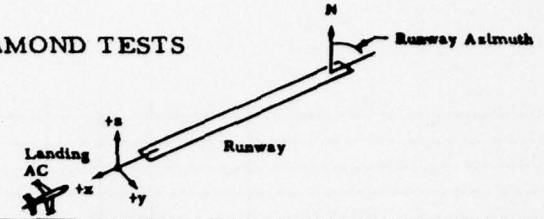

Run ID		Spectrum Analyser						Scanner						Computer		Time		Estimated Wind Azimuth (from)	azimuth 42° is normal to runway. Comments
				Freq. Span (MHz)				Range			Elevation								
No.	AC Type or VAD	B.W. (kHz)	Log Lin	Min.	f_c	Max.	Rate (msec)	Max.	Min.	Rate	Max.	Min.	Rate	Tape No.	No. Records	Start	Stop		
1	VAD	10	LN	0	2cm.	.5	1							DR901		6:46:00	6:49:30	est. from North	alt. at 31, 46, 61, 76, 91, 122, 244, 488 at 1 Rev/alt.
2	VAD															6:50:00	6:59:00		same alt.
3	AC 1	30		1	0	2		57			63	3	.1kg			7:04:44	7:06:06		
4	AC 2	100		1		6							.5kg			7:09:37	7:11:25		
5	AC 3															7:15:08	7:17:17		
6	AC 4			0	1cm	5		60								7:20:49	7:22:53		
7	AC 5							118			63	20				7:25:56	7:27:40		Time mark'em sight, not hear AV going 5-10° past 90°
8	AC 6	30						118			63	03				7:31:47	7:33:35		
9	AC 7										63	30				7:35:53	7:37:42		Run stop-comp. halt; Gen. fail; Processor run number still No. 6
10	AC 8							240			63	21				7:40:39	7:42:46		azimuth 180° + 42° (= 222°)
11	VAD	10		0		.5	1									7:50:00	7:58:00		Same alt. as run 1. Sync. clock 07:56:00 Our clock 07:56:03
12	AC 9	30		0	1/2cm	5		58			63	03	.5			8:12:49	8:15:37		222° azimuth
13	AC 10							120			63	15				8:18:08	8:19:56		
14	AC 11							183			63	25				8:23:37	8:25:39		
15	AC 12							240			62	35				8:29:21	8:31:31		
16	AC 13							57			62	03				8:35:07	8:36:58		
17	AC 14							57								8:40:36	8:42:59		Precisely in middle for 1st min (or longer) / Analog tape run out this run.
18	AC 15							57								8:46:06	8:48:19		
19	AC 16							68								8:51:47	8:53:41		Range, 68 m; Az. at 42°; Amplitude threshold not changed.
20	VAD	10		0	1.3cm	.5										8:58:00	9:07:08	Rel. from north	same alt. as run 1.
21	AC 17	30		0	.6cm	5		35			62	03				9:32:12	9:33:32		Az. 42°. Corrected time code this run.
22	AC 18															9:37:44	9:38:56		repeat of previous run (run 17)
23	AC 19															9:42:16	9:43:28		

Appendix A (Continued)

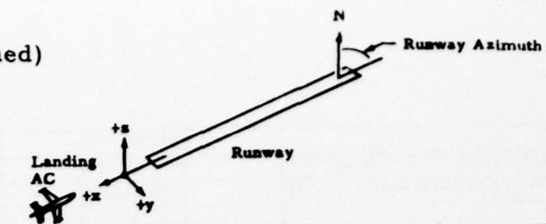

Location: Rosamond Dry Lake Van X Position: ____ Ref. Pt. ____ Runway Azimuth: ____

Date: 12/2/75 - Day 1 Van Y Position: Ref. Pt. Center of RW Mirror Azimuth for Switch ____

Sheet 2 of 2

Run ID		Spectrum Analyser						Scanner						Computer		Time		Estimated Wind Azimuth (from)	Comments
				Freq. Span (MHs)				Range			Elevation								
No.	AC Type or VAD	B.W. (kHs)	Log / Lin	Min.	f_c	Max.	Rate (msec)	Max.	Min.	Rate	Max.	Min.	Rate	Tape No.	No. Records	Start	Stop		
24	AC 19	30		0	.6cm	5		63			62	03				9:46:21	9:48:22		
25	AC 20							63								9:50:58	9:52:53		
26	AC 21							90								9:55:08	9:57:53		Good Run. Vortices over van - high velocities
27	AC 22																		*4 [illegible]
28	VAD	10		0	1¼cm	.5										10:03	10:12	[illegible] north	same [illegible]. as run 1.
																			* NOTE: 3rd SORTIE aborted due to
																			hydraulic problem on 747.

Appendix A (Continued)

Location: Panama City Dev Locs
Date: 12/3/75 - Day 2
Sheet 1 of 2

Van X Position Ref. Pt.: _____
Van Y Position Ref. Pt.: 200' N of RW

Runway Azimuth: _____
Mirror Azimuth for Switch: _____

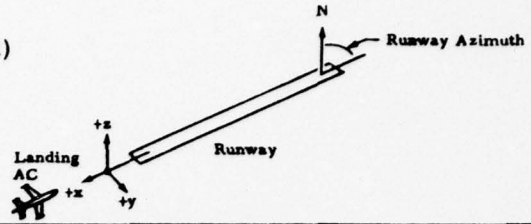

Run ID		Spectrum Analyzer						Scanner						Computer		Time		Estimated Wind Azimuth (from)	Comments
				Freq. Span (MHz)				Range			Elevation								
No.	AC Type or VAD	B.W. (kHz)	Log Lin	Min.	f_c	Max.	Rate (msec)	Max.	Min.	Rate	Max.	Min.	Rate	Tape No.	No. Records	Start	Stop		
1	VAD	10	Lin	0	2cm	.5	1							Dev02		6:29	6:35	est. from south	alt. at 31, 46, 61, 76, 91, 122, 244, 488 at 1 rev./alt.
2	AC 23	30		0	1cm	5	1	190	35	3.5	63	10	.2			6:55:06	6:57:03		processor ran RD. not updated for run 3 (AC run 24)
3	AC 24															6:59:04	7:01:12		
4	AC 25															7:03:32	7:05:38		
5	AC 26															7:07:47	7:10:01		
6	AC 27										45	17				7:12:33	7:14:41		
7	AC 28										40	17				7:16:50	7:18:58		
8	AC 29															7:21:23	7:23:37		
9	AC 30										45	17				7:25:17	7:27:18		
10	VAD	10		0	2cm	.5										7:31	7:39		alt. same as run 1.
11	AC 31	30		0	8cm	5		190	35	3.5	45	17	.2			7:56:09	1:58:30		pilot came in at 350 ft. instead of 200.
12	AC 32															8:00:47	8:04:11		elev. scanner inverted up prior to this run but reversed
13	AC 33										55	30				8:06:09	8:08:36	←	to work alt. before run started.
14	AC 34															8:11:02	8:13:09	→	Run AC 33: pilot came in at 210 ft. Alt,
15	AC 35															8:15:44	8:17:59	←	Mel switch run no. in processor to 34
16	AC 36															8:18:47	8:22:45	←	during runs.
17	AC 37															8:25:17	8:27:19	→	Run AC 35: Analog tape run start this run,
18	AC 38															8:30:30	8:32:35	→	Run AC 36: Lost CRT power during run 36. Plug to mainframe pulled out. noticed at 8:32:30. Also, our tone "mark" and AV "work" not synchronous for run 36.
19	VAD	10		0	1.5cm	.5										8:34	8:46		alt. same as run 1.

Appendix A (Concluded)

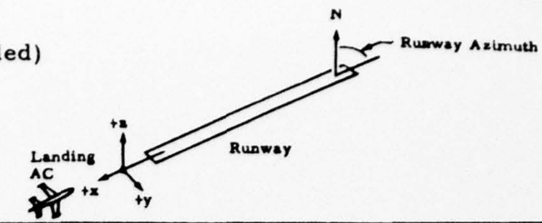

Location: Rosamond Dry Lake
Date: 12/3/75 - Day 2
Sheet 2 of 2

Van X Position: ______
Ref. Pt. ______
Van Y Position:
Ref. Pt. 200' N of RW

Runway Azimuth: ______
Mirror Azimuth for Switch ______

Run ID		Spectrum Analyzer						Scanner						Computer		Time		Estimated Wind Azimuth (from)	Comments
				Freq. Span (MHz)				Range			Elevation								
No.	AC Type or VAD	B. W. (kHz)	Log Lin	Min.	f_c	Max.	Rate (msec)	Max.	Min.	Rate	Max.	Min.	Rate	Tape No.	No. Records	Start	Stop		
20	AC 39	30	Lin	0	.6cm	5	1	140	35	3.5			.2			9:01:11	9:02:39	wd. from N.W.	
21	AC 40										55	23				9:06:52	9:08:57		
22	AC 41															9:12:36	9:14:34		
23	AC 42															9:18:06	9:20:26		
24	AC 43							150	35							9:23:37	9:26:24		
25	AC 44							160	35							9:28:40	9:30:55		
26	AC 45															9:33:57	9:36:46		
27	AC 46							180	35							9:39:09	9:42:11		
28	VAD	10		0	2cm	.5										9:44	9:52		alt. same as run 1. (sheet 1)
29	AC 47	30		0	.8cm	5		140	35	3.5	63	23	.2			10:10:57	10:13:11		
30	AC 48							160	35							10:15:23	10:17:37		wind from south. both vortices drift toward van.
31	AC 49															10:20:26	10:23:10		interesting run, 100 ft. flyby. dust stormes, [illegible] fly by van.
32	AC 50							140	35							10:24:49	10:27:44		Rotated scan 180° at 10:25:07
33	AC 51															10:29:31	10:32:13		Rotated scan 90° @ 10:30:46 (aft)
34	AC 52															10:33:37	10:36:26		Rotated scan forward 90° @ 10:35:00
35	AC 53															10:37:50	10:41:50		Rotated scan aft 90° @ 10:38:58; rotated 90° @ 10:39:55
36	AC 54															10:41:59	10:44:56		Rotated scan aft 90° @ 10:43:29
																			NOTE: AC RUN 53: picked up vortices at 10:39:16 after 1st rotation.
37	VAD	10		0	2cm	.5										10:49:00	10:54:15		alt. same as run 1. (sheet 1)
						NOTES:		TIME	CHECK & END OF SORTIE 4										
									OUR TIME			AV TIME							
									10:46:13			10:48:10							

Range checkout after runs O.K.

Appendix B

SAMPLE OUTPUT FROM VELOCITY AZIMUTH DISPLAY AND VORTEX TRACKER PROGRAM FOR ROSAMOND FLYBY 25

Page B-2 indicates the relative intensity (INTENSITY) and V_{ms} (SPEED (ft/sec)) of the LDV signal as a function of time and space for one sweep between the minimum and maximum elevation-angle setting in the finger-scan mode. A list of the data sorted according to INTENSITY is given on page B-3 followed by the list of the values selected for determining the vortex location on page B-4. A "scatter plot" showing the location of the intensity points in units of ft and their relative magnitude (on a scale of A to 0) is given on page B-5 along with the selected center of the two correlation circles (labeled Z) and the centroid of the correlation circles (the vortex locations labeled P and S for port and starboard, respectively). On page B-6, the points used in determining the vortex location are listed. The data are printed out on pages B-7 through B-12 and B-13 through B-17 for two other sample scans during flyby 25. A summary of the port and starboard locations from each of the scans is given on pages B-18 through B-20. The vortex trajectories are displayed on the last two pages of Appendix B, including time versus lateral displacement of the vortices (page B-21) and time versus vertical location as a function of time (page B-22).

TIME OF SWEEP START = 3.272 SEC.
TIME OF SWEEP END = 4.841 SEC.
MID TIME OF SWEEP = 4.056 SEC.

IP	TIME	RANGE	ANGLE	YP	ZP	DELTA TIME	C WIND	SPEED	IFREQ	INTENSITY
1	3.272	386.2	62.6	22.1	349.7	.784	.00	15.65	18	256
2	3.287	359.2	62.3	33.2	325.2	.769	.00	13.04	15	190
3	3.302	326.9	62.0	46.3	295.5	.754	.00	16.52	19	158
4	3.317	293.8	61.8	61.0	265.8	.740	.00	18.26	21	200
5	3.332	259.7	61.6	76.3	235.4	.725	.00	19.13	22	112
6	3.451	267.6	59.5	64.9	237.4	.605	.00	23.47	27	126
7	3.466	291.0	59.3	51.6	257.3	.590	.00	13.04	15	126
8	3.496	350.1	58.8	18.9	306.4	.560	.00	16.52	19	124
9	3.511	380.4	58.6	1.6	331.6	.545	.00	13.91	16	128
10	3.541	437.9	58.1	-31.6	378.4	.515	.00	27.82	32	124
11	3.795	319.1	53.9	12.0	264.8	.261	.00	20.87	24	126
12	3.810	341.7	53.6	-2.8	281.9	.247	.00	8.69	10	148
13	3.825	376.4	53.4	-24.6	309.1	.232	.00	16.52	19	158
14	3.855	432.6	52.9	-61.2	351.9	.202	.00	29.56	34	126
15	3.869	434.6	52.5	-64.9	351.8	.187	.00	35.65	41	124
16	3.884	418.5	52.3	-55.7	338.1	.172	.00	23.47	27	144
17	3.899	391.2	52.1	-40.1	315.8	.157	.00	26.95	31	166
18	3.914	360.5	51.8	-22.8	290.4	.142	.00	39.99	46	112
19	3.929	331.7	51.5	-6.9	266.7	.127	.00	35.65	41	126
20	3.944	310.2	51.4	6.3	249.4	.112	.00	10.43	12	126
21	3.959	274.9	51.2	27.9	220.7	.097	.00	15.65	18	120
22	3.974	240.0	51.0	48.8	193.4	.082	.00	16.52	19	128
23	4.079	262.2	49.1	28.3	205.1	-.022	.00	46.95	54	184
24	4.094	292.1	48.9	8.0	227.1	-.037	.00	46.08	53	220
25	4.109	322.0	48.6	-13.1	248.4	-.052	.00	50.43	58	256
26	4.123	348.1	48.3	-31.6	266.9	-.067	.00	42.60	49	256
27	4.138	375.3	48.1	-50.5	286.4	-.082	.00	36.52	42	192
28	4.153	402.2	47.9	-69.5	305.4	-.097	.00	30.43	35	280
29	4.168	434.0	47.7	-91.9	328.2	-.112	.00	26.08	30	318
30	4.183	438.8	47.4	-97.2	329.8	-.127	.00	13.04	15	320
31	4.198	425.8	47.2	-89.4	319.1	-.142	.00	9.56	11	190
32	4.213	401.4	47.0	-73.9	300.6	-.157	.00	9.56	11	192
33	4.228	371.4	46.7	-54.6	277.4	-.172	.00	29.56	34	222
34	4.243	348.9	46.6	-39.9	260.4	-.187	.00	7.82	9	320
35	4.258	308.0	46.1	-13.5	229.0	-.202	.00	33.04	38	164
36	4.273	277.6	45.9	7.0	206.5	-.217	.00	24.34	28	168
37	4.467	393.9	42.8	-89.2	274.4	-.411	.00	17.39	20	158
38	4.482	420.7	42.6	-109.9	291.5	-.426	.00	20.87	24	128
39	4.497	438.9	42.3	-124.5	302.6	-.441	.00	16.52	19	174
40	4.512	427.5	42.0	-117.9	292.8	-.456	.00	17.39	20	128
41	4.527	406.9	41.8	-103.5	278.0	-.471	.00	16.52	19	192
42	4.781	384.1	37.6	-104.4	241.9	-.725	.00	8.69	10	128
43	4.796	409.6	37.4	-125.5	255.7	-.740	.00	8.69	10	118
44	4.811	437.7	37.2	-148.8	271.1	-.754	.00	9.56	11	196
45	4.826	435.6	36.8	-148.9	267.8	-.769	.00	8.69	10	190
46	4.841	414.7	36.6	-133.0	254.1	-.784	.00	8.69	10	174

ORDER	VELOCITY	INTENSITY
1	25	30
2	23	39
3	24	29
4	26	28
5	18	1

6	27	25
7	15	26
8	19	33
9	35	24
10	28	4
11	14	44
12	33	27
13	10	32
14	17	41
15	29	2
16	36	31
17	6	45
18	16	23
19	11	39
20	38	46
21	5	36
22	4	17
23	37	35
24	40	3
25	3	13
26	8	37
27	13	12
28	22	16
29	39	9
30	41	22
31	1	38
32	21	40
33	9	42
34	2	6
35	7	7
36	30	11
37	20	14
38	31	19
39	32	20
40	44	8
41	12	10
42	42	15
43	43	21
44	45	43
45	46	5
46	34	18

II	II3	N1	N2	R2
30	29	2	2	30.15
30	28	3	3	1355.06
30	32	4	4	1405.40
30	41	5	5	2727.48
30	31	6	6	171.75
30	39	7	7	1492.69
30	17	8	8	3453.66
30	37	9	9	3134.18
30	16	10	10	1796.11
30	38	11	11	1633.05
30	40	12	12	1798.91
30	14	13	13	1782.36
30	15	14	14	1556.26

KV = 1 JJJ = 30 YC = -81.6 ZC = 316.6

II	III	N1	N2	R2
24	23	2	2	897.96
24	36	3	3	425.12
24	35	4	4	463.56
24	12	5	5	3123.12
24	22	6	6	2803.32
24	6	7	7	3296.32
24	7	8	8	2819.10
24	11	9	9	1438.20
24	19	10	10	1772.69
24	20	11	11	499.09
24	21	12	12	440.48

KV = 2 JJJ = 24 YC = 15.2 ZC = 229.4

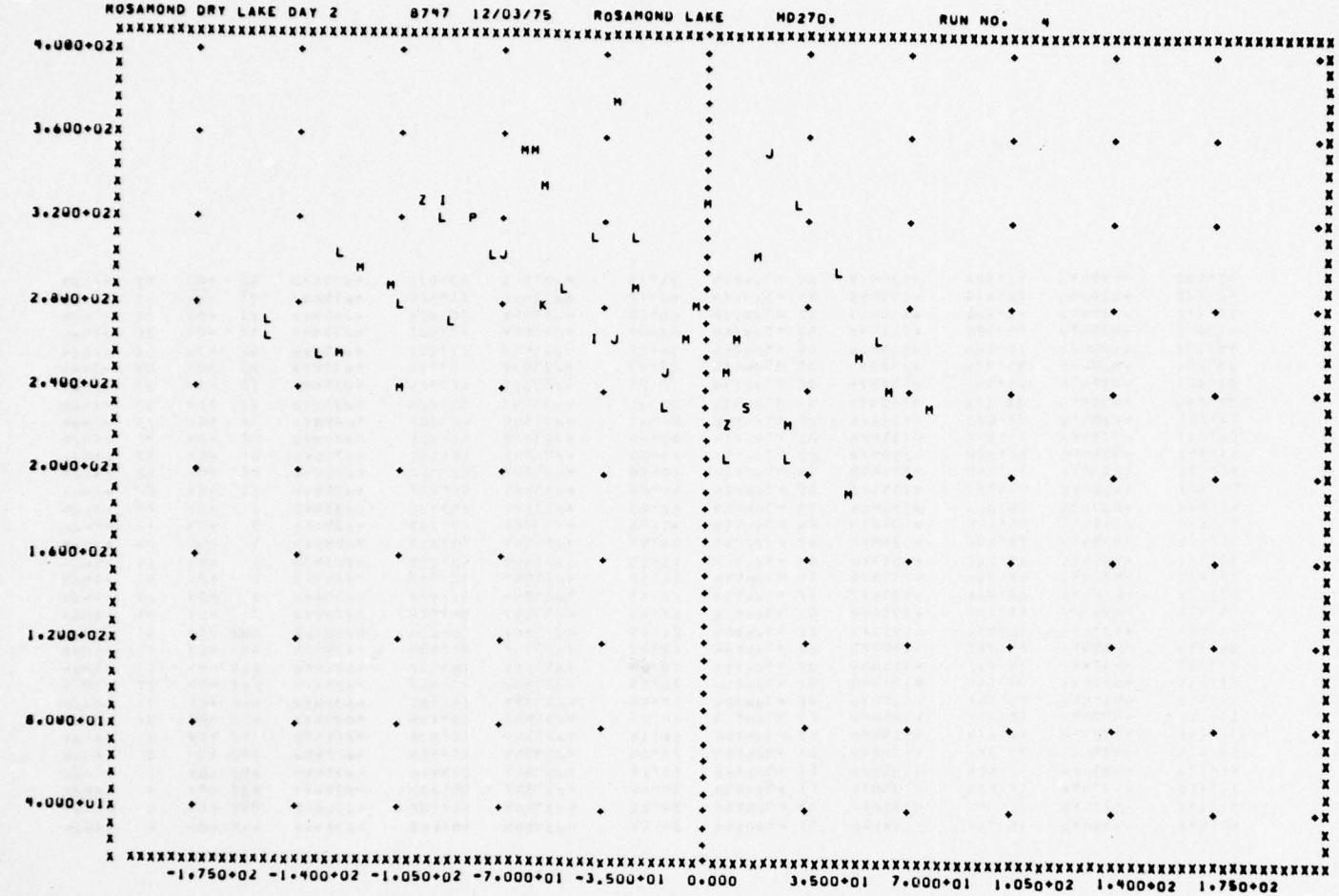
ROSAMOND DRY LAKE DAY 2 8747 12/03/75 ROSAMOND LAKE MD270. RUN NO. 4
4.080+02
3.600+02
3.200+02
2.800+02
2.400+02
2.040+02
1.600+02
1.200+02
8.040+01
4.040+01
-1.750+02 -1.400+02 -1.050+02 -7.000+01 -3.500+01 0.000 3.500+01 7.000+01 1.050+02 1.400+02 1.750+02
O=0-5 N=5-10 M=10-15 L=15-20 K=20-25 J=25-30 I=30-35 H=35-40 G=40-45 F=45-50 E=50-55 D=55-60 C=60-65 B=65-70 A=70-
NPHV= 1 KD= 239 RANGEP= 432.88 ANGLEP= 44.42 NSAMPL= 9 RANGEI= 434.71 RANGEN= 414.37
NPHV= 2 KD= 241 RANGEP= 388.45 ANGLEP= 44.84 NSAMPL= 9 RANGEI= 391.08 RANGEN= 361.88
NPHV= 3 KD= 243 RANGEP= 326.44 ANGLEP= 45.42 NSAMPL= 9 RANGEI= 329.40 RANGEN= 296.59

NPHV=	4	KD=	244	RANGEP=	293.44	ANGLEP=	45.62	NSAMPL=	10	RANGEI=	296.59	RANGEN=	265.09
NPHV=	5	KD=	256	RANGEP=	351.49	ANGLEP=	48.62	NSAMPL=	11	RANGEI=	347.77	RANGEN=	381.64
NPHV=	6	KD=	258	RANGEP=	407.88	ANGLEP=	49.05	NSAMPL=	13	RANGEI=	403.87	RANGEN=	434.71
NPHV=	7	KD=	259	RANGEP=	435.10	ANGLEP=	49.43	NSAMPL=	13	RANGEI=	434.71	RANGEN=	437.66
NPHV=	8	KD=	260	RANGEP=	435.54	ANGLEP=	49.62	NSAMPL=	12	RANGEI=	437.66	RANGEN=	419.95
NPHV=	9	KD=	261	RANGEP=	416.27	ANGLEP=	49.83	NSAMPL=	14	RANGEI=	419.95	RANGEN=	393.70
NPHV=	10	KD=	264	RANGEP=	332.55	ANGLEP=	50.62	NSAMPL=	12	RANGEI=	336.29	RANGEN=	305.12
NPHV=	11	KD=	275	RANGEP=	291.67	ANGLEP=	53.30	NSAMPL=	26	RANGEI=	283.14	RANGEN=	315.94
NPHV=	12	KD=	277	RANGEP=	345.14	ANGLEP=	53.82	NSAMPL=	10	RANGEI=	341.86	RANGEN=	374.67
NPHV=	13	KD=	278	RANGEP=	381.86	ANGLEP=	54.06	NSAMPL=	30	RANGEI=	374.67	RANGEN=	398.62
NPHV=	14	KD=	279	RANGEP=	408.18	ANGLEP=	54.33	NSAMPL=	32	RANGEI=	398.62	RANGEN=	428.48
NPHV=	15	KD=	280	RANGEP=	438.03	ANGLEP=	54.73	NSAMPL=	32	RANGEI=	428.48	RANGEN=	428.48
NPHV=	16	KD=	1	RANGEP=	435.45	ANGLEP=	54.87	NSAMPL=	35	RANGEI=	440.62	RANGEN=	425.85
NPHV=	17	KD=	2	RANGEP=	416.75	ANGLEP=	55.07	NSAMPL=	37	RANGEI=	425.85	RANGEN=	401.25
NPHV=	18	KD=	3	RANGEP=	390.35	ANGLEP=	55.28	NSAMPL=	41	RANGEI=	401.25	RANGEN=	374.67
NPHV=	19	KD=	4	RANGEP=	360.89	ANGLEP=	55.57	NSAMPL=	42	RANGEI=	374.67	RANGEN=	341.86
NPHV=	20	KD=	5	RANGEP=	329.96	ANGLEP=	55.88	NSAMPL=	39	RANGEI=	341.86	RANGEN=	311.35
NPHV=	21	KD=	6	RANGEP=	297.67	ANGLEP=	56.09	NSAMPL=	43	RANGEI=	311.35	RANGEN=	279.53
NPHV=	22	KD=	7	RANGEP=	272.57	ANGLEP=	56.24	NSAMPL=	21	RANGEI=	279.53	RANGEN=	246.39
NPHV=	23	KD=	17	RANGEP=	287.93	ANGLEP=	58.54	NSAMPL=	35	RANGEI=	276.90	RANGEN=	308.40
NPHV=	24	KD=	18	RANGEP=	320.95	ANGLEP=	58.89	NSAMPL=	45	RANGEI=	308.40	RANGEN=	336.29
NPHV=	25	KD=	19	RANGEP=	351.24	ANGLEP=	59.09	NSAMPL=	47	RANGEI=	336.29	RANGEN=	368.11
NPHV=	26	KD=	20	RANGEP=	375.79	ANGLEP=	59.26	NSAMPL=	30	RANGEI=	368.11	RANGEN=	393.70
NPHV=	27	KD=	21	RANGEP=	405.09	ANGLEP=	59.48	NSAMPL=	39	RANGEI=	393.70	RANGEN=	422.90
NPHV=	28	KD=	22	RANGEP=	430.70	ANGLEP=	59.78	NSAMPL=	44	RANGEI=	422.90	RANGEN=	440.62
NPHV=	29	KD=	23	RANGEP=	436.37	ANGLEP=	60.07	NSAMPL=	35	RANGEI=	440.62	RANGEN=	428.48
NPHV=	30	KD=	24	RANGEP=	419.37	ANGLEP=	60.27	NSAMPL=	37	RANGEI=	428.48	RANGEN=	403.87
NPHV=	31	KD=	25	RANGEP=	395.17	ANGLEP=	60.48	NSAMPL=	39	RANGEI=	403.87	RANGEN=	381.56
NPHV=	32	KD=	26	RANGEP=	370.74	ANGLEP=	60.74	NSAMPL=	34	RANGEI=	381.56	RANGEN=	349.74
NPHV=	33	KD=	27	RANGEP=	339.06	ANGLEP=	61.07	NSAMPL=	35	RANGEI=	349.74	RANGEN=	319.23
NPHV=	34	KD=	28	RANGEP=	305.17	ANGLEP=	61.28	NSAMPL=	42	RANGEI=	319.23	RANGEN=	285.76
NPHV=	35	KD=	29	RANGEP=	273.09	ANGLEP=	61.48	NSAMPL=	39	RANGEI=	285.76	RANGEN=	253.28

TIME OF SWEEP START = 23.516 SEC.
TIME OF SWEEP END = 25.114 SEC.
MID TIME OF SWEEP = 24.315 SEC.

IP	TIME	RANGE	ANGLE	YP	ZP	DELTA TIME	C WIND	SPEED	IFREQ	INTENSITY
1	23.516	378.9	36.8	-103.2	234.1	.799	.00	7.82	9	148
2	23.770	392.6	40.8	-97.1	263.7	.545	.00	13.04	15	144
3	23.799	440.0	41.2	-130.8	297.1	.515	.00	9.56	11	128
4	23.844	381.9	42.0	-83.7	262.7	.471	.00	13.04	15	112
5	23.889	288.2	42.8	-11.4	203.0	.426	.00	18.26	21	126
6	24.029	273.4	45.1	6.9	200.5	.291	.00	23.47	27	126
7	24.053	333.0	45.5	-33.3	244.6	.261	.00	26.08	30	208
8	24.068	361.0	45.9	-51.4	266.1	.247	.00	28.69	33	128
9	24.083	392.0	46.1	-72.0	289.3	.232	.00	31.30	36	188
10	24.098	416.2	46.3	-87.7	307.7	.217	.00	26.95	31	158
11	24.113	437.7	46.6	-100.8	324.9	.202	.00	39.99	46	348
12	24.128	432.2	46.9	-95.5	322.3	.187	.00	23.47	27	318
13	24.143	405.5	47.1	-76.1	304.0	.172	.00	39.12	45	256
14	24.158	381.2	47.3	-58.6	287.1	.157	.00	33.91	39	152
15	24.173	353.0	47.6	-38.2	267.4	.142	.00	35.65	41	156
16	24.188	324.6	47.9	-17.8	247.7	.127	.00	26.95	31	128
17	24.203	297.1	48.0	1.3	227.9	.112	.00	13.04	15	128
18	24.337	267.1	50.3	29.2	212.4	-.022	.00	25.21	29	126
19	24.352	299.5	50.5	9.4	238.0	-.037	.00	35.65	41	128
20	24.367	327.3	50.7	-7.2	260.4	-.052	.00	28.69	33	136
21	24.382	348.5	51.0	-19.2	277.9	-.067	.00	12.17	14	192
22	24.397	381.6	51.2	-38.9	304.6	-.082	.00	16.52	19	200
23	24.412	412.0	51.5	-56.7	329.2	-.097	.00	27.82	32	256
24	24.427	436.5	51.7	-70.4	349.7	-.112	.00	26.95	31	256
25	24.442	435.1	52.1	-67.5	350.2	-.127	.00	26.95	31	192
26	24.457	414.8	52.3	-53.9	335.0	-.142	.00	26.08	30	358
27	24.472	389.6	52.5	-37.4	315.9	-.157	.00	23.47	27	254
28	24.487	364.3	52.6	-21.0	296.6	-.172	.00	21.74	25	160
29	24.502	333.5	52.9	-1.2	273.0	-.187	.00	19.13	22	232
30	24.517	301.9	53.2	19.4	248.9	-.202	.00	20.00	23	192
31	24.531	266.4	53.5	41.4	221.0	-.217	.00	23.47	27	224
32	24.546	234.3	53.6	61.1	195.7	-.232	.00	18.26	21	126
33	24.636	225.3	55.2	71.5	192.1	-.321	.00	18.26	21	126
34	24.651	259.4	55.5	52.9	220.4	-.336	.00	22.60	26	118
35	24.666	283.5	55.6	39.9	241.0	-.351	.00	10.43	12	136
36	24.681	317.0	55.8	21.9	269.3	-.366	.00	13.91	16	172
37	24.711	375.5	56.4	-7.6	319.9	-.396	.00	17.39	20	352
38	24.726	402.2	56.6	-21.2	342.9	-.411	.00	16.52	19	128
39	24.741	430.7	56.8	-35.6	367.6	-.426	.00	15.65	18	192
40	24.771	424.1	57.4	-28.3	364.4	-.456	.00	13.91	16	200
41	24.785	397.1	57.6	-12.6	342.4	-.471	.00	14.78	17	238
42	24.800	372.9	57.8	1.4	322.8	-.486	.00	11.30	13	112
43	24.815	341.0	58.1	19.6	296.4	-.500	.00	13.91	16	126
44	24.830	310.4	58.4	37.5	271.4	-.515	.00	14.78	17	126
45	24.845	278.4	58.6	55.1	244.7	-.530	.00	12.17	14	124
46	24.950	217.7	60.3	92.0	196.0	-.635	.00	13.04	15	176
47	24.965	251.3	60.6	76.8	226.0	-.650	.00	19.13	22	160
48	24.980	279.7	60.8	63.7	251.2	-.665	.00	12.17	14	126
49	24.995	311.9	61.0	49.0	279.9	-.680	.00	20.00	23	318
50	25.010	340.8	61.3	36.3	305.9	-.695	.00	18.26	21	190
51	25.024	369.0	61.6	24.7	331.7	-.710	.00	16.52	19	152
52	25.039	396.3	61.8	13.0	356.4	-.725	.00	15.65	18	126
53	25.054	424.0	62.0	1.2	381.5	-.740	.00	14.78	17	190

54	25.069	441.8	62.3	-5.6	398.0	-.754	.00	19.78	17	158
55	25.099	401.7	62.8	16.9	364.1	-.784	.00	18.26	21	190
56	25.119	376.6	62.8	27.6	341.8	-.799	.00	20.87	24	126

ORDER	VELOCITY	INTENSITY
1	11	26
2	13	37
3	15	11
4	19	12
5	14	49
6	9	13
7	8	23
8	20	24
9	23	27
10	10	41
11	16	29
12	24	31
13	25	7
14	7	22
15	26	40
16	18	21
17	6	25
18	12	30
19	27	39
20	31	50
21	34	53
22	28	55
23	56	9
24	30	46
25	49	36
26	29	28
27	47	47
28	5	10
29	32	54
30	33	15
31	50	14
32	55	51
33	37	1
34	22	2
35	38	20
36	51	35
37	39	3
38	52	8
39	41	16
40	44	17
41	53	19
42	54	38
43	36	5
44	40	6
45	43	18
46	2	32
47	4	33
48	17	43
49	46	44
50	21	48
51	45	52
52	48	56

53	42	45
54	35	34
55	3	4
56	1	42

11	113	N1	N2	N2
26	37	2	2	2371.59
26	11	3	3	2301.73
26	12	4	4	1895.58
26	13	5	5	1955.59
26	23	6	6	91.29
26	24	7	7	487.28
26	27	8	8	637.90
26	41	9	9	1761.82
26	22	10	10	1155.79
26	40	11	11	1514.96
26	25	12	12	914.05
26	39	13	13	1389.69
26	9	14	14	2415.77
26	28	15	15	2556.98
26	10	16	16	1891.93
26	14	17	17	2329.28
26	38	18	18	1133.86
26	42	19	19	3215.93

NV = 1 JJJ = 26 YC = -60.9 ZC = 323.2

11	113	N1	N2	N2
31	30	2	2	1260.28
31	46	3	3	3191.45
31	36	4	4	2711.50
31	47	5	5	1280.65
31	35	6	6	902.98
31	17	7	7	1655.47
31	19	8	8	1310.45
31	5	9	9	3104.77
31	6	10	10	1611.90
31	18	11	11	221.90
31	32	12	12	1029.38
31	33	13	13	1742.47
31	44	14	14	2559.26
31	48	15	15	1410.64
31	45	16	16	749.01
31	34	17	17	133.03

NV = 2 JJJ = 31 YC = 37.2 ZC = 225.8

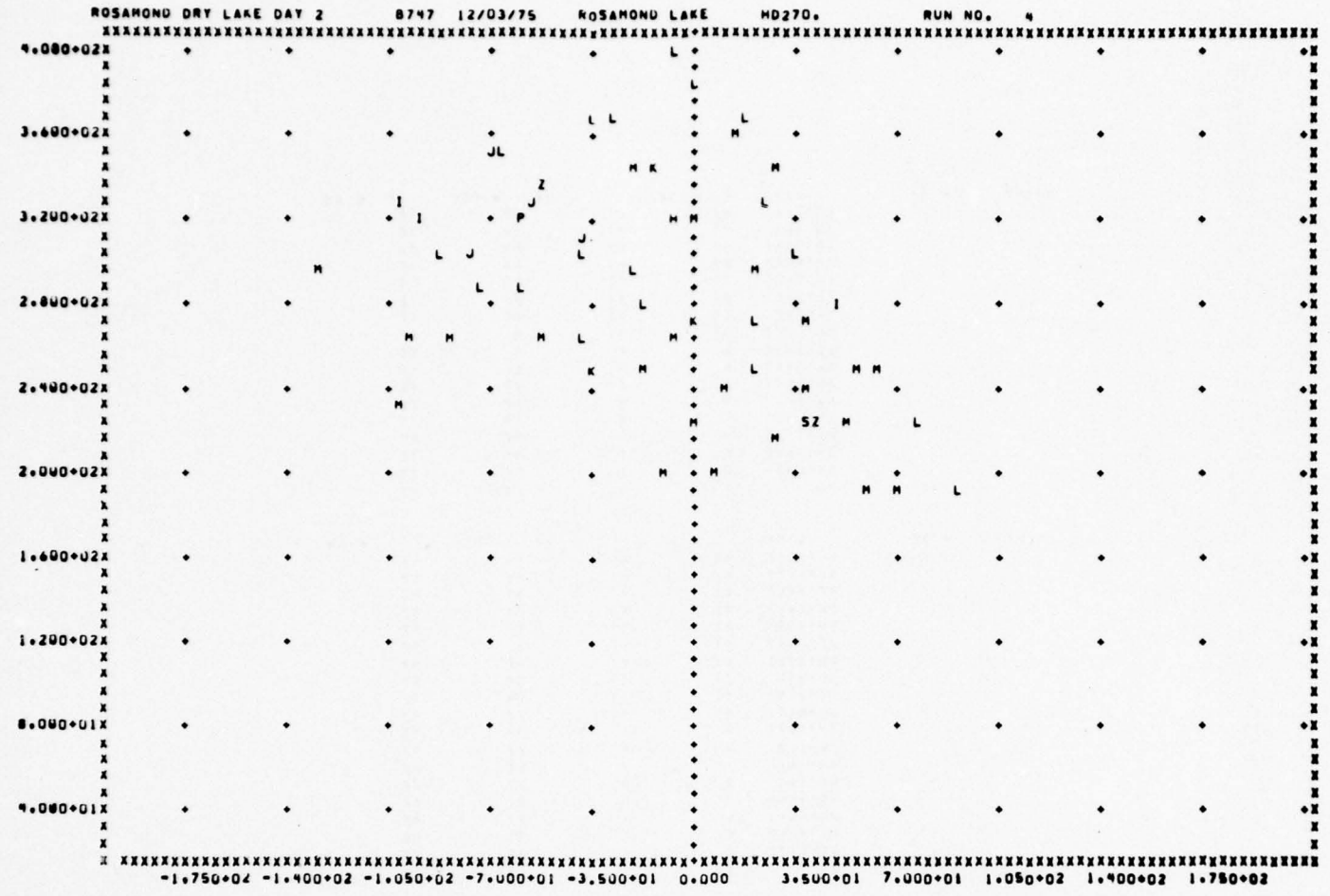

0=0-5 N=5-10 M=10-15 L=15-20 K=20-25 J=25-30 I=30-35 H=35-40 G=40-45 F=45-50 E=50-55 D=55-60 C=60-65 B=65-70 A=70-

NPHV=	1	KD= 276	RANGEP=	346.19	ANGLEP=	62.55	NSAMPL= 24	RANGEI=	353.67	RANGEN=	322.61		
NPHV=	2	KD= 277	RANGEP=	314.30	ANGLEP=	62.30	NSAMPL= 25	RANGEI=	322.51	RANGEN=	289.70		
NPHV=	3	KD= 278	RANGEP=	281.08	ANGLEP=	61.95	NSAMPL= 26	RANGEI=	289.70	RANGEN=	256.56		

NPHV=	4	KD=	279	RANGEP=	249.61	ANGLEP=	61.76	NSAMPL=	20	RANGEI=	256.56	RANGEN=	221.78
NPHV=	5	KD=	280	RANGEP=	214.83	ANGLEP=	61.56	NSAMPL=	20	RANGEI=	221.78	RANGEN=	221.78
NPHV=	6	KD=	5	RANGEP=	209.80	ANGLEP=	60.37	NSAMPL=	13	RANGEI=	205.71	RANGEN=	237.20
NPHV=	7	KD=	6	RANGEP=	245.00	ANGLEP=	60.10	NSAMPL=	24	RANGEI=	237.20	RANGEN=	269.69
NPHV=	8	KD=	7	RANGEP=	278.56	ANGLEP=	59.73	NSAMPL=	33	RANGEI=	269.69	RANGEN=	296.59
NPHV=	9	KD=	8	RANGEP=	305.63	ANGLEP=	59.54	NSAMPL=	29	RANGEI=	296.59	RANGEN=	327.76
NPHV=	10	KD=	9	RANGEP=	335.79	ANGLEP=	59.34	NSAMPL=	31	RANGEI=	327.76	RANGEN=	353.67
NPHV=	11	KD=	10	RANGEP=	361.82	ANGLEP=	59.09	NSAMPL=	27	RANGEI=	353.67	RANGEN=	383.86
NPHV=	12	KD=	11	RANGEP=	391.95	ANGLEP=	58.74	NSAMPL=	29	RANGEI=	383.86	RANGEN=	411.75
NPHV=	13	KD=	12	RANGEP=	420.04	ANGLEP=	58.54	NSAMPL=	32	RANGEI=	411.75	RANGEN=	437.66
NPHV=	14	KD=	15	RANGEP=	403.30	ANGLEP=	57.73	NSAMPL=	33	RANGEI=	411.75	RANGEN=	386.15
NPHV=	15	KD=	16	RANGEP=	376.45	ANGLEP=	57.53	NSAMPL=	34	RANGEI=	386.15	RANGEN=	357.61
NPHV=	16	KD=	17	RANGEP=	347.46	ANGLEP=	57.33	NSAMPL=	34	RANGEI=	357.61	RANGEN=	327.76
NPHV=	17	KD=	18	RANGEP=	318.99	ANGLEP=	57.15	NSAMPL=	27	RANGEI=	327.76	RANGEN=	295.28
NPHV=	18	KD=	19	RANGEP=	283.56	ANGLEP=	56.86	NSAMPL=	35	RANGEI=	295.28	RANGEN=	261.81
NPHV=	19	KD=	20	RANGEP=	250.89	ANGLEP=	56.54	NSAMPL=	32	RANGEI=	261.81	RANGEN=	227.69
NPHV=	20	KD=	21	RANGEP=	217.85	ANGLEP=	56.34	NSAMPL=	30	RANGEI=	227.69	RANGEN=	194.88
NPHV=	21	KD=	26	RANGEP=	207.05	ANGLEP=	55.15	NSAMPL=	24	RANGEI=	199.80	RANGEN=	229.99
NPHV=	22	KD=	27	RANGEP=	240.91	ANGLEP=	54.87	NSAMPL=	32	RANGEI=	229.99	RANGEN=	264.11
NPHV=	23	KD=	28	RANGEP=	269.99	ANGLEP=	54.55	NSAMPL=	23	RANGEI=	264.11	RANGEN=	289.70
NPHV=	24	KD=	30	RANGEP=	300.20	ANGLEP=	54.34	NSAMPL=	32	RANGEI=	289.70	RANGEN=	322.51
NPHV=	25	KD=	31	RANGEP=	330.09	ANGLEP=	54.14	NSAMPL=	30	RANGEI=	322.51	RANGEN=	347.77
NPHV=	26	KD=	32	RANGEP=	358.24	ANGLEP=	53.88	NSAMPL=	31	RANGEI=	347.77	RANGEN=	381.56
NPHV=	27	KD=	33	RANGEP=	388.25	ANGLEP=	53.54	NSAMPL=	30	RANGEI=	381.56	RANGEN=	403.87
NPHV=	28	KD=	34	RANGEP=	411.56	ANGLEP=	53.35	NSAMPL=	25	RANGEI=	403.87	RANGEN=	434.71
NPHV=	29	KD=	35	RANGEP=	434.71	ANGLEP=	53.14	NSAMPL=	31	RANGEI=	434.71	RANGEN=	434.71
NPHV=	30	KD=	37	RANGEP=	409.97	ANGLEP=	52.69	NSAMPL=	28	RANGEI=	417.32	RANGEN=	391.08
NPHV=	31	KD=	38	RANGEP=	384.00	ANGLEP=	52.34	NSAMPL=	28	RANGEI=	391.08	RANGEN=	365.81
NPHV=	32	KD=	39	RANGEP=	357.71	ANGLEP=	52.15	NSAMPL=	26	RANGEI=	365.81	RANGEN=	334.65
NPHV=	33	KD=	40	RANGEP=	326.20	ANGLEP=	51.95	NSAMPL=	26	RANGEI=	334.65	RANGEN=	302.17
NPHV=	34	KD=	41	RANGEP=	293.72	ANGLEP=	51.70	NSAMPL=	26	RANGEI=	302.17	RANGEN=	269.69
NPHV=	35	KD=	42	RANGEP=	260.98	ANGLEP=	51.35	NSAMPL=	26	RANGEI=	269.69	RANGEN=	236.22
NPHV=	36	KD=	43	RANGEP=	228.27	ANGLEP=	51.15	NSAMPL=	24	RANGEI=	236.22	RANGEN=	203.08
NPHV=	37	KD=	49	RANGEP=	229.23	ANGLEP=	49.73	NSAMPL=	17	RANGEI=	223.43	RANGEN=	257.55
NPHV=	38	KD=	50	RANGEP=	263.43	ANGLEP=	49.35	NSAMPL=	23	RANGEI=	257.55	RANGEN=	283.14
NPHV=	39	KD=	51	RANGEP=	290.68	ANGLEP=	49.15	NSAMPL=	23	RANGEI=	263.14	RANGEN=	315.94
NPHV=	40	KD=	52	RANGEP=	321.53	ANGLEP=	48.95	NSAMPL=	23	RANGEI=	315.94	RANGEN=	340.22
NPHV=	41	KD=	53	RANGEP=	346.42	ANGLEP=	48.76	NSAMPL=	18	RANGEI=	340.22	RANGEN=	374.67
NPHV=	42	KD=	54	RANGEP=	379.46	ANGLEP=	48.52	NSAMPL=	20	RANGEI=	374.67	RANGEN=	398.62
NPHV=	43	KD=	55	RANGEP=	406.17	ANGLEP=	48.15	NSAMPL=	23	RANGEI=	398.62	RANGEN=	431.43
NPHV=	44	KD=	59	RANGEP=	392.37	ANGLEP=	47.17	NSAMPL=	17	RANGEI=	396.00	RANGEN=	374.67
NPHV=	45	KD=	60	RANGEP=	369.50	ANGLEP=	46.97	NSAMPL=	15	RANGEI=	374.67	RANGEN=	340.22
NPHV=	46	KD=	61	RANGEP=	334.73	ANGLEP=	46.76	NSAMPL=	18	RANGEI=	340.22	RANGEN=	309.71
NPHV=	47	KD=	62	RANGEP=	304.25	ANGLEP=	46.54	NSAMPL=	16	RANGEI=	309.71	RANGEN=	275.59
NPHV=	48	KD=	63	RANGEP=	270.77	ANGLEP=	46.17	NSAMPL=	15	RANGEI=	275.59	RANGEN=	243.44
NPHV=	49	KD=	64	RANGEP=	238.08	ANGLEP=	45.97	NSAMPL=	16	RANGEI=	243.44	RANGEN=	209.97
NPHV=	50	KD=	65	RANGEP=	204.57	ANGLEP=	45.77	NSAMPL=	16	RANGEI=	209.97	RANGEN=	176.18
NPHV=	51	KD=	69	RANGEP=	191.67	ANGLEP=	44.76	NSAMPL=	20	RANGEI=	185.04	RANGEN=	218.18
NPHV=	52	KD=	70	RANGEP=	223.48	ANGLEP=	44.57	NSAMPL=	16	RANGEI=	218.18	RANGEN=	251.31
NPHV=	53	KD=	71	RANGEP=	256.67	ANGLEP=	44.32	NSAMPL=	19	RANGEI=	251.31	RANGEN=	279.53
NPHV=	54	KD=	72	RANGEP=	284.06	ANGLEP=	43.97	NSAMPL=	15	RANGEI=	279.53	RANGEN=	309.71
NPHV=	55	KD=	73	RANGEP=	315.03	ANGLEP=	43.76	NSAMPL=	20	RANGEI=	309.71	RANGEN=	336.29
NPHV=	56	KD=	74	RANGEP=	341.40	ANGLEP=	43.57	NSAMPL=	15	RANGEI=	336.29	RANGEN=	370.41
NPHV=	57	KD=	75	RANGEP=	375.07	ANGLEP=	43.32	NSAMPL=	20	RANGEI=	370.41	RANGEN=	393.70
NPHV=	58	KD=	76	RANGEP=	399.81	ANGLEP=	42.96	NSAMPL=	19	RANGEI=	393.70	RANGEN=	425.85
NPHV=	59	KD=	77	RANGEP=	428.81	ANGLEP=	42.76	NSAMPL=	20	RANGEI=	425.85	RANGEN=	440.62
NPHV=	60	KD=	78	RANGEP=	437.37	ANGLEP=	42.56	NSAMPL=	22	RANGEI=	440.62	RANGEN=	425.85

```
NPHV=  81   KD=  79   RANGEP=   420.44   ANGLEP=   42.36   NSAMPL= 22   RANGEI=   425.85   RANGEN=   401.25
NPHV=  82   KD=  80   RANGEP=   395.97   ANGLEP=   42.10   NSAMPL= 24   RANGEI=   401.25   RANGEN=   379.27
NPHV=  83   KD=  81   RANGEP=   372.97   ANGLEP=   41.76   NSAMPL= 20   RANGEI=   379.27   RANGEN=   347.77
NPHV=  84   KD=  82   RANGEP=   342.03   ANGLEP=   41.56   NSAMPL= 19   RANGEI=   347.77   RANGEN=   317.59
NPHV=  85   KD=  83   RANGEP=   311.38   ANGLEP=   41.36   NSAMPL= 18   RANGEI=   317.59   RANGEN=   283.14
NPHV=  86   KD=  84   RANGEP=   276.57   ANGLEP=   41.12   NSAMPL= 20   RANGEI=   283.14   RANGEN=   260.33
NPHV=  87   KD=  85   RANGEP=   243.91   ANGLEP=   40.76   NSAMPL= 19   RANGEI=   250.33   RANGEN=   216.54
NPHV=  88   KD=  86   RANGEP=   212.85   ANGLEP=   40.58   NSAMPL= 11   RANGEI=   216.54   RANGEN=   183.07
NPHV=  89   KD=  92   RANGEP=   252.79   ANGLEP=   39.08   NSAMPL= 30   RANGEI=   243.44   RANGEN=   274.61
NPHV=  70   KD=  93   RANGEP=   282.60   ANGLEP=   38.74   NSAMPL= 29   RANGEI=   274.61   RANGEN=   302.17
NPHV=  71   KD=  94   RANGEP=   311.42   ANGLEP=   38.54   NSAMPL= 30   RANGEI=   302.17   RANGEN=   333.01
NPHV=  72   KD=  95   RANGEP=   342.53   ANGLEP=   38.33   NSAMPL= 33   RANGEI=   333.01   RANGEN=   361.88
NPHV=  73   KD=  96   RANGEP=   372.10   ANGLEP=   38.13   NSAMPL= 35   RANGEI=   361.88   RANGEN=   391.08
NPHV=  74   KD=  97   RANGEP=   401.05   ANGLEP=   37.85   NSAMPL= 38   RANGEI=   391.08   RANGEN=   417.32
NPHV=  75   KD=  98   RANGEP=   423.38   ANGLEP=   37.55   NSAMPL= 26   RANGEI=   417.32   RANGEN=   440.62
NPHV=  76   KD=  99   RANGEP=   438.25   ANGLEP=   37.33   NSAMPL= 36   RANGEI=   440.62   RANGEN=   428.48
NPHV=  77   KD= 100   RANGEP=   419.57   ANGLEP=   37.11   NSAMPL= 46   RANGEI=   428.48   RANGEN=   409.12
NPHV=  78   KD= 101   RANGEP=   394.77   ANGLEP=   36.85   NSAMPL= 37   RANGEI=   409.12   RANGEN=   383.86
NPHV=  79   KD= 102   RANGEP=   371.18   ANGLEP=   36.52   NSAMPL= 42   RANGEI=   383.86   RANGEN=   363.67
NPHV=  80   KD= 103   RANGEP=   349.54   ANGLEP=   36.37   NSAMPL= 14   RANGEI=   363.67   RANGEN=   329.15
NPHV=  81   KD= 105   RANGEP=   279.09   ANGLEP=   35.87   NSAMPL= 33   RANGEI=   289.70   RANGEN=   267.55
NPHV=  82   KD= 112   RANGEP=   219.44   ANGLEP=   34.11   NSAMPL= 45   RANGEI=   205.71   RANGEN=   236.22
NPHV=  83   KD= 113   RANGEP=   239.47   ANGLEP=   33.98   NSAMPL= 10   RANGEI=   236.22   RANGEN=   268.70
NPHV=  84   KD= 114   RANGEP=   280.13   ANGLEP=   33.63   NSAMPL= 43   RANGEI=   268.70   RANGEN=   295.28
NPHV=  85   KD= 115   RANGEP=   308.70   ANGLEP=   33.31   NSAMPL= 44   RANGEI=   295.28   RANGEN=   325.79
NPHV=  86   KD= 116   RANGEP=   336.66   ANGLEP=   33.12   NSAMPL= 39   RANGEI=   325.79   RANGEN=   353.67
NPHV=  87   KD= 117   RANGEP=   365.04   ANGLEP=   32.93   NSAMPL= 35   RANGEI=   353.67   RANGEN=   386.15
NPHV=  88   KD= 118   RANGEP=   391.53   ANGLEP=   32.72   NSAMPL= 21   RANGEI=   386.15   RANGEN=   411.75
NPHV=  89   KD= 119   RANGEP=   420.04   ANGLEP=   32.54   NSAMPL= 32   RANGEI=   411.75   RANGEN=   437.66
NPHV=  90   KD= 120   RANGEP=   436.69   ANGLEP=   32.13   NSAMPL= 33   RANGEI=   437.66   RANGEN=   434.71
NPHV=  91   KD= 121   RANGEP=   428.20   ANGLEP=   31.94   NSAMPL= 32   RANGEI=   434.71   RANGEN=   414.37
NPHV=  92   KD= 122   RANGEP=   409.48   ANGLEP=   31.72   NSAMPL= 21   RANGEI=   414.37   RANGEN=   391.08
NPHV=  93   KD= 124   RANGEP=   356.35   ANGLEP=   31.17   NSAMPL= 17   RANGEI=   361.88   RANGEN=   329.40
NPHV=  94   KD= 126   RANGEP=   292.69   ANGLEP=   30.78   NSAMPL= 12   RANGEI=   296.59   RANGEN=   264.11
NPHV=  95   KD= 136   RANGEP=   292.82   ANGLEP=   28.17   NSAMPL= 13   RANGEI=   288.39   RANGEN=   322.51
NPHV=  96   KD= 140   RANGEP=   408.19   ANGLEP=   27.17   NSAMPL= 14   RANGEI=   403.87   RANGEN=   434.71
NPHV=  97   KD= 141   RANGEP=   435.18   ANGLEP=   26.97   NSAMPL= 16   RANGEI=   434.71   RANGEN=   437.66
NPHV=  98   KD= 142   RANGEP=   435.01   ANGLEP=   26.77   NSAMPL= 15   RANGEI=   437.66   RANGEN=   419.95
NPHV=  99   KD= 143   RANGEP=   416.01   ANGLEP=   26.57   NSAMPL= 15   RANGEI=   419.95   RANGEN=   393.70
NPHV= 100   KD= 144   RANGEP=   390.89   ANGLEP=   26.36   NSAMPL= 11   RANGEI=   393.70   RANGEN=   368.11
NPHV= 101   KD= 145   RANGEP=   364.93   ANGLEP=   25.98   NSAMPL= 10   RANGEI=   368.11   RANGEN=   336.29
NPHV= 102   KD= 146   RANGEP=   332.39   ANGLEP=   25.78   NSAMPL= 12   RANGEI=   336.29   RANGEN=   303.81
```

TIME OF SWEEP START = 57.474 SEC.
TIME OF SWEEP END = 57.655 SEC.
MID TIME OF SWEEP = 58.565 SEC.

IP	TIME	RANGE	ANGLE	YP	ZP	DELTA TIME	C WIND	SPEED	IFREQ	INTENSITY
1	57.474	485.8	62.6	68.4	260.7	1.091	.00	10.43	12	254
2	57.489	453.5	62.4	62.5	231.4	1.076	.00	10.43	12	240
3	57.504	418.9	62.1	57.7	200.4	1.061	.00	11.30	13	174
4	57.519	384.9	61.8	112.6	169.9	1.046	.00	10.43	12	128
5	57.579	410.4	60.8	97.3	190.4	.986	.00	11.30	13	318
6	57.594	438.9	60.6	82.6	215.1	.971	.00	9.56	11	320
7	57.609	471.9	60.4	65.6	243.4	.956	.00	10.43	12	318
8	57.624	499.8	60.2	50.9	267.1	.941	.00	12.17	14	192
9	57.639	331.1	59.9	39.2	293.4	.926	.00	11.30	13	320
10	57.668	384.6	59.4	3.1	339.7	.896	.00	9.56	11	158
11	57.683	414.3	59.2	-11.2	361.0	.881	.00	9.56	11	124
12	57.758	354.0	58.0	12.1	307.1	.807	.00	10.43	12	112
13	57.773	323.5	57.6	26.5	280.1	.792	.00	11.30	13	224
14	57.788	290.9	57.4	43.1	252.0	.777	.00	12.17	14	222
15	57.803	260.0	57.2	59.1	225.5	.762	.00	10.43	12	240
16	57.818	225.9	57.0	76.8	196.4	.747	.00	10.43	12	160
17	57.833	192.1	56.6	99.2	167.3	.732	.00	10.43	12	190
18	57.892	202.4	55.8	86.1	179.3	.672	.00	9.56	11	124
19	57.907	232.8	55.4	67.7	198.4	.657	.00	11.30	13	256
20	57.922	266.1	55.2	48.0	225.5	.642	.00	11.30	13	288
21	57.937	292.1	55.0	32.3	248.2	.627	.00	9.56	11	238
22	57.952	325.3	54.8	12.3	272.7	.613	.00	9.56	11	200
23	57.982	383.7	54.2	-24.6	318.1	.583	.00	9.56	11	128
24	58.072	362.4	52.8	-19.2	295.4	.493	.00	9.56	11	144
25	58.087	331.1	52.6	-1.3	269.9	.478	.00	9.56	11	188
26	58.102	296.7	52.2	16.8	243.0	.463	.00	9.56	11	256
27	58.117	267.4	52.0	35.3	217.4	.448	.00	9.56	11	190
28	58.132	234.1	51.8	55.2	190.9	.433	.00	9.56	11	374
29	58.146	200.0	51.6	75.7	163.4	.418	.00	9.56	11	172
30	58.206	195.6	50.6	75.7	158.1	.359	.00	8.69	10	126
31	58.221	226.5	50.2	55.0	180.9	.344	.00	9.56	11	256
32	58.236	259.8	50.0	32.9	206.0	.329	.00	11.30	13	278
33	58.251	285.9	49.8	15.4	225.1	.314	.00	10.43	12	176
34	58.266	316.4	49.6	-6.5	249.3	.299	.00	8.69	10	142
35	58.281	344.7	49.2	-25.4	267.8	.284	.00	11.30	13	180
36	58.296	378.0	49.0	-48.1	292.2	.269	.00	12.17	14	144
37	58.311	401.6	48.8	-64.6	309.1	.254	.00	8.69	10	112
38	58.341	435.6	48.3	-89.5	332.6	.224	.00	12.17	14	128
39	58.371	394.1	47.8	-64.9	296.8	.194	.00	16.52	19	164
40	58.386	369.5	47.6	-49.3	279.7	.179	.00	13.04	15	152
41	58.400	335.6	47.3	-27.4	253.8	.164	.00	13.04	15	148
42	58.415	305.1	47.0	-8.2	230.0	.149	.00	12.17	14	152
43	58.430	273.8	46.8	12.5	206.6	.134	.00	8.69	10	254
44	58.445	242.0	46.6	33.7	182.8	.120	.00	8.69	10	432
45	58.535	220.4	45.2	44.6	163.1	.030	.00	8.69	10	128
46	58.550	252.1	44.8	21.1	189.4	.015	.00	8.69	10	128
47	58.565	280.4	44.6	.3	203.8	.000	.00	9.56	11	192
48	58.580	311.5	44.4	-22.6	224.8	-.015	.00	9.56	11	172
49	58.595	340.7	44.1	-44.5	244.1	-.030	.00	12.17	14	126
50	58.610	371.2	43.8	-68.0	263.8	-.045	.00	10.43	12	128
51	58.639	425.0	43.4	-108.9	298.9	-.075	.00	10.43	12	124
52	58.669	425.3	42.8	-112.4	295.8	-.105	.00	11.30	13	128
53	58.684	401.4	42.6	-95.6	278.4	-.120	.00	9.56	11	152

54	58.699	376.2	42.4	-77.9	260.5	-.134	.00	13.91	16	190
55	58.729	314.3	41.8	-34.4	216.4	-.164	.00	8.69	10	128
56	58.744	280.6	41.6	-9.9	193.2	-.179	.00	10.43	12	128
57	58.908	335.7	39.0	-61.0	218.1	-.344	.00	8.69	10	144
58	58.938	391.9	38.4	-107.2	250.3	-.373	.00	10.43	12	126
59	58.953	418.0	38.2	-128.6	265.4	-.388	.00	12.17	14	136
60	58.968	439.6	38.0	-146.6	277.4	-.403	.00	9.56	11	126
61	59.013	380.2	37.2	-102.9	236.7	-.448	.00	11.30	13	238
62	59.028	346.1	37.0	-78.2	216.2	-.463	.00	20.87	24	128
63	59.207	299.8	34.0	-48.6	174.5	-.642	.00	12.17	14	126
64	59.267	412.5	33.0	-146.1	231.5	-.702	.00	10.43	12	160
65	59.566	381.5	20.0	-136.9	186.0	-1.001	.00	8.69	10	128
66	59.581	404.6	27.8	-158.0	195.4	-1.016	.00	8.69	10	112
67	59.655	364.9	26.6	-126.9	170.3	-1.091	.00	8.69	10	192

UNDER	VELOCITY	INTENSITY
1	62	44
2	39	28
3	54	6
4	40	9
5	41	5
6	8	7
7	14	20
8	36	32
9	38	19
10	42	26
11	44	31
12	59	1
13	63	43
14	3	4
15	5	15
16	9	21
17	13	61
18	19	13
19	20	14
20	32	22
21	35	8
22	52	47
23	61	67
24	1	17
25	2	27
26	4	54
27	7	25
28	12	35
29	15	33
30	16	3
31	17	29
32	33	48
33	50	39
34	51	16
35	56	64
36	58	10
37	64	40
38	0	42
39	10	53
40	11	41
41	18	24

42	21	36
43	22	57
44	23	34
45	24	59
46	25	4
47	26	23
48	27	38
49	28	45
50	29	46
51	31	50
52	47	52
53	48	55
54	53	56
55	60	62
56	30	65
57	34	30
58	37	49
59	43	58
60	44	60
61	45	63
62	46	11
63	55	18
64	57	51
65	65	12
66	66	37
67	67	66

II	III	N1	N2	R2
44	28	2	2	528.17
44	6	3	3	3443.30
44	20	4	4	2028.29
44	32	5	5	539.24
44	19	6	6	1408.77
44	31	7	7	456.58
44	43	8	8	1009.41
44	15	9	9	2470.52
44	47	10	10	1555.29
44	27	11	11	1216.85
44	33	12	12	2144.54
44	29	13	13	2129.46
44	16	14	14	2044.82
44	45	15	15	498.80
44	46	16	16	162.32
44	56	17	17	2007.23
44	30	18	18	2380.44
44	18	19	19	2824.32

KV = 1 JJJ = 44 YC = 46.4 ZC = 198.7

II	III	N1	N2	R2
61	54	2	2	1190.72
61	64	3	3	1888.51
61	53	4	4	1807.21
61	57	5	5	2106.69
61	59	6	6	1481.17
61	50	7	7	1952.76

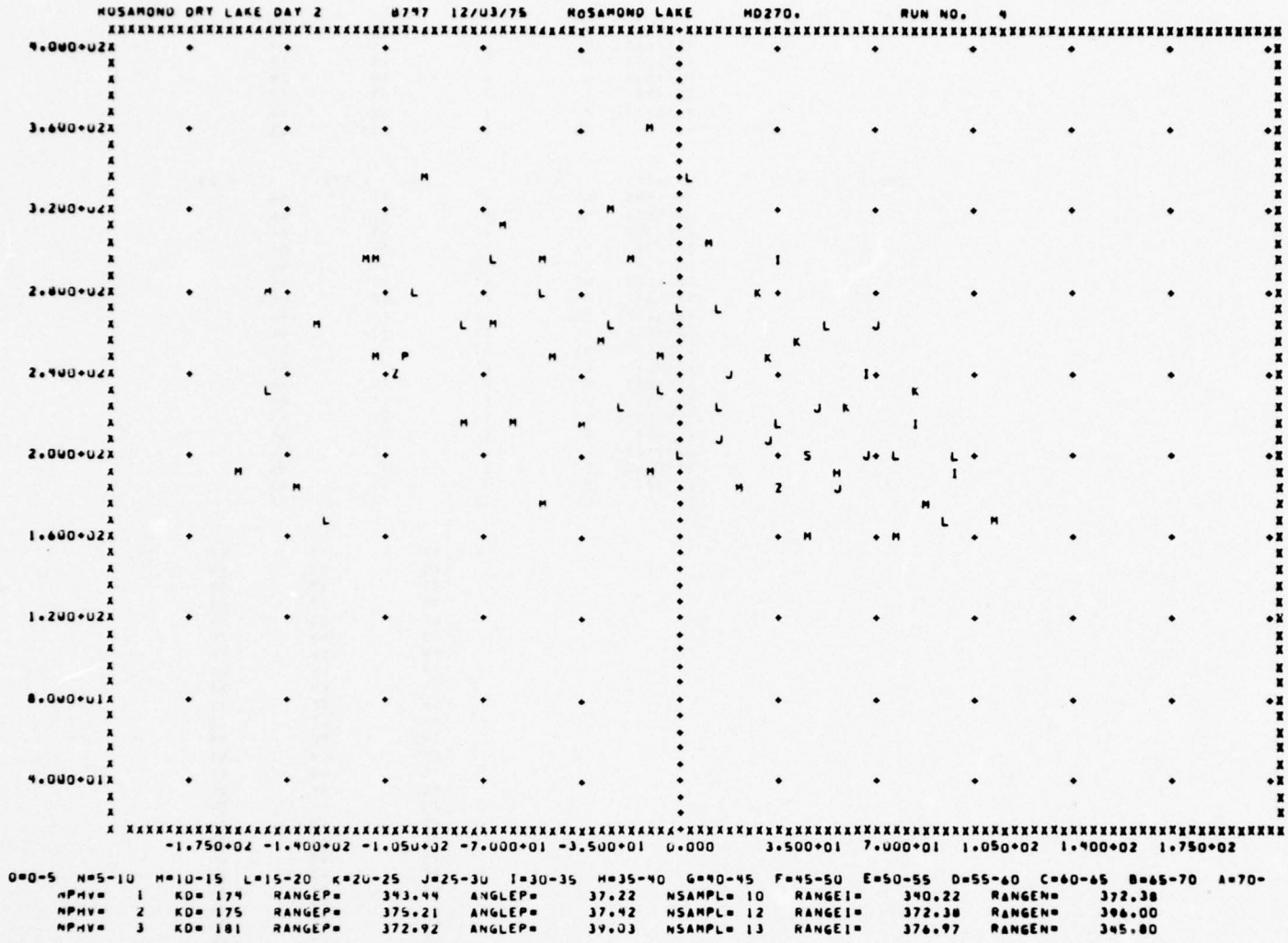
ROSAMOND DRY LAKE DAY 2 8797 12/03/75 ROSAMOND LAKE HD270. RUN NO. 4
9.000+02
3.600+02
3.200+02
2.800+02
2.400+02
2.000+02
1.600+02
1.200+02
8.000+01
4.000+01
-1.750+02 -1.400+02 -1.050+02 -7.000+01 -3.500+01 0.000 3.500+01 7.000+01 1.050+02 1.400+02 1.750+02
0=0-5 N=5-10 M=10-15 L=15-20 K=20-25 J=25-30 I=30-35 H=35-40 G=40-45 F=45-50 E=50-55 D=55-60 C=60-65 B=65-70 A=70-
NPHV= 1 KD= 179 RANGEP= 393.44 ANGLEP= 37.22 NSAMPL= 10 RANGEI= 340.22 RANGEN= 372.38
NPHV= 2 KD= 175 RANGEP= 375.21 ANGLEP= 37.42 NSAMPL= 12 RANGEI= 372.38 RANGEN= 306.00
NPHV= 3 KD= 181 RANGEP= 372.92 ANGLEP= 39.03 NSAMPL= 13 RANGEI= 376.97 RANGEN= 345.80

NPHV=	4	KD= 219	RANGEP=	538.75	ANGLEP=	48.56	NSAMPL= 12	RANGEI=	411.75	RANGEN=	1970.19
NPHV=	5	KD= 226	RANGEP=	337.17	ANGLEP=	60.22	NSAMPL= 10	RANGEI=	340.22	RANGEN=	309.71
NPHV=	6	KD= 227	RANGEP=	305.62	ANGLEP=	60.42	NSAMPL= 12	RANGEI=	309.71	RANGEN=	276.59
NPHV=	7	KD= 228	RANGEP=	271.84	ANGLEP=	60.62	NSAMPL= 11	RANGEI=	275.59	RANGEN=	241.47
NPHV=	8	KD= 229	RANGEP=	237.20	ANGLEP=	60.65	NSAMPL= 13	RANGEI=	241.47	RANGEN=	208.66
NPHV=	9	KD= 230	RANGEP=	204.94	ANGLEP=	61.22	NSAMPL= 11	RANGEI=	208.66	RANGEN=	174.87
NPHV=	10	KD= 235	RANGEP=	222.18	ANGLEP=	62.42	NSAMPL= 10	RANGEI=	218.83	RANGEN=	282.30
NPHV=	11	KD= 236	RANGEP=	255.02	ANGLEP=	62.62	NSAMPL= 10	RANGEI=	252.30	RANGEN=	279.53
NPHV=	12	KD= 237	RANGEP=	283.21	ANGLEP=	62.80	NSAMPL= 11	RANGEI=	279.53	RANGEN=	312.99
NPHV=	13	KD= 238	RANGEP=	315.52	ANGLEP=	62.78	NSAMPL= 10	RANGEI=	312.99	RANGEN=	338.25

ROSAMOND DRY LAKE DAY 2 B747 12/03/75
TIME IS 7: 3:50
ROSAMOND LAKE HD270. RUN NO. 4

STARBOARD VORTEX

TIME	Z	Y
4.05621	260.652	44.1498
8.27676	260.229	38.5139
13.8568	212.365	47.6868
15.5002	278.173	6.46237
18.7123	271.046	30.3668
20.6620	257.905	26.2682
24.3148	224.413	55.0379
26.2645	177.873	46.3209
29.8949	259.492	26.9209
31.6056	171.146	59.0845
34.7579	230.324	46.7477
37.0064	220.007	5.36603
40.5472	241.469	61.3459
42.5118	244.896	40.6397
45.4176	230.303	52.5408
47.4121	192.493	60.0888
51.1471	205.975	83.2493
53.0743	192.320	58.7777
63.6145	233.186	37.4797
69.2095	220.445	35.1234

PORT VORTEX

TIME	∠	Y
4.05621	316.589	-81.6382
8.27676	357.333	-29.5650
13.8568	349.730	-34.7920
15.5002	258.296	-114.384
18.7123	323.249	-69.0965
20.6620	269.113	-123.139
24.3148	323.246	-60.4487
26.2645	273.360	14.0868
29.8949	323.499	-74.6053
31.6056	232.370	-37.9057
34.7579	334.106	-23.4391
37.0064	243.742	-125.949
40.5472	289.022	-84.2635
42.5118	258.368	-105.767
45.4176	318.621	-45.9242
47.4121	269.746	-97.0168
51.1471	354.548	-20.3668
53.0743	237.969	-126.092
63.6145	297.511	-90.3922
69.2095	308.295	-82.9007

UNKNOWN TYPE OF VORTEX

TIME	Z	Y
2.89089	286.775	31.5946
9.94257	297.216	-87.3446
56.5852	253.098	45.4470
58.5648	198.678	46.4100
61.9412	252.638	67.2202
67.1926	342.761	-.433675
73.0118	342.916	-59.9073
77.9868	296.564	-91.7344
80.8926	230.220	-141.526
89.0200	261.570	-43.6382
91.4552	235.385	-136.489
94.5179	262.498	-29.0438
96.8784	248.933	-124.571

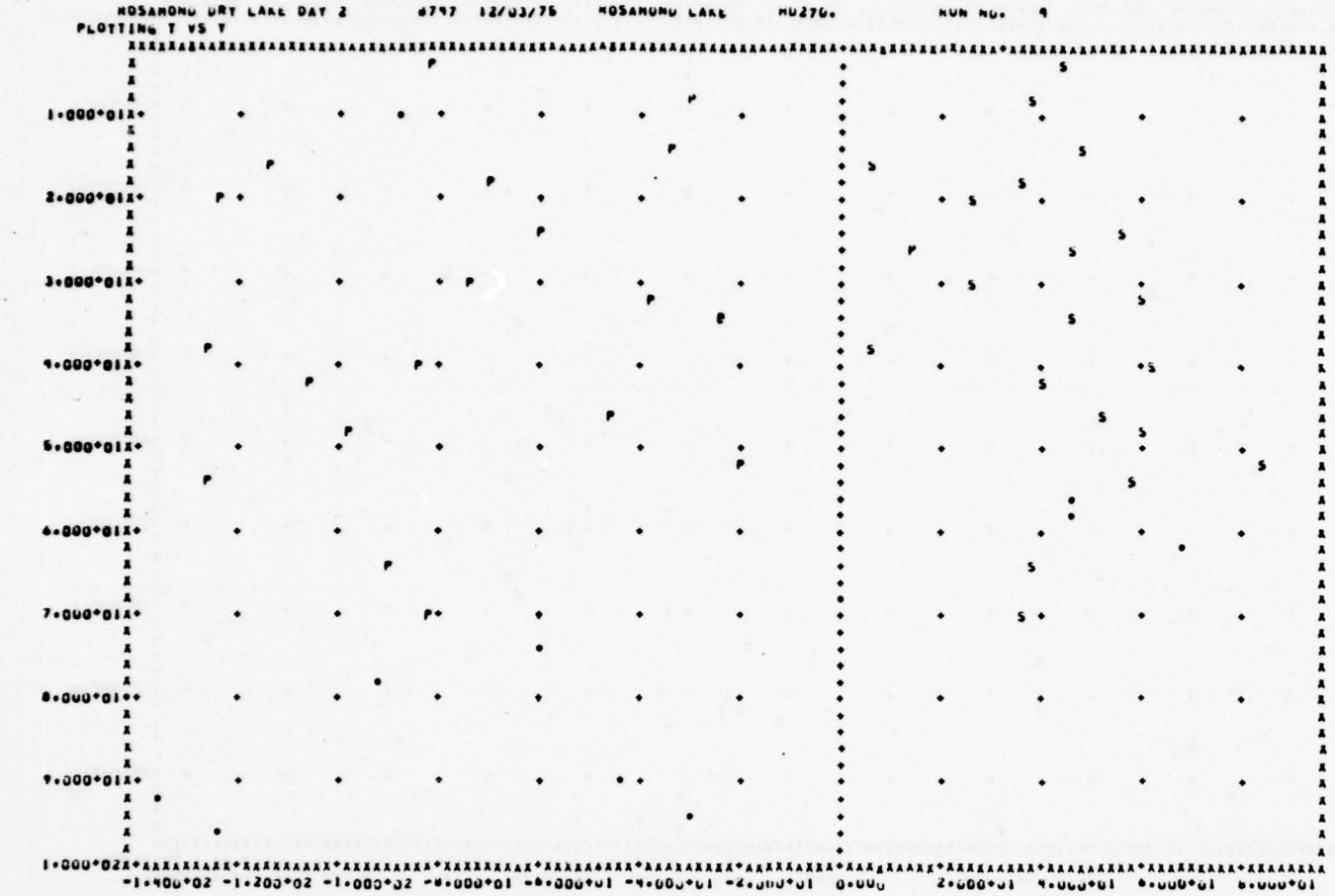

THE INTERPRETATION OF MEANINGLESS INPUT WAS ATTEMPTED.
THE FOLLOWING RECORD IS ERRONEOUS OR DOES NOT CORRESPOND TO FORMAT SPECIFICATIONS:

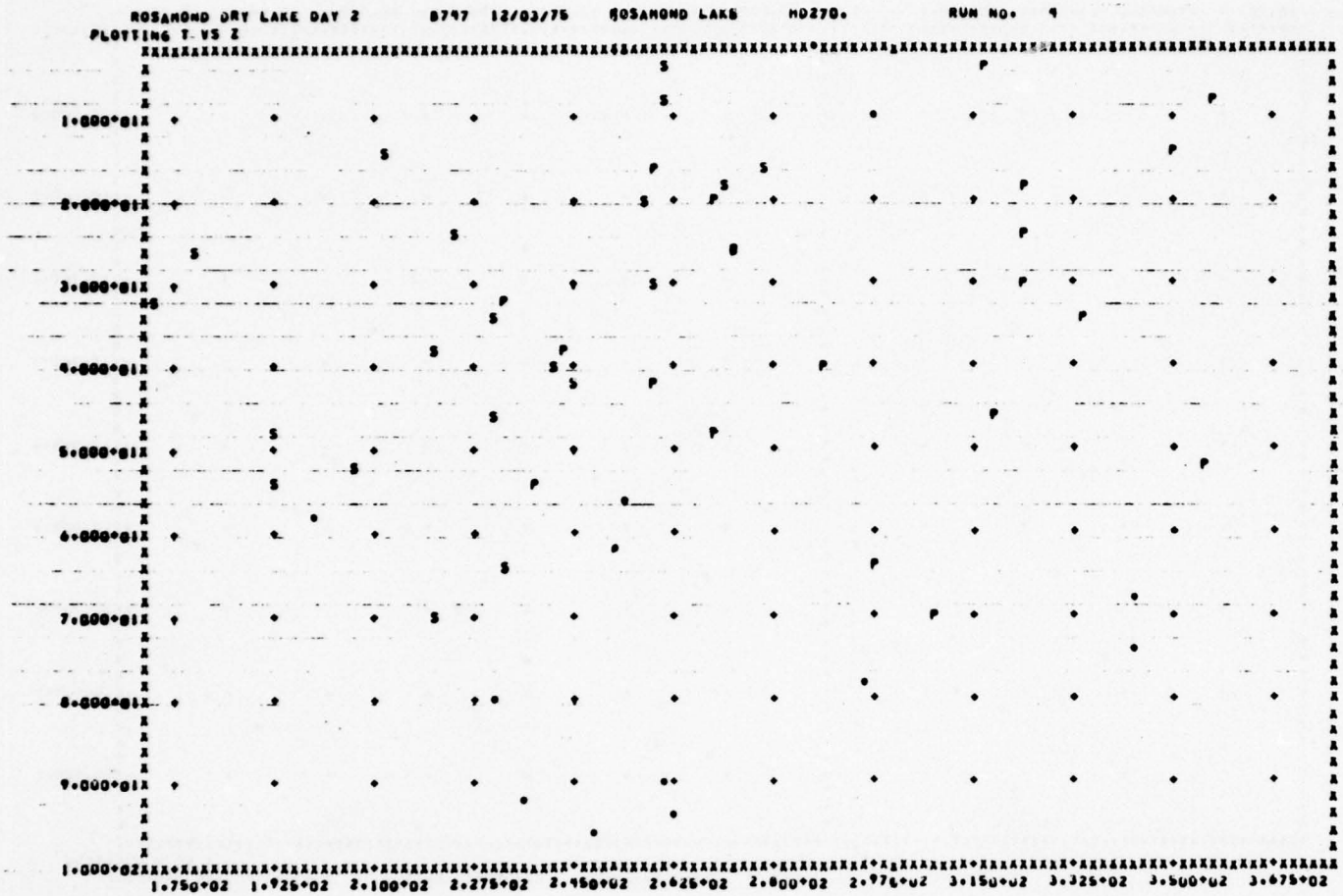
ROSAMOND DRY LAKE DAY 2 8747 12/03/75 ROSAMOND LAKE MD270. RUN NO. 9
PLOTTING T VS Z
1.000+01
2.000+01
3.000+01
4.000+01
5.000+01
6.000+01
7.000+01
8.000+01
9.000+01
1.000+02
1.750+02 1.925+02 2.100+02 2.275+02 2.450+02 2.625+02 2.800+02 2.975+02 3.150+02 3.325+02 3.500+02 3.675+02

Appendix C

SAMPLE OUTPUT FROM NASA-MSFC LASER DOPPLER VELOCIMETER DATA PROCESSING ROUTINES FOR ROSAMOND FLYBY 47

Results from the Rosamond high-speed data are given on page C-2 including a printout of the relative intensity of the LDV signal (IPEAK) and the frequency (or velocity) of the flow field including V_{ms} and V_{pk} in units of meters per second (VMAX and VPEAK, respectively). The sweep count from the start of the flyby is shown by the column labeled SCAN while the lateral and vertical location and range and elevation angle of the focal volume are given by X (m), Y (m), R (m), and T (deg), respectively. The time at which the LDV signal was sampled is contained in the frame count (1 FRAME = 1/500 sec).

From the array of LDV sample points illustrated on page C-2, plots of VPEAK versus the scan elevation angle in degrees, THETA, are generated as illustrated on pages C-3 through C-6. Note that the characteristic double peak signature of the wake vortex is evident in the sample plots.

Applying the "I_{pk}" algorithm (p. 4-7 of Ref. 7) to the threshold LDV spectrum illustrated above, the vortex location is determined. The vortex trajectory for flyby 47 as computed from the high speed data is shown on pages C-7 through C-9. On page C-7 the vertical and lateral motion of the vortices is given as a function of time, while page C-8 shows the altitude versus lateral position of the wake vortex. Page C-9 lists the vortex locations. For additional information regarding the vortex location, criteria, and coefficients used in the "I_{pk}" algorithm and shown in the plots, refer to Ref. 7.

Note that the coordinate system used in the NASA-MSFC data processing routines is not the same as the coordinate system used in the text earlier. The runway centerline is located at y = -200 ft in the NASA plots.

SCAN	FRAME	X	Y	R	T	IPEAK	VMAX	VPEAK	VAVG	VWIDTH
4	4150	219.4	245.0	328.9	48.2	127	9.8	10.9	9.0	8
4	4151	216.9	242.5	325.3	48.2	131	8.2	10.4	8.7	8
4	4152	218.8	240.0	324.7	47.7	134	8.2	10.9	8.8	8
4	4153	216.9	237.5	321.6	47.6	134	9.3	10.4	9.0	8
4	4154	208.7	235.0	314.3	48.4	123	10.4	10.9	9.1	8
4	4155	206.2	232.5	310.8	48.4	121	9.3	10.4	8.5	8
4	4156	208.1	229.4	309.7	47.8	121	10.4	10.4	8.8	8
4	4157	205.0	226.2	305.3	47.8	124	8.2	10.4	8.5	8
4	4158	196.9	223.7	298.0	48.7	118	8.2	10.4	8.2	8
4	4159	199.4	221.2	297.8	48.0	131	8.2	10.9	8.5	9
4	4160	196.9	217.5	293.4	47.8	136	7.1	10.4	8.0	9
4	4161	189.4	215.6	287.0	48.7	128	9.3	10.4	8.7	7
4	4162	186.2	212.5	282.6	48.8	125	9.3	10.9	9.4	8
4	4163	187.5	209.4	281.1	48.2	116	10.9	10.9	9.1	8
4	4164	185.6	206.9	277.9	48.1	123	8.7	10.9	8.8	5
4	4165	178.1	204.4	271.1	48.9	117	8.7	10.9	9.4	6
4	4166	179.4	201.2	269.6	48.3	111	7.1	10.4	7.8	4
4	4167	177.5	198.7	266.5	48.2	116	9.3	10.4	9.0	6
4	4168	169.4	195.6	258.8	49.1	118	9.3	9.8	8.8	5
4	4169	166.2	192.5	254.4	49.2	131	8.7	9.3	8.5	4
4	4170	169.4	190.6	255.0	48.4	119	8.7	10.9	8.8	4
4	4171	166.2	187.5	250.6	48.4	130	8.7	10.4	8.9	5
4	4172	158.7	185.0	243.8	49.4	126	8.7	8.7	8.3	3
4	4173	156.6	181.9	239.4	49.4	131	8.2	8.7	8.2	3
4	4174	158.1	179.4	239.1	48.6	136	8.2	10.4	8.5	5
4	4175	155.0	176.2	234.7	48.7	128	8.7	10.4	7.5	6
4	4176	147.5	173.1	227.4	49.6	129	8.7	9.8	8.1	5
4	4177	145.0	170.6	223.9	49.6	136	8.7	9.3	8.1	6
4	4178	146.9	168.1	223.2	48.9	120	8.2	8.7	7.5	5
4	4179	139.4	165.0	216.8	49.8	132	7.6	8.7	7.7	4
4	4180	136.2	161.9	211.6	49.9	134	8.2	9.3	8.0	5
4	4181	138.7	159.4	211.3	49.0	128	8.2	8.7	7.5	6
4	4182	136.2	156.3	207.3	48.9	130	8.2	8.7	8.4	2
4	4183	128.1	153.2	200.1	50.2	130	8.2	9.3	8.1	5
4	4184	126.2	151.2	197.0	50.1	117	9.3	9.3	8.5	5
4	4185	128.1	148.1	195.8	49.1	121	7.6	8.7	7.8	4
4	4186	125.6	145.0	191.9	49.1	116	6.0	9.3	7.3	5
4	4187	118.1	141.9	184.6	50.2	106	8.2	8.2	8.2	1
4	4188	115.0	139.4	180.7	50.5	115	8.2	8.7	8.2	2
4	4189	117.5	136.9	180.4	49.9					
4	4190	115.0	134.4	176.9	49.4					
4	4191	107.5	131.2	169.7	50.7					
4	4192	109.4	127.5	168.0	49.4					
4	4193	106.9	125.0	164.5	49.5					
4	4194	99.4	121.9	157.3	50.8					
4	4195	96.2	120.0	153.8	51.3					
4	4196	99.4	117.5	153.9	49.8					
4	4197	96.2	114.4	149.5	49.9					
4	4198	88.7	111.2	142.3	51.4					
4	4199	86.6	108.7	138.4	51.8					

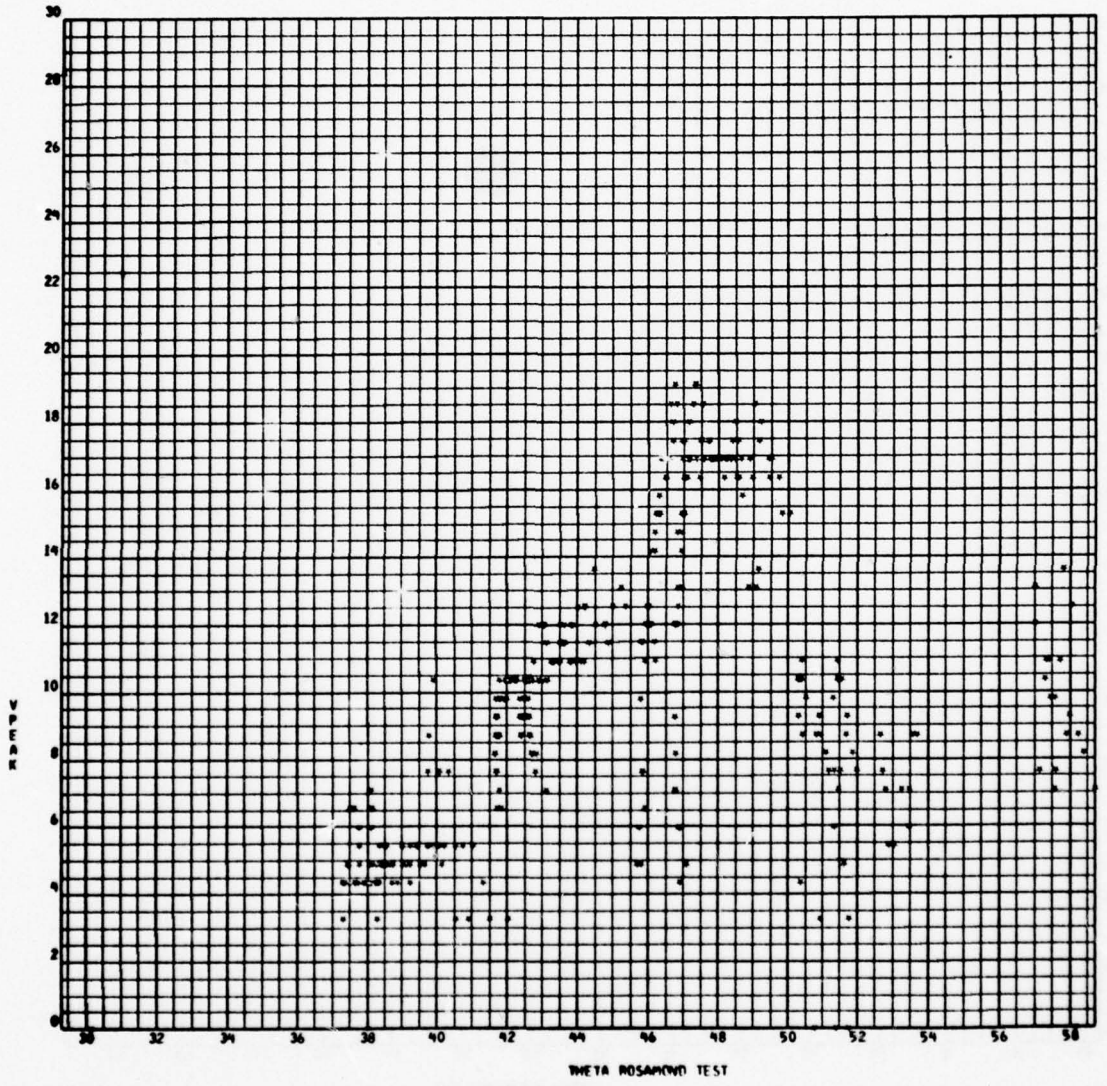
30
28
26
24
22
20
18
16
14
12
10
8
6
4
2
0
VPER
30
32
34
36
38
40
42
44
46
48
50
52
54
56
58
THETA ROSAMOND TEST

SCAN = 3

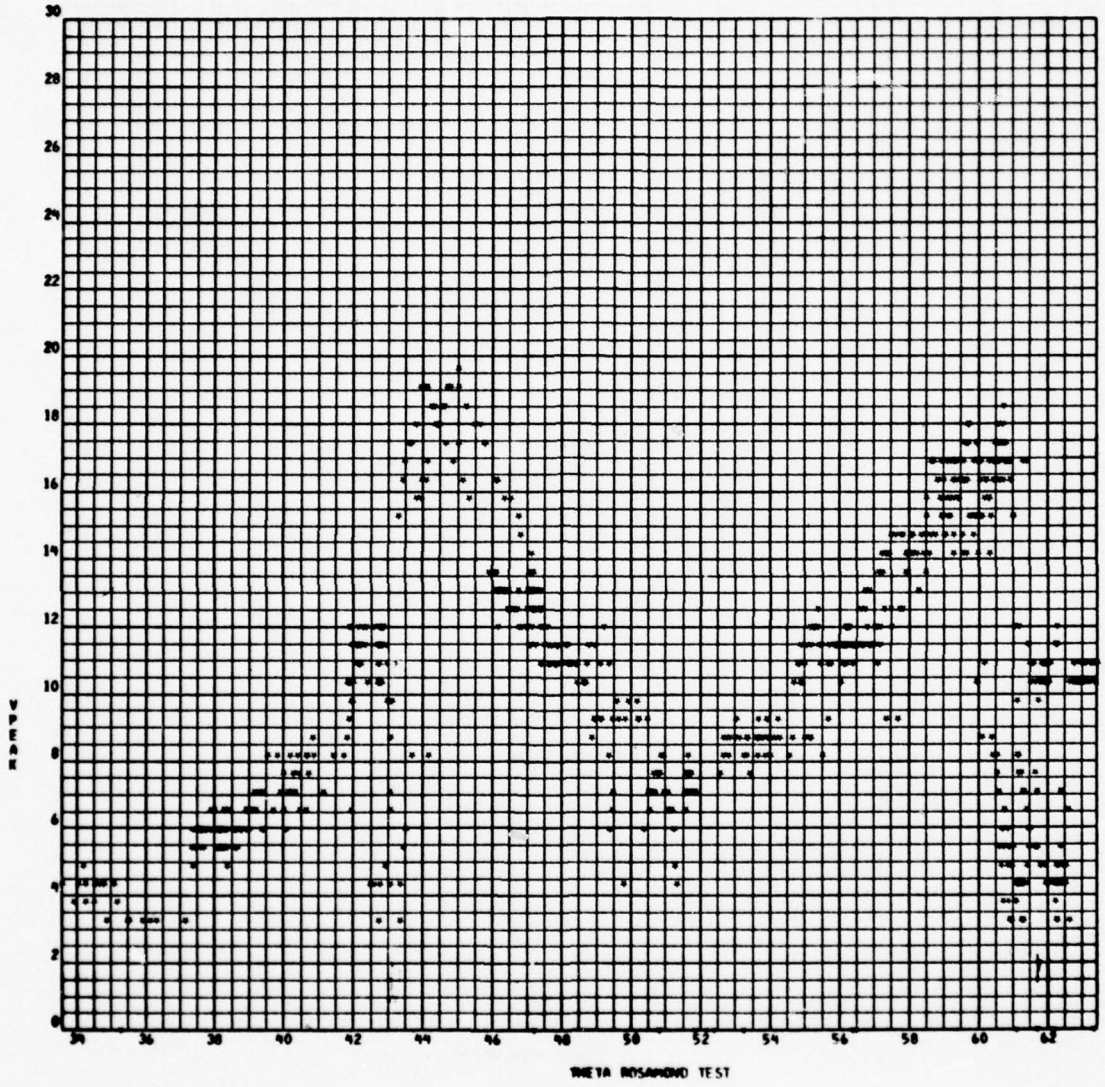

SCAN = 4

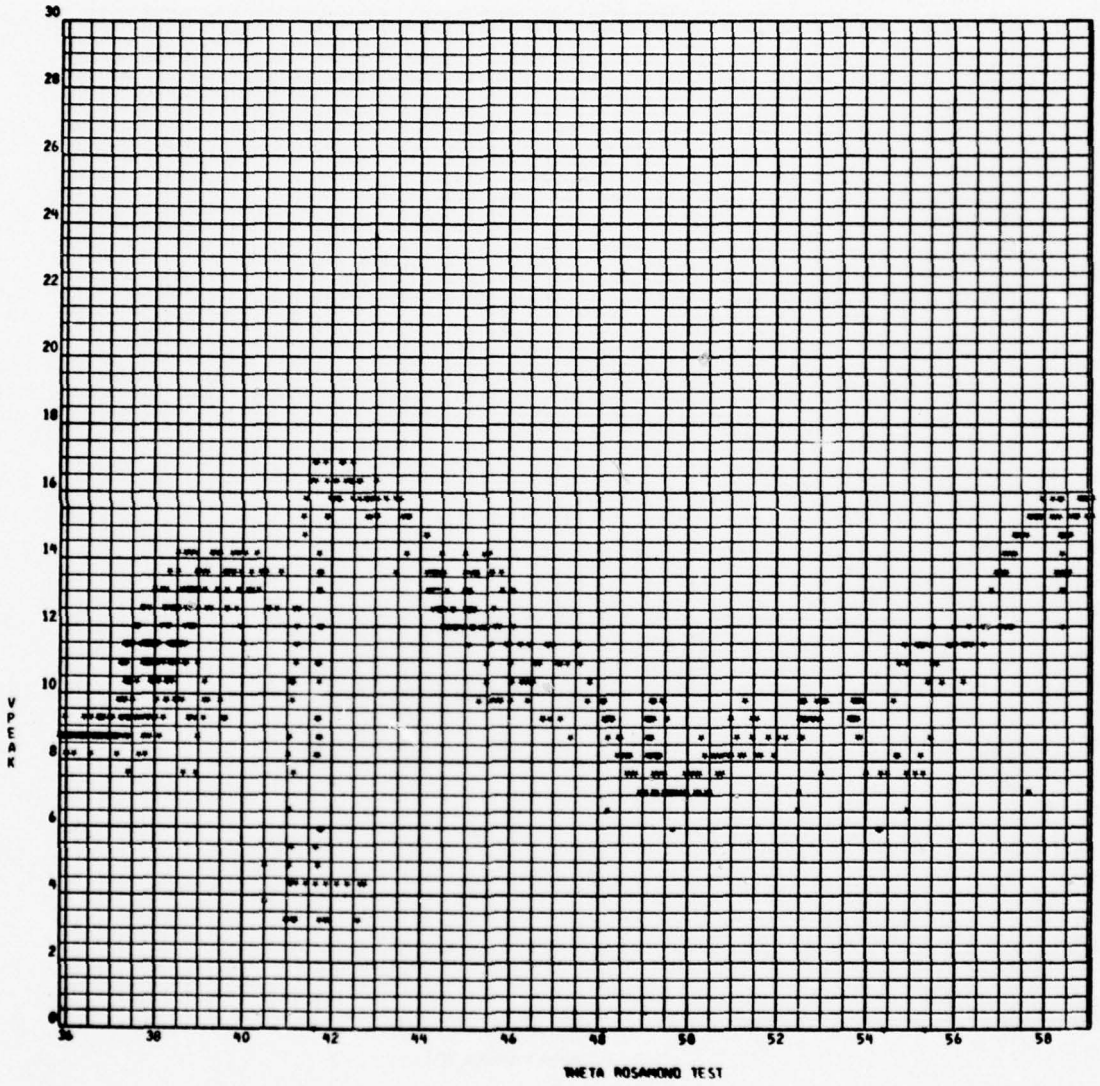
VPEAK
30
28
26
24
22
20
18
16
14
12
10
8
6
4
2
0
36
38
40
42
44
46
48
50
52
54
56
58
THETA ROSAMOND TEST

SCAN = 5

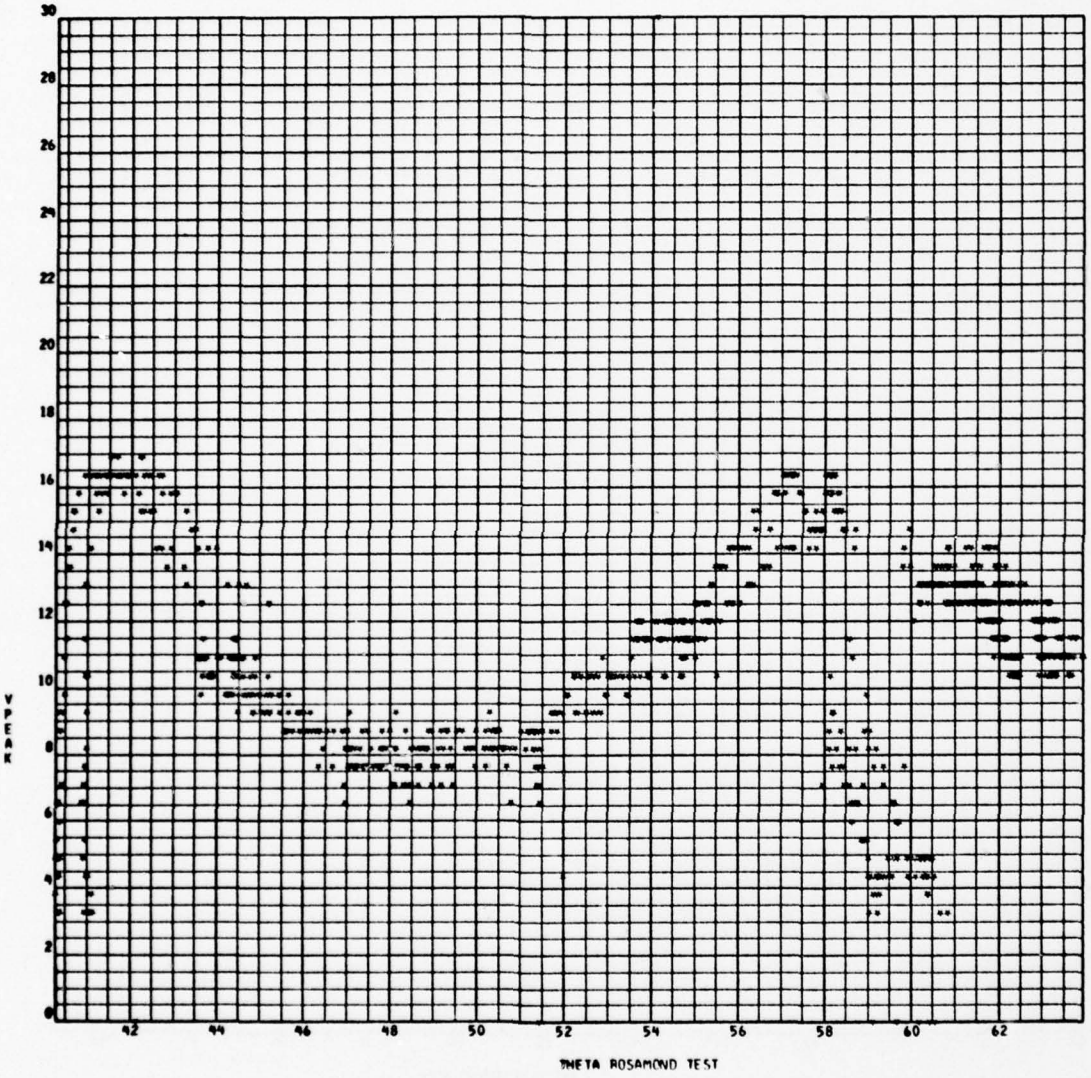
30
28
26
24
22
20
18
16
14
12
10
8
6
4
2
0
VPEAK
42
44
46
48
50
52
54
56
58
60
62
THETA ROSAMOND TEST

SCAN = 6

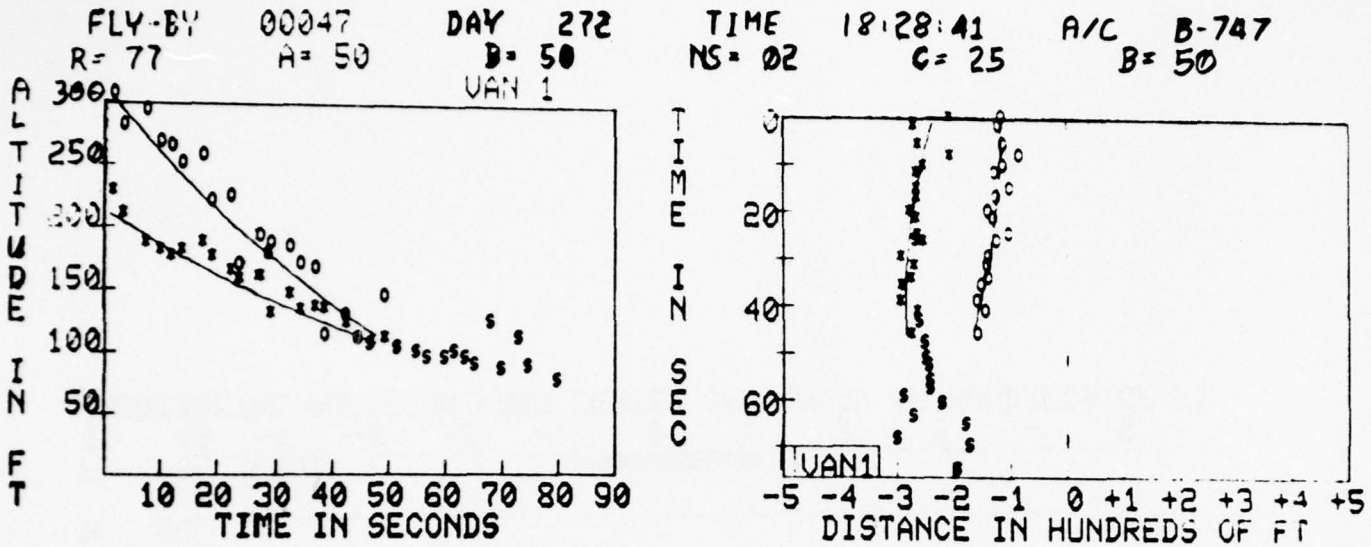
FLY-BY 00047 DAY 272
R= 77 A= 50 B= 50
VAN 1
ALTITUDE IN FT
300
250
200
150
100
50
10 20 30 40 50 60 70 80 90
TIME IN SECONDS
TIME 18:28:41 A/C B-747
NS= 02 C= 25 B= 50
TIME IN SEC
0
20
40
60
VAN1
-5 -4 -3 -2 -1 0 +1 +2 +3 +4 +5
DISTANCE IN HUNDREDS OF FT

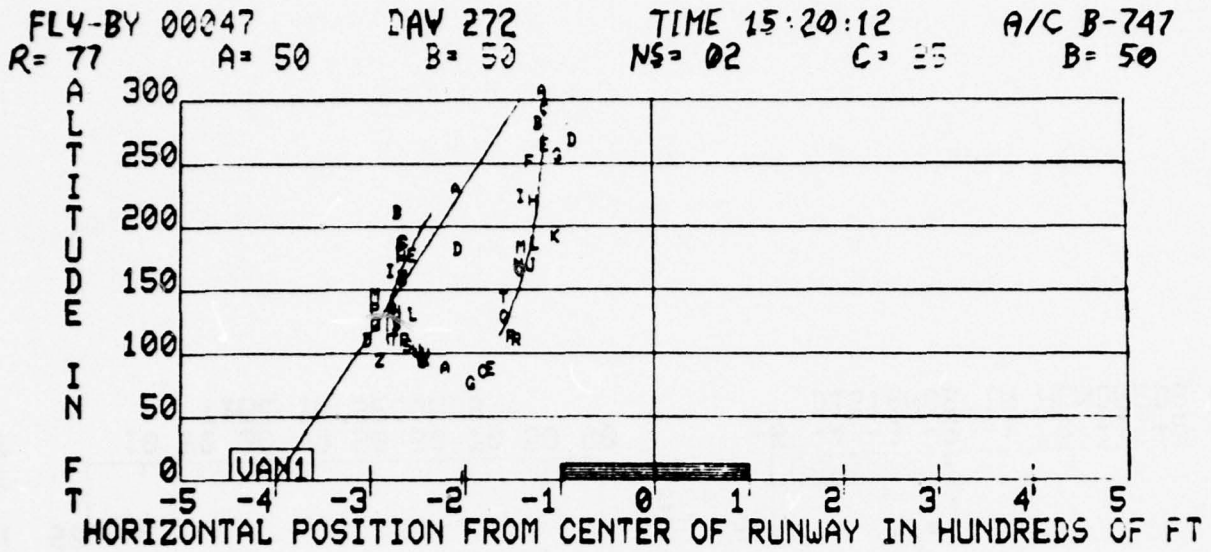
FLY-BY 00047
DAY 272
TIME 15:20:12
A/C B-747
R= 77
A= 50
B= 50
NS= 02
C= 35
B= 50
ALTITUDE IN FT
300
250
200
150
100
50
0
VAN1
-5
-4
-3
-2
-1
0
1
2
3
4
5
HORIZONTAL POSITION FROM CENTER OF RUNWAY IN HUNDREDS OF FT

FLY-BY 00047 DAY 272 TIME 15:28:32 A/C B-747

R = 77 A = 50 B = 50 NS = 02 C = 25 D = 50

FR	DATA PTS	COR PT P	S	NOISE P	S	ANGLE MN	MX	PK P	PAR S	TIME	PORT POS X	Y	STARB POS X	Y
01	2270	151	055	00	00	44	61	230	200	000 8	-211	225	-120	303
02	0491	128	128	00	00	37	62	230	221	002 8	-274	207	-124	277
03	2529	150	099	00	00	33	60	241	210	006 8	-268	183	-117	288
04	0753	250	146	00	00	37	61	222	208	009 4	-210	178	-089	263
05	2931	250	238	00	00	37	61	257	225	011 4	-259	173	-117	260
06	2817	238	250	00	00	36	61	258	209	013 2	-270	177	-133	247
07	2685	250	112	00	00	37	63	248	214	016 7	-271	183	-104	252
08	2719	233	222	00	00	38	61	260	220	018 3	-270	171	-130	216
09	0569	186	135	00	00	38	60	249	185	021 6	-281	160	-144	219
10	0680	209	224	00	00	29	59	248	196	023 2	-269	153	-133	165
11	2577	250	125	00	00	28	62	262	189	026 5	-268	156	-107	187
12	0086	088	088	00	00	88	89	250	000	028 0	-298	128	-129	181
13	0494	151	179	00	00	31	62	265	189	031 8	-298	141	-143	179
14	0401	158	098	00	00	29	60	272	172	033 6	-276	128	-146	165
15	0286	111	088	00	00	30	61	265	170	036 3	-280	131	-144	162
16	0311	056	114	00	00	18	61	276	176	038 0	-297	130	-154	108
17	0187	036	077	00	00	20	63	273	176	041 7	-298	118	-162	124
18	0178	057	025	00	00	18	62	237	145	043 8	-268	105	-148	105
19	0167	062	000	00	02	18	62	238	000	046 0	-264	101		
20	0142	043	019	00	00	19	62	212	144	048 7	-278	106	-162	139
21	0132	062	000	00	00	19	61	218	000	050 9	-254	098		
22	0116	054	000	00	00	19	54	220	000	054 0	-252	094		
23	0297	051	000	00	00	18	51	202	000	055 9	-248	090		
24	0088	003	000	00	00	82	60	188	000	059 2	-246	090		
25	0062	040	000	00	00	20	45	188	000	060 8	-246	094		
26	0082	002	000	00	00	37	42	174	000	062 8	-293	089		
27	0250	048	000	00	00	30	36	198	000	064 3	-224	084		
28	0026	006	000	00	00	39	45	166	000	067 1	-276	118		
29	0290	020	078	00	00	23	32	000	186	069 1			-184	080
30	0222	002	000	00	00	47	49	174	000	072 3	-306	106		
31	0268	000	068	00	00	24	25	000	176	073 8			-176	083
32	0200	000		00		90	90	000						
33	0233	000	024	00	00	19	21	000	196	079 1			-198	072
34	0000	000		00		90	90	000						
35	0000	000		00		90	90	000						
36	0000	000		00		90	90	000						

Appendix D

WAKE VORTEX TRACKS COMPUTED FROM LOW-SPEED MEASUREMENTS

The circles, triangles and diamond symbols represent the port, starboard and undefined vortex, respectively. For each flyby, the predicted wake vortex trajectory assuming zero crosswind is shown by the solid lines. The vortex tracks were computed from the predicted model described in Ref. 10 for a circulation strength of $\Gamma = 662\ m^2/sec$ and an initial vortex spacing of $b' = 41.8\,m$. Available photographic and acoustic measurements also appear on the plots, the solid circles and triangles representing the former and the x's the latter measurements. The dashed line is a smooth curve drawn through the photographic vortex tracks.

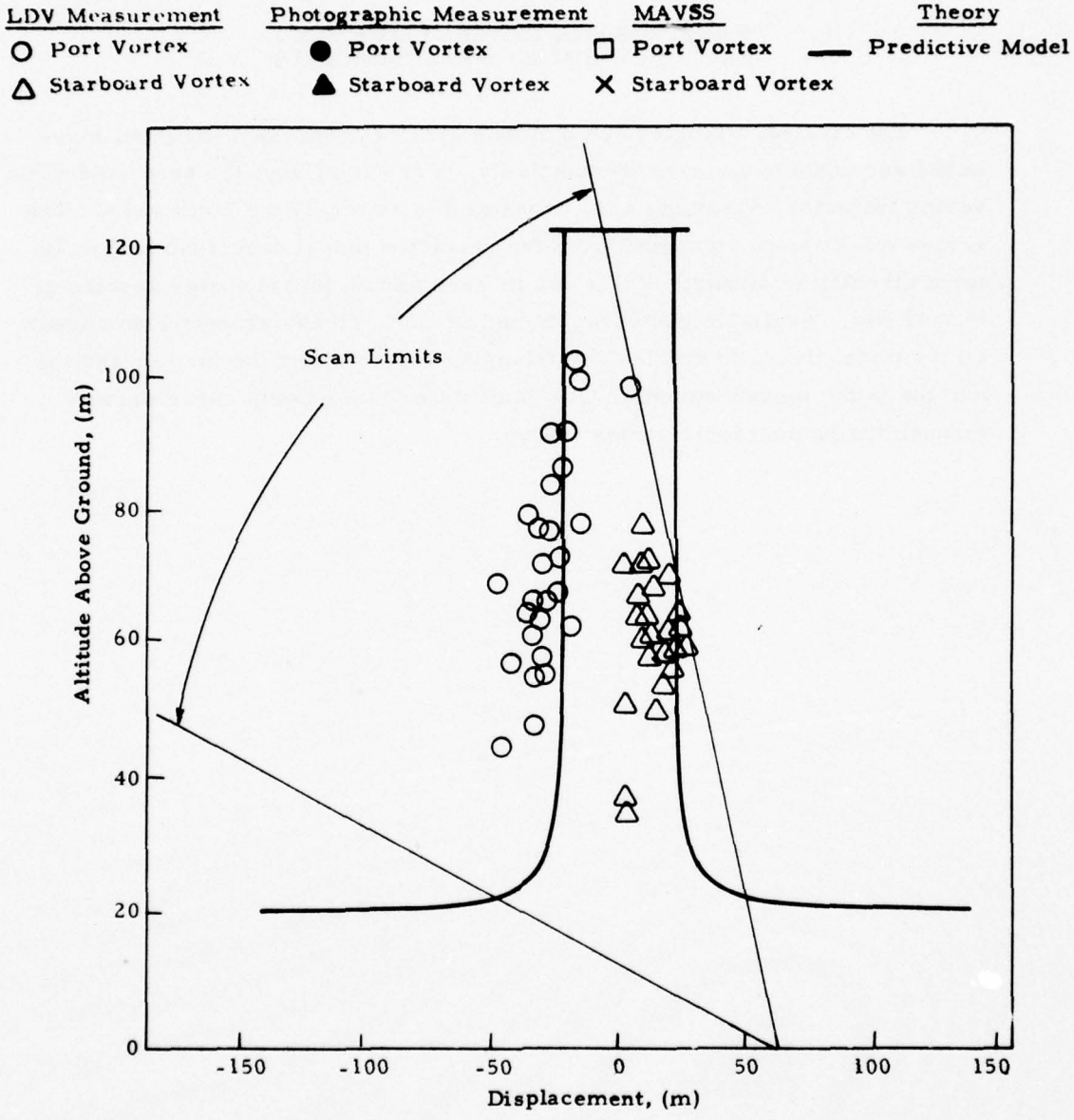

Fig. D-1 - Wake Vortex Trajectory for Rosamond Flyby 23

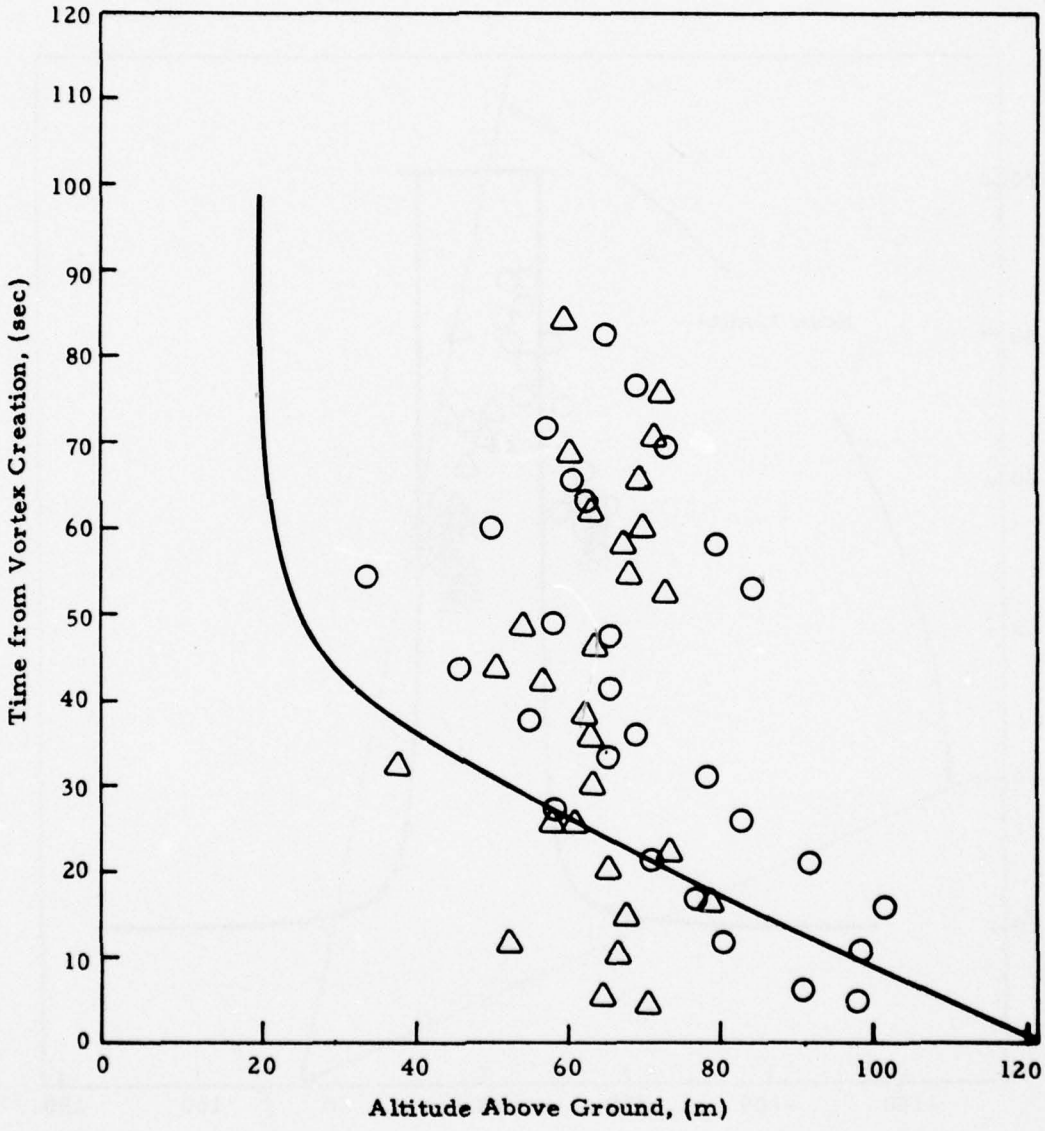

Fig. D-1 - (Concluded)

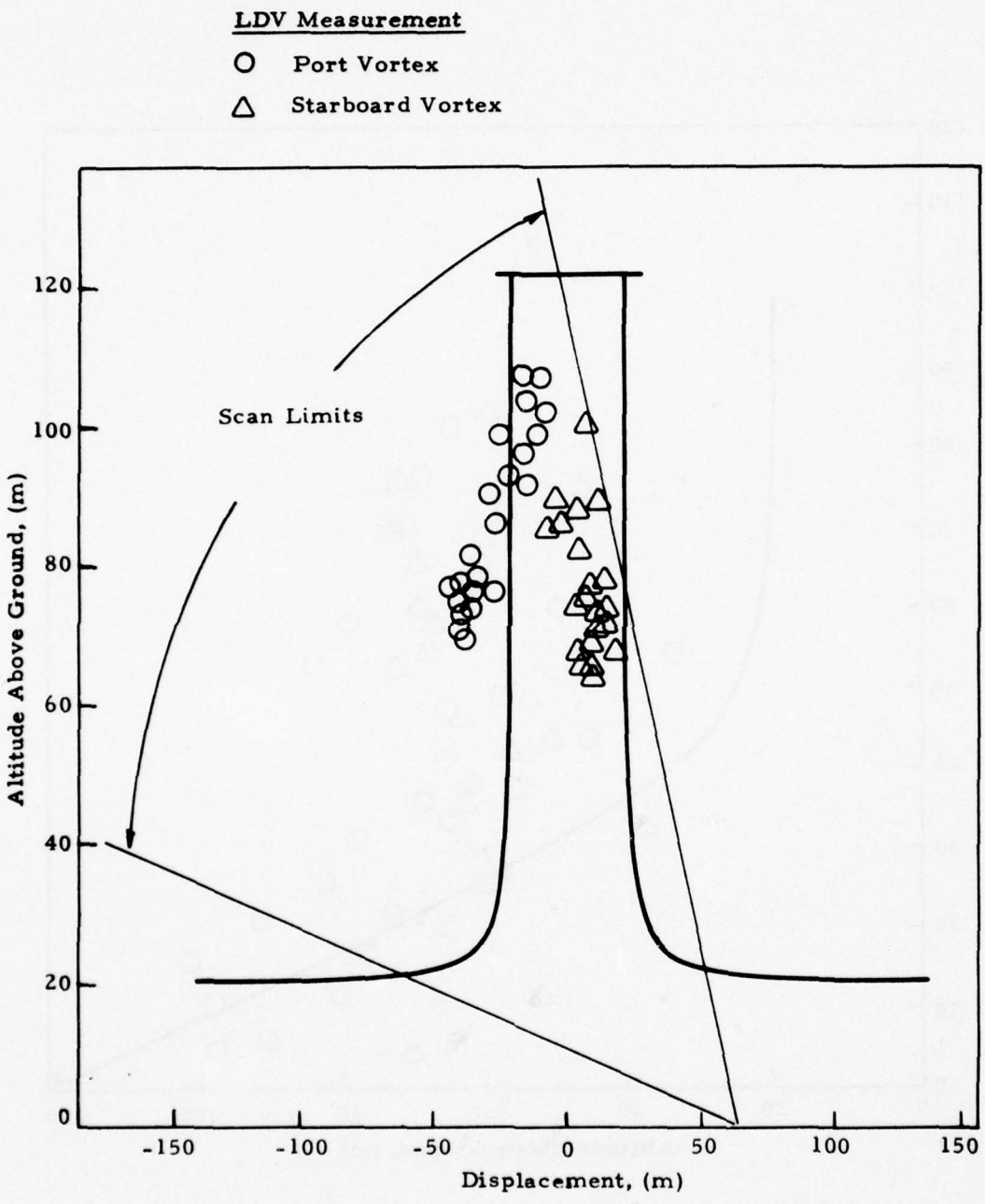

Fig. D-2 - Wake Vortex Trajectory for Rosamond Flyby 24

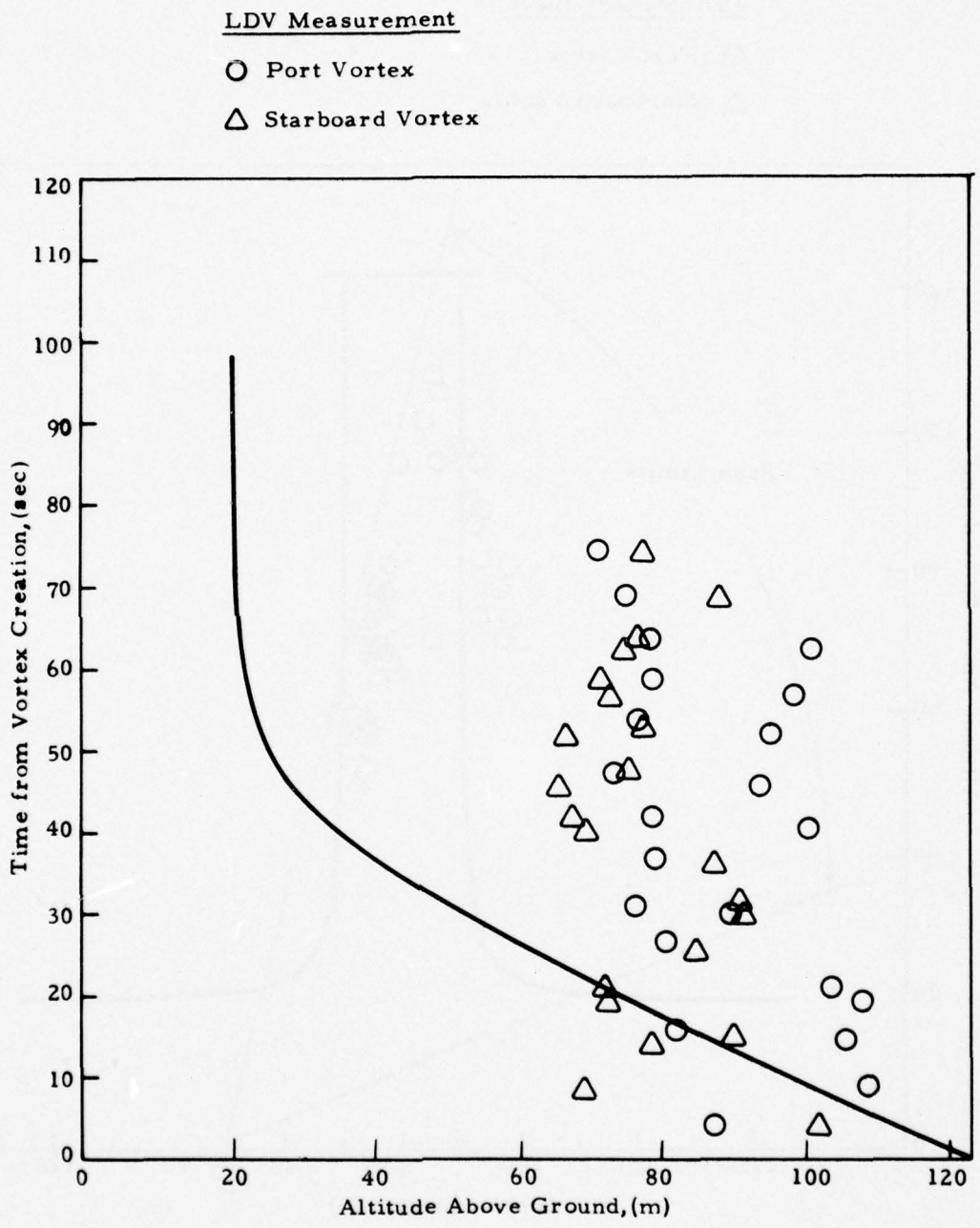

Fig. D-2 - (Concluded)

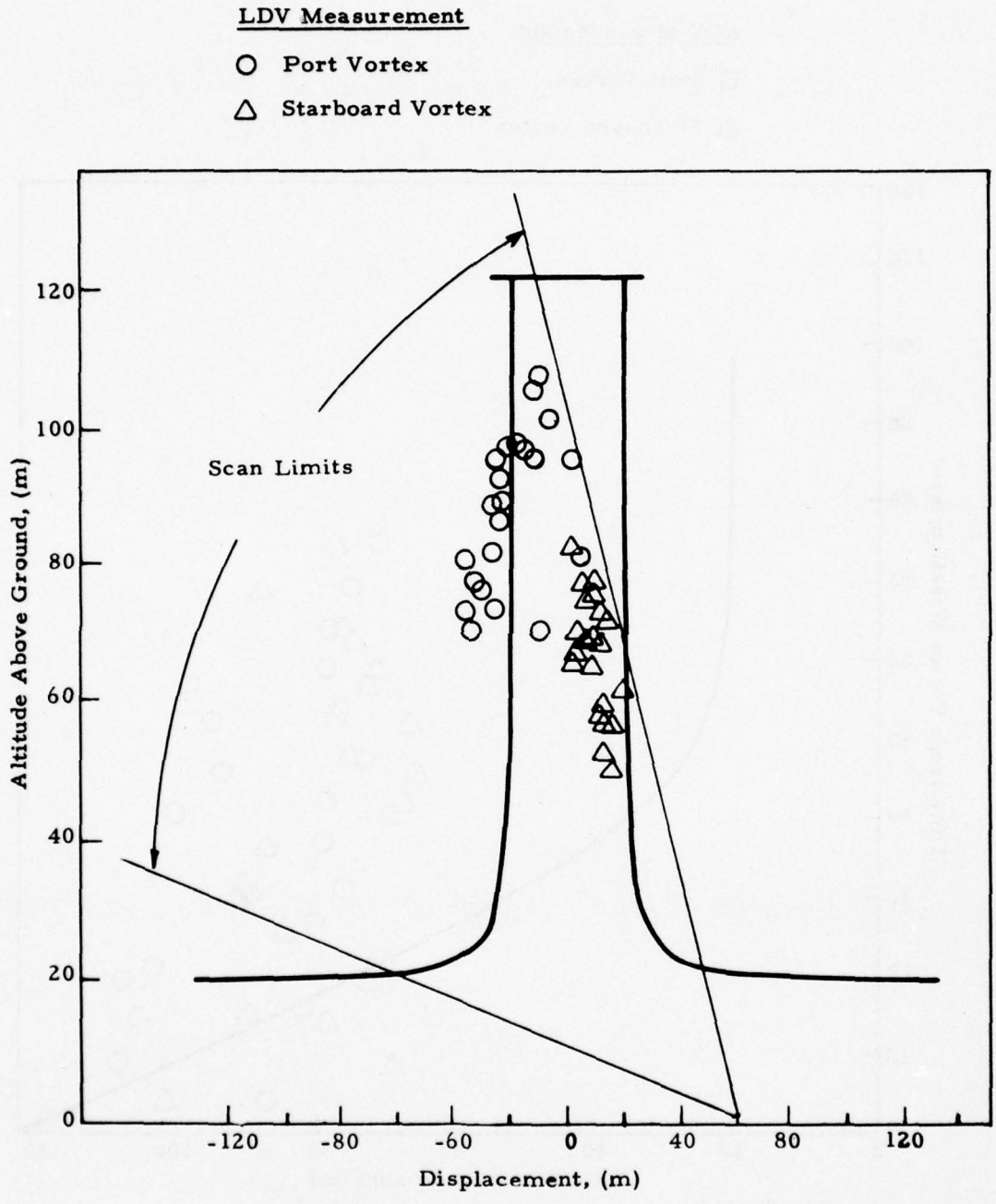

Fig. D-3 - Wake Vortex Trajectory for Rosamond Flyby 25

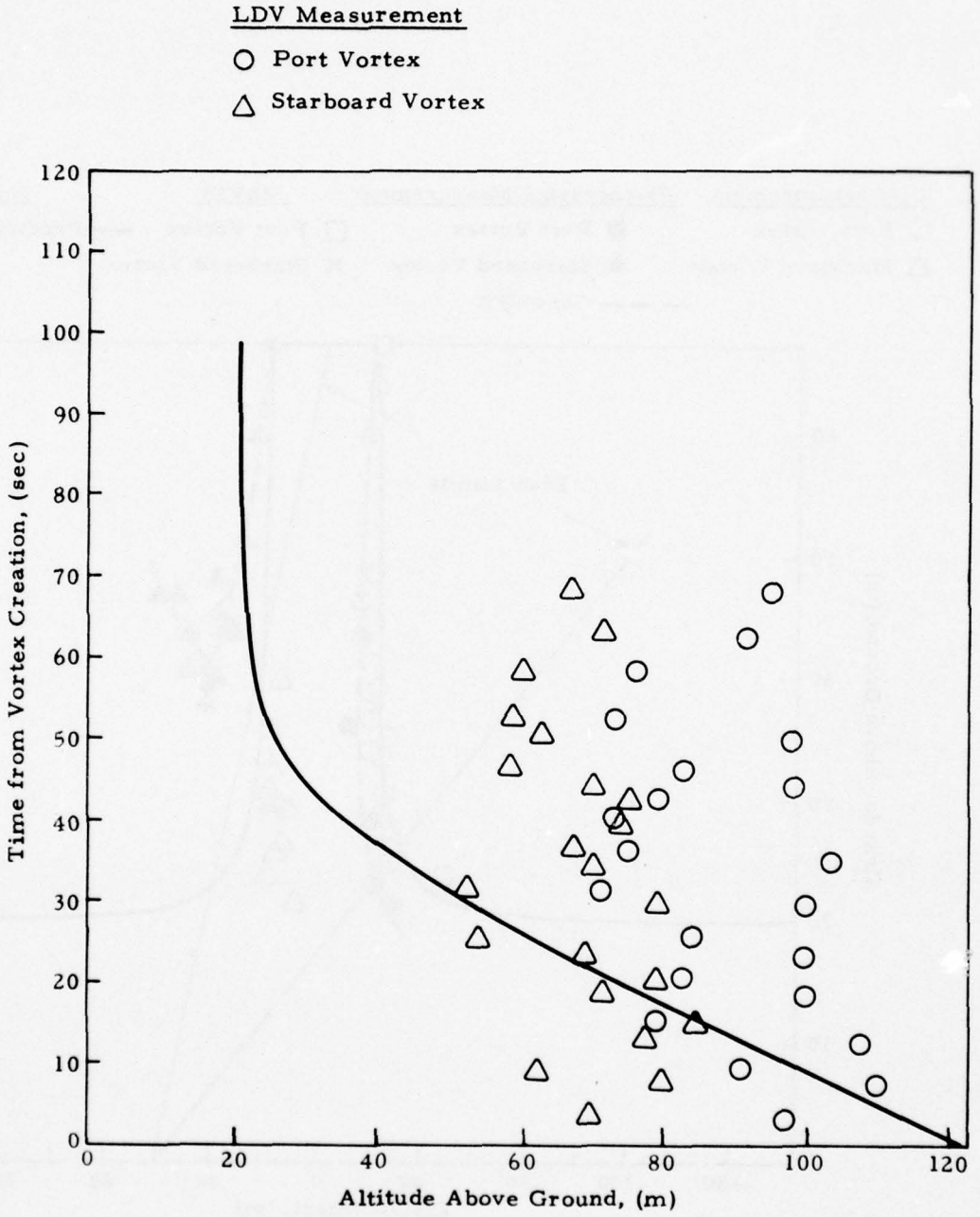

Fig. D-3 - (Concluded)

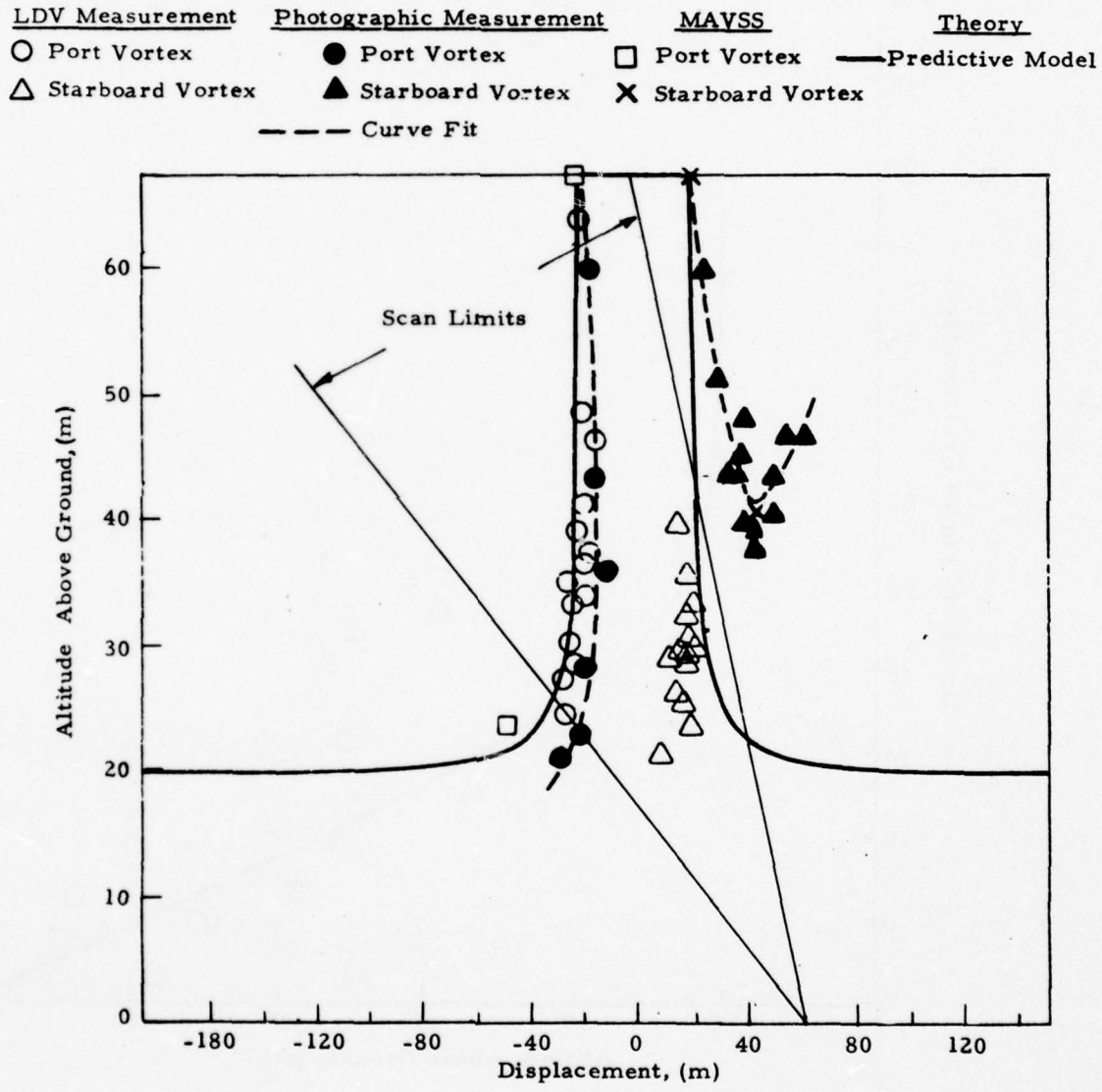

Fig. D-4 - Wake Vortex Trajectory for Rosamond Flyby 27

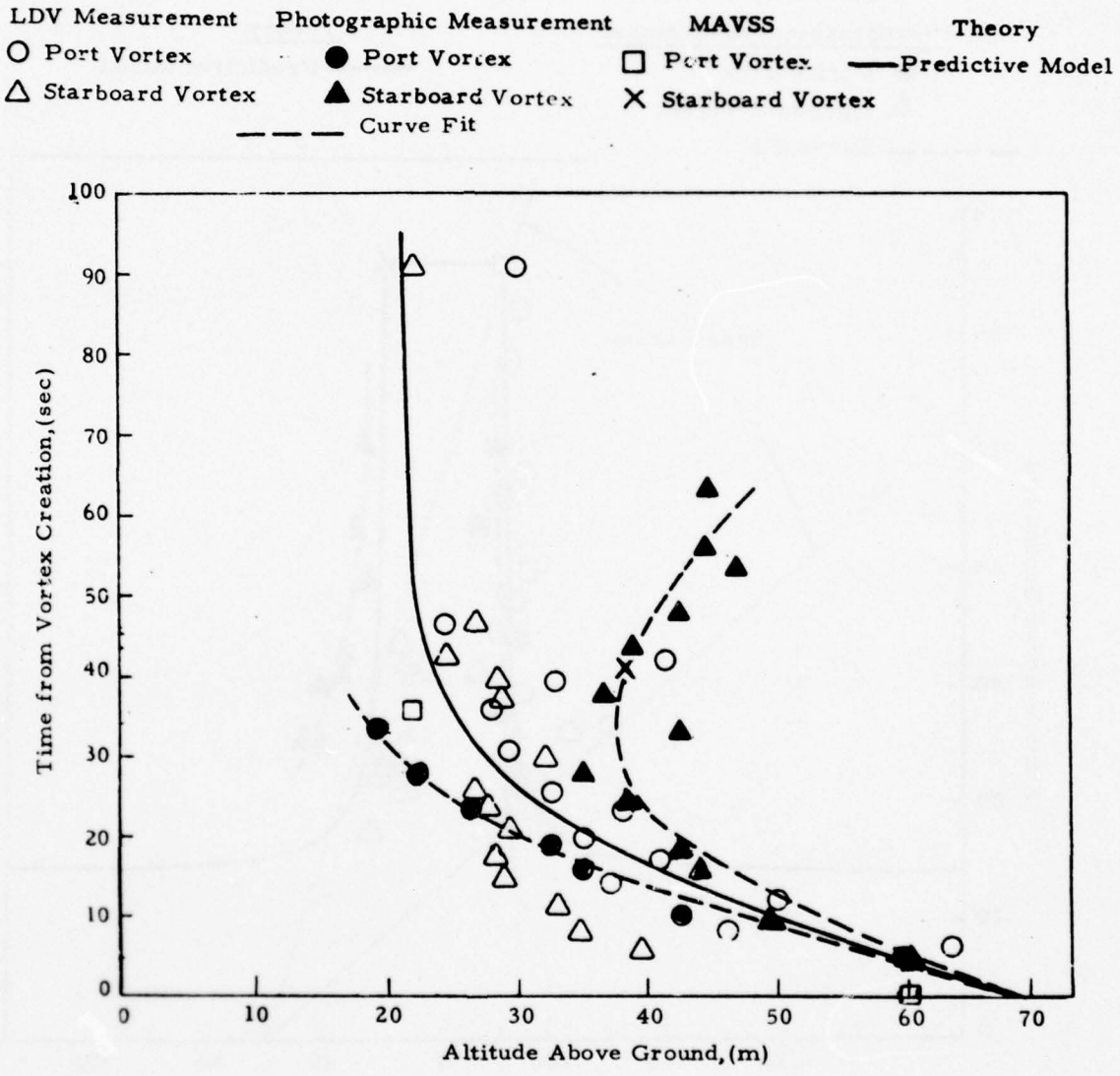

Fig. D-4 - (Concluded)

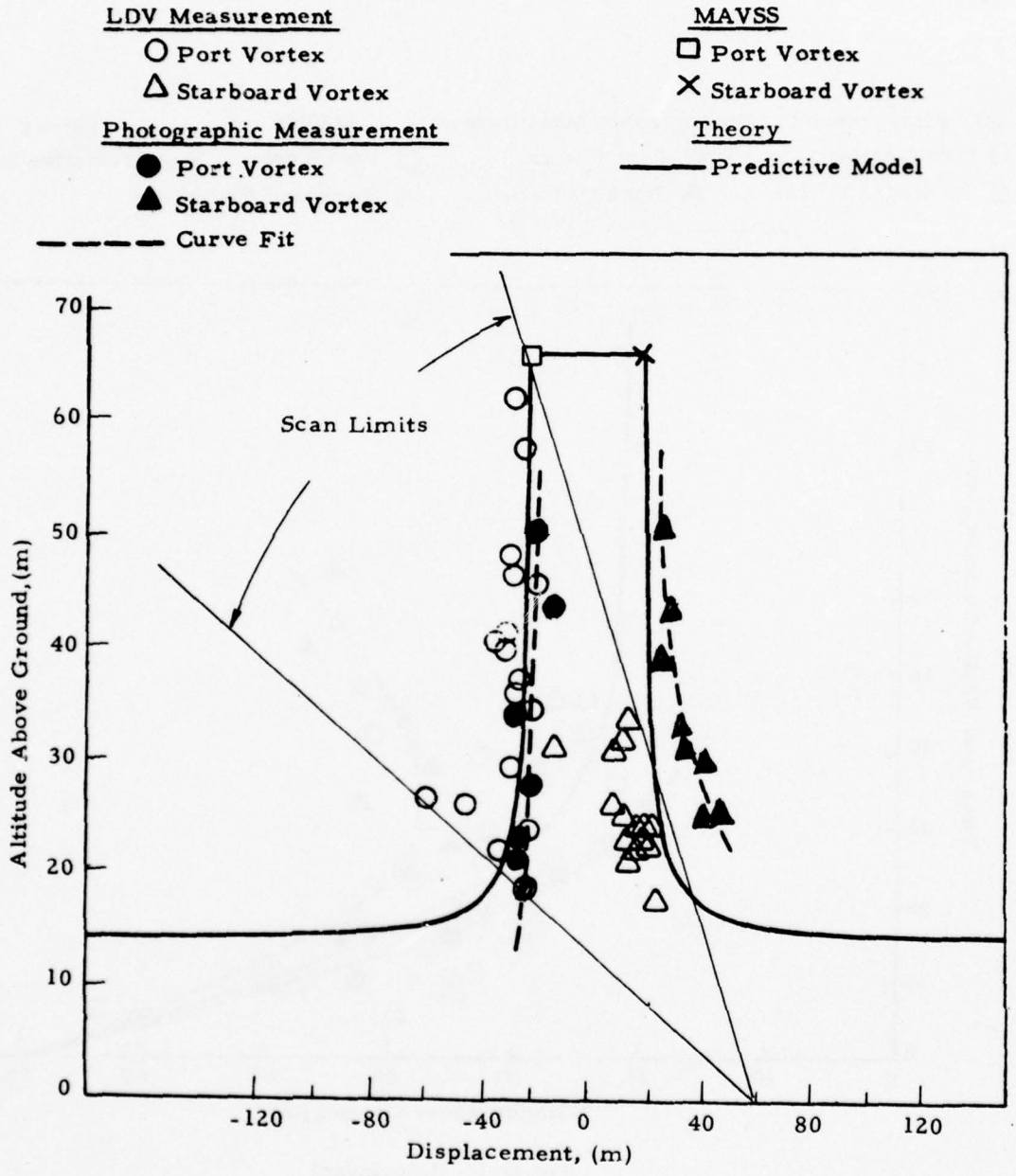

Fig. D-5 - Wake Vortex Trajectory for Rosamond Flyby 28

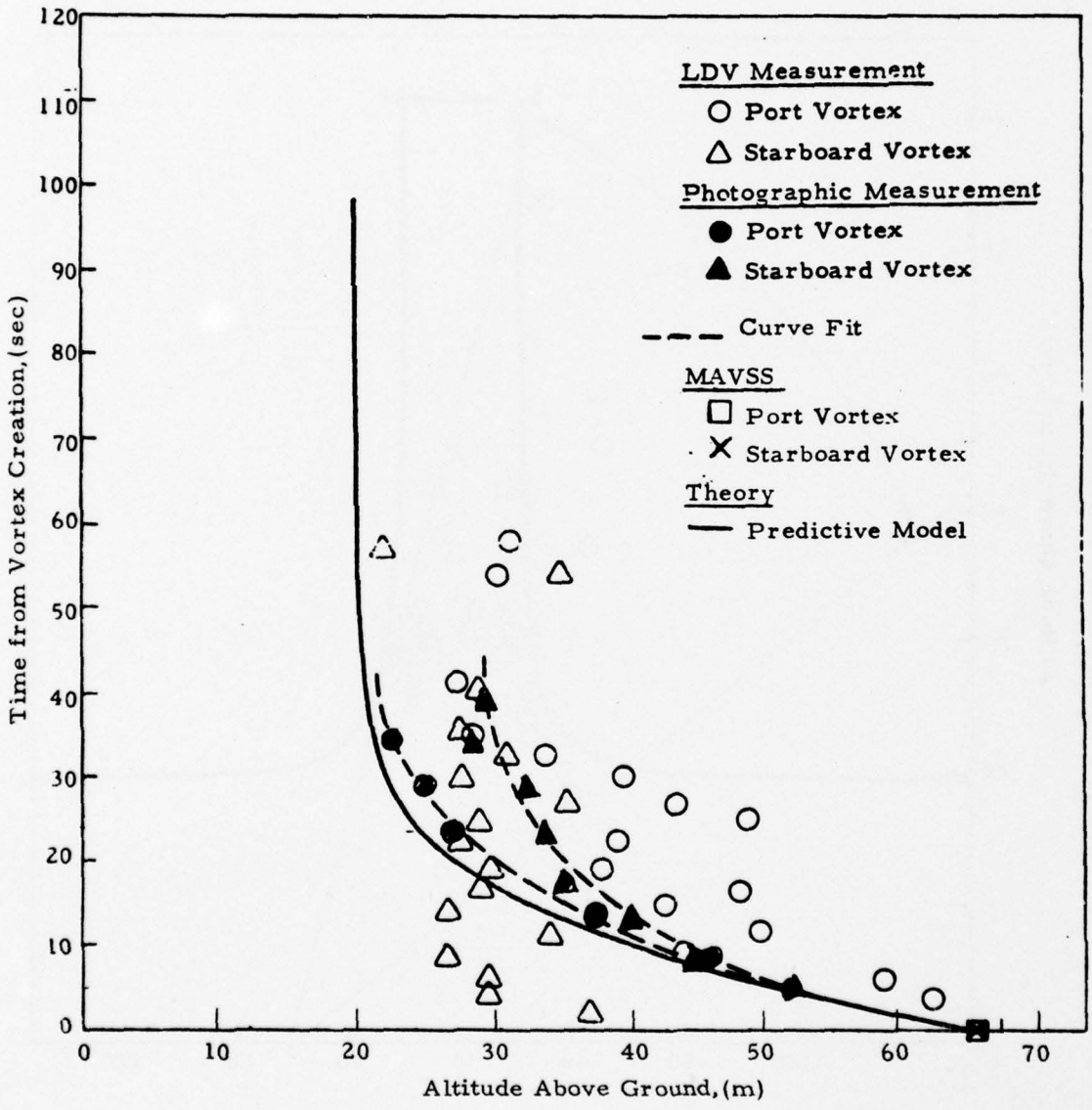

Fig. D-5 - (Concluded)

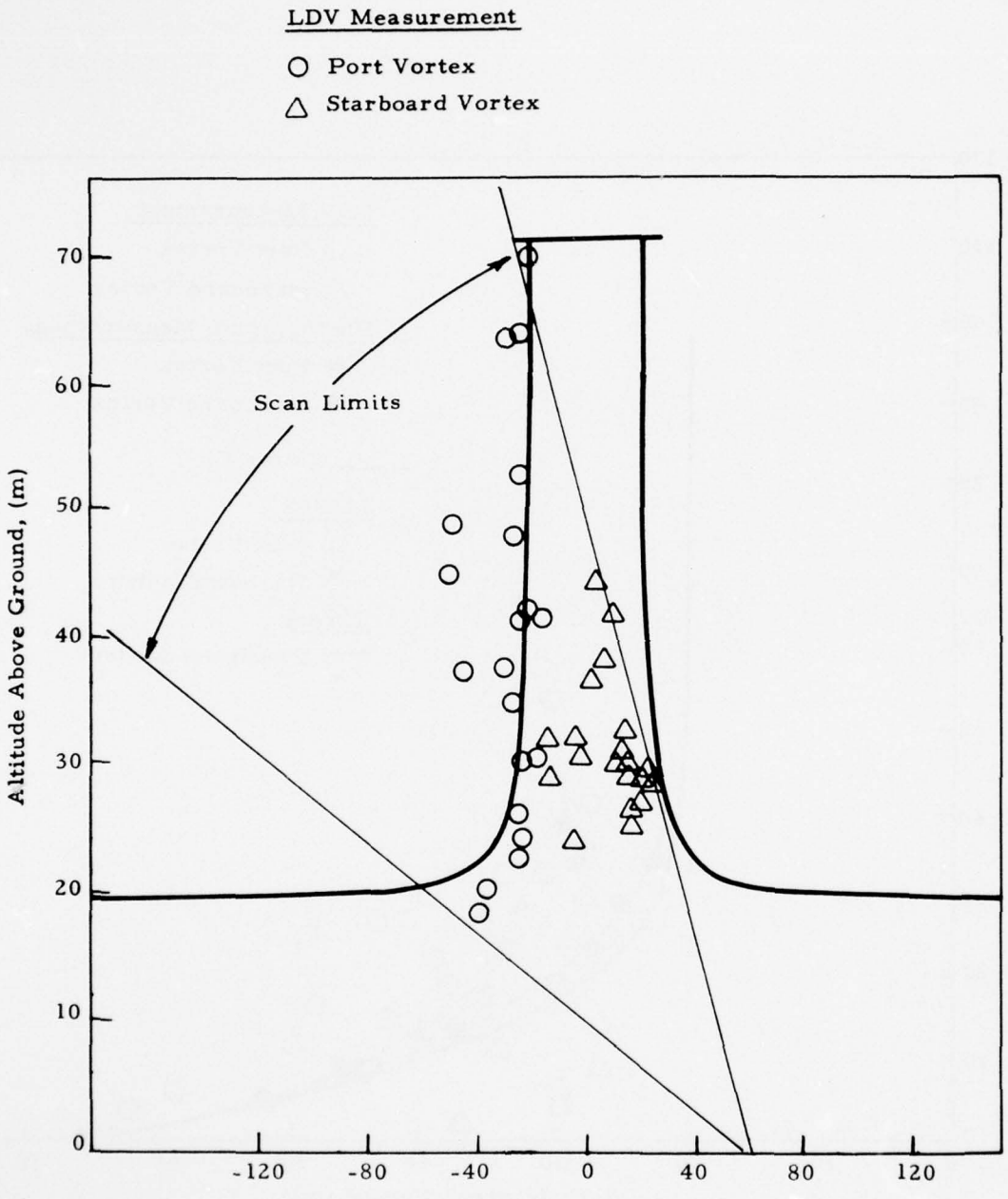

Fig. D-6 - Wake Vortex Trajectory for Rosamond Flyby 29

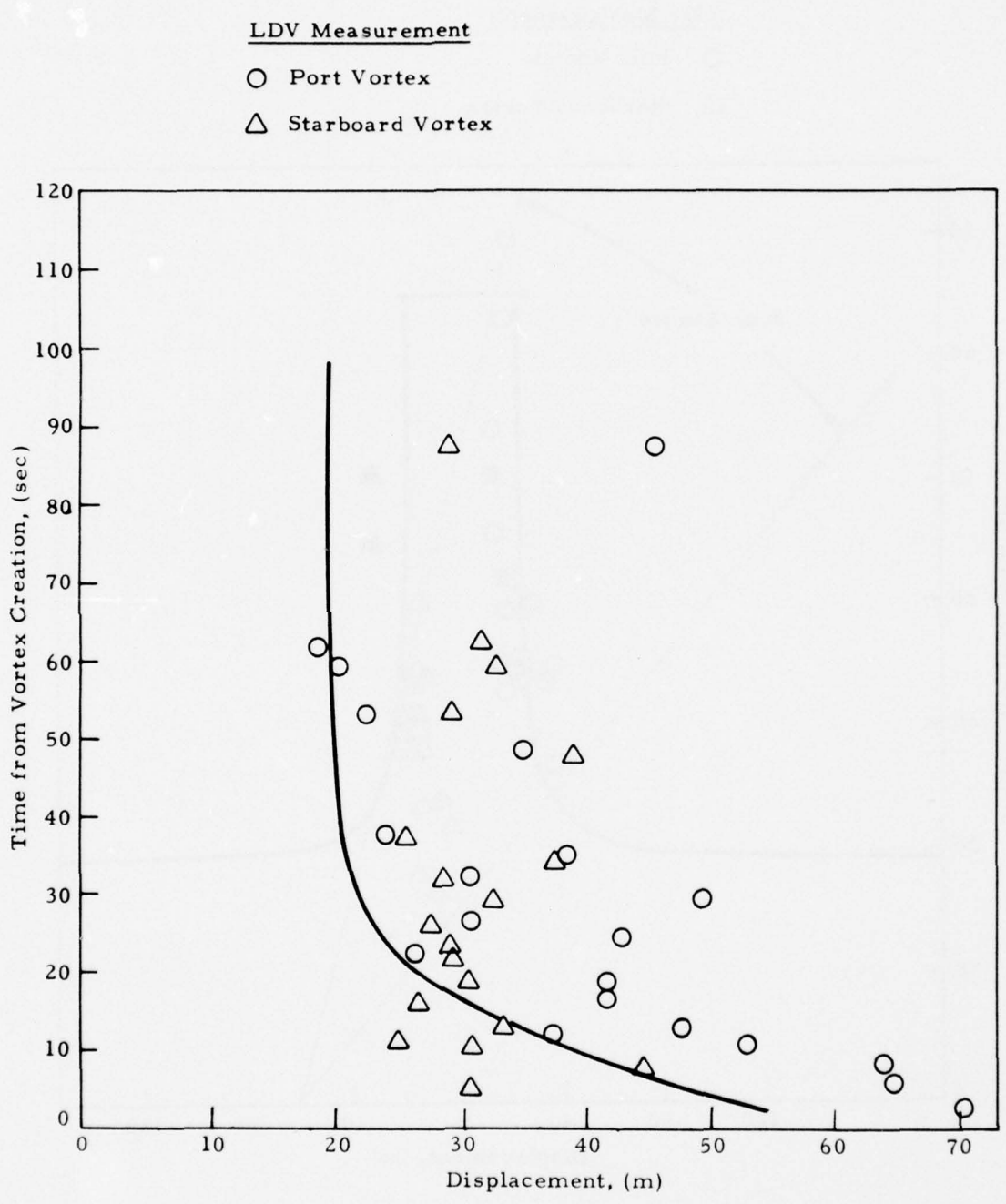

Fig. D-6 - (Concluded)

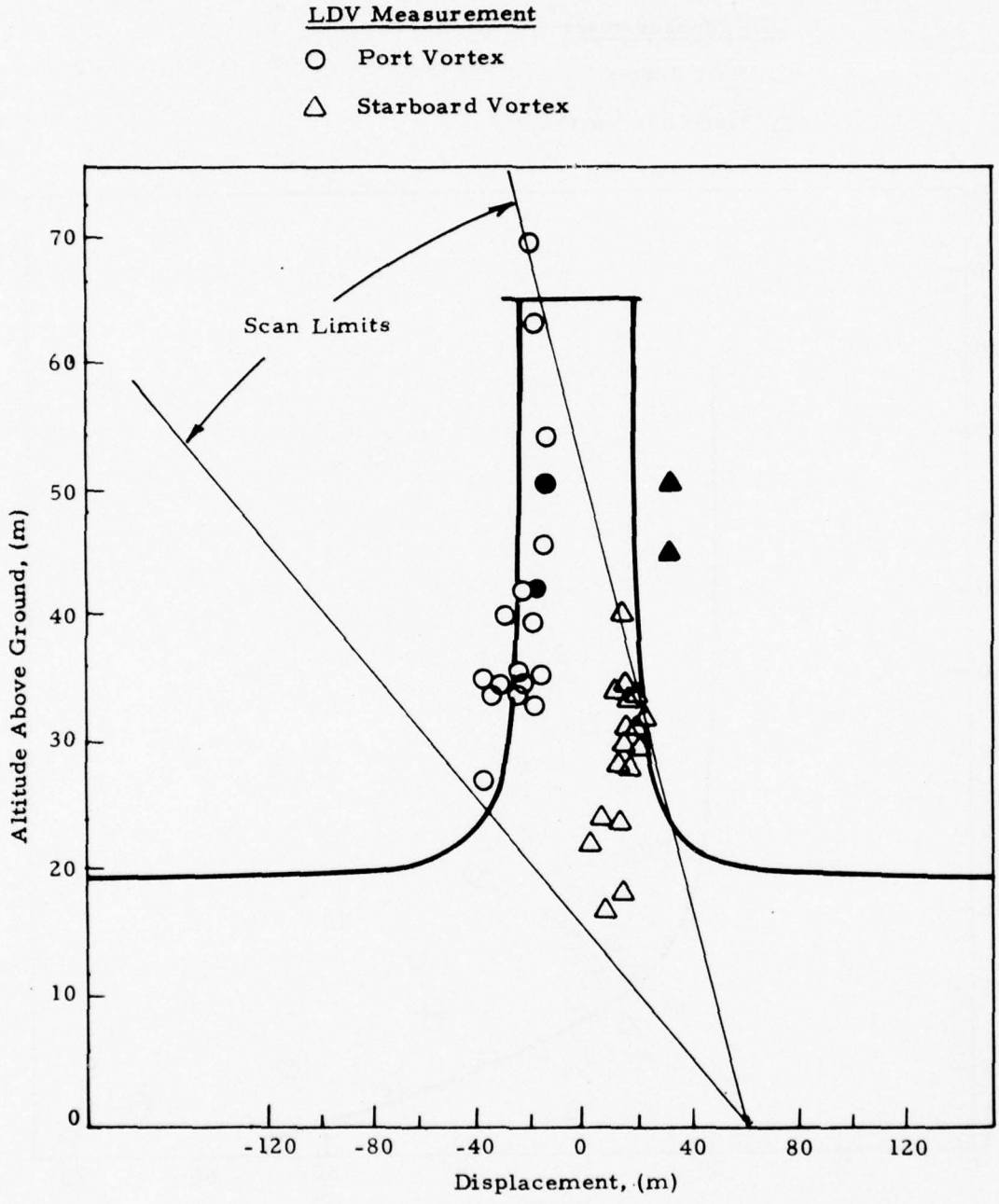

Fig. D-7 - Wake Vortex Trajectory for Rosamond Flyby 30

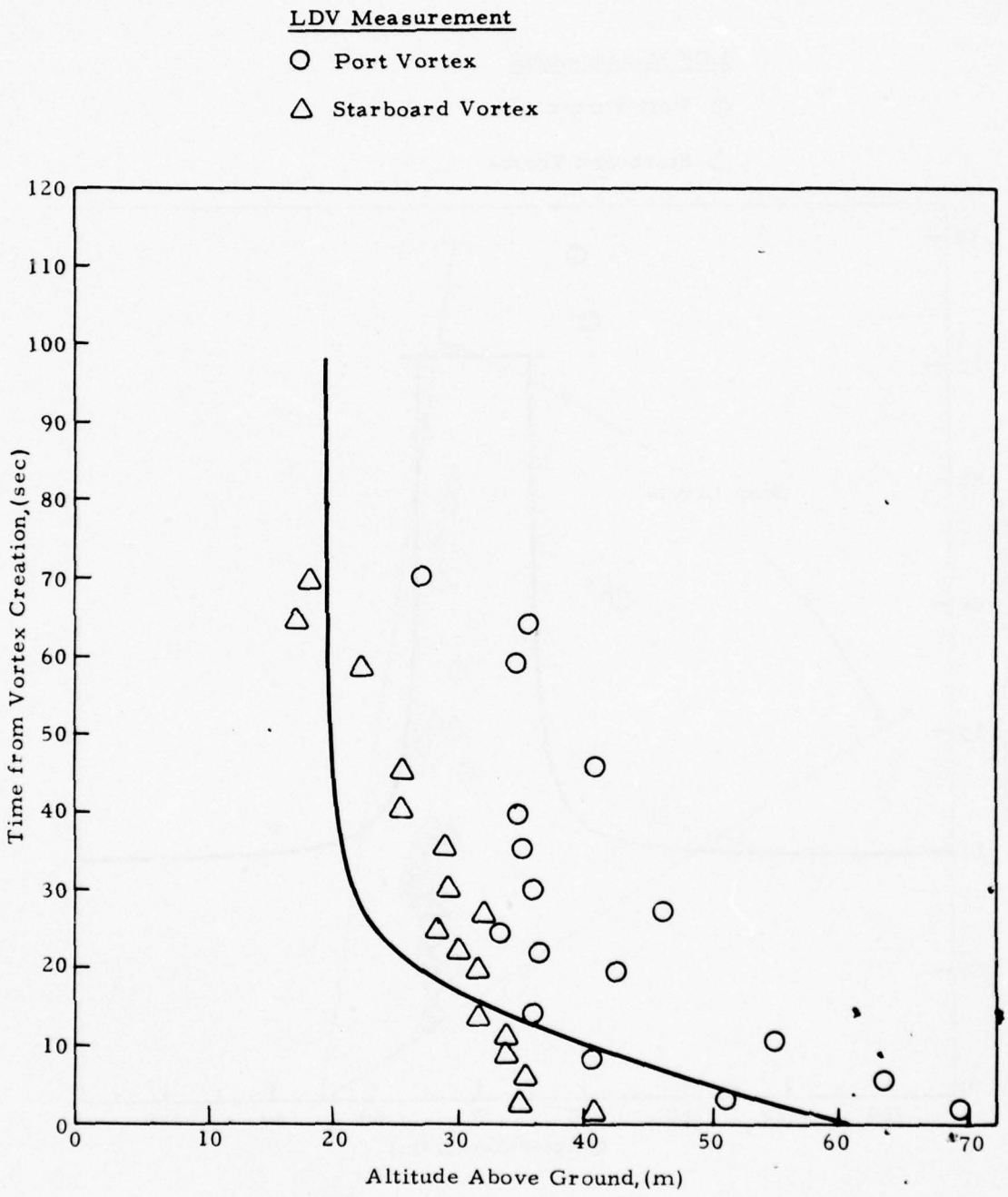

Fig. D-7 - (Concluded)

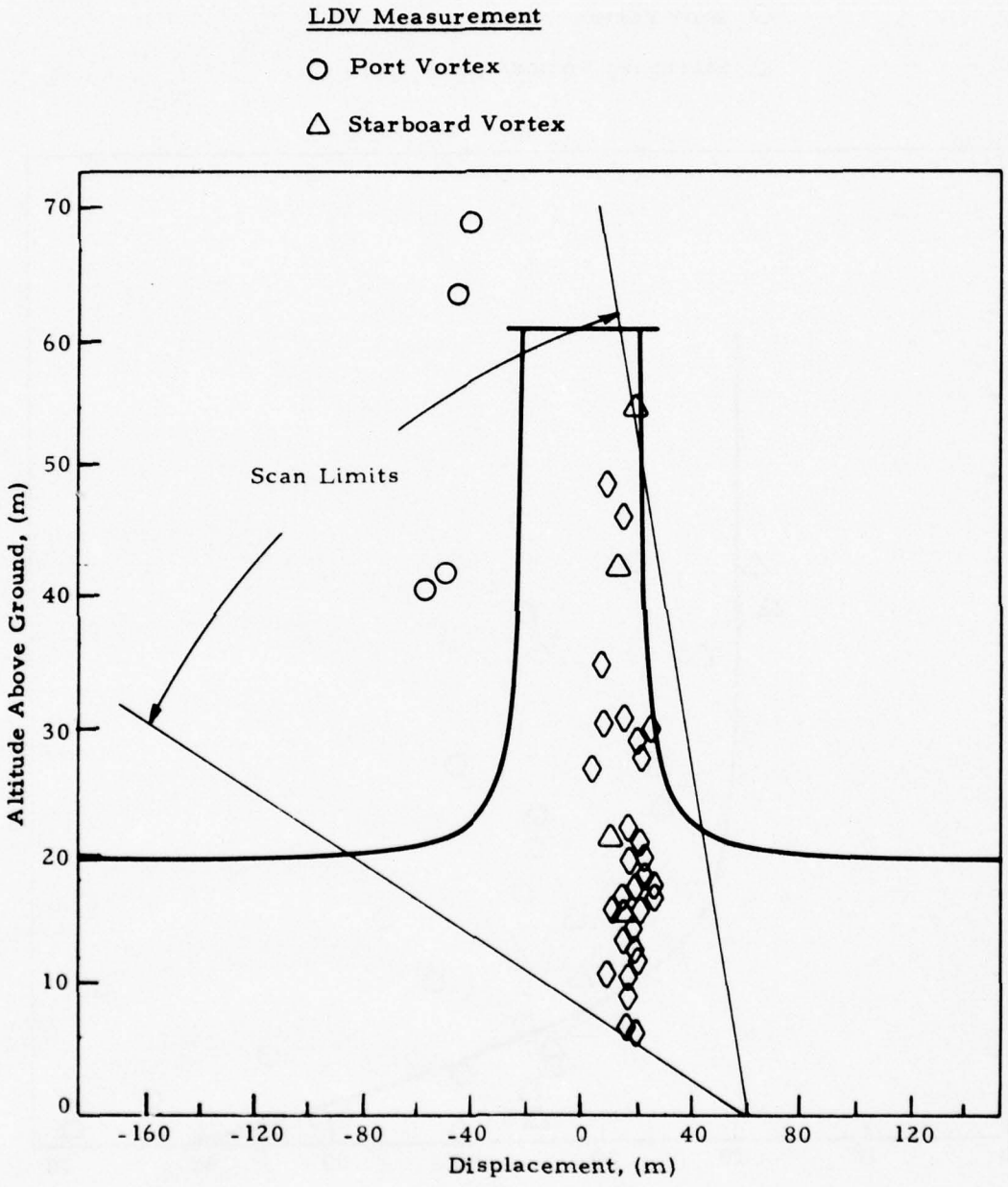

Fig. D-8 - Wake Vortex Trajectory for Rosamond Flyby 40

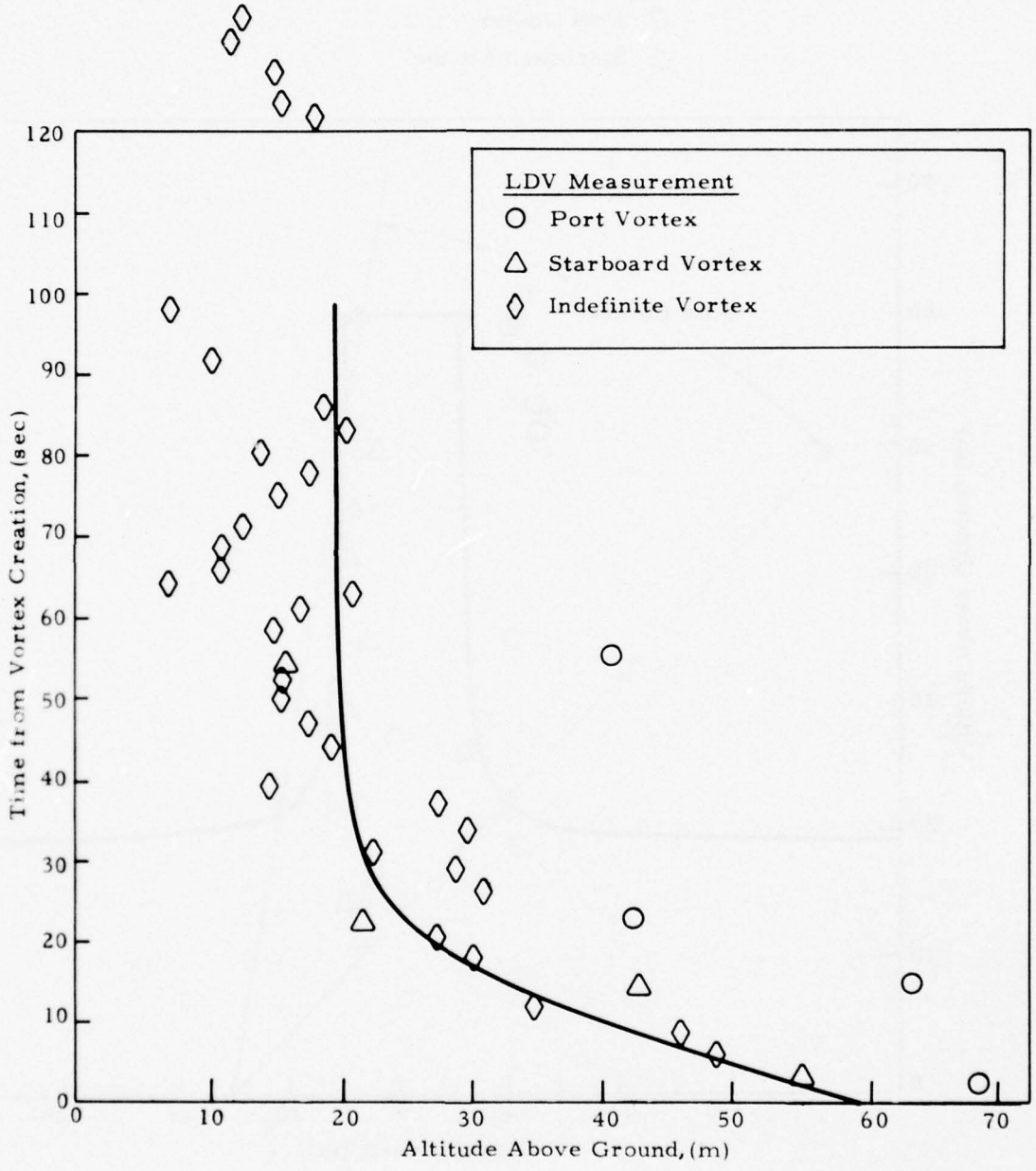

Fig. D-8 - (Concluded)

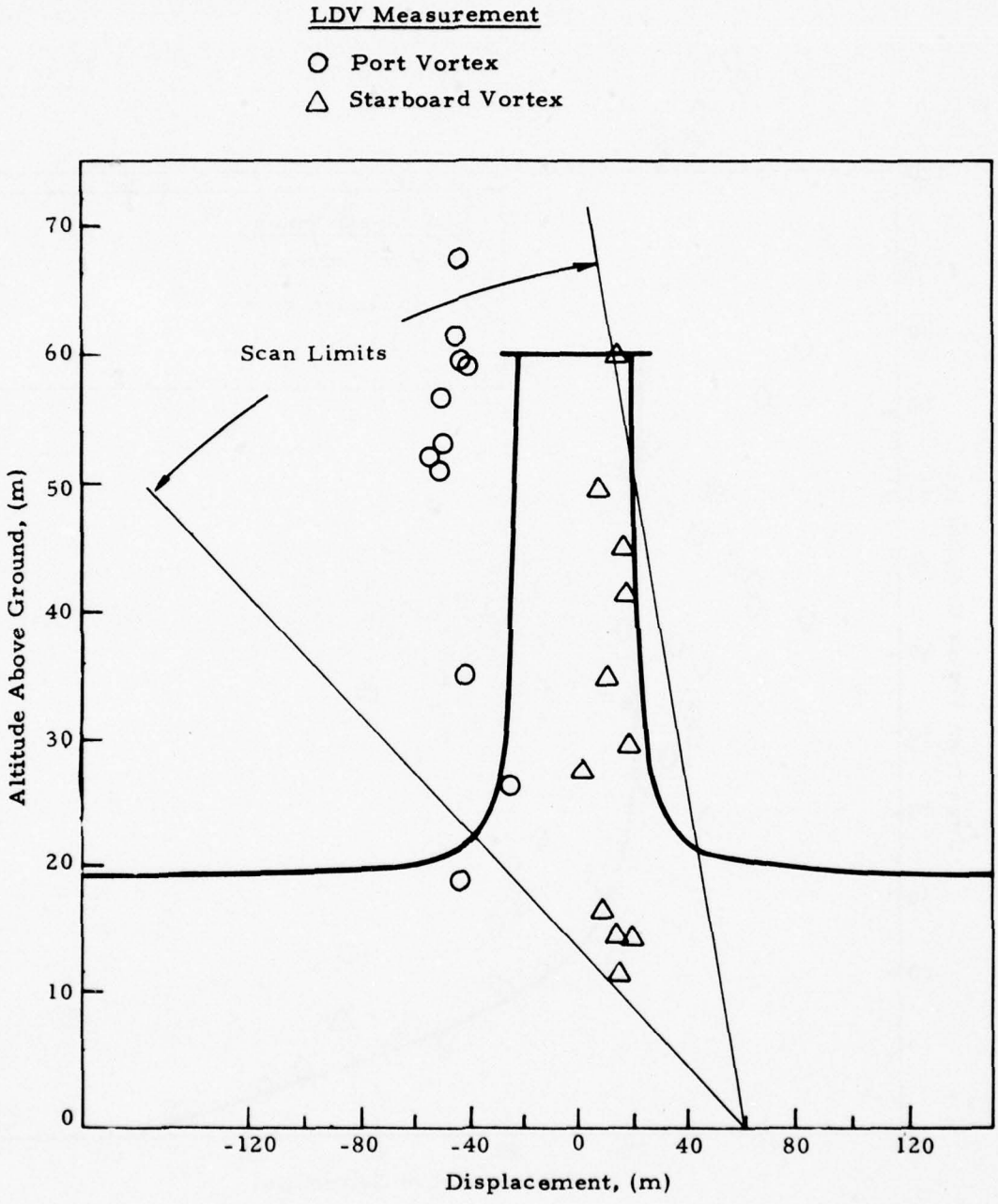

Fig. D-9 - Wake Vortex Trajectory for Rosamond Flyby 42

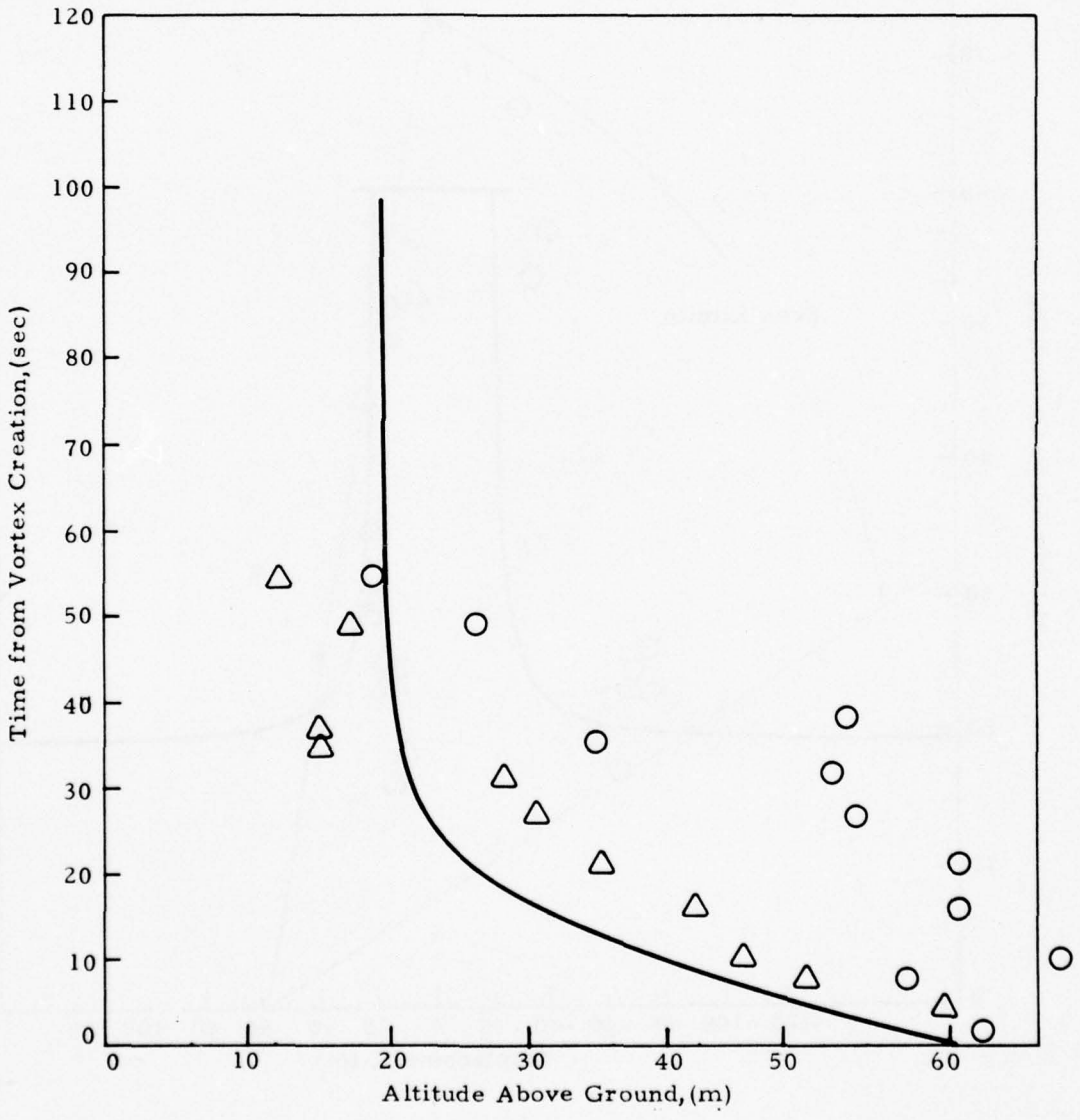

Fig. D-9 - (Concluded)

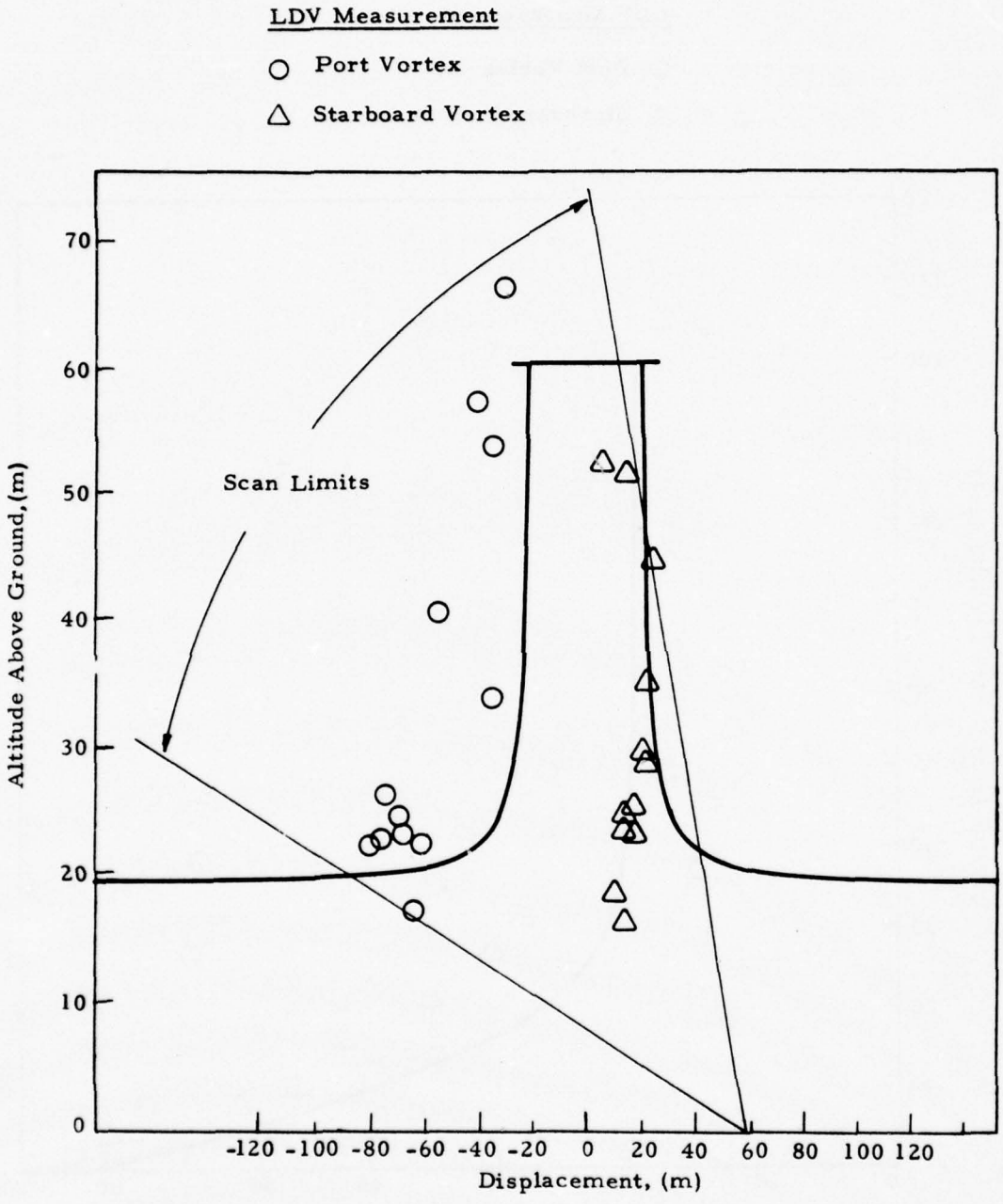

Fig. D-10 - Wake Vortex Trajectory for Rosamond Flyby 44

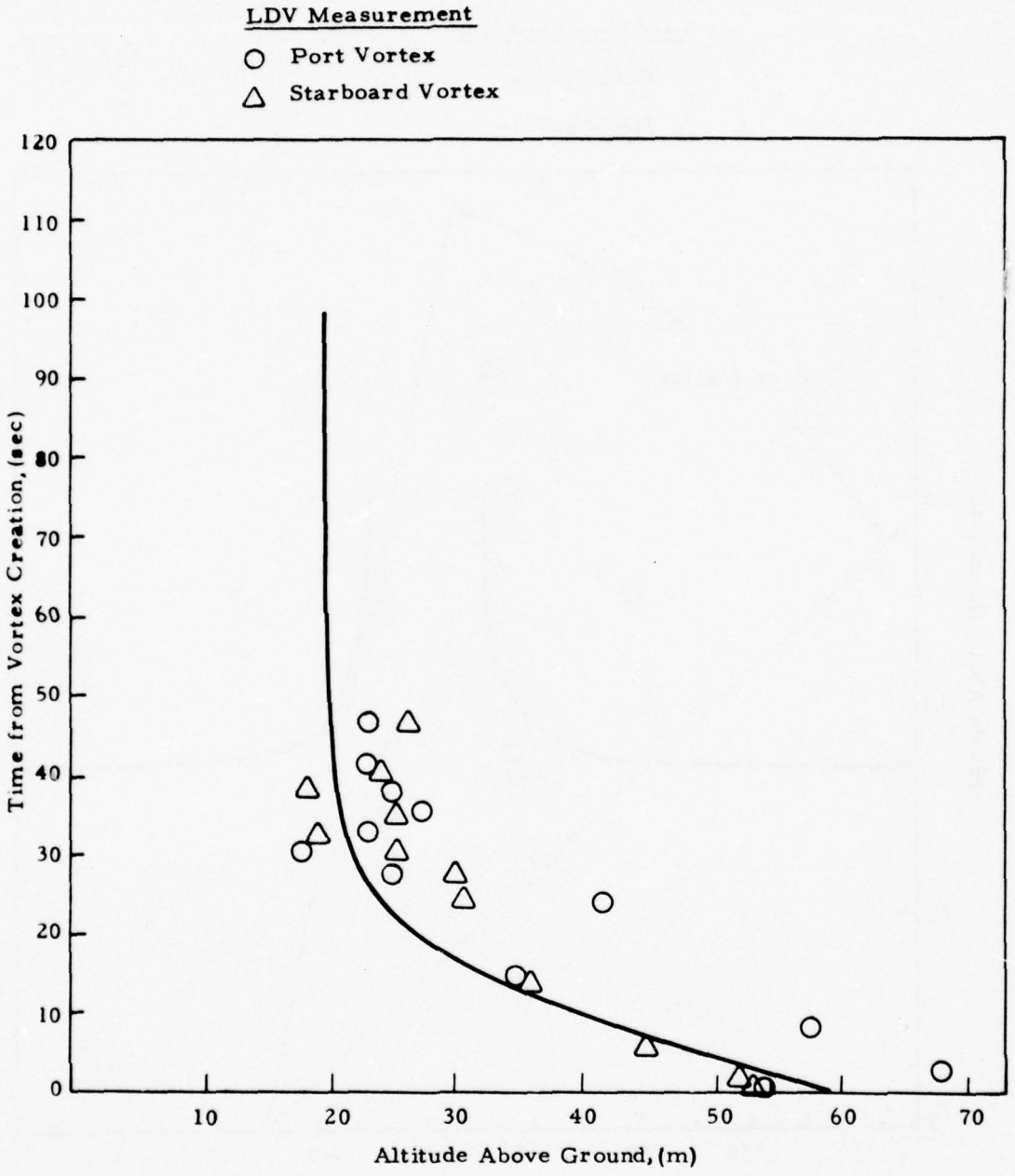

Fig. D-10 - (Concluded)

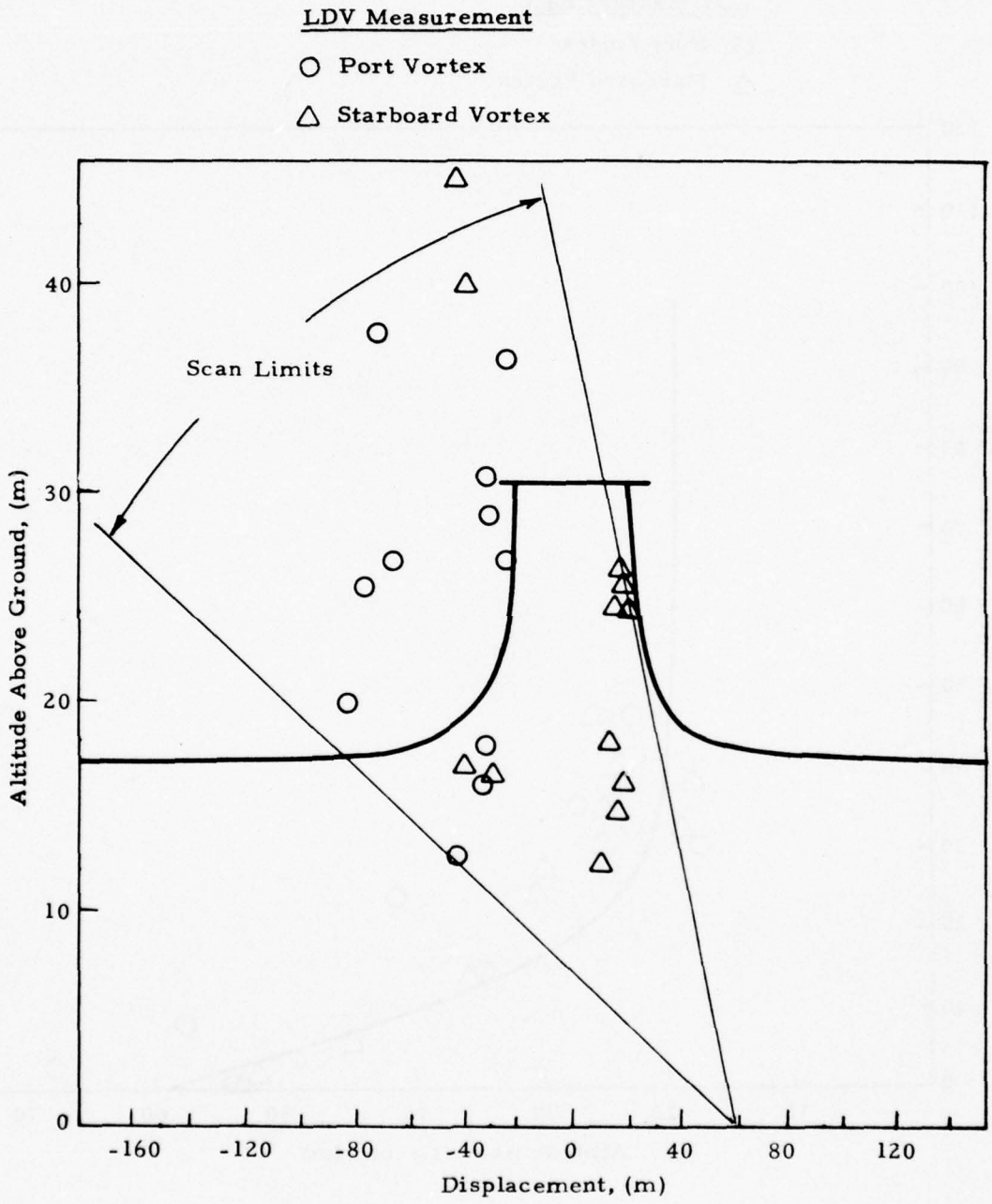

Fig. D-11 - Wake Vortex Trajectory for Rosamond Flyby 46

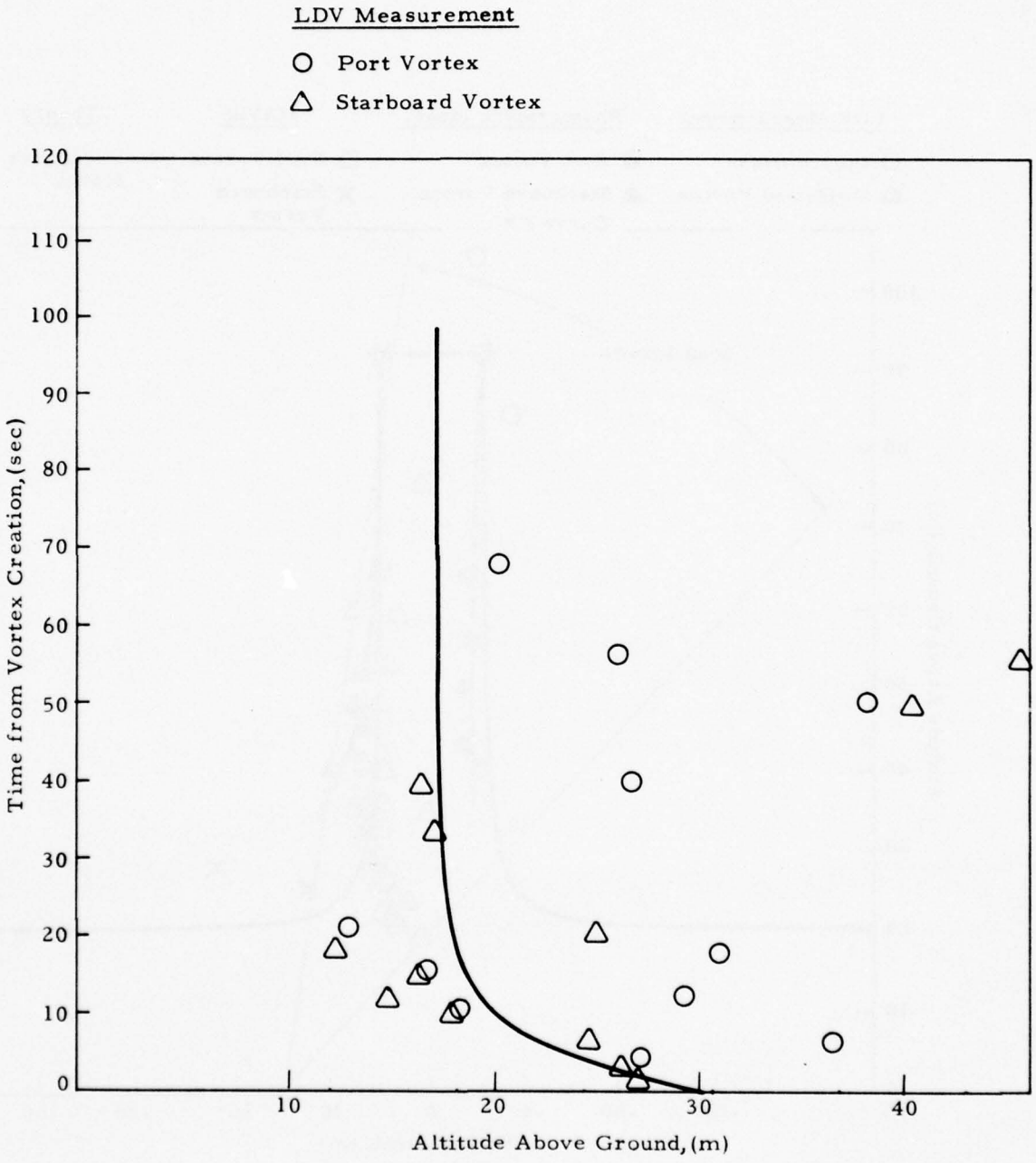

Fig. D-11 - (Concluded)

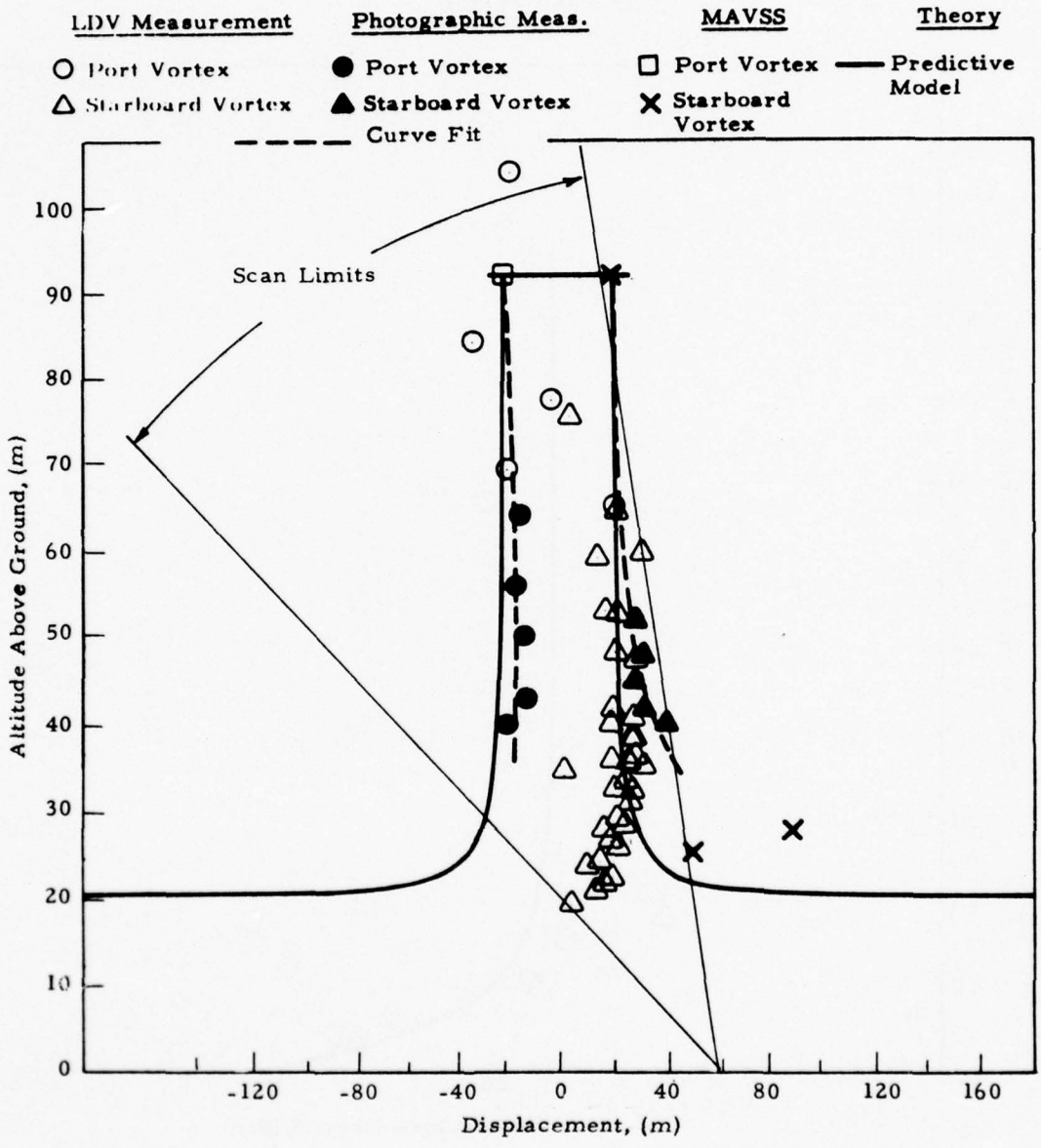

Fig. D-12 - Wake Vortex Trajectory for Rosamond Flyby 47

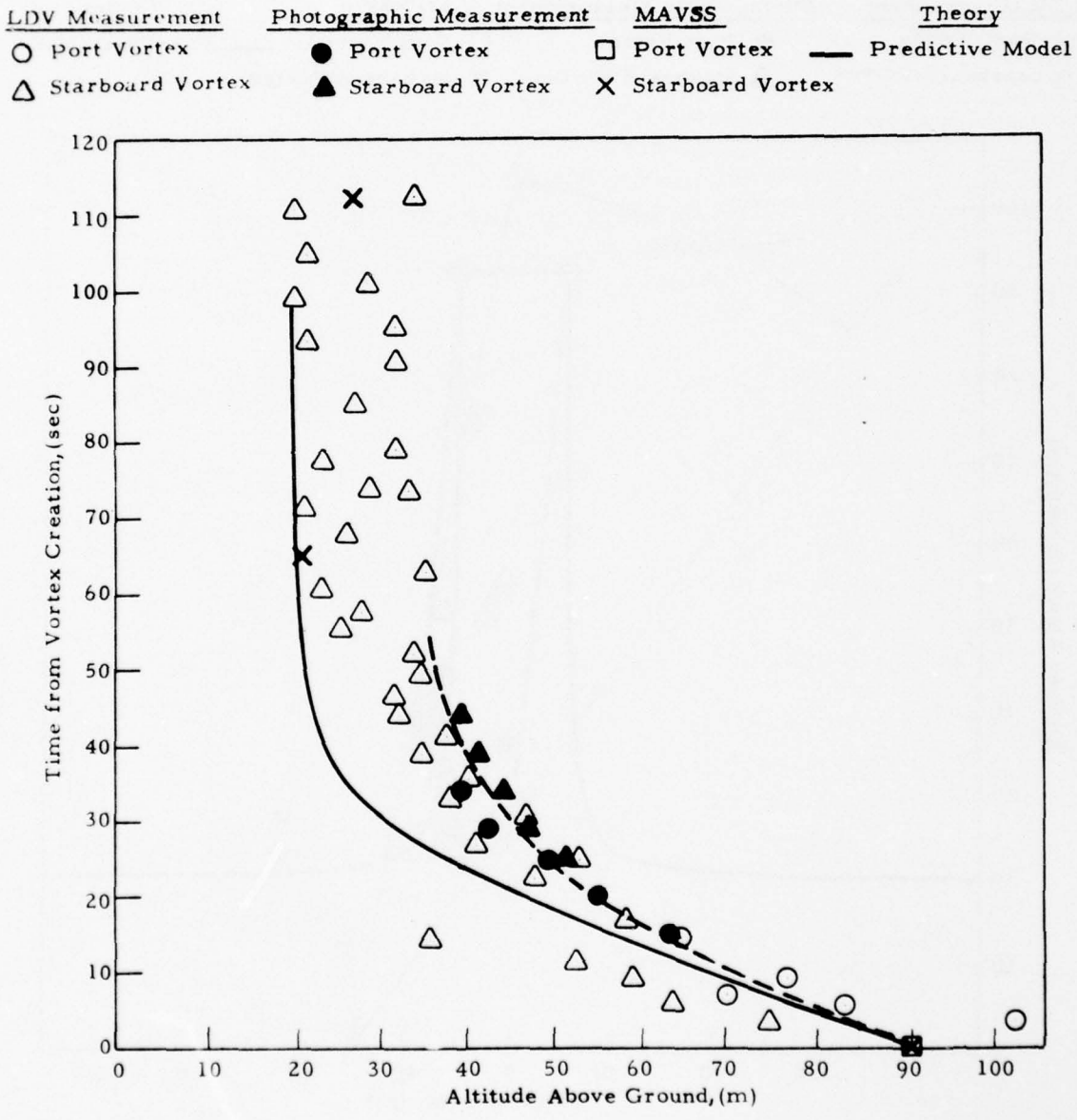

Fig. D-12 - (Concluded)

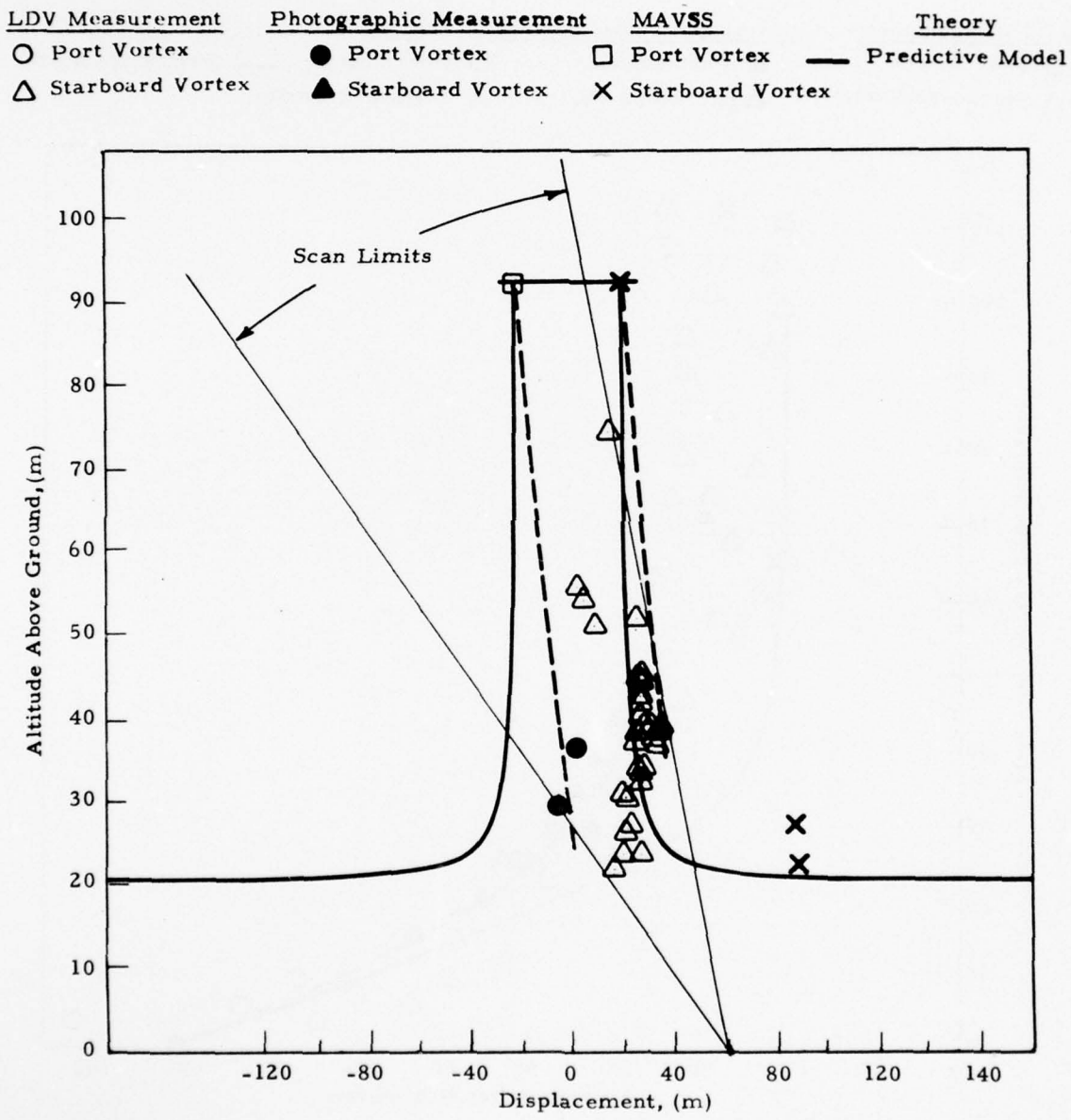

Fig. D-13 - Wake Vortex Trajectory for Rosamond Flyby 48

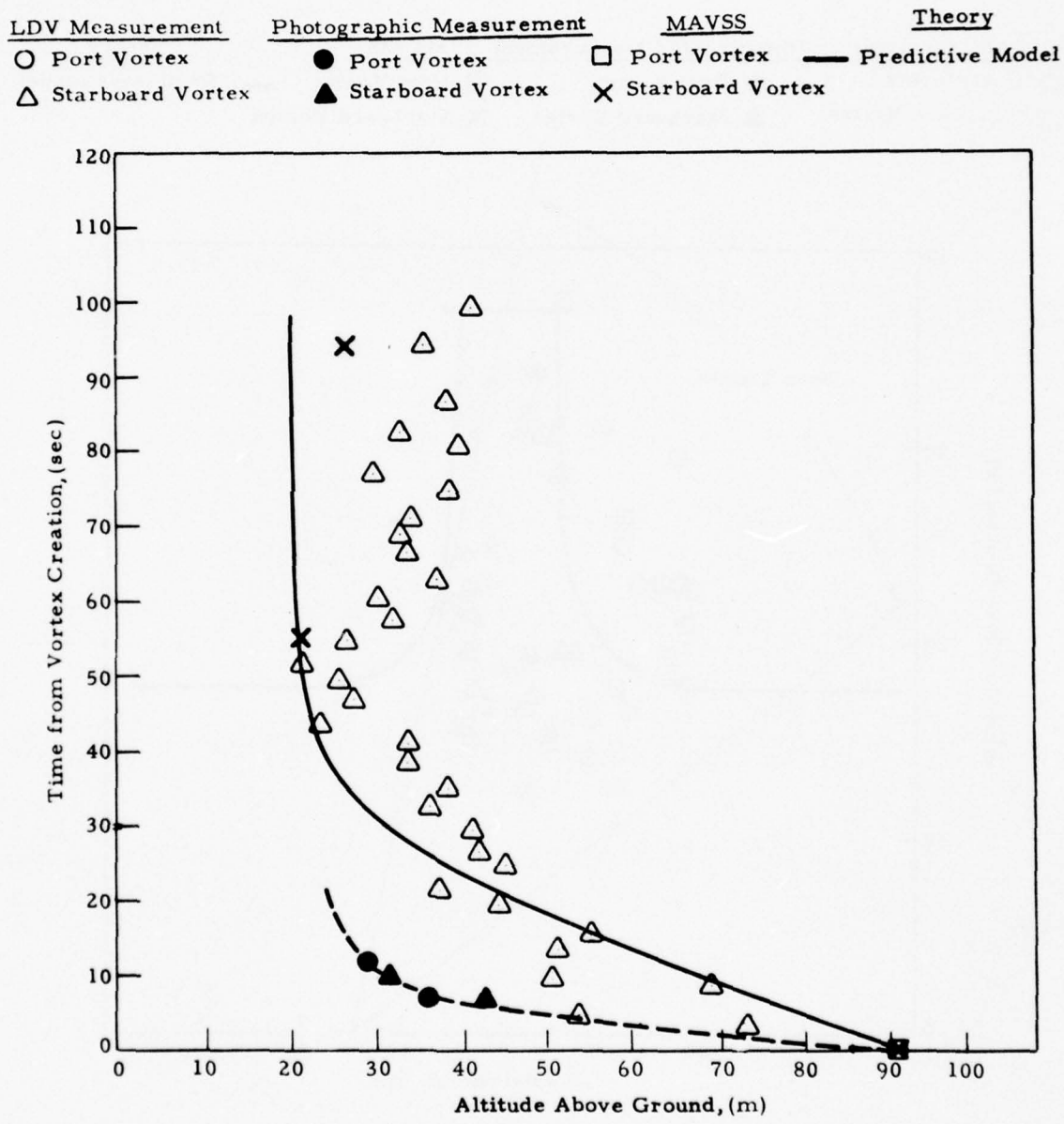

Fig. D-13 - (Concluded)

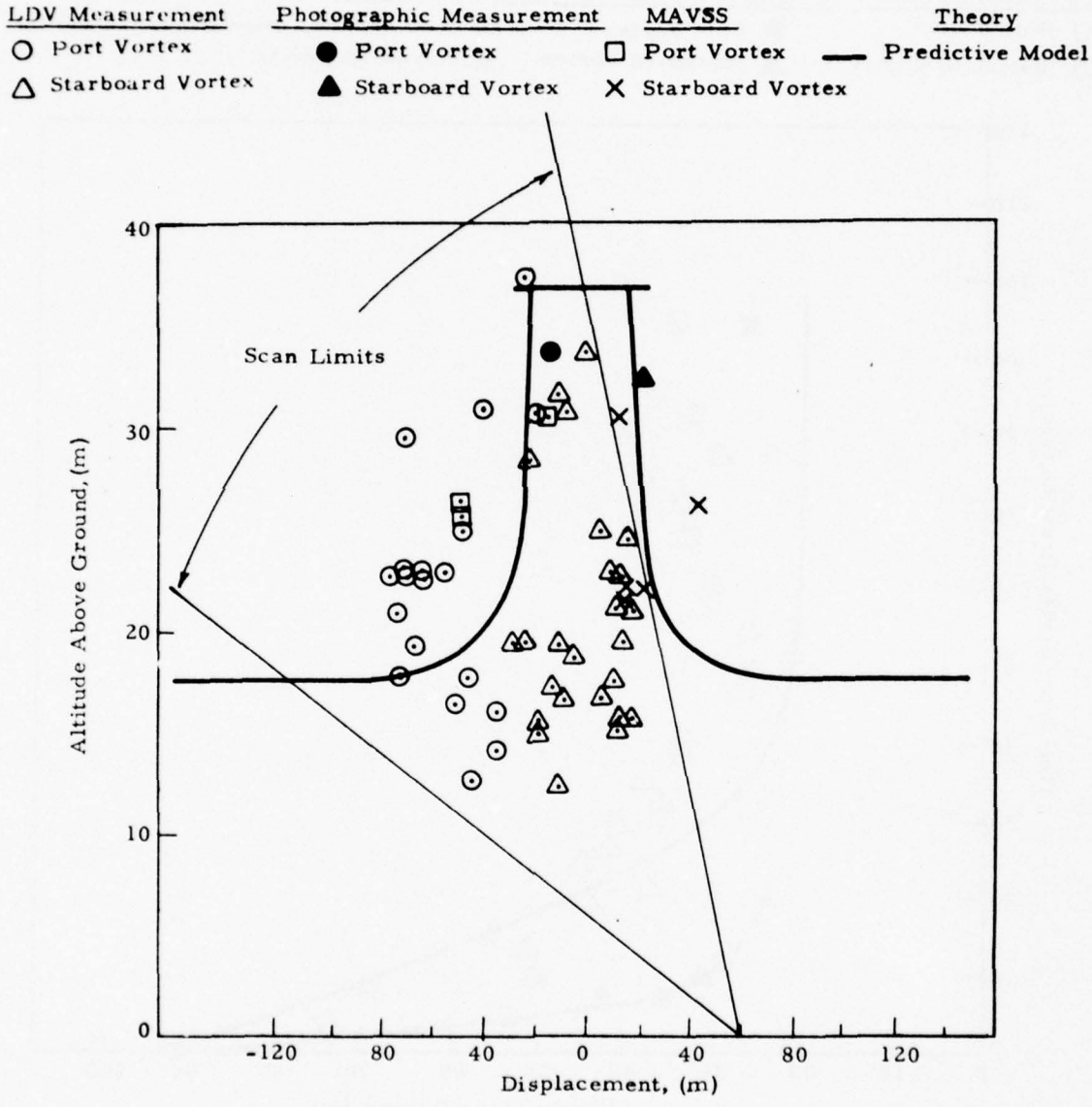

Fig. D-14 - Wake Vortex Trajectory for Rosamond Flyby 49

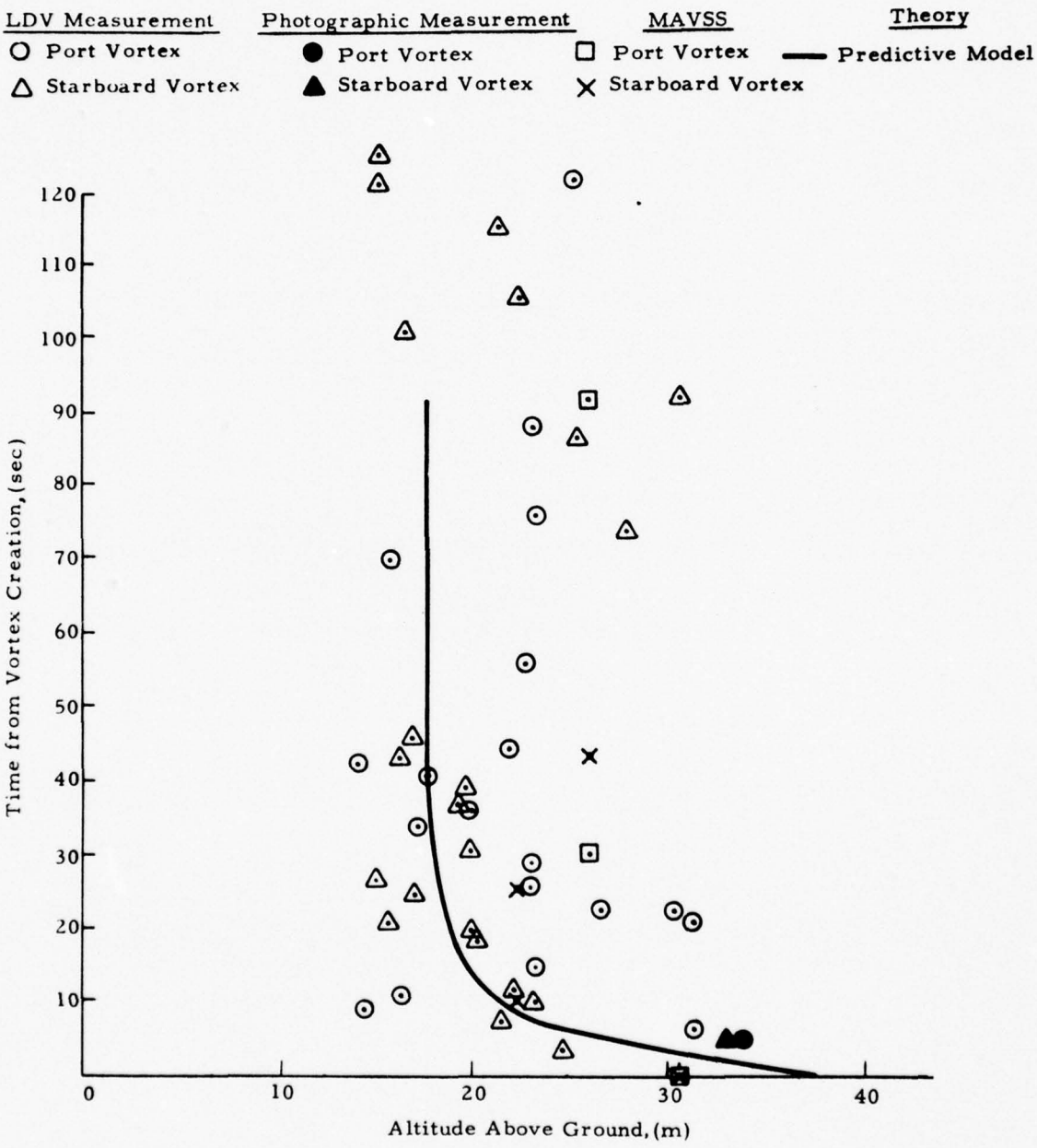

Fig. D-14 - (Concluded)

Appendix E

WAKE VORTEX TRACKS COMPUTED FROM HIGH-SPEED MEASUREMENTS

The measurements obtained with the NASA high-speed filter bank and processor and software system are summarized in this appendix. The output consists of three plots: (1) vortex altitude versus time; (2) lateral distance versus time; and (3) altitude versus lateral distance. A listing of the vortex locations is given in a table following the three plots. The port and starboard vortices are indicated by (0*) and (*) on the altitude and lateral distance versus time plots. The vortices are labeled by letters A to Z on the lateral distance plots (each pair of letters corresponds to a successive elevation scan frame).

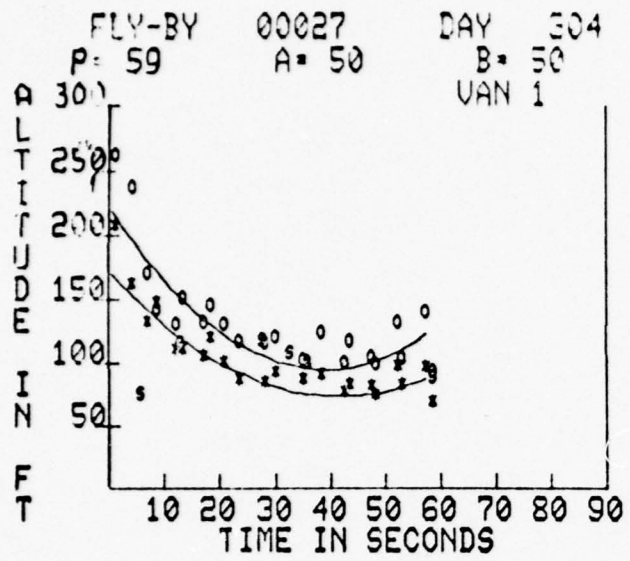

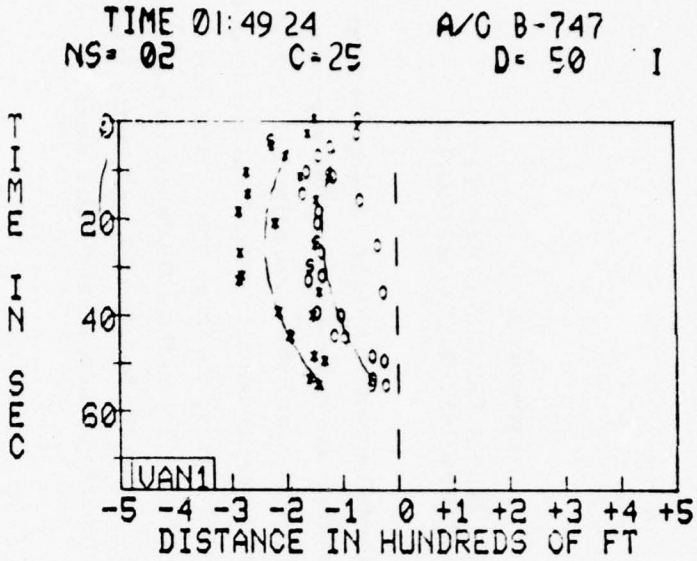

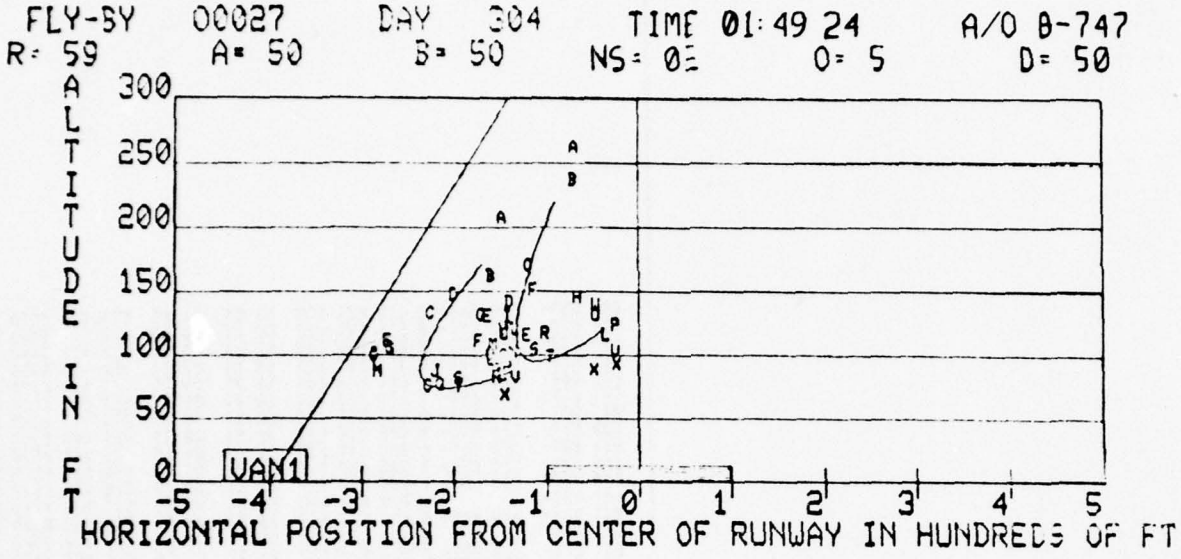

FLY-BY 00027 DAY 304 TIME 01 49 24 A/C B-747

[illegible] 59 A= 50 B= 50 NS= 02 C= 25 D= 50 I

FR	DATA PTS	COR PT P	COR PT S	NOISE P	NOISE S	ANGLE MN	ANGLE MX	PK P	PAR S	TIME	PORT POS X	PORT POS Y	STARB POS X	STARB POS Y
01	0747	250	059	00	00	24	44	258	216	020 6	-150	203	-073	258
02	0713	250	141	00	00	23	43	273	218	023 7	-163	158	-074	233
03	[illegible]	[illegible]	[illegible]	00	00	20	83	[illegible]	[illegible]	026 5	-220	020	-121	166
04	0533	169	250	01	00	22	43	229	265	029 2	-223	143	-143	138
05	[illegible]	[illegible]	[illegible]	00	00	23	[illegible]	[illegible]	269	012 8	-274	107	-188	128
06	[illegible]	250	183	00	01	21	43	277	260	012 9	-176	107	-117	147
07	0749	275	247	00	00	22	45	245	265	016.7	-272	101	-173	128
08	0750	250	031	00	01	21	42	261	233	017.8	-148	116	-071	141
09	0555	033	155	00	00	20	45	281	258	020.3	-289	097	-144	126
10	0642	124	250	01	00	20	43	222	268	022.9	-222	083	-147	113
11	0465	033	180	05	00	18	43	210	253	026.9			-149	114
12	[illegible]	070	[illegible]	00	00	18	[illegible]	280	[illegible]	029.5	-288	089	-023	118
13	0444	025	158	05	00	17	45	225	244	032.0			-160	104
14	0533	011	226	00	00	17	41	256	240	034.4	-284	083	-139	098
15	0354	016	165	00	00	19	42	241	229	035.1	-259	095	-164	097
16	0534	174	137	00	00	17	33	224	177	037.7	-144	037	-029	120
17	0333	040	144	01	00	15	46	183	230	042.0	-218	073	-148	095
18	0433	165	117	00	01	15	36	221	193	042.8	-155	078	-105	112
19	[illegible]	033	133	01	00	16	35	170	224	047.1	-197	078	-117	101
20	[illegible]	033	181	01	00	16	29	160	218	047.7	-197	071	-099	094
21	0215	121	034	00	03	17	20	224	163	051.8	-153	093	-050	127
22	0411	204	[illegible]	00	00	17	26	242	158	052.5	-135	070	-029	099
23	0218	165	[illegible]	00	00	17	33	203	164	055.8	-162	093	-050	135
24	[illegible]	[illegible]	[illegible]	00	00	13	18	[illegible]	160	057.8	-148	065	-088	080

FR	DATA PTS	COR PT P	COR PT S	NOISE P	NOISE S	ANGLE MN	ANGLE MX	PK P	PAR S	TIME	PORT POS X	PORT POS Y	STARB POS X	STARB POS Y

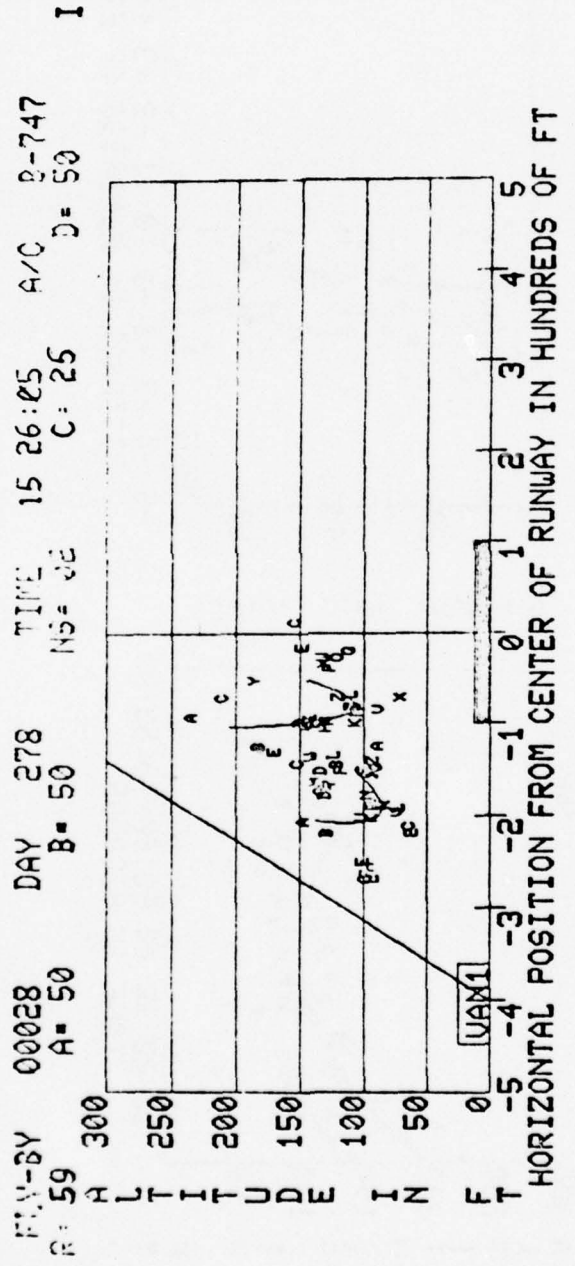

FLY-BY 00028 DAY 278 TIME 15:32:27 A/C B-747

R= 59 A= 50 B= 50 NS= 03 C= 25 D= 50 I

FR	DATA PTS	COR P	COR S	PT P	PT S	NOISE P	NOISE S	ANGLE MN	ANGLE MX	PK P	PK S	PHR	TIME	PORT X	PORT Y	STARB X	STARB Y	POS
01	0887	250	192	00	00	21	40	261	273	000	3	-209	144	-056	230			
02	0900	178	250	00	00	21	40	226	282	004	0	-221	125	-127	178			
03	0903	000	003	00	00	00	00	000	000	000	2	-146	148	0000	000			
04	0900	000	250	00	00	00	00	000	000	000	2	-180	126	-102	145			
05	0000	003	000	00	00	00	00	000	000	000	9	-053	057	-053	109			
06	0953	250	213	00	00	21	40	264	000	014	2	-206	093	-103	136			
07	0974	000	250	00	00	00	00	000	000	016	2	-271	004	-175	130			
08	0000	073	233	00	00	21	41	242	000	017	7	-258	052	-107	126			
09	0000	250	181	00	01	19	42	257	000	021	4	-172	126	-056	138			
10	0753	150	213	01	00	19	39	217	237	023	0	-167	130	-102	133			
11	0000	000	193	00	00	18	39	238	000	027	4	-205	000	-101	103			
12	0000	000	000	00	00	18	00	000	000	000	9	-000	000	-073	183			
13	0000	000	160	01	00	16	39	000	057	033	2	-192	050	-091	101			
14	0000	173	233	01	00	16	39	238	000	033	1	-180	000	-100	126			
15	0712	173	160	00	00	14	41	248	152	037	0	-190	037	-030	117			
16	0000	164	000	00	00	14	41	240	194	037	9	-154	000	-041	123			
17	0000	000	165	00	00	15	34	246	204	041	9	-150	000	-038	108			
18	0007	073	244	01	00	16	33	192	240	043	4	-191	079	-100	124			
19	0734	169	197	00	00	13	34	200	245	046	9	-198	000	-034	104			
20	0000	115	148	00	00	13	37	213	242	000	0	-103	031	-024	105			
21	0000	070	237	02	00	13	00	173	231	051	6	-204	000	-105	141			
22	0000	119	000	00	00	18	00	173	000	000	5	-100	070	-037	004			
23	0000	000	187	00	00	14	00	000	172	057	5	-183	153	-031	109			
24	0000	000	000	00	00	14	00	000	151	000	0	-157	000	-070	037			
25	0007	000	107	00	00	15	00	231	103	000	5	-109	103	-000	101			
26	0101	000	000	01	00	16	21	140	180	004	6	-142	000	-075	116			
27	0000	074	000	00	04	17	21	173	000	000	0	-127	000					
28	0000	000	000	00	00	20	00	184	000	070	0	-143	117					
29	0000	000	000	00	00	17	18	146	000	071	3	-215	000					
30	0103	103	000	00	00	21	21	180	000	075	0	-154	129					
31	0000	000	000	00	00	17	18	178	000	075	8	-000	058					
32	0000	000	000	00	00	19	27	140	000	070	1	-153	113					
33	0000	000		00		00	00	000										
34	0000	000	000	00	00	00	00	153	000	005	0	-165	133					
35	0000	000		00		00	00	000										
36	0000	000		00		00	00	000										

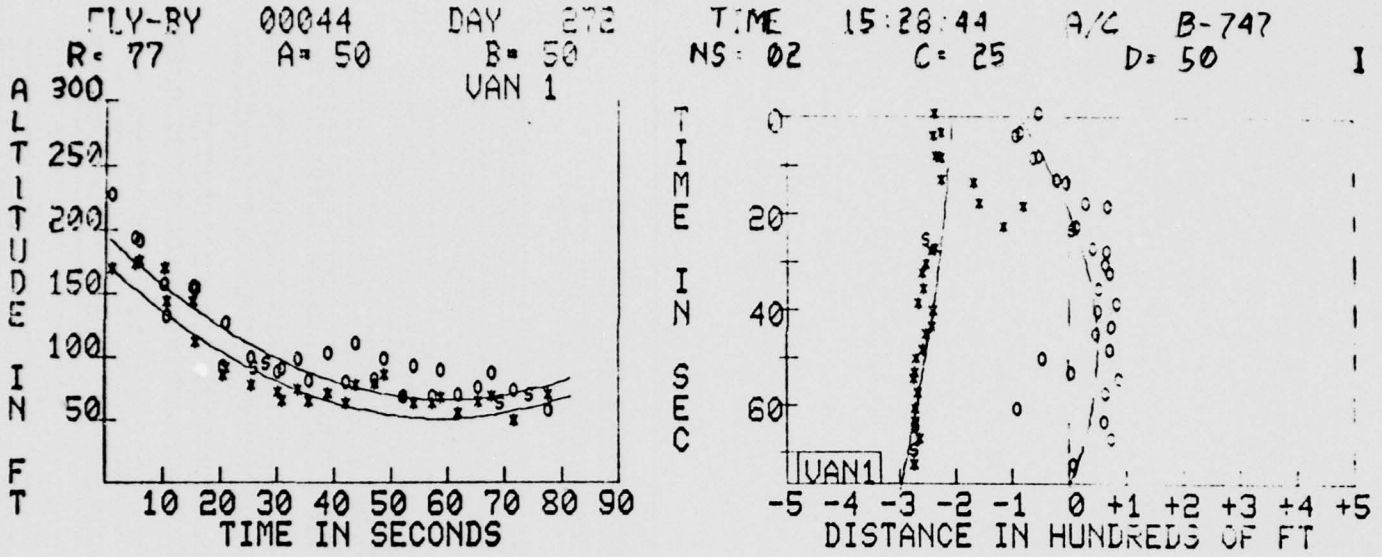

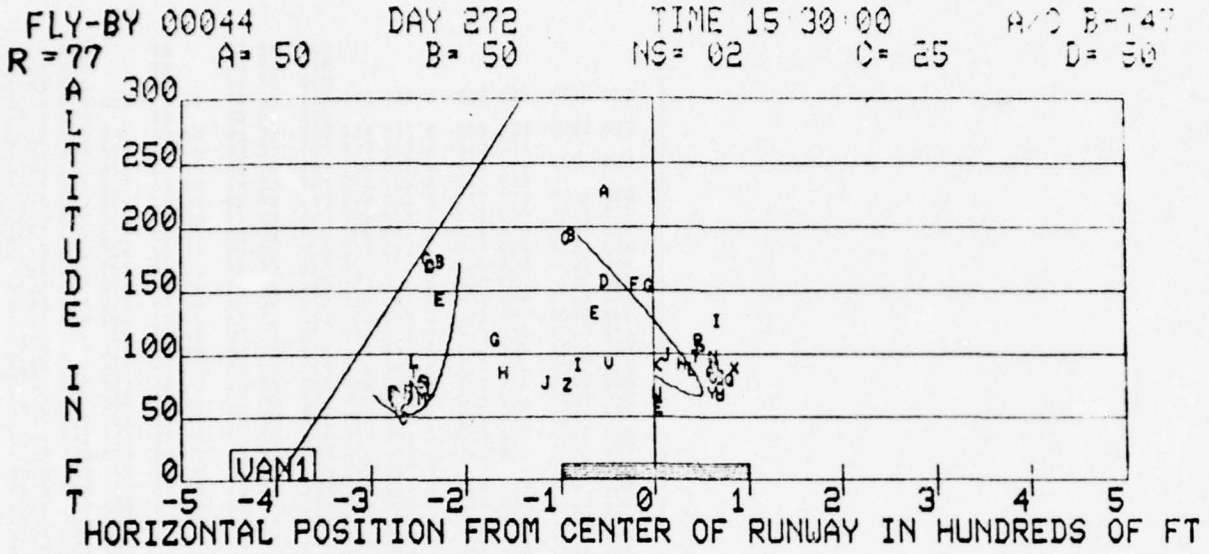

FLY-BY 00044 DAY 272 TIME 15:28:32 A/C B-747

R = 77 A= 50 B= 50 NS= 02 C= 25 D= 50

FR	DATA PTS	COR P	COR S	PT	NOISE P	NOISE S	ANGLE MN	ANGLE MX	PK P	PAR S	TIME	PORT X	PORT Y	STARB X	STARB Y	POS
01	0076	194	220	00	00	27	54	262	282	200	5	-240	165	-056	223	
02	0065	241	224	00	00	27	53	262	270	004	5	-228	168	-050	189	
03	0097	174	187	00	00	27	54	248	274	005	3	-243	170	-097	186	
04	0062	156	221	00	00	19	53	234	266	009	6	-238	164	-055	153	
05	0782	178	154	00	00	19	53	249	281	010	1	-228	139	-065	127	
06	0086	166	134	00	00	17	54	253	258	014	7	-230	159	-054	150	
07	0058	131	141	00	00	17	52	197	237	015	2	-172	107	-009	149	
08	0053	123	146	00	00	09	54	224	252	019	8	-163	081	0035	087	
09	0061	132	050	00	00	09	55	256	234	020	3	-085	086	0063	121	
10	0519	119	122	01	00	10	51	224	256	024	8	-119	073	0009	094	
11	0312	035	218	05	00	08	33	223	249	025	3			0000	087	
12	0053	058	000	00	00	02	38	230	000	033	6	-231	003	0036	083	
13	0030	041	131	00	00	07	32	250	260	030	3	-249	060	0061	085	
14	0441	028	108	00	00	08	33	245	224	033	1	-257	070	0059	094	
15	0406	021	084	00	00	08	36	232	240	035	0	-265	060	0056	076	
16	0392	021	123	00	00	10	35	229	200	038	4	-263	066	0046	098	
17	0480	021	081	00	00	08	34	214	214	041	5	-271	058	0076	076	
18	0178	036	079	00	00	08	33	214	178	043	2	-246	072	0044	106	
19	0343	024	126	00	00	08	36	217	194	046	6	-249	074	0036	077	
20	0033	024	040	00	00	09	37	208	169	048	2	-257	081	0040	093	
21	0150	014	039	00	00	11	34	225	176	051	5	-263	064	0035	094	
22	0048	010	023	00	00	11	34	212	153	053	4	-275	053	-031	087	
23	0132	029	101	00	00	09	33	193	165	056	6	-276	058	-031	094	
24	0010	000	004	00	00	00	00	000	134	058	1	-278	003	0033	004	
25	0005	003	005	00	00	09	35	173	163	061	1	-272	050	0038	054	
26	0008	002	006	00	00	11	29	153	163	064	7	-278	059	-013	071	
27	0019	004	014	00	00	08	28	158	148	067	3	-276	063	0037	082	
28	0033	008	020	00	00	14	33	184	000	000	5	-276	058			
29	0018	010	006	00	00	09	30	180	135	071	1	-269	044	0067	068	
30	0024	004	003	00	00	23	33	150	000	073	7	-279	065			
31	0008	005	002	00	00	07	33	196	134	077	0	-270	065	0000	053	
32	0000	000		00		00	00	000								
33	0008	004	003	00	01	10	27	172	140	081	6	-273	050	0050	077	
34	0000	000		00		00	00	000								
35	0000	000		00		00	00	000								
36	0000	000		00		00	00	000								

FR	DATA PTS	COR P	COR S	PT	NOISE P	NOISE S	ANGLE MN	ANGLE MX	PK P	PAR S	TIME	PORT X	PORT Y	STARB X	STARB Y	POS

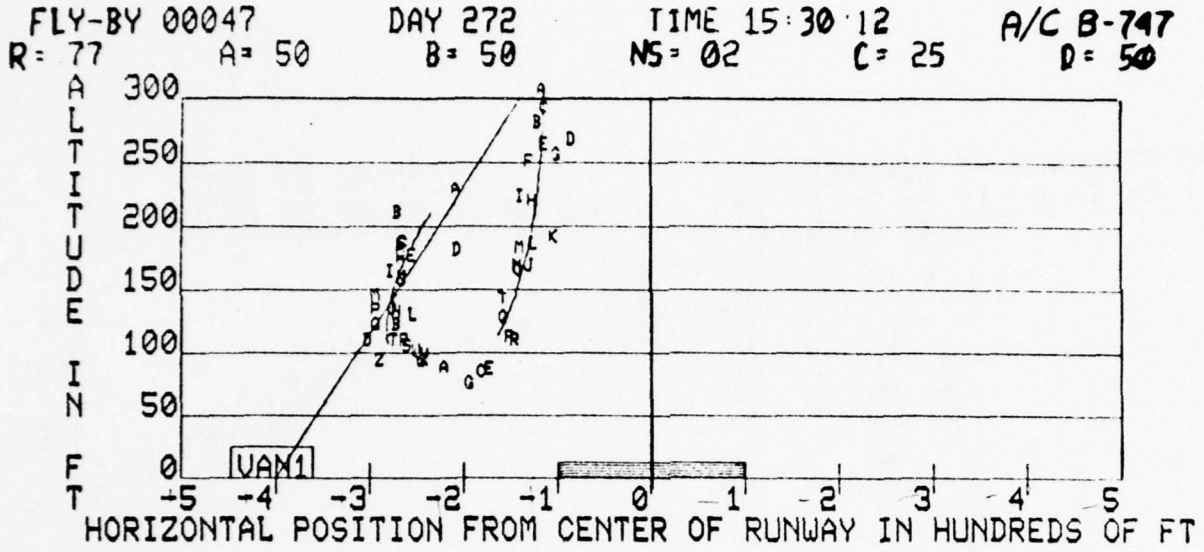

FLY-BY 00047 DAY 272 TIME 15 88:88 A/C B-747

R=77 A= 50 B= 50 NS= 02 C= 25 D= 50

FR	DATA PTS	COR P	COR S	PT	NOISE P	NOISE S	ANGLE MN	ANGLE MX	PK P	PAR S	TIME	PORT X	PORT Y	STARB X	STARB Y	POS
01	2270	151	055		00	00	44	61	230	200	000 8	-211	225	-120	303	
02	0491	128	128		00	00	37	62	230	221	002 8	-274	207	-124	277	
03	0509	150	099		00	00	33	60	241	210	006 8	-268	183	-117	288	
04	0753	250	146		00	00	37	61	222	208	009 4	-210	178	-089	263	
05	0931	250	238		00	00	37	61	257	225	011 4	-259	173	-117	260	
06	0817	238	250		00	00	36	61	258	209	013 2	-270	177	-133	247	
07	0685	250	112		00	00	37	63	248	214	016.7	-271	183	-104	252	
08	0719	233	222		00	00	38	61	260	220	018 3	-270	171	-130	216	
09	0569	186	135		00	00	38	60	249	185	021 6	-281	160	-144	219	
10	0680	209	224		00	00	29	59	248	196	023 2	-269	153	-133	165	
11	0577	250	125		00	00	28	62	262	189	026.5	-268	156	-107	187	
12	0486	038	087		00	00	88	89	250	000	028 0	-298	126	-129	181	
13	0494	151	179		00	00	31	62	265	189	031 8	-298	141	-143	179	
14	0481	158	098		00	00	29	60	272	172	033 6	-276	128	-146	165	
15	0286	111	088		00	00	30	61	265	170	036.3	-280	131	-144	162	
16	0311	056	114		00	00	18	61	276	176	038.0	-297	130	-154	108	
17	0187	036	077		00	00	20	63	273	176	041.7	-298	118	-162	124	
18	0178	057	025		00	00	18	62	237	145	043.8	-268	105	-148	105	
19	0167	062	000		00	02	18	62	238	000	046.0	-264	101			
20	0142	043	019		00	00	19	62	212	144	048.7	-278	106	-162	139	
21	0132	062	000		00	00	19	61	218	000	050.9	-254	098			
22	0116	054	000		00	00	19	54	220	000	054.0	-252	094			
23	0097	051	000		00	00	18	51	202	000	055.9	-248	090			
24	0092	033	000		00	00	81	52	181	000	059.2	-246	090			
25	0092	040	000		00	00	20	45	188	000	060.8	-246	094			
26	0092	002	000		00	00	37	42	174	000	062.8	-293	089			
27	0090	048	000		00	00	30	36	198	000	064.3	-224	084			
28	0086	036	000		00	00	39	45	166	000	067.1	-276	118			
29	0090	000	078		00	00	23	32	000	185	069.1			-184	080	
30	0092	002	000		00	00	47	49	174	000	072.3	-306	106			
31	0088	020	068		00	00	24	25	000	176	073.8			-176	083	
32	0000	000			00		99	99	000							
33	0033	003	024		00	00	19	21	003	196	079.1			-198	072	
34	0000	000			00		99	99	000							
35	0000	000			00		99	99	000							
36	0000	000			00		99	99	000							

FR	DATA PTS	COR P	COR S	PT	NOISE P	NOISE S	ANGLE MN	ANGLE MX	PK P	PAR S	TIME	PORT X	PORT Y	STARB X	STARB Y	POS

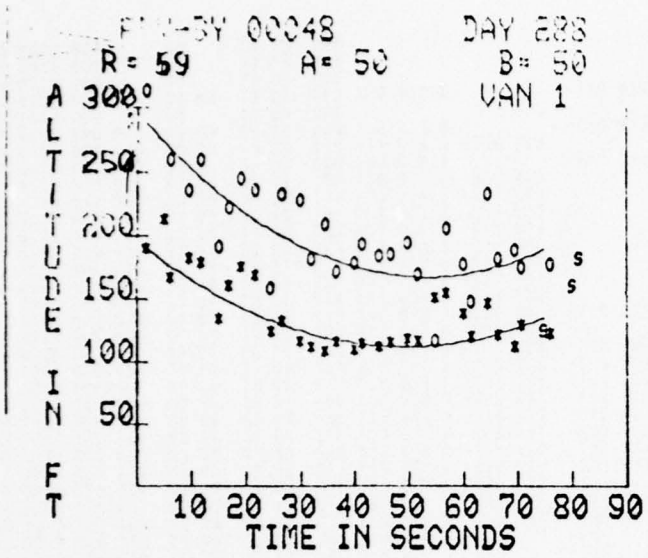

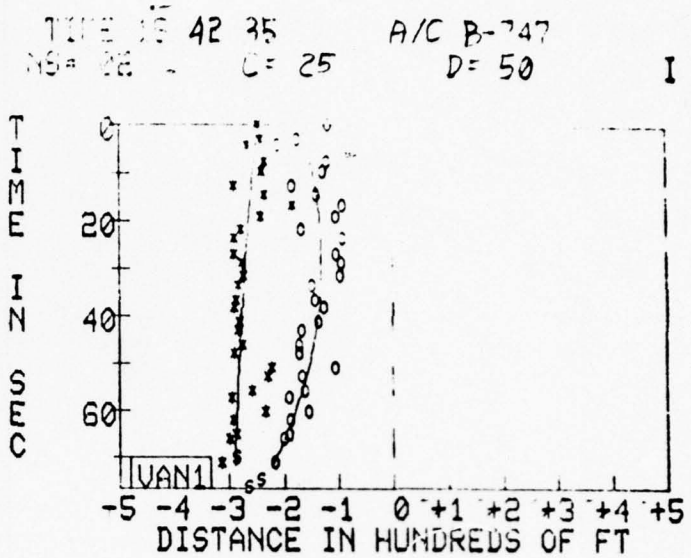

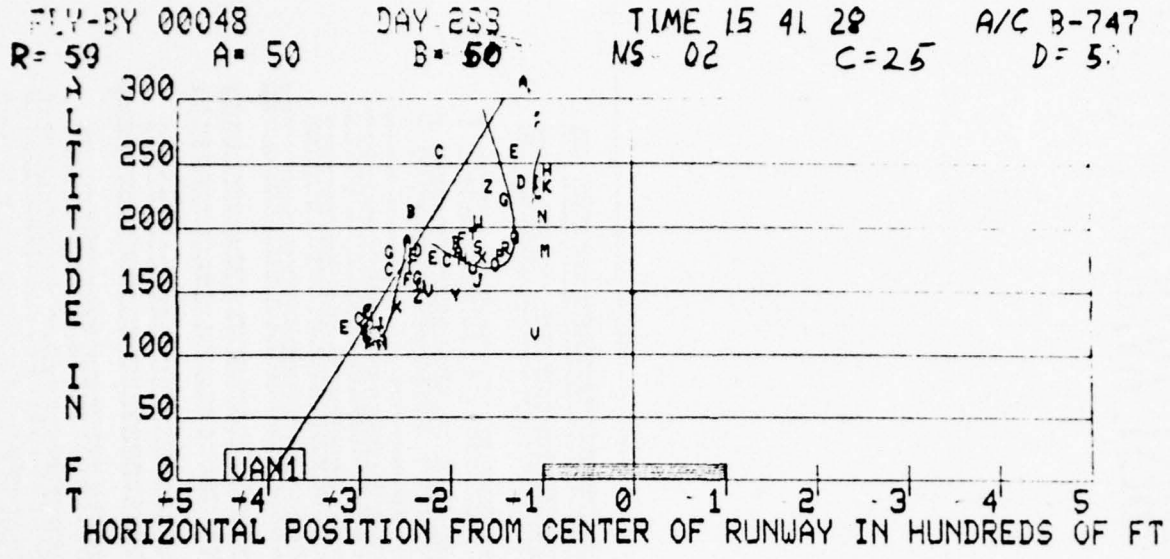

FLY-BY 00048 DAY 288 TIME 15:44:12 A/C B-[illegible]

R = 59 A = 50 B = 50 NB = 02 C = 25 D = 50

FR	DATA PTS	COR P	COR S	PT P	PT S	NOISE P	NOISE S	ANGLE MN	ANGLE MX	PK P	PK S	PAR TIME	PORT POS X	PORT POS Y	STARB POS X	STARB POS Y
01	0409	068	079	00	00	35	61	234	218	020	9		-250	186	-121	328
02	0609	154	073	00	00	33	61	248	192	004	2		-246	209	-180	326
03	0673	059	129	00	00	30	62	225	235	005	6		-270	162	-214	254
04	0602	159	108	00	00	26	63	241	202	008	9		-239	177	-124	231
05	0644	148	110	00	00	27	63	238	208	011	0		-243	174	-132	255
06	0584	043	144	00	00	23	61	229	212	014	3		-252	130	-189	187
07	0526	137	116	00	00	27	61	233	209	016	3		-239	156	-143	217
08	0495	133	084	00	00	25	60	217	214	018	4		-189	170	-096	239
09	0500	149	058	00	00	23	61	233	206	020	9		-247	164	-108	231
10	0537	026	104	00	00	21	62	222	214	024	0		-281	120	-171	153
11	0508	008	107	00	00	03	63	000	212	025	8		-294	127	-097	228
12	0450	022	095	00	00	22	60	258	201	029	1		-294	111	-107	203
13	0407	032	091	00	00	21	61	276	197	031	2		-279	107	-099	176
14	0472	043	095	00	00	19	58	250	202	033	8		-278	104	-102	203
15	0494	041	127	00	00	21	63	222	205	036	1		-286	110	-153	166
16	0397	017	103	00	00	19	54	200	213	039	3		-292	105	-148	173
17	0387	032	117	00	00	21	59	209	210	040	9		-294	110	-131	188
18	0433	040	106	00	00	21	57	203	224	044	0		-284	107	-142	178
19	0393	022	106	00	00	25	56	245	184	046	0		-287	110	-171	179
20	0400	033	096	00	00	25	53	243	182	049	1		-283	112	-178	189
21	0347	021	119	00	00	24	63	241	213	051	1		-283	112	-178	193
22	0337	003	092	00	00	21	52	221	177	054	1		-287	146	-111	112
23	0003	000	019	00	00	00	00	000	140	056	1		-254	149	-172	200
24	0153	000	041	00	00	19	53	213	104	059	3		-282	133	-167	171
25	0165	005	055	00	00	27	58	217	104	000	8		-287	114	-195	142
26	0151	006	018	00	00	00	51	005	146	004	0		-280	141	-160	227
27	0116	024	047	00	00	00	55	244	173	006	7		-287	116	-193	176
28	0000	010	045	00	00	00	55	217	168	008	9		-282	103	-196	183
29	0007	021	031	00	00	05	53	225	176	070	1		-303	124	-206	169
30	0005	004	000	00	00	00	58	103	000	074	2		-280	120		
31	0005	002	007	00	00	00	57	002	142	076	3		-318	117	-221	172
32	0003	000	003	00	00	40	47	000	156	079	3				-248	154
33	0002	001	000	00	00	53	54	104	000	000	6		-278	178		
34	0000	000		00		00	00	000								
35	0000	000		00		00	00	000								

FR	DATA PTS	COR P	COR S	PT P	PT S	NOISE P	NOISE S	ANGLE MN	ANGLE MX	PK P	PK S	PAR TIME	PORT POS X	PORT POS Y	STARB POS X	STARB POS Y

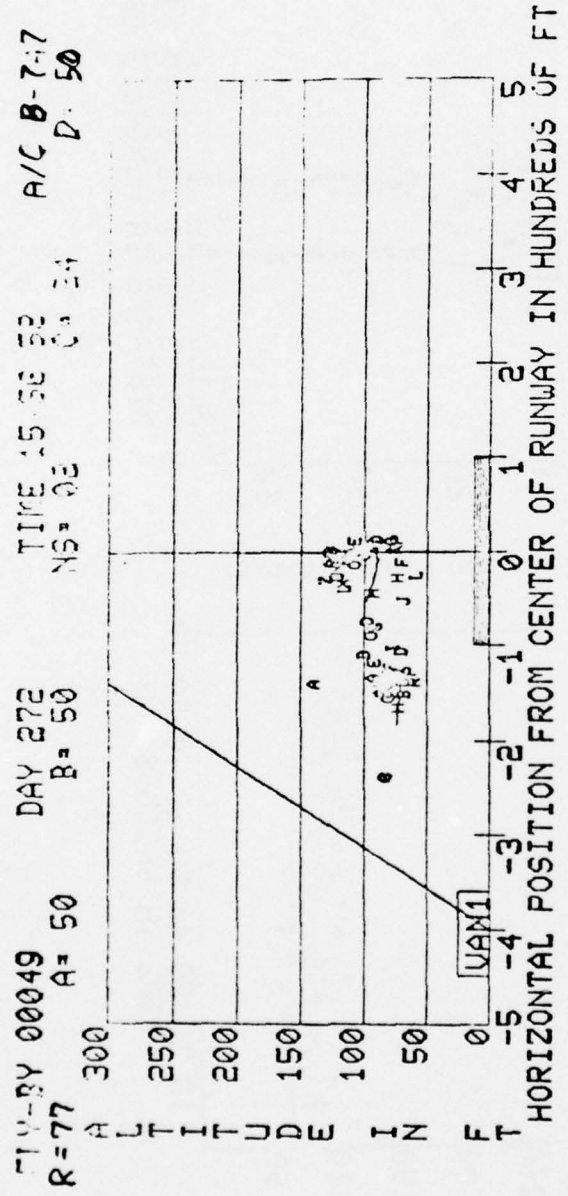

FLY-BY 00049 DAY 272 TIME 15 51 55 A/C = B-747
R = 77 A = 50 B = 50 NS = 02 C = 24 D = 50 I

FR	DATA PTS	COR P	COR S	PT P	PT S	NOISE P	NOISE S	ANGLE MN	ANGLE MX	PK P	PK S	PAR TIME	PORT POS X	PORT POS Y	STARB POS X	STARB POS Y
01	0893	062	250	00	00	07	35	220	262	000.6	-241	080	-144	135		
02	0969	250	229	00	00	07	34	273	213	003.1	-154	064	-013	116		
03	0937	068	250	00	00	08	33	262	268	006.7	-240	079	-093	090		
04	0838	250	099	00	00	08	33	266	240	007.9	-110	066	0009	086		
05	0711	250	106	00	00	08	32	261	214	011.5	-122	087	0007	103		
06	0690	250	156	00	00	08	33	261	244	013.3	-153	074	-014	066		
07	0679	250	056	00	00	07	33	278	269	016.5	-158	076	0007	075		
08	0697	227	214	00	00	07	28	252	276	017.9	-169	068	-031	069		
09	0587	248	000	00	02	09	28	269	000	021.9	-106	073				
10	0528	016	250	05	00	08	22	170	288	022.8			-056	065		
11	0376	000	221	00	00	08	23	000	249	026.2			-085	090		
12	0283	000	089	05	00	08	20	000	268	027.6			-028	058		
13	0367	131	120	00	00	08	21	214	244	031.6	-132	075	0004	089		
14	0505	190	139	00	00	08	25	241	250	032.8	-142	064	0002	074		
15	0371	126	171	00	00	10	23	214	242	035.6	-145	077	-017	104		
16	0470	169	122	00	00	09	20	216	242	037.6	-130	059	0009	071		
17	0297	109	118	00	00	09	22	209	228	041.2	-137	074	-012	110		
18	0507	159	190	00	00	09	22	217	236	042.7	-142	056	0000	071		
19	0315	078	145	00	00	10	23	196	240	046.6	-139	080	-003	103		
20	0465	131	191	00	00	09	22	200	226	048.1	-141	065	0000	053		
21	0240	067	000	00	00	12	21	184	225	051.8	-139	074	-004	103		
22	0522	134	250	00	00	09	10	209	226	055.0	-134	068	-007	095		
23	0215	000	000	04	00	08	24	000	224	056.4			-020	117		
24	0[illegible]	000	193	00	00	50	00	000	217	058.7			-037	113		
25	0[illegible]	000	110	00	00	10	25	209	220	061.1	-148	003	-011	123		
26	0[illegible]	005	163	00	00	10	25	178	208	063.5	-153	080	-033	126		
27	0272	084	133	00	00	07	23	196	222	066.7	-137	008	-015	123		
28	0354	136	041	00	00	11	22	212	176	068.3	-113	095	-002	122		
29	0219	057	108	00	00	12	21	188	203	071.4	-138	083	-005	114		
30	0291	186	000	00	00	10	29	200	000	074.2	-077	094				
31	0164	050	075	00	00	08	28	174	201	075.7	-133	077	-003	101		
32	0174	050	076	00	00	11	29	180	202	079.7	-126	075	0001	100		
33	0128	006	000	00	00	09	28	184	000	000.9	-033	087				
34	0201	000	146	04	00	09	31	000	200	004.6			-048	089		
35	0105	051	033	00	00	09	18	196	177	006.8	-138	074	-008	106		
36	0000	000		00		00	00	000								

Appendix F

TIME HISTORY OF VORTEX ROTATIONAL VELOCITY

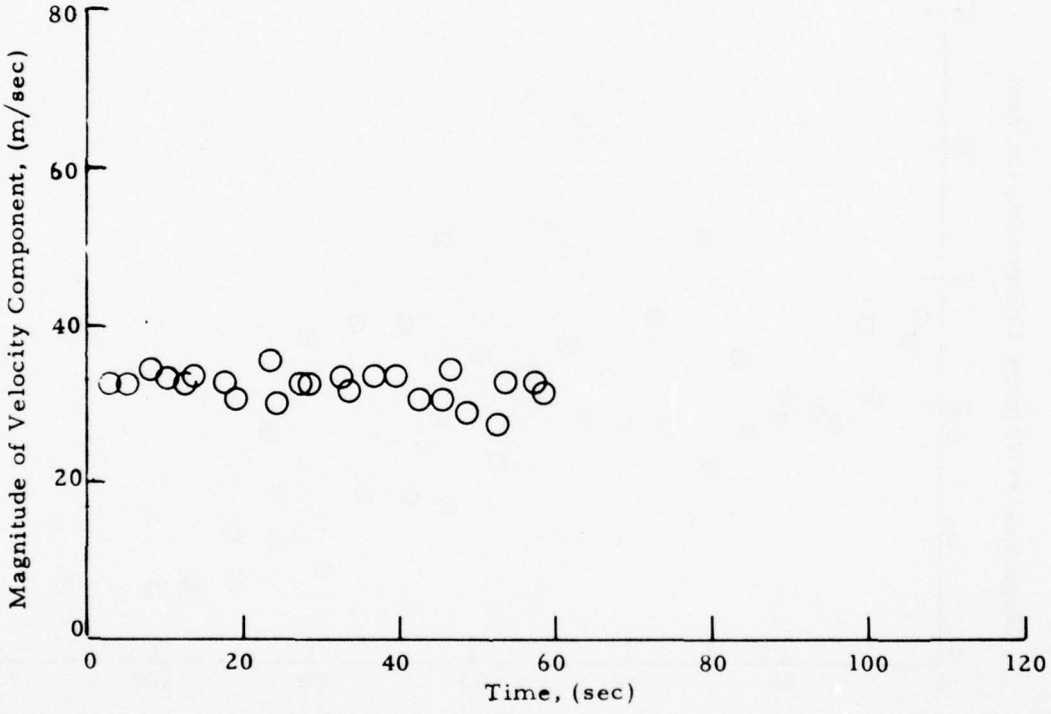

Fig. F-1 - $|V_{pk}|$ as a Function of Time for Rosamond B-747 Flyby 24 (from High-Speed Data)

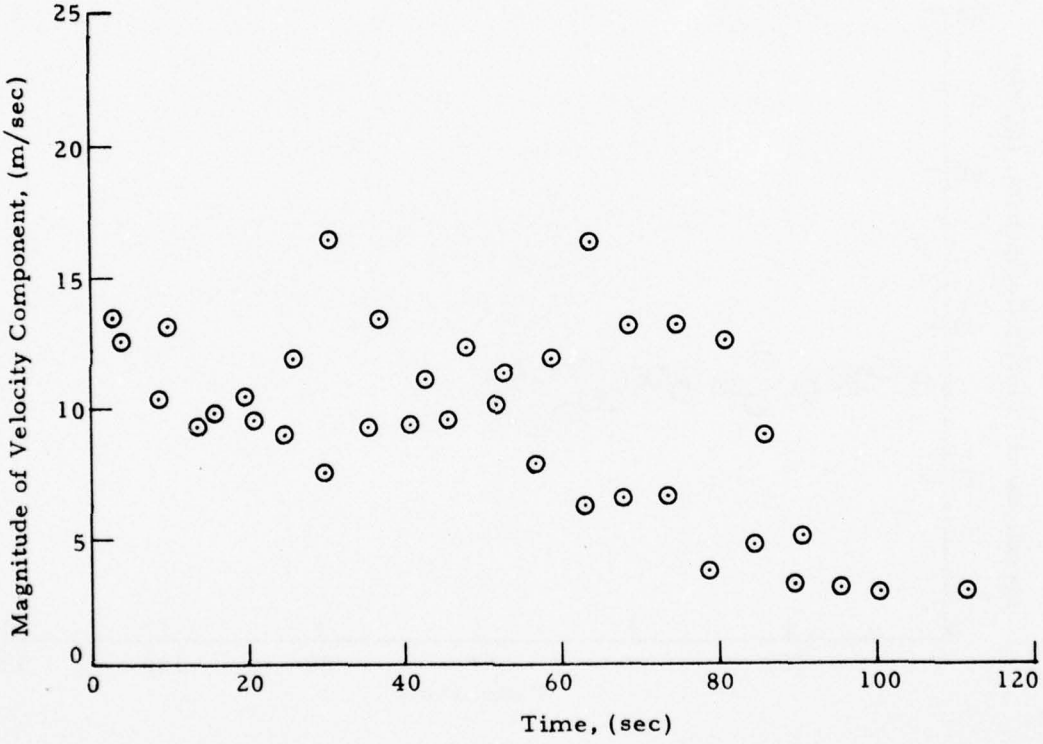

Fig. F-2 - $|V_{ms}|$ as a Function of Time for Rosamond B-747 Flyby 24 (from Low-Speed Data)

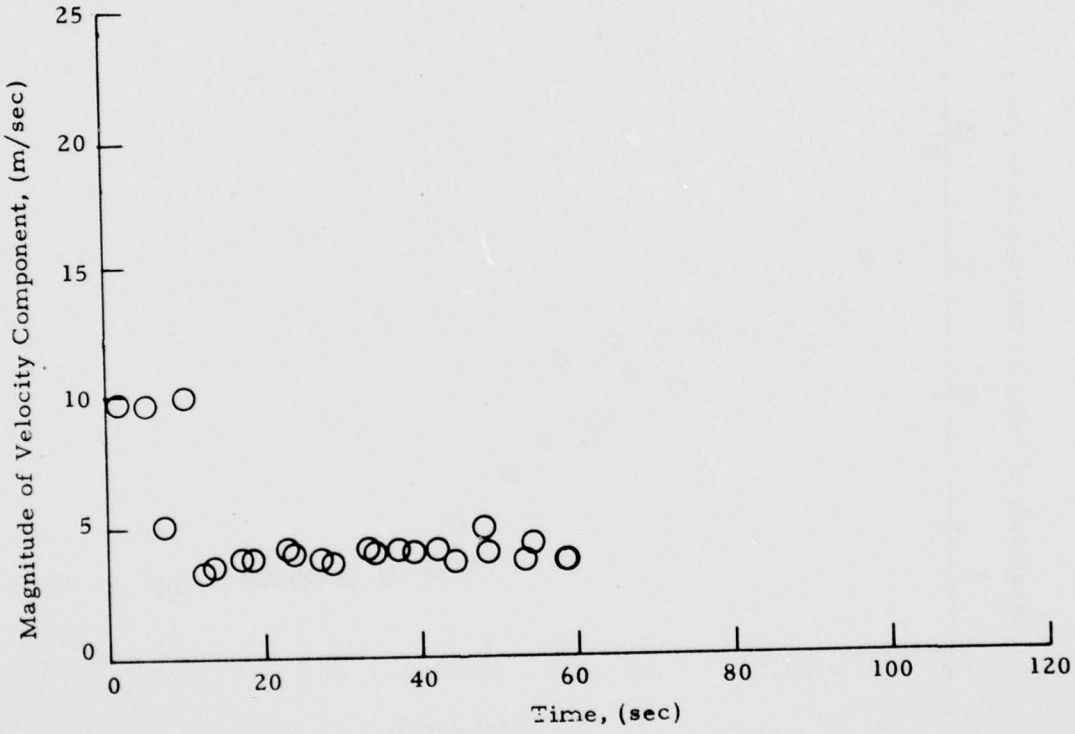

Fig. F-3 - $|V_{ms}|$ as a Function of Time for Rosamond B-747 Flyby 24 (from High-Speed Data)

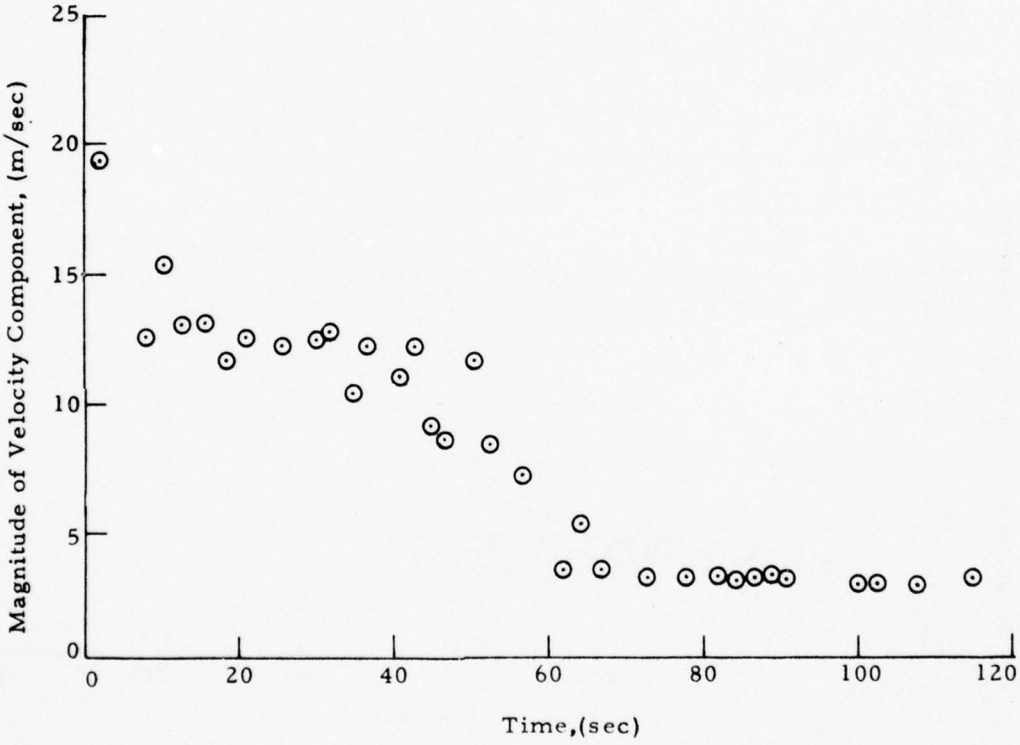

Fig. F-4 - $|V_{ms}|$ as a Function of Time for Rosamond B-747 Flyby 25 (from Low-Speed Data)

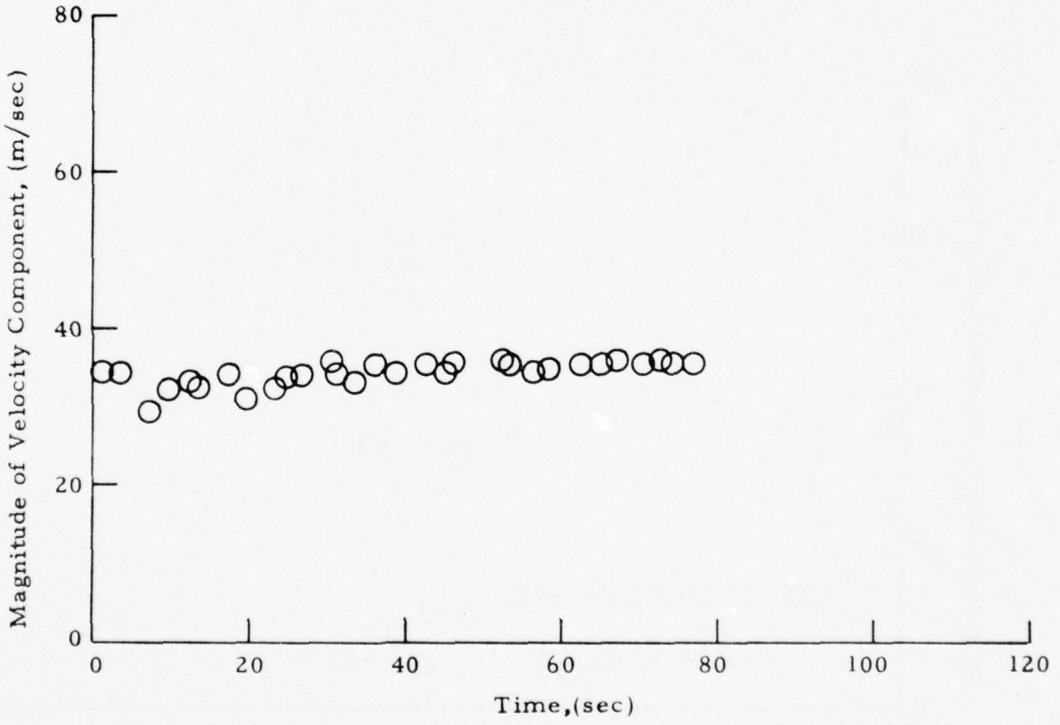

Fig. F-5 - $|V_{pk}|$ as a Function of Time for Rosamond B-747 Flyby 27 (from high speed data)

AD-A048 275 LOCKHEED MISSILES AND SPACE CO INC HUNTSVILLE ALA HU--ETC F/G 1/1
LASER DOPPLER VELOCIMETER MEASUREMENTS OF B-747 WAKE VORTEX CHA--ETC(U).
SEP 77 M R BRASHEARS, A D ZALAY DOT-TSC-1145

UNCLASSIFIED LMSC-HREC-TR-D496975 FAA-RD-77-85 NL

3 OF 3
AD
A048275

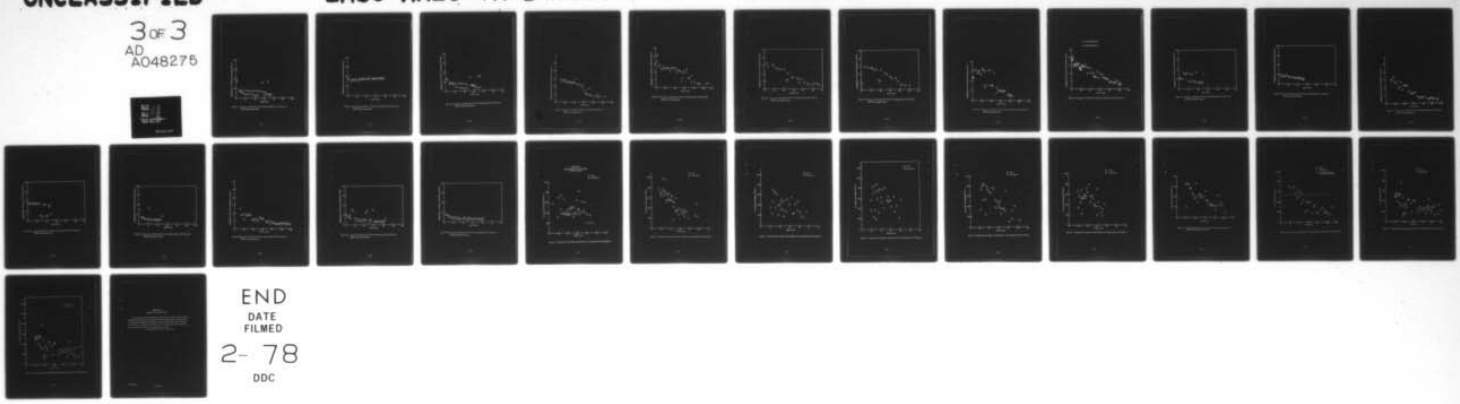

END
DATE
FILMED
2-78
DDC

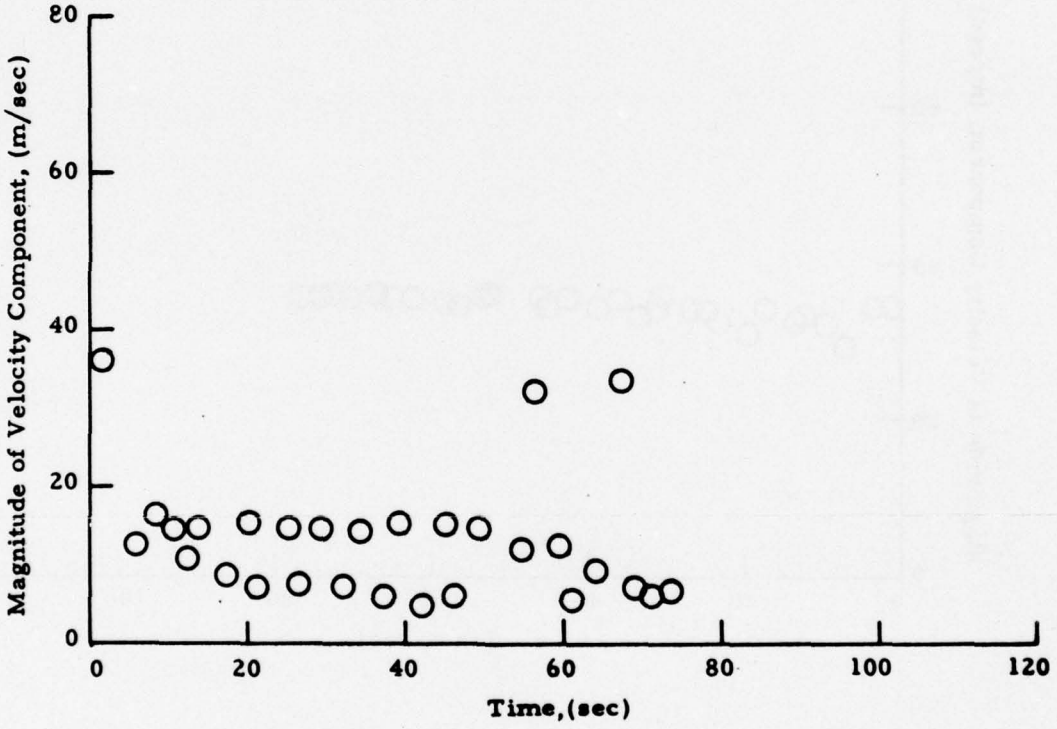

Fig. F-6 - $|V_{ms}|$ as a Function of Time for Rosamond B-747 Flyby 27 (from High-Speed Data)

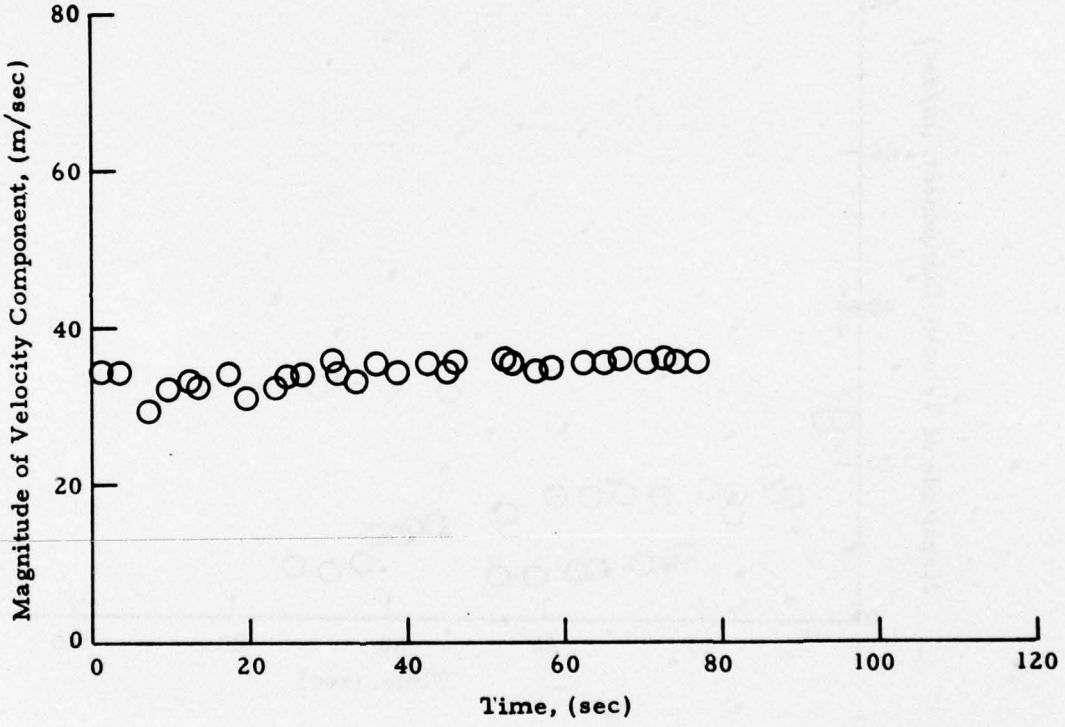

Fig. F-7 - $|V_{pk}|$ as a Function of Time for Rosamond B-747 Flyby 28 (from High-Speed Data)

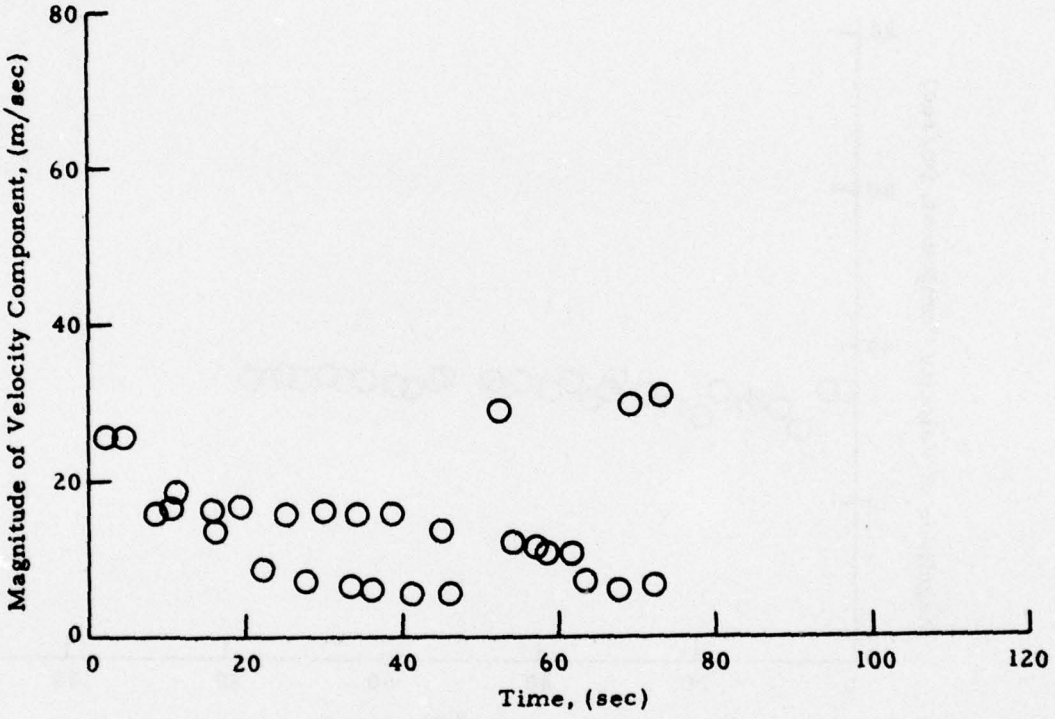

Fig. F-8 - $|V_{ms}|$ as a Function of Time for Rosamond B-747 Flyby 28 (from High-Speed Data)

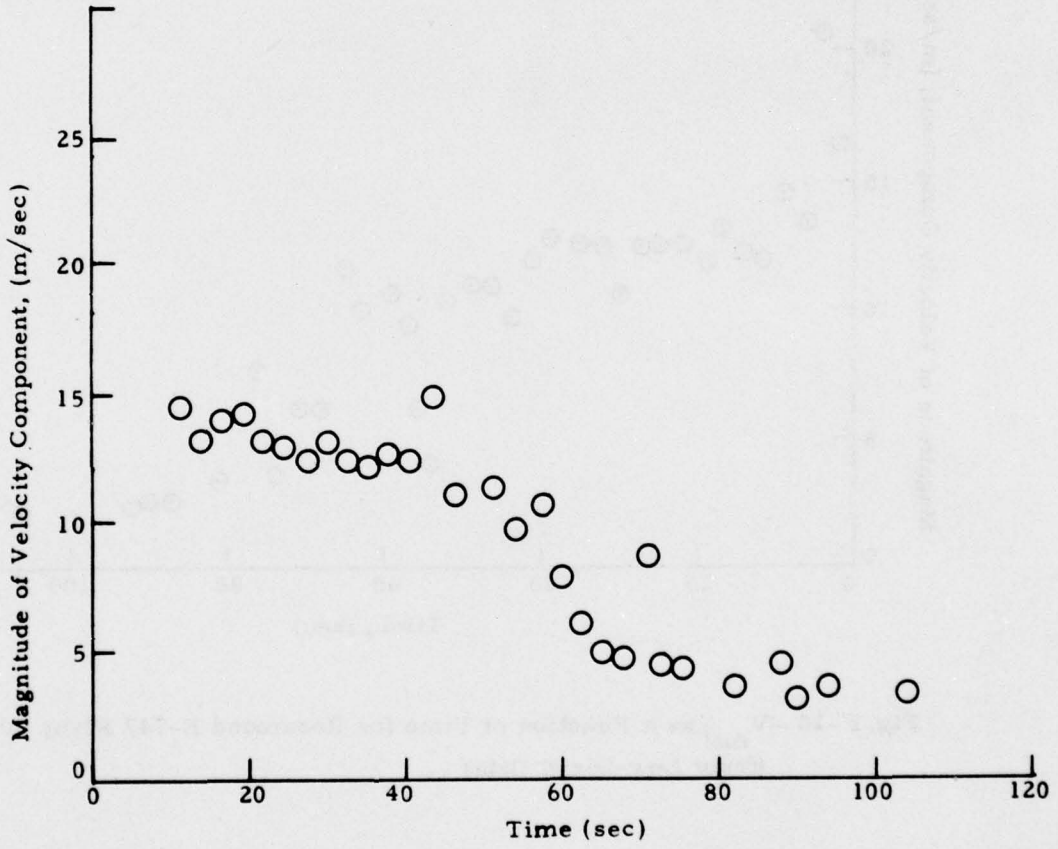

Fig. F-9 - $|V_{ms}|$ as a Function of Time for Rosamond Flyby 29 (from Low-Speed Data)

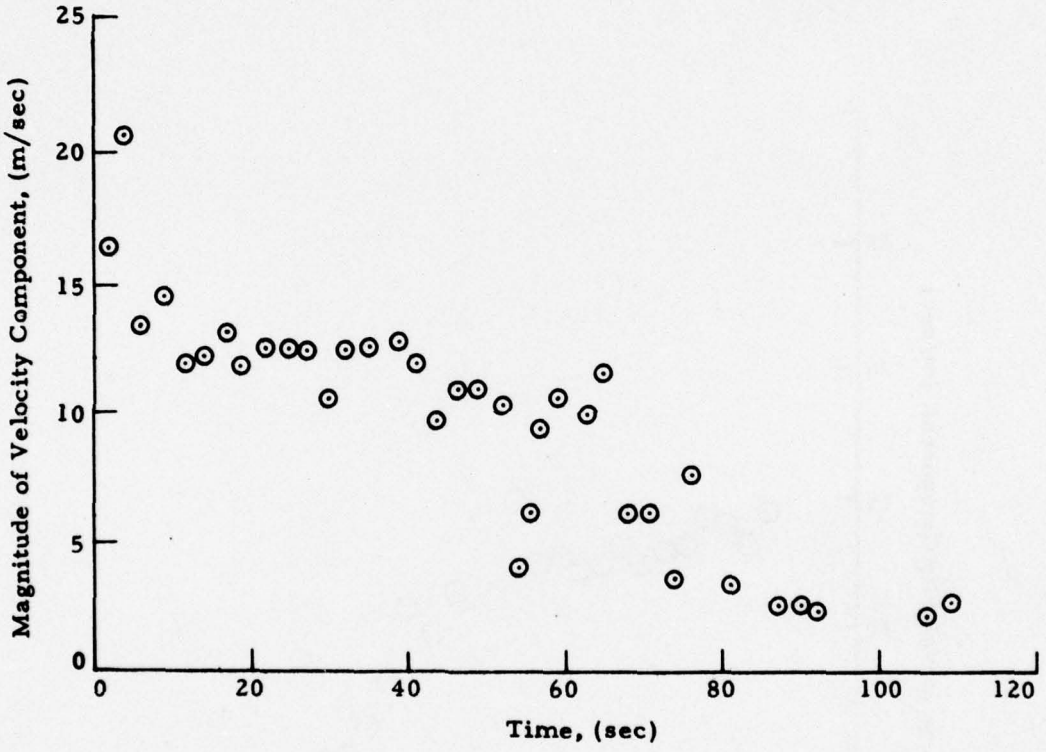

Fig. F-10 - $|V_{ms}|$ as a Function of Time for Rosamond B-747 Flyby 30 (from Low-Speed Data)

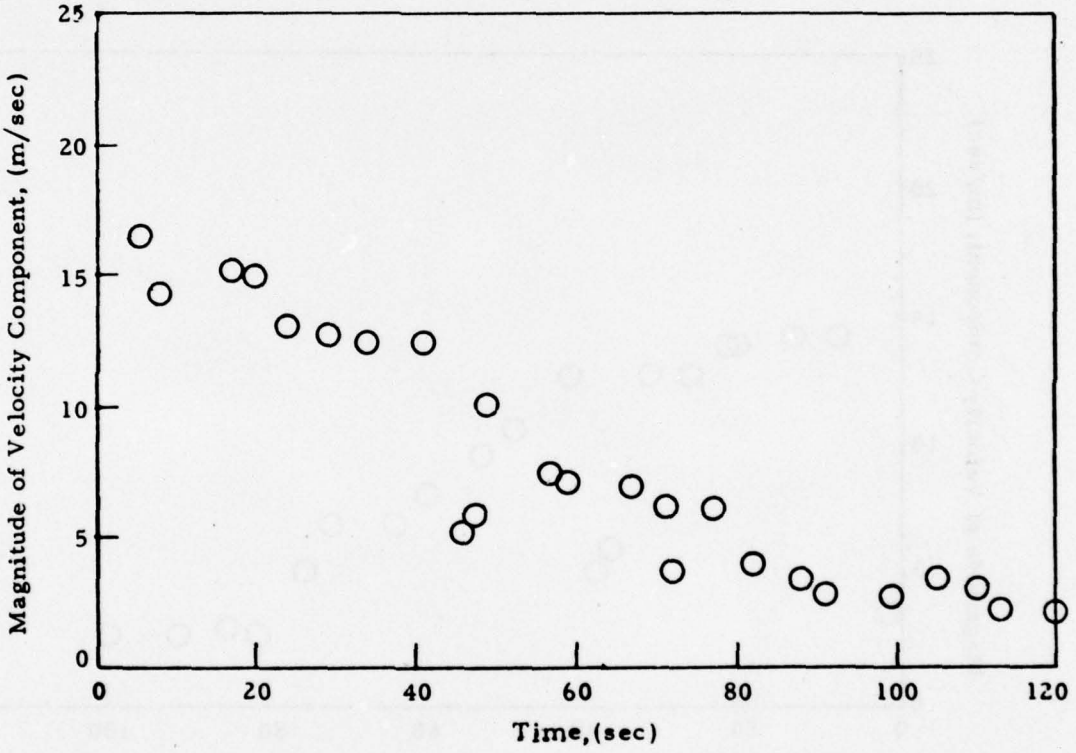

Fig. F-11 - $|V_{ms}|$ as a Function of Time for Rosamond B-747 Flyby 35 (from Low-Speed Data)

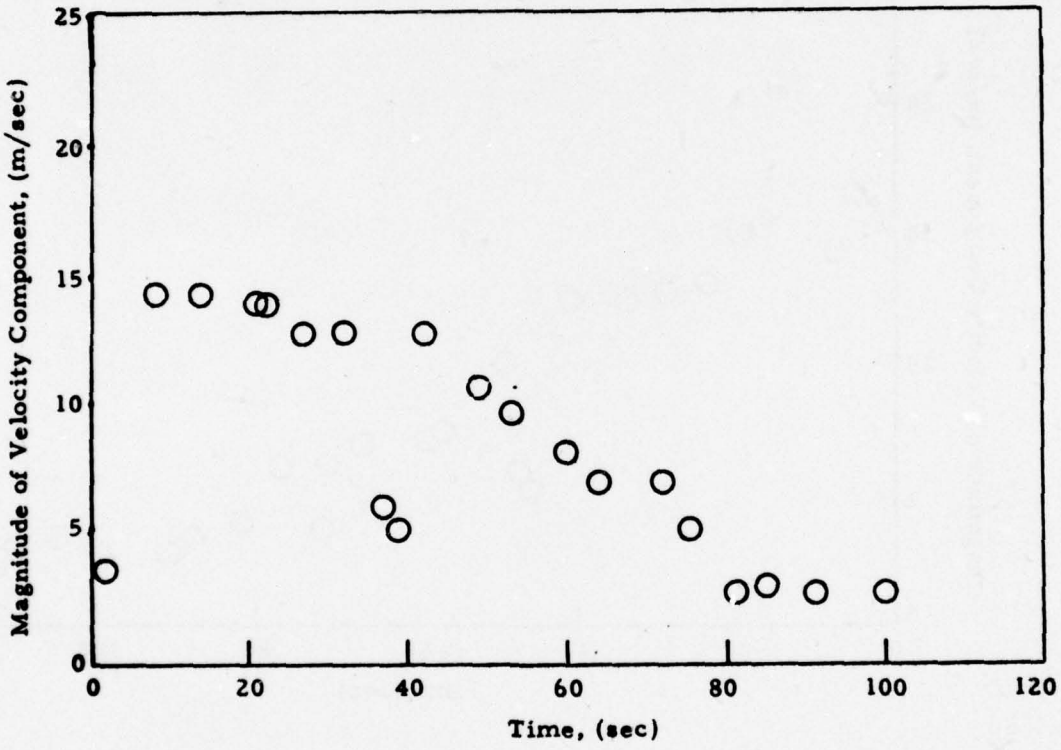

Fig. F-12 - $|V_{ms}|$ as a Function of Time for Rosamond B-747 Flyby 38 (from Low-Speed Data)

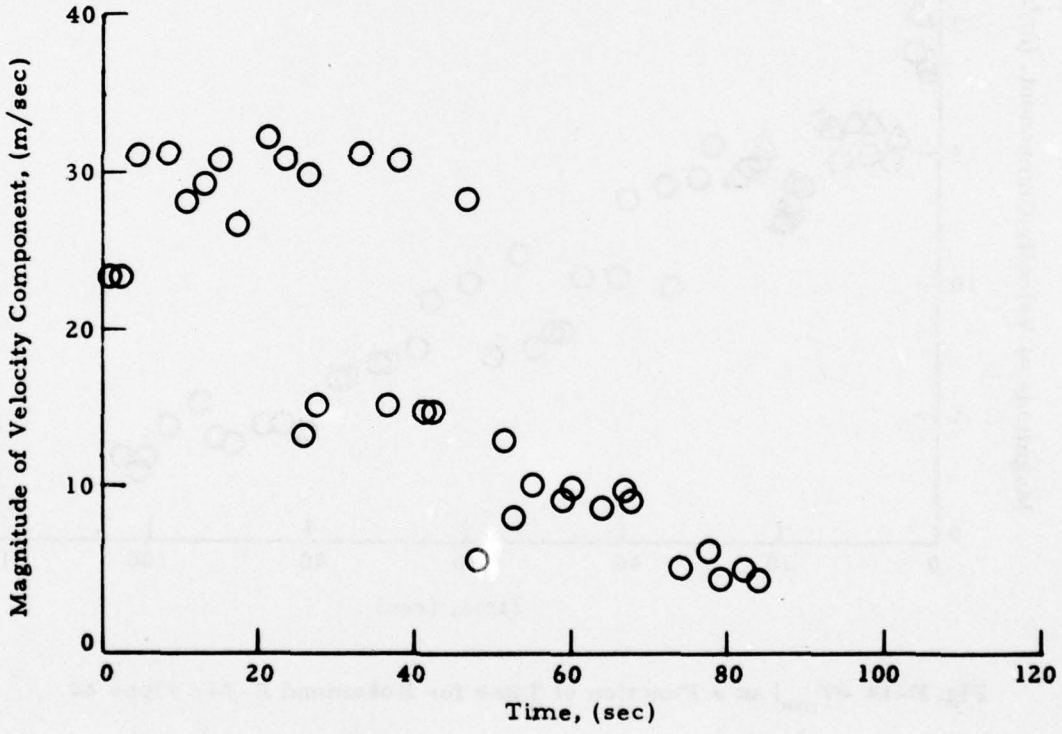

Fig. F-13 - $|V_{pk}|$ as a Function of Time for Rosamond B-747 Flyby 44 (from High Speed Data)

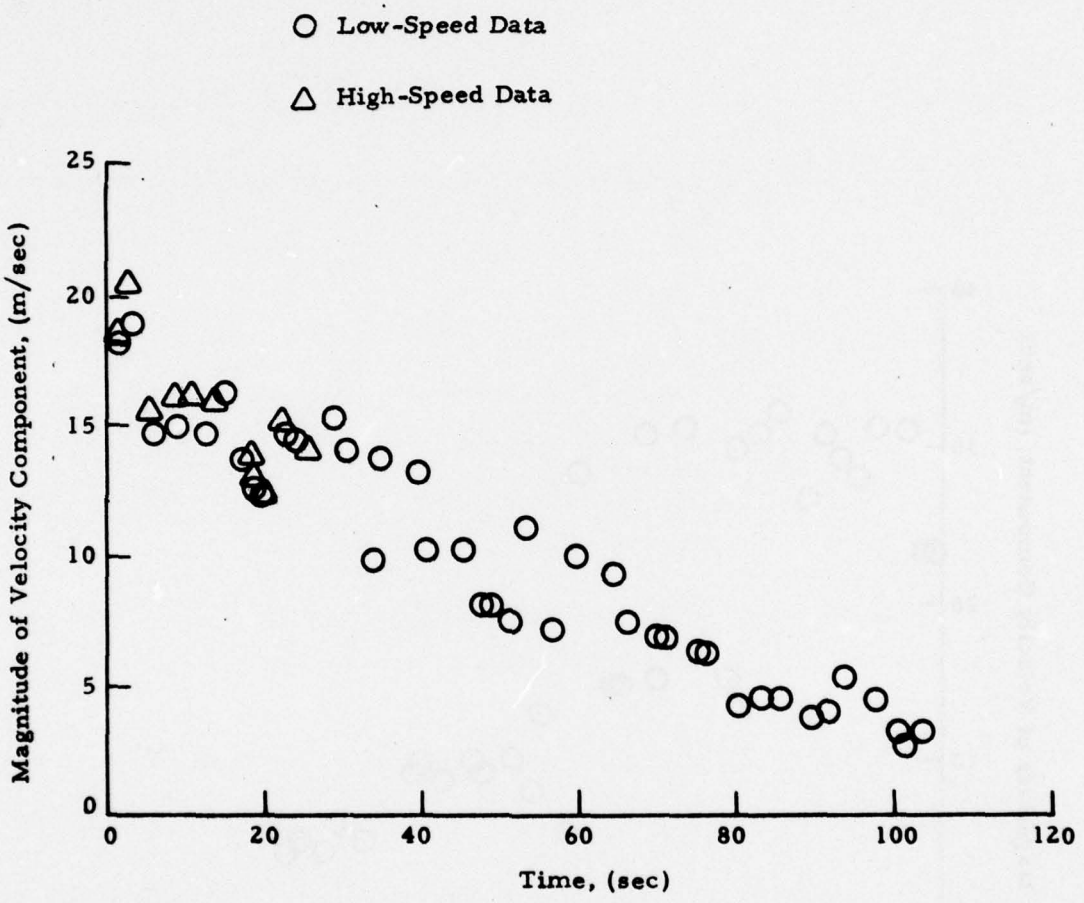

Fig. F-14 $-|V_{ms}|$ as a Function of Time for Rosamond B-747 Flyby 44

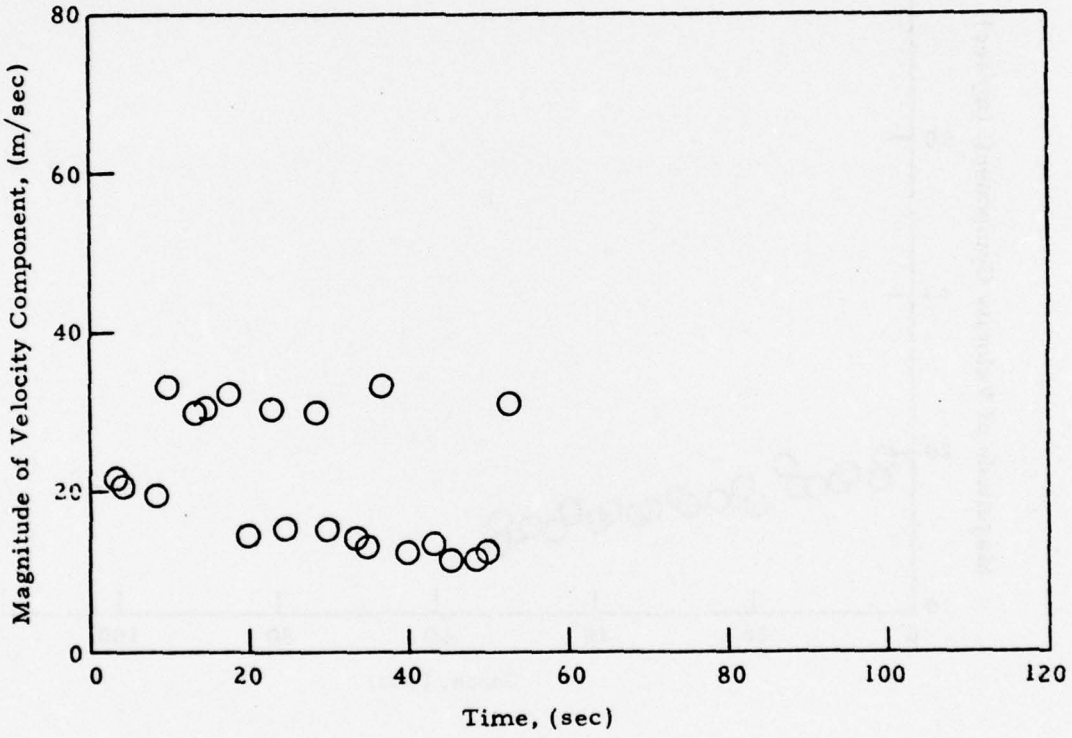

Fig. F-15 - $|V_{pk}|$ as a Function of Time for Rosamond B-747 Flyby 47 (from High-Speed Data)

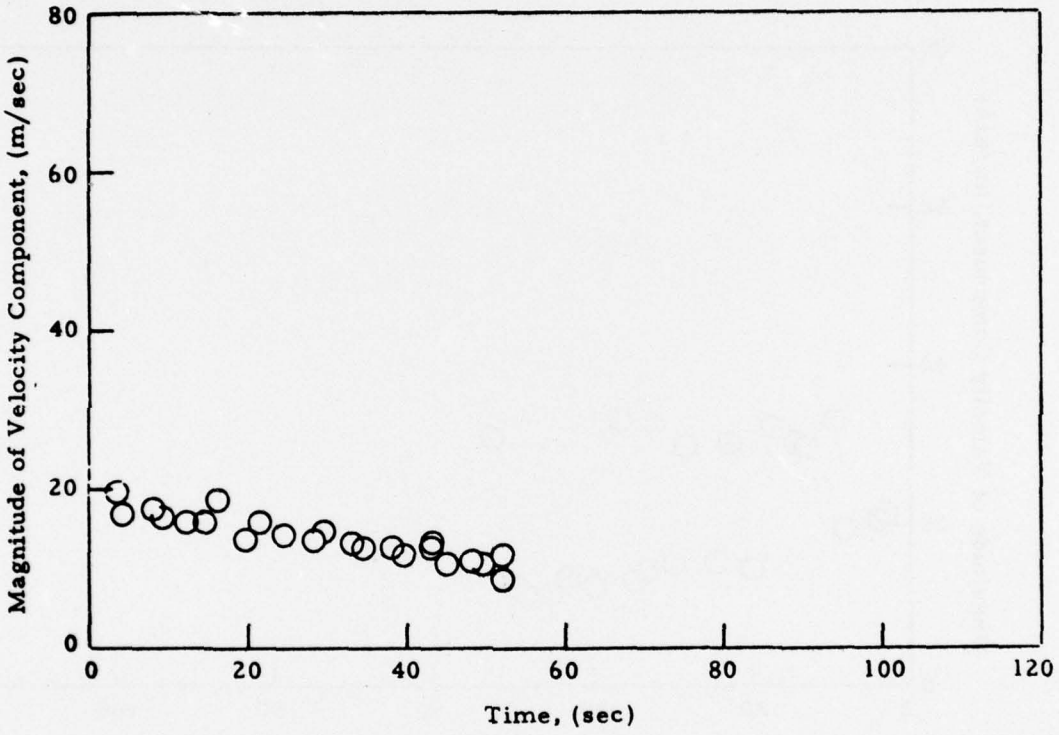

Fig. F-16 - $|V_{ms}|$ as a Function of Time for Rosamond B-747 Flyby 47 (from High-Speed Data)

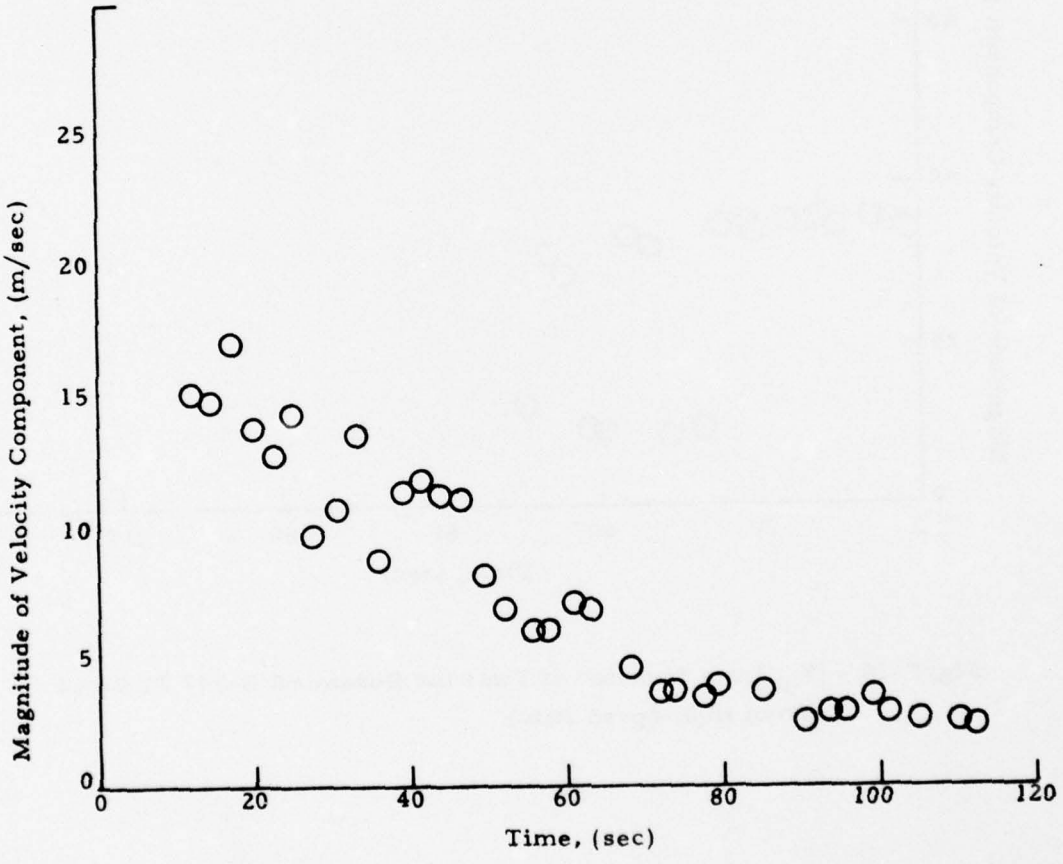

Fig. F-17 - $|V_{ms}|$ as a Function of Time for Rosamond B-747 Flyby 47 (from Low-Speed Data)

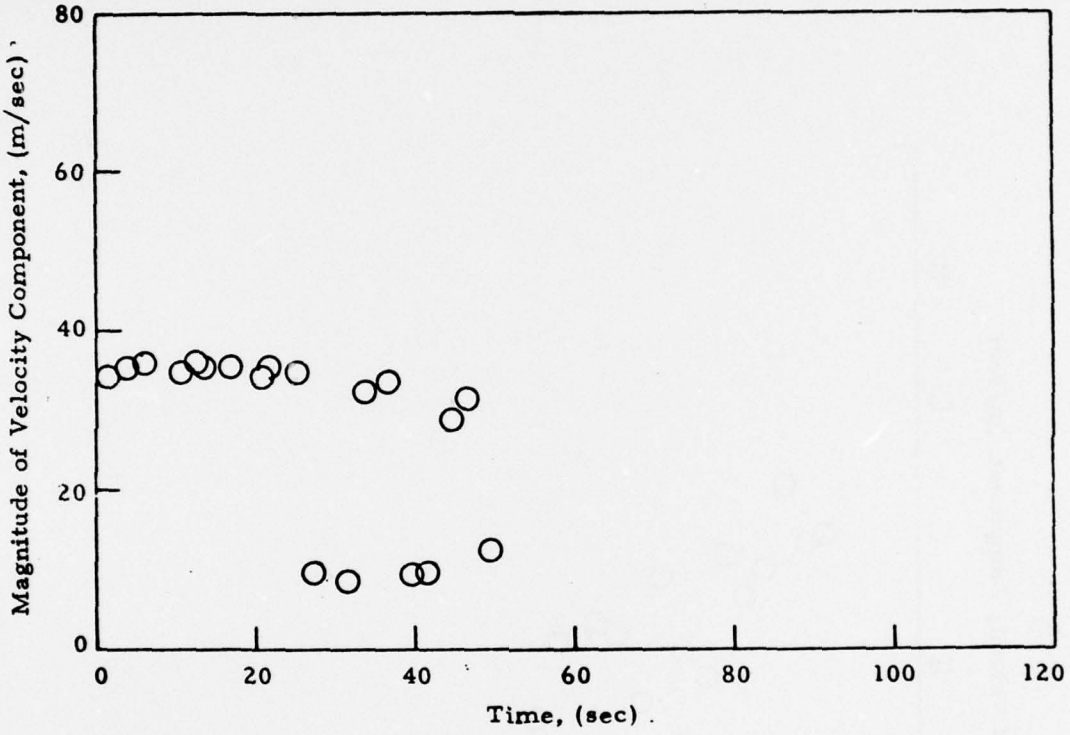

Fig. F-18 - $|V_{pk}|$ as a Function of Time for Rosamond B-747 Flyby 48 (from High-Speed Data)

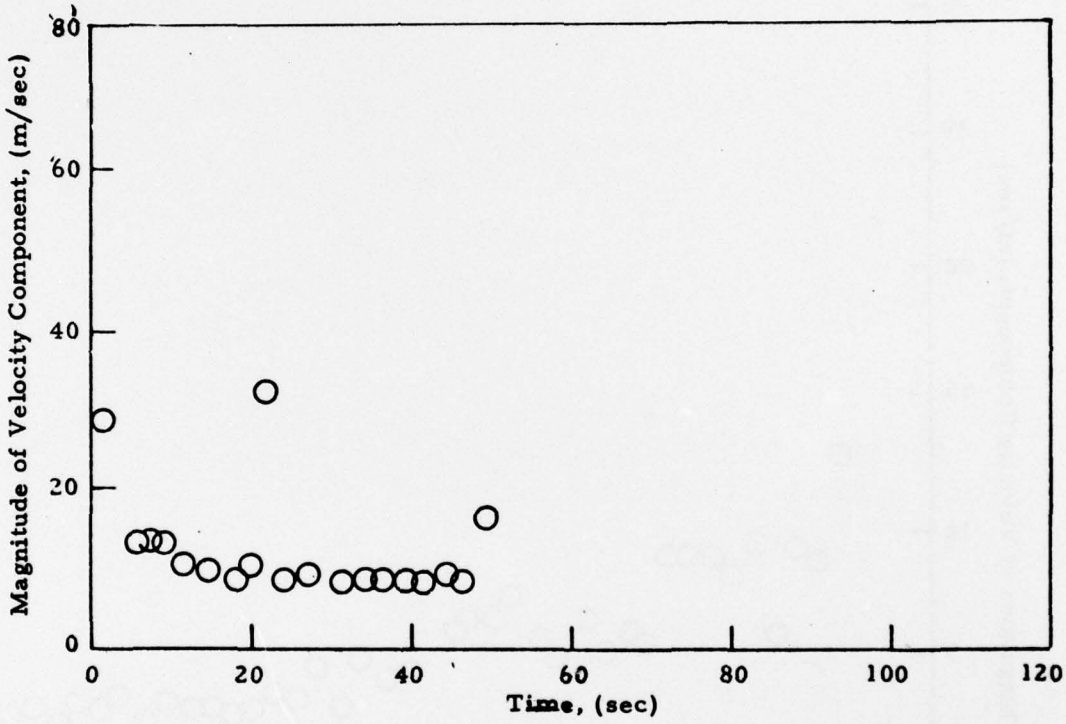

Fig. F-19 - $|V_{ms}|$ as a Function of Time for Rosamond B-747 Flyby 48 (from High-Speed Data)

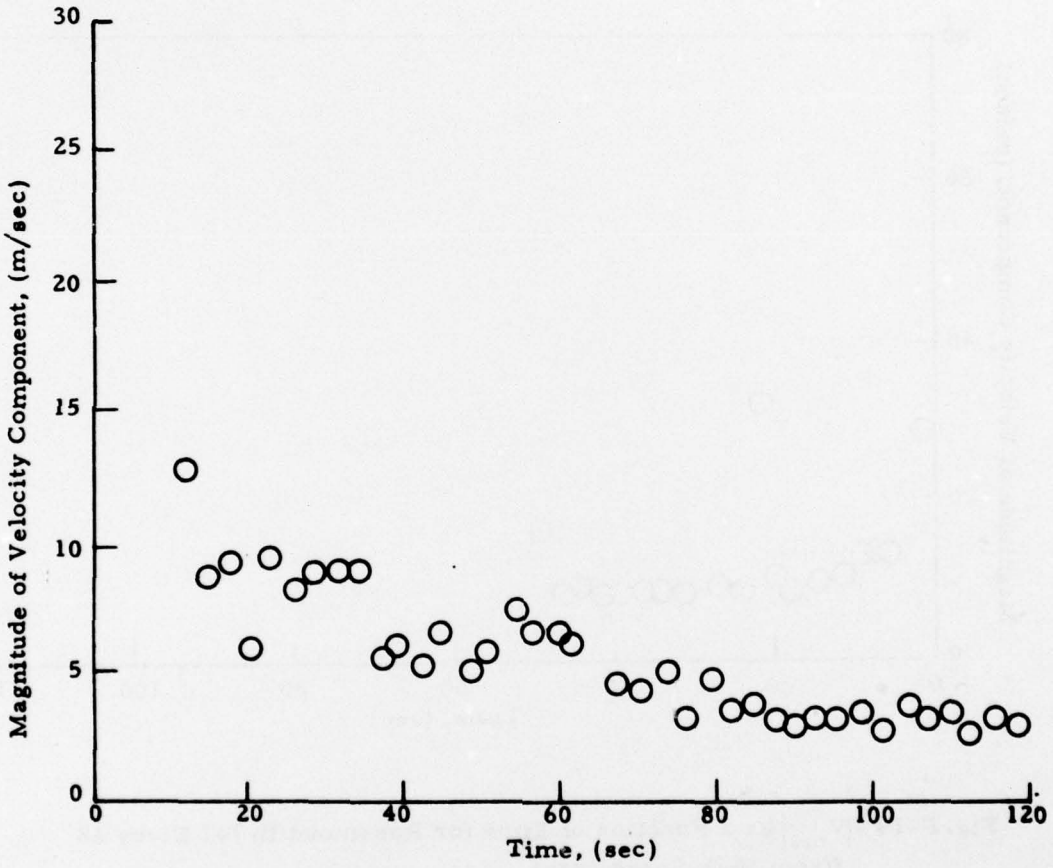

Fig. F-20-$|V_{ms}|$ as a Function of Time for Rosamond B-747 Flyby 48 (from Low-Speed Data)

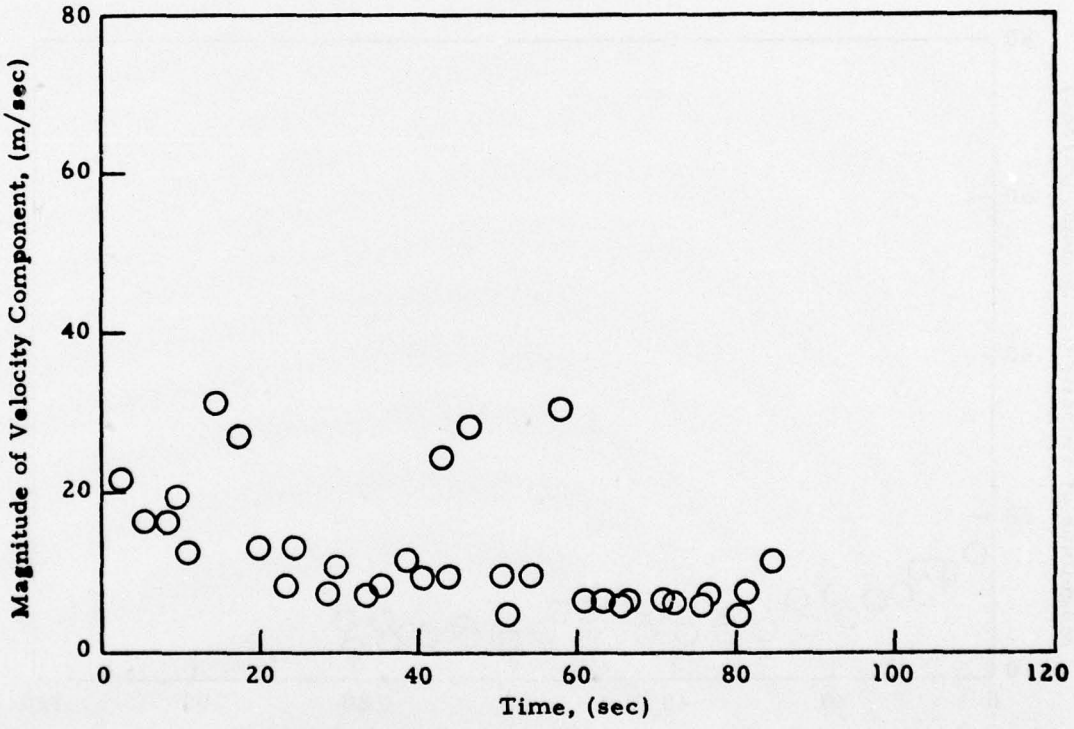

Fig. F-21 - $|V_{pk}|$ as a Function of Time for Rosamond B-747 Flyby 49 (from High-Speed Data)

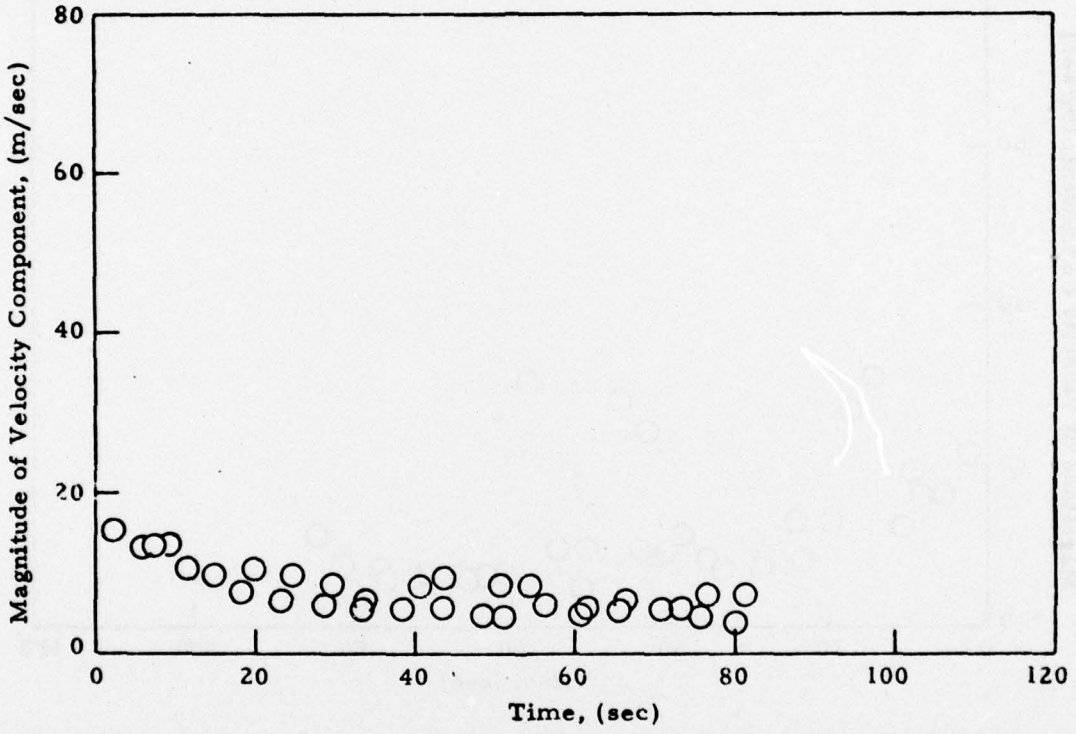

Fig. F-22 - $|V_{ms}|$ as a Function of Time for Rosamond B-747 Flyby 49 (from High-Speed Data)

Appendix G

TIME HISTORY OF VORTEX CIRCULATION

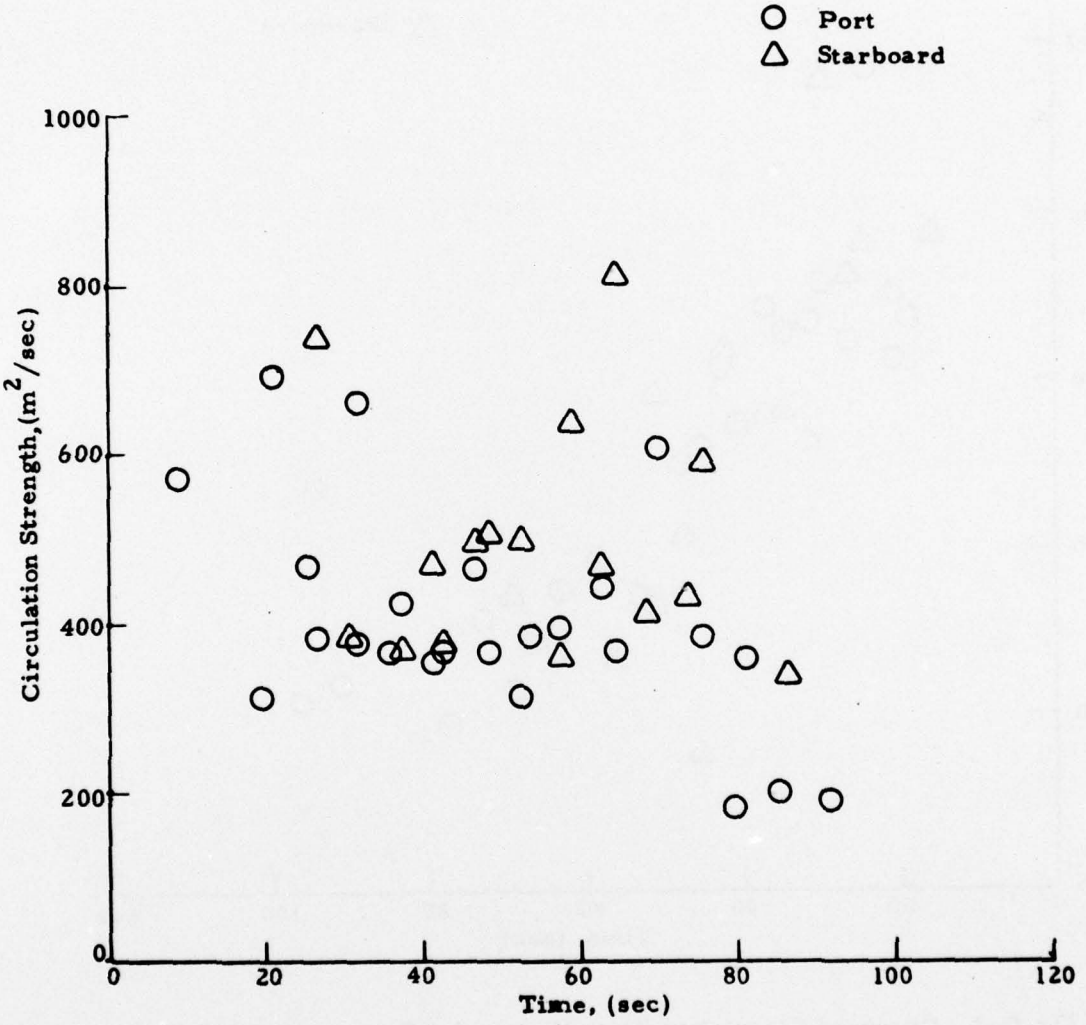

Fig. G-1 - Observed Circulation Time History for Rosamond B-747 Flyby 24

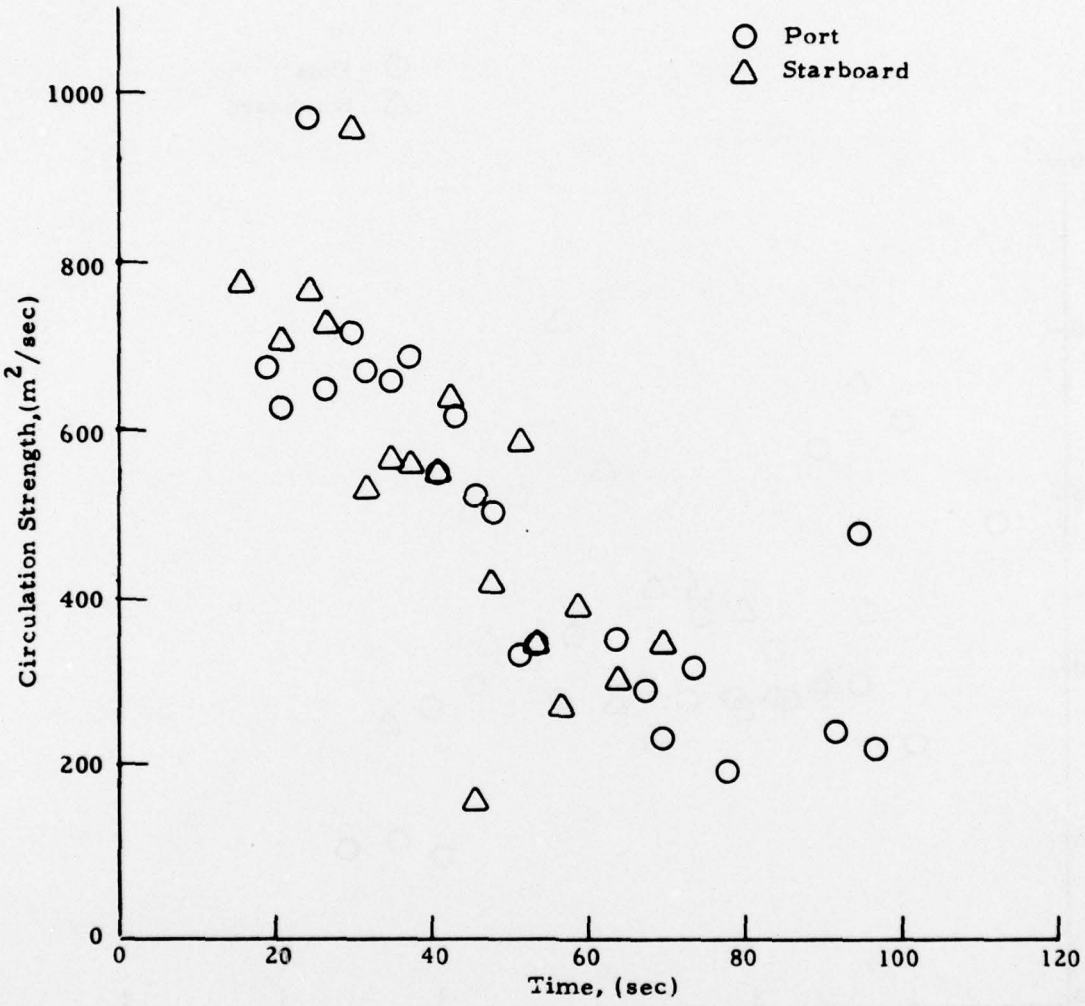

Fig. G-2 - Observed Circulation Time History for Rosamond B-747 Flyby 25

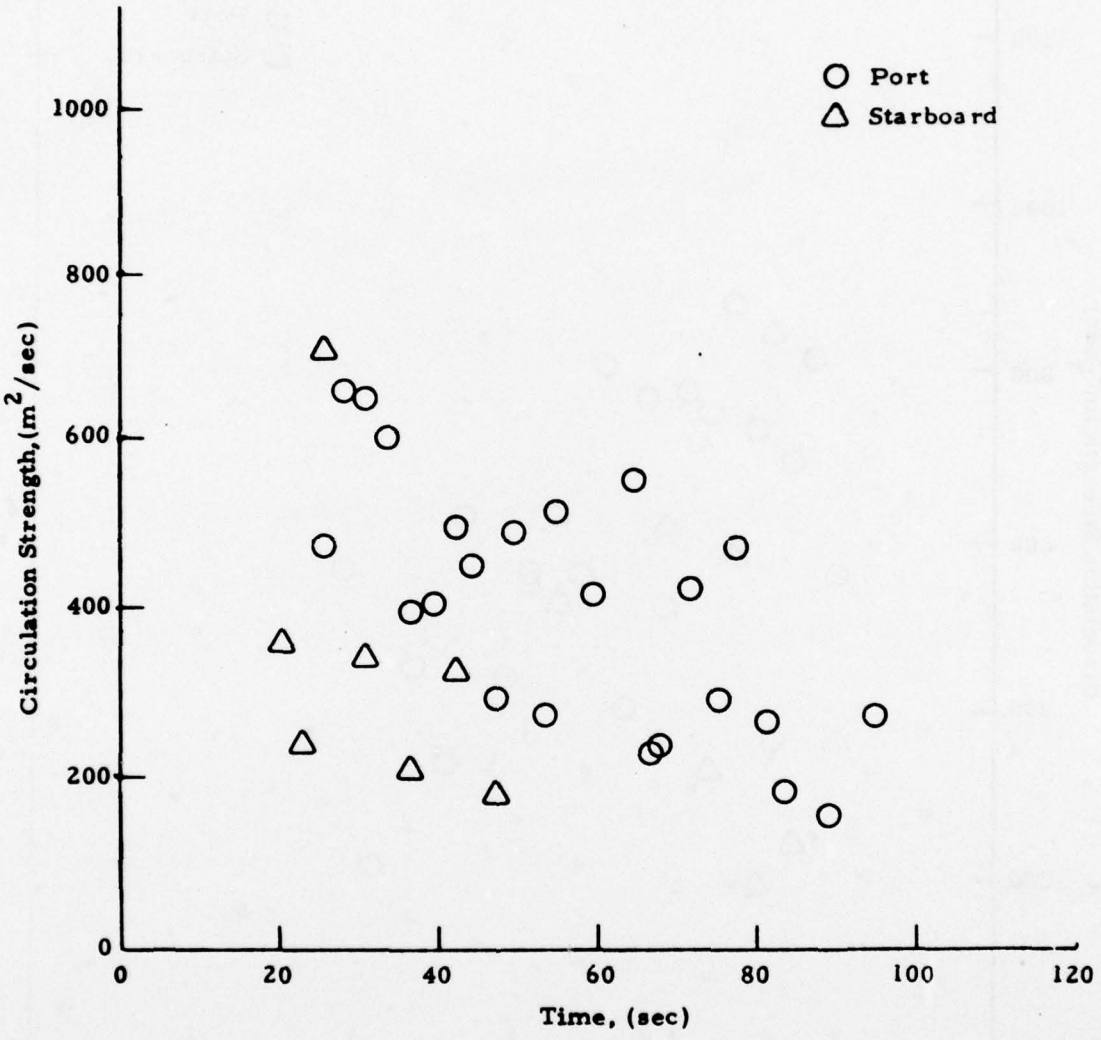

Fig.G-3 - Observed Circulation Time History for Rosamond B-747 Flyby 27

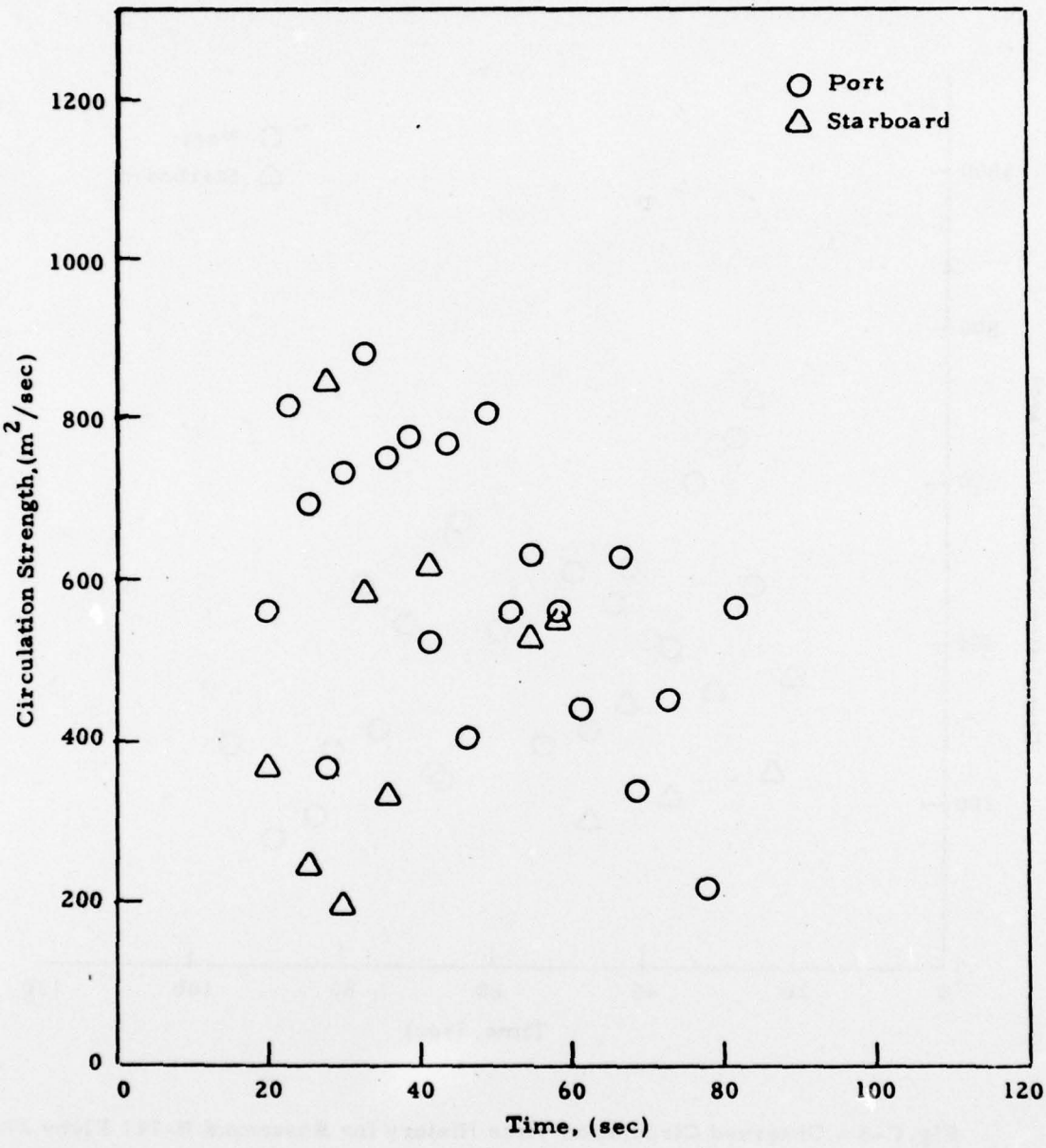

Fig. G-4 - Observed Circulation Time History for Rosamond B-747 Flyby 28

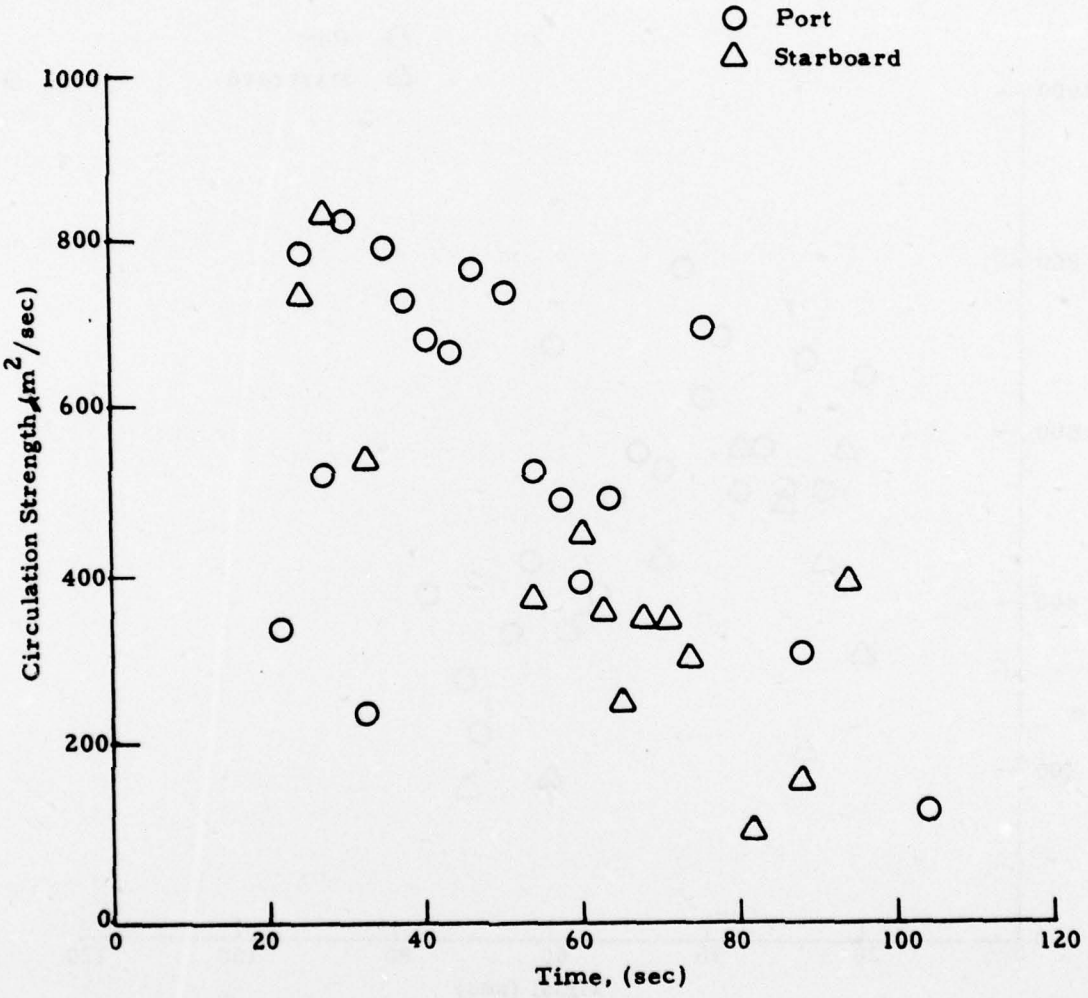

Fig. G-5 - Observed Circulation Time History for Rosamond B-747 Flyby 29

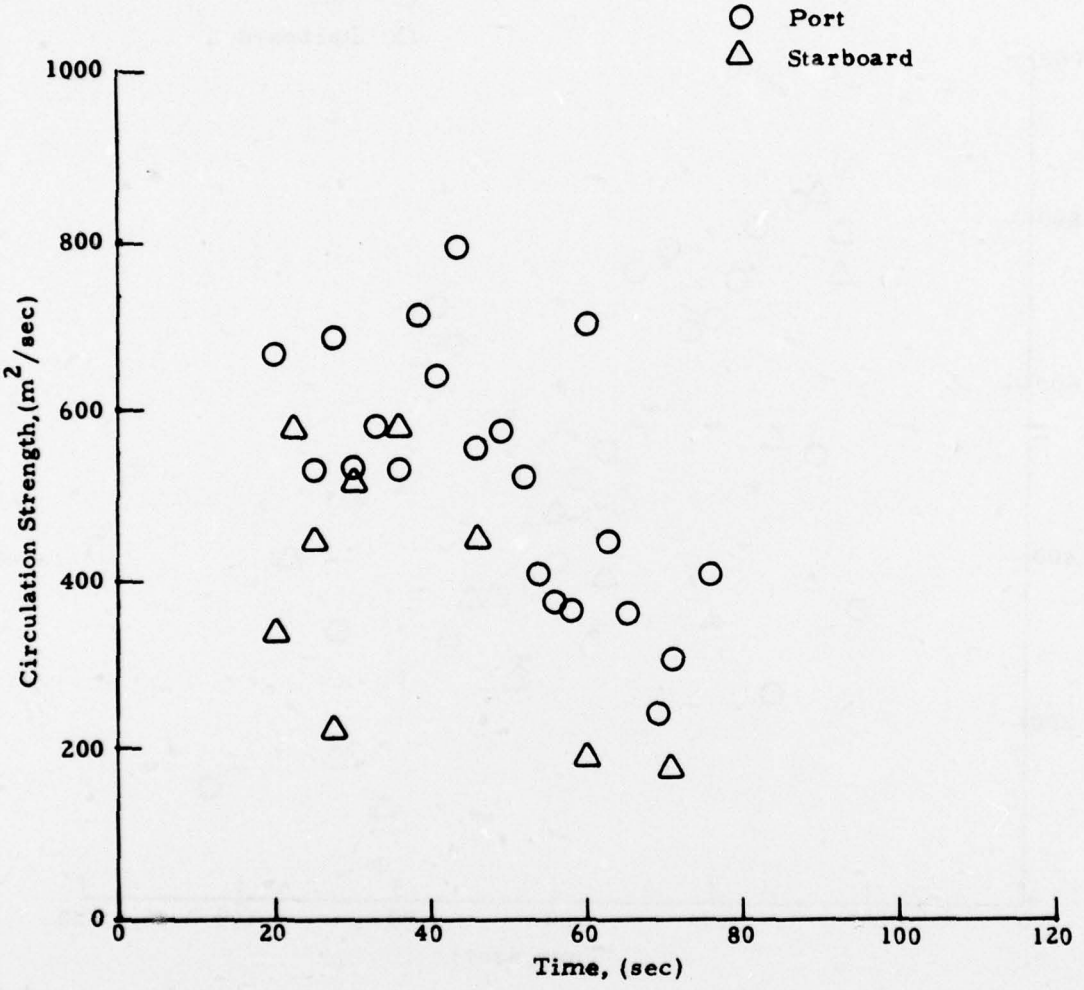

Fig. G-6 - Observed Circulation Time History for Rosamond B-747 Flyby 30

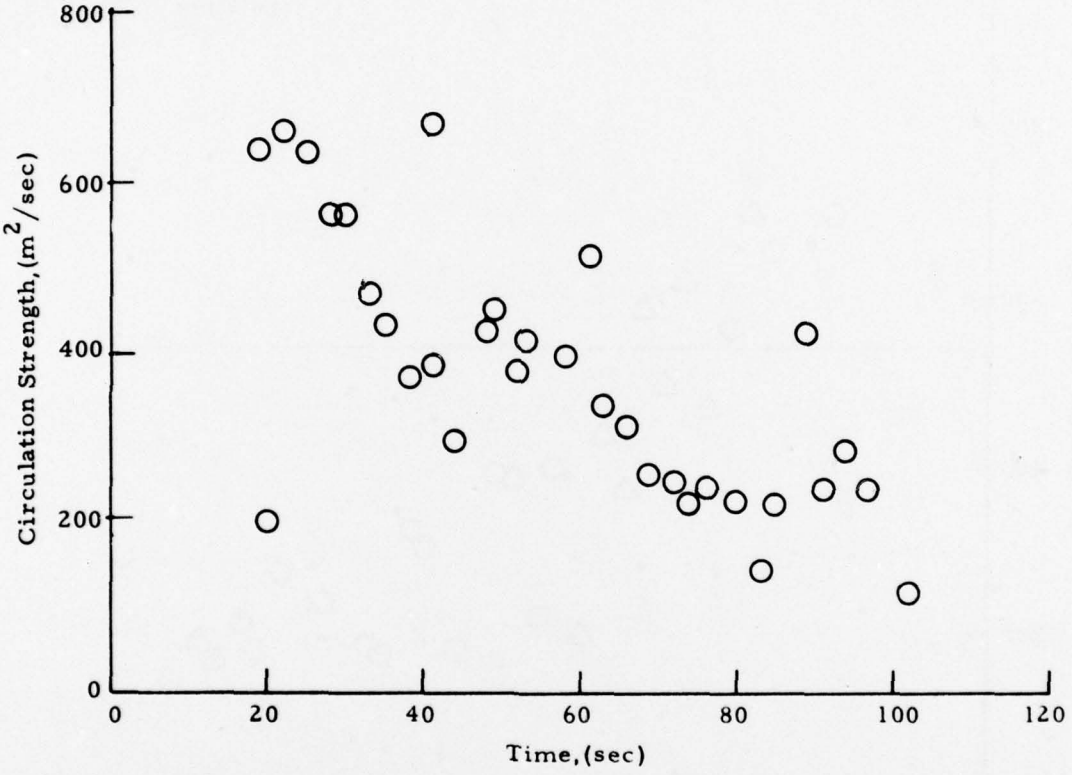

Fig. G-7 - Observed Circulation Time History for Rosamond B-747 Flyby 44, Starboard Vortex

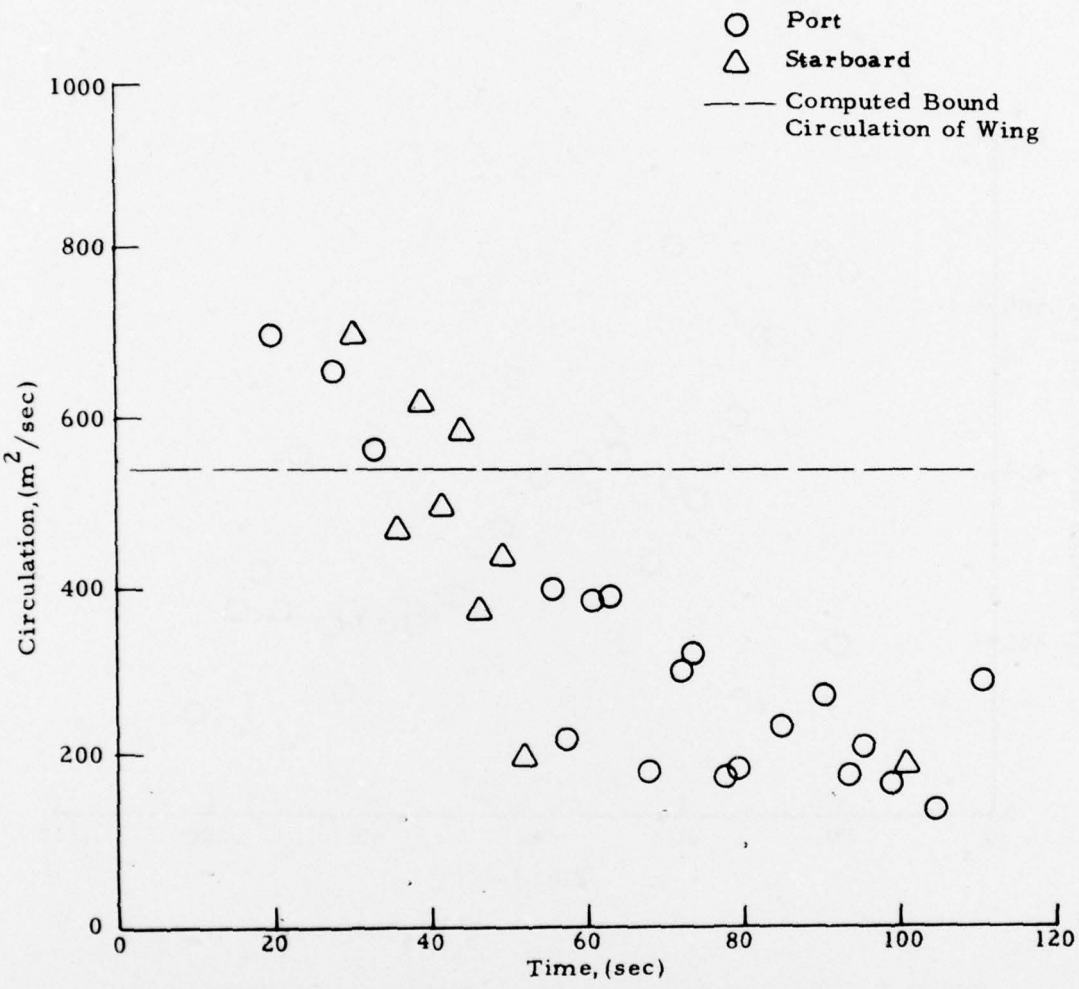

Fig. G-8 - Observed Circulation Time History for Rosamond B-747 Flyby 47

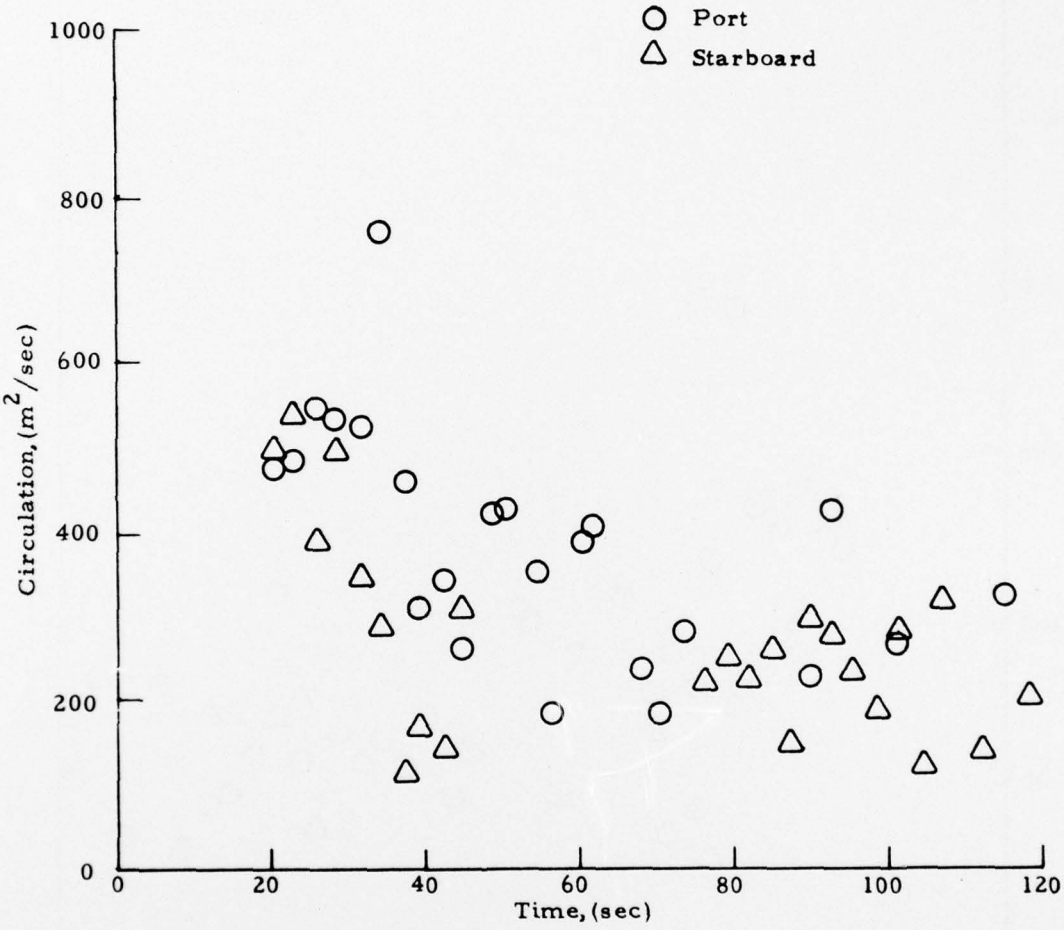

Fig. G-9 - Observed Circulation Time History for Rosamond B-747 Flyby 48

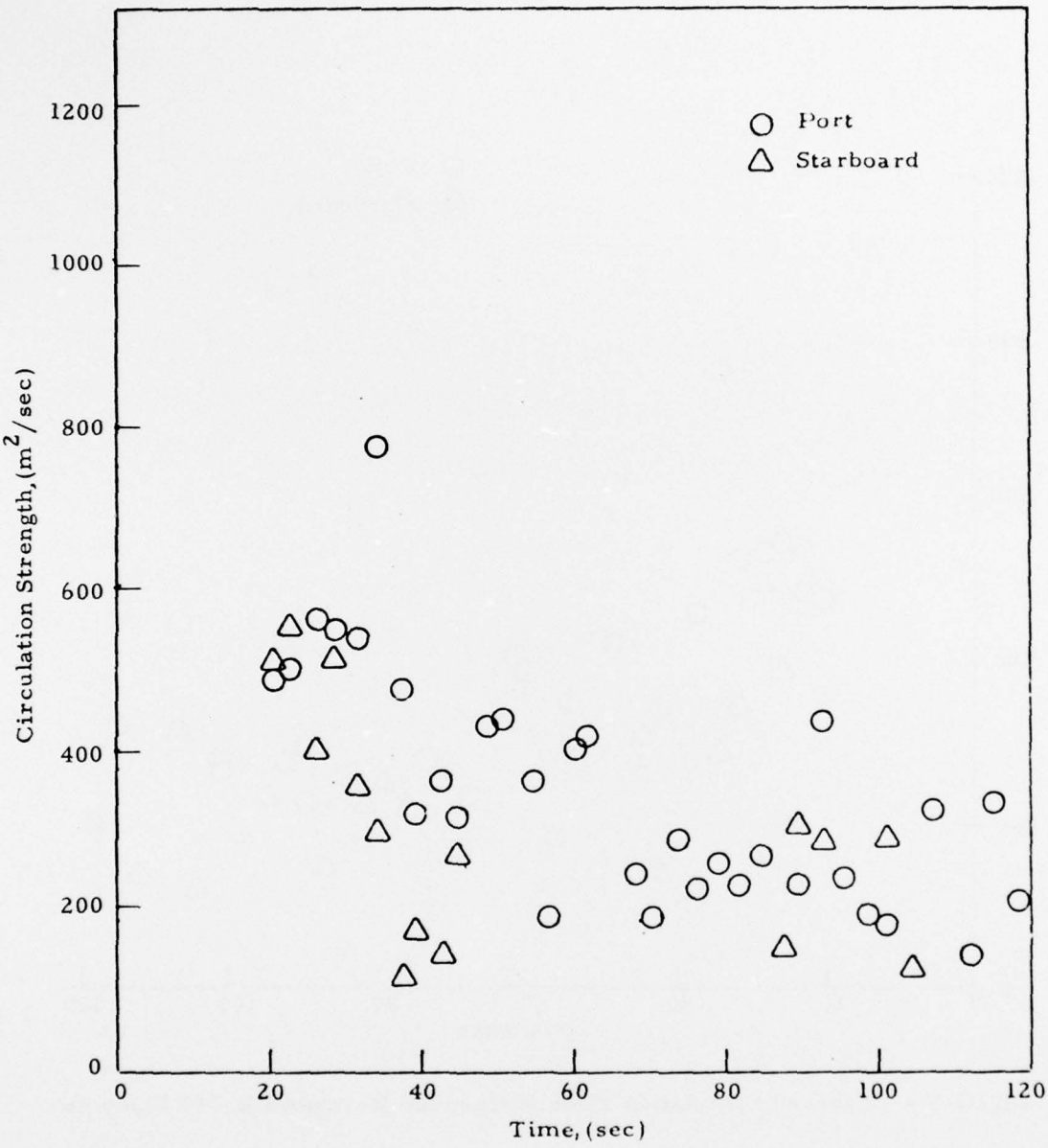

Fig. G-10 - Observed Circulation Time History for Rosamond B-747 Flyby 49

Appendix H
REPORT OF INVENTIONS

In accordance with the objectives of the contract, wake vortex and wind measurements were carried out at the Rosamond, California, test site with a scanning laser Doppler velocimeter system, and the LDV measurements were processed, reduced, and analyzed. The contract objectives were met, and no invention, discovery, or innovation was found.

☆U.S. GOVERNMENT PRINTING OFFICE: 1977—701-663/179

200Copies